TABLE OF CONTENTS

Page

LIST OF TABLES

Page

LIST OF FIGURES

Page

LIST OF ABREVIATIONS

AoA	Angle of attack
ABCA	Artificial Bee colony algorithm
ATAG	Air Transport Action Group
BFGS	Broyden-Fletcher-Goldfarb-Shanno optimization algorithm
CIRA	Italian Aerospace Research Center
CNRC	Canadian National Research Council
CO2	Carbon dioxide
CRIAQ	Consortium for Research and Innovation in Aerospace in Québec
DFEM	Detailed Finite Element Model
DLM	Dublet Lattice Method
DLR	German Aerospace Research Center (Deutsches Zentrum fur Luft und Raumfahrt)
ETS	Ecole de Techonolgie Superieure
FEM	Finite Element Model
FLDS	Flight, Loads and Dynamics Solver
GA	Genetic Algorithm
GARDN	Green Aviation Research Development Network
GFEM	General Finite Element Model
Hz	Herz
IAR-CNRC	Institute for Aerospace Research – Canadian National Research Center
ICAO	International Civil Aviation Organization
IR	Infra Red Termography

XXX

IPS	Infinite Plate Spline
LARCASE	Laboratory of Applied Research in Active Control, Avionics and Aeroservoelasticity
LE	Leading Edge
M	Mach
MDO	Multi-Disciplinary Objective
MPC	Multi Point Constraint
NASA	National Aeronautics and Space Administration
PID	Proportional Integral Derivative

PTA – Pressure Transducer Array

RMS	Root Mean Square
SMA	Shape Memory Alloy
SPC	Single Point Constraint
TE	Trailing Edge
TPS	Thin Plate Spline
UAV	Unmanned Aerial Vehicle
UD/1D	Uni-dimensional

LIST OF SYMBOLS AND UNITS OF MEASUREMENTS

0D	Zero dimensional
1D	Uni-dimensional
2D	Bi-dimensional
3D	Tri-dimensional
α	Angle of attack
β	Aileron deflection angle
Δactuator	Difference between the displacement of two actuators situated on the same chord line
δ	Random value
ε	Percentage of improvement
ε	Probability of selection parameter
$\Phi_{x(y,z)}$	Phase on the X (Y, Z) direction
λ	Describes the delay in the Laminar flow
μ	Dynamic viscosity
ρ	Density (kg/m3)
τ	Describes the onset of turbulence flow
A	Aerodynamic forces matrice
A_f	Attraction factor
A_m	Amplitude of mutation
$A_{x(y, z)}$	Acceleration amplitude of the torsional mode on the X (Y, Z) direction
a	Spline polynomial parameter
b	Spline polynomial parameter

C	Structural damping matrice
C_D	Wing drag coefficient
C_d	Airfoil drag coefficient
C_{d_o}	Drag coefficient for the original airfoil
C_{d_m}	Drag coefficient for the morphed airfoil
C_f	Skin friction coefficient
C_{l_o}	Lift coefficient for the original airfoil
C_{l_m}	Lift coefficient for the morphed airfoil
$\frac{C_L}{C_D}$	Airfoil Lift-to-Drag ratio
C_p	Pressure coefficient
c	Wing or airfoil chord
E_1	Longitudinal Elastic Modulus
E_2	Transversal Elastic Modulus
F_f	Fitness or objective function
$f_{x(y,z)}$	Frequency (Hz)
f(x)	Exact function that describes the curve to be interpolated
G_{12}	Longitudinal Shear Strength
g	Damping coefficient
H	Wind Tunnel Height
h	Spline interval
I	Integral of the exact function approximated by the spline interpolation
K	Generalized Stiffness matrice

k	Reduced frequency
L	Length of reference
L	Wind tunnel length
M	Generalized mass matrice
m_i	Spline polynomial slope
P	Pressure
P_m	Probability of mutation
P_n	Spline polynomial of nth degree
P_s	Probability of Selection Function
p	Laplace non-dimenssional parameter
p	Spectre of all the eigenvalues
Q	Matrice of external forces
Q^I	Imaginary part of the Q matrice
Q^R	Real part of the Q matrice
q	Modal displacements
Re	Reynolds number
S_{1T}	Longitudinal Tension Strength
S_{2T}	Transversal Tension Strength
S_{1C}	Longitudinal Compression Strength
S_{2C}	Transversal Compression Strength
Tr	Non-dimensional transition x coordinate
Up_{TR}	Transition point value on the upper surface of the airfoil
u	x direction speed component

V	Speed (m/s)
v	y direction speed component
W	Wind tunnel width
w	z direction speed component
w_i	Fitness function weights
x	Probability of Selection function parameter
x_i	x coordinate of the spline points
y	Probability of Selection function parameter
y_i	y coordinate of the spline point
z	Probability of Selection function parameter

INTRODUCTION

In the present chapter, the global and historical context of the thesis and the problem for which solutions were researched are presented. Also, the solution found and the context in which it was applied is presented, as well as the main and secondary objectives of the thesis. Finally, a description of the methodology and models applied for attaining these objectives is given.

From ancient times, we have tried to overcome our limitations as humans, and one such limitation was the ability to fly. During ancient China, hot air lanterns, human carrying kite or bamboo-copter toys were invented. During the medieval era in Europe, Leonardo da Vinci draws the first designs of flying machines with humans on board and notes the first ideas and studies airflows and streamlined shapes, while during the 18th century, the first aerodynamic studies were developed and the era of balloon flight begun. Thus, men have always tried to conquer the air and fly. The 19th century has seen more development of aerodynamic and control theories, while its end has seen the first trials of engine powered heavier - than - air aircrafts with pilots on board.

In 1903, the Wright brothers, after many years of research and development, have done four flights which were considered the first controlled and powered heavier-than-air flights and also the flights photographed for the first time.

After the first successful flights of the Wright brothers, the 20th century has seen an explosion in the research and development of aviation. In less than 15 years it became one of the leading domains and industrial fields. During the first half of the First World War, the aircrafts were used mainly for reconnaissance, but during the second half of the war they became more commonly used as fighters and bombers. During the period between the First and Second World Wars, research was devoted to studies of the aerodynamic performances of different configurations of aircrafts. More theories were developed for airplane design and

manufacturing, culminating with the development of the best aircraft fighters used during the Second World War.

After the wars, the aviation concentrated on pushing the boundaries of flight until the sound barrier was broken, and the first supersonic flight was achieved by the development of the fastest and highest aircraft fighter SR71. The notion of active modification (morphing) of aircraft geometries, especially wings, has been introduced as a result of the researches conducted on supersonic aircrafts. At the same time, the Boeing 707 commercial civil aircraft became the first successful commercial jet aircraft. Then, in 1976, the Concorde became the first supersonic commercial aircraft. Finally, the largest and most fuel economical commercial aircraft, Airbus A380, was developed over a period of over 17 years, from 1988, when its development started, to 2005 when the maiden flight took place.

Today, the increase in concern over the climate changes and the influence of mankind on it, lead to increase in research regarding the quantity of carbon footprint due to the aeronautical industry and the need in its minimization. The research conducted by various aeronautical organizations, such as IATA and ICAO or companies such as Boeing and Airbus, has shown that 2% of the global quantity of green gases was produced by the aeronautical industry (ATAG, 2015). This research has also shown that following the development of more airlines and aircrafts, the production of green gases has an ascending trend (Anderson and Bows, 2008). An overview of some of the leading figures for aerospace impact on the green gas levels are given in Figure 0.1.

The research has sparked interest in the development of aircraft technologies that would lead to less fuel consumption (Peeters, Middel and Hoolhorst, 2005), (News, 2008), or to the replacement of the classic fuel with biological fuel, such as the biodiesel (Engineer, 2009). In addition, aircrafts that used solar energy to power their flight were developed and in 2010, Solar Impulse demonstrated that it was possible to fly an aircraft completely powered by solar cells (Impulse, 2010).

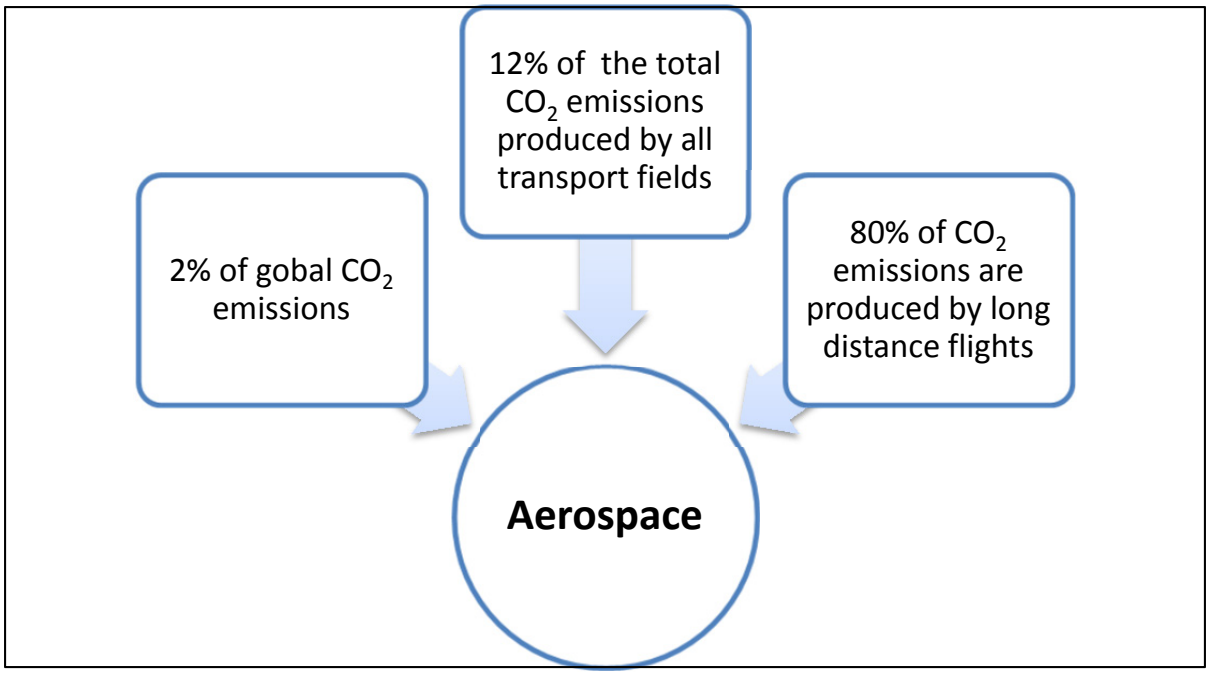

Figure 0.1 Influence of the aerospace industry on the green gas emissions, particularly CO_2

In this context on the influence of the aerospace industry on the world climate and economy, several major project networks were developed as collaborations between industry, academia and research institutions to design, manufacture and test new technologies that would lead to a marked decrease of the impact the aerospace field has on the environment. The main networks are in Europe, the 'Clean Sky', and in Canada, the Green Aviation Research and Development Network (GARDN). These networks were developed for collaboration between various fields inside the aerospace domain: structures, aerodynamics, flight dynamics, aircraft control, flight management, etc; many solutions were researched for the development of optimal technologies that helped achieve various objectives.

0.1 Problem Statement

One such objective is the development of aircraft structures that have higher performance and better control than previous aircrafts. This type of objective, in order to be achieved, needs a multidisciplinary approach in which aerodynamics, structure, control and optimization methods combine to find the best solutions in terms of performances and shapes

of aircrafts, that could be controlled in an optimal manner. If successful, these types of multidisciplinary optimization (MDO) objectives pave the way towards the development of new types of aircrafts that would have higher performances, lower fuel consumption, better control, and larger mission flight envelope than the today existing aircrafts.

The approach for this MDO type of problem is morphing, that represents an active or passive modification of the structure or shape of an aircraft in order to obtain specific performances improvements, either structural or aerodynamic. Morphing can be applied to a wide range of aircraft components, both 'internal' – such as optimization of interior design – and 'external' – such as optimization of wings, fuselage, engines, horizontal or vertical tail, etc

.

Morphing is mainly important for the improvement of aircraft performances in terms of aerodynamics, control or mission envelope; for these aspects, wing morphing is of particular importance.

0.1.1 CRIAQ MDO 505 Morphing Architectures and Related Technologies for Wing Efficiency Improvement

In this context of morphing wings development, for the purpose of optimizing performances and under the umbrella of the Consortium for Research and Innovation in Canada (CRIAQ), the level 5 project MDO 505 'Morphing Architectures and Related Technologies for Wing Efficiency Improvement' took place. The CRIAQ MDO 505 project took place between teams from Canadian industries – Bombardier Aerospace and Thales Canada – Canadian academic and research partners – Ecole de Technologie Superieure (ETS), Ecole Polytechnique and the National Research Council (NRC) – and the Italian industries and academia – Aelania Aermacchi, University of Naples and the Italian Center for Reasearch in Aerospace (CIRA). This project was realized in continuation of the CRIAQ 7.1 project.

The purpose of the CRIAQ MDO 505 project was the development of a wing demonstrator equipped with an aileron system that had an optimized structure representative for a real

wing, an active morphing upper surface of the wing and an alternative active morphing aileron. Figure 0.2 presents the concept and design of the CRIAQ MDO 505 wing tip structure.

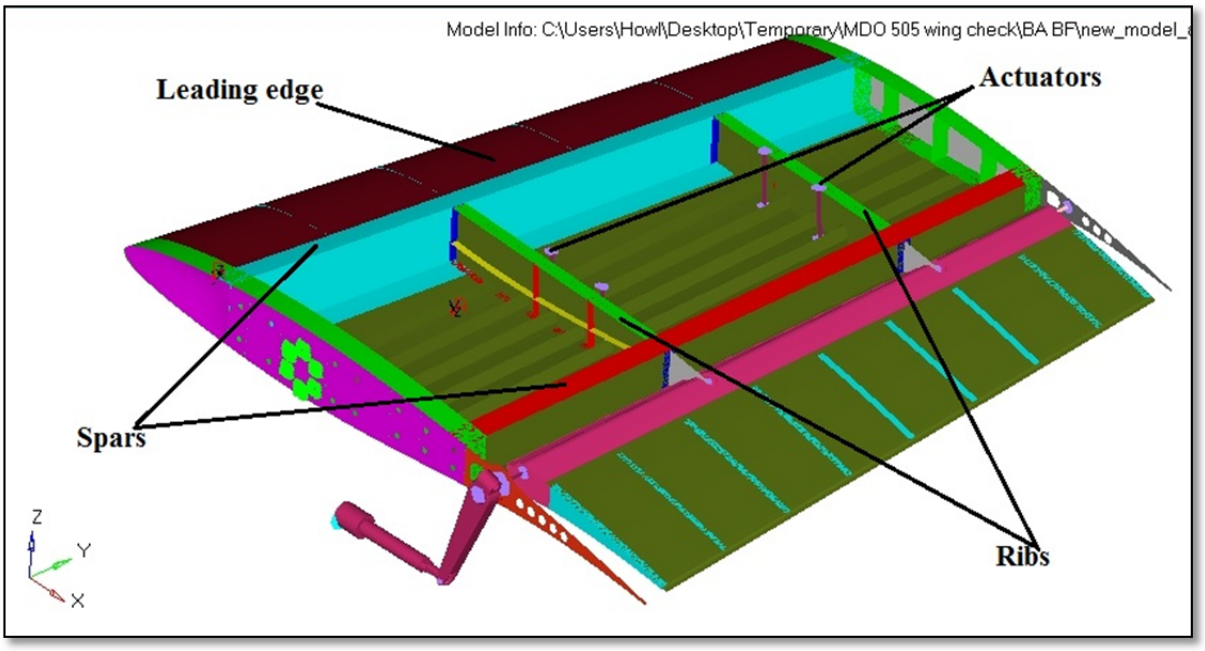

Figure 0.2 The CRIAQ MDO 505 Morphing Wing concept

The technology was tested for aerodynamic, structural and control performance improvements using bench test techniques, without aerodynamic loads but under structural loading, and wind tunnel experimental testing. The objective of the first set of bench tests was to observe that the optimized wing box structure, which had a large part of the upper surface manufactured from a combination of composite material, resisted to the 1g loads demanded by certification authorities while its shape was morphed using electrical actuation system integrated inside the wing box. The second set of bench tests was used to develop and integrate different types of controller methodologies, such as Proportional-Integrator-Derivative (PIDs), Neural Network, Fuzzy Logic, etc. with the aim to achieve the desired displacements of the optimized wing airfoil. The wind tunnel experimental testing was done to achieve several objectives: 1) aerodynamic improvement of the flow behaviour on the upper surface through the morphing of the composite upper surface shape of the wing; 2)

modification of the aerodynamic lift and drag ratio through the use of a morphing aileron; 3) validation of the control system methodologies under loading conditions; 4) verification of numerical prediction for aeroelastic stability – particularly flutter; 5) validation of the numerical predictions of the pressure distribution for the actuation section; 6) validation of the optimization prediction for the achievements of the aerodynamic improvement objectives.

0.1.2 ATR-42 Morphing Wing Project

Another project, that preceded and provided a first step in understanding the magnitude of the MDO 505 project, was developed at the Laboratory of Applied Research in Active Control, Avionics and AeroServoElasticity (LARCASE). The objective of this project was to develop a morphing wing entirely from composite materials on which optimization techniques were tested, and which was experimentally tested in the Price-Païdoussis subsonic wind tunnel. The knowledge accumulated during this ongoing project was of extreme importance in the beginning of the CRIAQ MDO 505 project. For this project, two rigid reduced scale wing models and an active morphing wing model were developed based on the ATR-42 wing airfoil; their shapes were rectangular to avoid three dimensional flow effects during wind tunnel tests. The wing models were manufactured from fiber glass-epoxy composite material that was specially designed for this project. The electrical actuation system for the active morphing wing model was manufactured with both external and internal (wing box) components. The objective of the project was three-fold; it followed the development and wind tunnel validation of (1) the knowledge needed for composite material optimization with morphing properties, (2) the first version of the optimization software that would provide the optimal shapes and (3) the control system for the morphing wing that would ensure the achievement of the desired shapes.

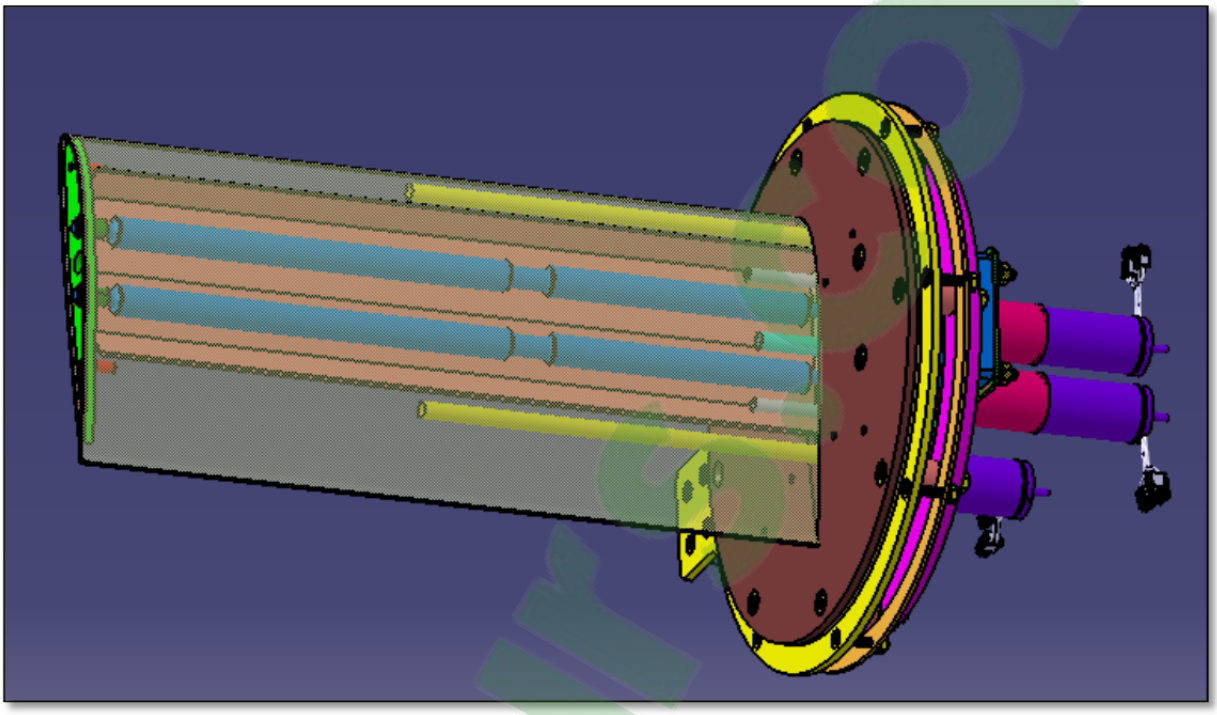

Figure 0.3 Model of the ATR42 morphing wing
(retrieved from (Baciu, 2012))

0.2 Research Objectives

The research presented in this thesis was done in the framework of the projects presented above and its objectives are related to those presented for each of the projects described.

The global objective of the research was to determine with reasonable accuracy the impact of optimized shapes of the airfoils for the ATR 42 wing and the CRIAQ MDO 505 wing-tip demonstrator, on the aerodynamic and aeroelastic behaviour. The numerical analysis was conducted for a range of angles of attack, speeds and aileron deflection angles, and these ranges were constrained by the dimensions and speed limits of the wind tunnels in which the wing models were tested. For the CRIAQ MDO 505 wing – tip demonstrator the wind tunnel test cases were chosen in agreement with the project partners with the aim to fulfill the project objectives.

To ensure the good progress of the research and to successfully achieve the proposed global objective, the following sub-objectives were established:

1) Conception of optimization process and the geometry parameterization of both the ATR-42 and MDO 505 wing airfoils

- Implementation of the 'cubic spline' methodology for recreating smooth curves such as those needed for optimized airfoil shape design;
- Development of the 'cubic spline' method for its application on a specific number of points for a certain region of the airfoil and ensure a smooth connection between the reconstructed curve and the rest of the airfoil;
- Implementation of different "global constraint" optimization algorithms such as Genetic Algorithm (GA), Artificial Bee Colony (ABC) and Gradient Descent (GD), with the aim to compare their obtained results, and choose the best optimization algorithm;
- Development of the Genetic Algorithm to ensure fast convergence by introducing particular functions such as 'Tournament' or 'Binary Cross-Over';
- Implementation of two aileron shape morphing methods coupled with the optimization algorithm and the geometric parameterization with the aim to choose the best structural and control morphing methodology;
- Development of the chosen aileron shape morphing method for both constrained and free optimization capabilities.

2) Application of the Genetic Algorithm for the improvement of the ATR-42 wing airfoil performances

- Two-dimensional analysis on the ATR-42 wing airfoil with the aim to minimize the drag coefficient through manipulation of the boundary layer behaviour at low speeds and small angles of attack;
- Two-dimensional analysis on the ATR 42 wing airfoil with the aim to improve the boundary layer behaviour at low speeds and high angles of attack.

Application of the Genetic Algorithm for the improvement of the CRIAQ MDO 505 wing airfoil performances

- Two-dimensional analysis on the CRIAQ MDO 505 wing airfoil with the aim to delay the transition region towards the trailing edge and reduce the drag coefficient, for speeds in the range of 34 to 102 m/s, a wide range of angles of attack between -5° and +10° and conventional aileron deflection angles between -15° and +15°;
- Two-dimensional analysis on the CRIAQ MDO 505 wing airfoil with the aim to advance the transition region towards the leading edge and ensure a more stable boundary layer, for speeds in the range of 50 to 102 m/s, a wide range of angles of attack between -5° and +10° and conventional aileron deflection angles between -15° and +15°;
- Two-dimensional analysis on the CRIAQ MDO 505 wing airfoil with morphing aileron with the aim to improve the lift coefficient and delay the transition region position for speeds in the range of 34 to 102 m/s, a wide range of angles of attack between -5° and +10° and morphing aileron deflection angles between 7° up and 7° down;
- Two-dimensional analysis on the CRIAQ MDO 505 wing airfoil with morphing aileron with the aim to minimize the aileron deflection needed for a given lift coefficient.

3) Flutter Analysis of the CRIAQ MDO 505 wing-tip demonstrator

- Development of the wing-tip General Finite Element Model (GFEM) with composite upper surface modeled by surface elements using Hypermesh software from the Hyperworks software package;
- Development of the wing-tip GFEM with aluminium upper surface modeled by surface elements using Hypermesh software from the Hyperworks software package;
- Development of the conventional aileron GFEM modeled by surface and solid elements using Hypermesh software from the Hyperworks software package.
- Performing a Natural Mode analysis of the wing – aileron (wing-tip) system with composite upper surface to evaluate the possibility of coupled modes occurence using Optistruct solver from the Hyperworks software package;

- Importing, checking for errors and correcting the GFEM of both wing – aileron (wing-tip) system with composite upper surface and wing-tip – aileron – system with aluminium upper surface in the analysis software using MSC Patran;
- Development of the aerodynamic and aeroelastic model for flutter analysis using Flight Loads and Dynamics Software (FLDS) from MSC Patran/Nastran;
- Development of the aero-structure coupling using FLDS from MSC Patran/Nastran;
- Performing the flutter analysis on both GFEM models using MSC Nastran solver from MSC Patran/Nastran software package;
- Exporting and interpreting the flutter analysis results using both numerical estimation and visualization software Hyperview from the Hyperworks software package.

4) Wind tunnel testing of the ATR-42 rigid wing models

- Installation of the ATR-42 rigid wing models in the Price Paidoussis subsonic wind tunnel chamber and their connection to the AeroLab pressure measurement system;
- Performing the experimental testing at three wind tunnel speeds and five angles of attack at each speed (for a total of 5 cases) for each ATR-42 wing model;
- Post-processing of the recorded pressure data to obtain the pressure coefficient distribution for each tested case;
- Estimation of the transition region on the upper surface of each ATR-42 wing model by applying the second derivative method to the pressure coefficient distribution;
- Validation of the numerically calculated transition from the two-dimensional analysis of the ATR-42 wing's airfoil using the transition region estimated from experimental data.

5) Wind tunnel testing of the CRIAQ MDO 505 wing-tip demonstrator

First set of wind tunnel tests

- Validation of the numerical (spline reconstruction of the upper surface) and manufactured original and morphed wing shapes using static scanning techniques after wind tunnel tests;

- Validation of the numerical transition prediction for 38 case expressed in terms of various speeds, angles of attack and conventional aileron deflection angles by using the Post Processed Infrared Thermography data;
- Validation of the numerical transition prediction for 38 case expressed in terms of various speeds, angles of attack and conventional aileron deflection angles by using the Post Processed Kulite pressure sensors data;
- Validation of the numerical pressure distribution for 38 cases expressed in terms of various speeds, angles of attack and conventional aileron deflections by using the Post Processed Kulite and pressure taps sensors data;
- Development of an aerodynamic data post processing procedure for calibration of the aerodynamic optimization and analyses based on the experimental Infrared Thermography Transition data.

Second set of wind tunnel tests

- Validation of the Infrared Thermography transition data from the first series of tests before and after change of photography procedure during wind tunnel tests;
- Validation of the numerical and manufactured original and morphed wing shapes using static scanning techniques after wind tunnel tests with the aim to check the values of deformations induced by aerodynamic loads during tests;
- Validation of the aerodynamic data post processing procedure and recalibration of the procedure based on the new experimental data;
- Validation of the new 59 numerical transition values with the experimental Infrared Thermography transition data;
- Validation of the new 59 numerical transition values with the experimental Kulite pressure sensor data;
- Validation of the numerical pressure distribution on the wing with the experimental pressure distribution obtained from the Kulite and pressure tap sensors;
- Selection of the test cases for the wing with morphing aileron based on the results validated during the second set of wind tunnel tests.

Third set of wind tunnel tests

- Validation of the numerical and manufactured original and morphed wing and aileron shapes using static scanning techniques after wind tunnel tests to check the values of the deformations induced by aerodynamic loads during tests;
- Validation of the morphing aileron deflection angles under wind tunnel aerodynamic loads;
- Validation of the optimization of the laminar region extension on the wing using the Infrared Thermography measurements;
- Validation of the numerical pressure distribution using Kulite pressure sensors and pressure taps on the morphing wing, and morphing aileron pressure taps.

0.3 Research Methodology and Models

In order to perform the numerical analysis of a morphing wing system, several different algorithms and codes, all originally developed or commercially available, were coupled and used:

- The cubic spline interpolation for reconstructing the upper surface of the morphing wing airfoil shapes;
- The Genetic, Artificial Bee Colony and Gradient Descent algorithms for determining the optimum wing shapes in function of the flight conditions;
- Morphing aileron – shape changing methods;
- The XFOIL solver for performing the two-dimensional airfoil analysis;
- The XFLR solver for performing the three-dimensional wing analysis;
- The Hypermesh code for developing the General Finite Element Model of the wing and aileron;
- The Optistruct solver for performing the modal analysis of the GFEM model;
- The Patran code for importing and correcting the GFEM model before performing its aeroelastic analysis;
- The Flight Loads and Dynamics software (FLDS) for performing the aero-structural coupling;

- The Nastran solver for performing the flutter analysis;
- The Hyperview code for visualizing the flutter analysis results.

Each one of these codes and models will be briefly presented and explained in the next subsections. All the algorithms developed during this research were programmed using FORTRAN and Matlab, saved and compiled as self-contained 32-bit applications, without requiring any additional libraries. They can be run on any computer using the Windows XP, Vista, Seven, Eight or Ten operating systems, both 32-bit and 64-bit versions. The desired configuration and setup was performed using input files of simple formatting (TXT or DAT files, modifiable by any text editor), and the output was presented in the same way, and was further post-processed.

0.3.1 Cubic Spline Interpolation

The *spline* functions are characterized by their shape on subintervals, between two control points. They are also known as piece-wise polynomial real functions. In interpolating problems, *spline* interpolation is often referred to as polynomial interpolation, due to the fact that it yields similar type of results.

When lower degree *splines* are used the resulted curve is as well traced as if it was interpolated with high degree polynomials, but has the benefit of avoiding instability due to Runge's phenomenon (Berbente, Mitran and Zancu, 1997).
The most used *spline* interpolation is the *cubic spline* that ensures continuity up to, and including, the second order derivatives, which permits the calculation of the curvature radius.

The *cubic spline* is represented by the 3rd degree polynomial function:

$$P_{3,i}(x) = y_i + m_i(x - x_i) + b_i(x - x_i)^2 + a_i(x - x_i)^3 \tag{0.1}$$

The polynomial function presented in equation (0.1) describes the behaviour of the *splines* on each interval.

The parameters a_i and b_i are written as functions of the slope m_i calculated in each node. The slope m_i is the solution to the tri-diagonal linear system:

$$\begin{aligned}
&\rho_i m_{i-1} + 2m_i + \lambda_i m_{i+1} = d_i,\ i \in \overline{2,(N-2)} \\
&\textit{where} \\
&\rho_i = \frac{h_i}{h_{i-1}+h_i},\ \lambda_i = 1-\rho_i,\ d_i = \frac{3\lambda_i(y_{i+1}-y_i)}{h_i} + \frac{\rho_i(y_i-y_{i-1})}{h_{i-1}} \\
&h_i = x_{i+1} - x_i;
\end{aligned} \tag{0.2}$$

To equation (0.2) boundary conditions are added, to replace the continuity conditions needed for the 1st and 2nd derivatives that cannot be imposed on the first and last nodes, x_1 and x_N.

$$p''(x_1) = p''(x_N) = 0; \tag{0.3}$$

By imposing continuity conditions, two degrees of freedom from the system presented in equation (0.2) remain undefined. These two degrees of freedom are the values of the boundary slopes m_1 and m_N. Under these circumstances, the values for the end slopes can be either imposed or calculated through relation with their neighbouring slopes.

In the present case, a more particular case of the *cubic spline* interpolation was used - the natural *cubic spline* interpolation defined by the boundary conditions presented in equation (0.3). The application of equation (0.3) to the polynomial function from equation (0.1) gives the following linear system for the calculation of the boundary slopes, m_1 and m_N:

$$\begin{cases} 2m_1 + m_2 = 3\dfrac{y_2 - y_1}{h_1} \\ m_{N-1} + m_N = 3\dfrac{y_N - y_{N-1}}{h_{N-1}} \end{cases} \tag{0.4}$$

It was demonstrated, that by imposing the conditions from eq. (0.4), the integral from equation (0.5) is minimized:

$$I = \int_{x_1}^{x_N} [f''(x)]^2 dx \tag{0.5}$$

In equation (0.5), *f(x)* represents the unknown exact function that describes the curve to be traced, which is approximated by the *spline* interpolation. The minimization of the integral from equation (0.5), by imposing the natural conditions, leads to the most smooth *cubic spline* interpolation. Figure 0.4 presents the application of the cubic spline method on the ATR-42 airfoil.

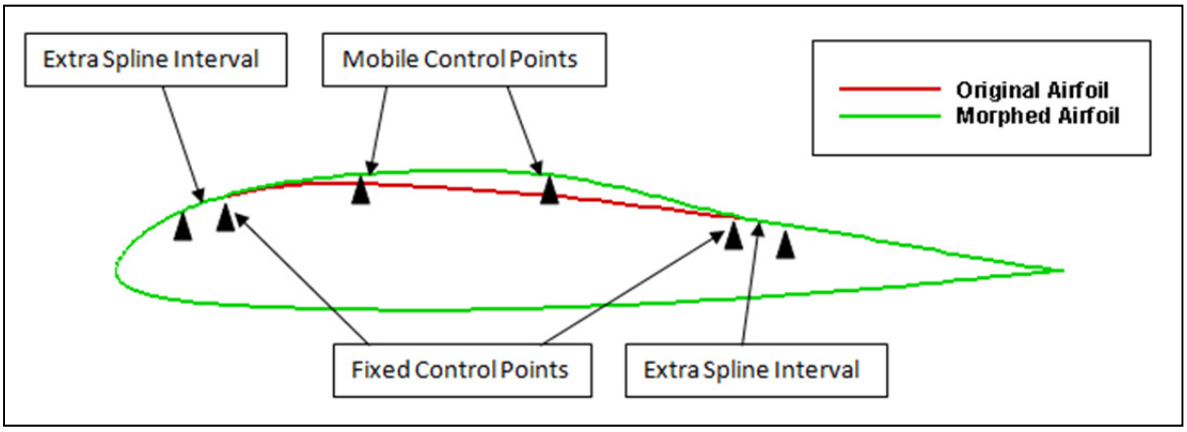

Figure 0.4 Application of cubic spline method on the ATR-42 airfoil for upper surface morphing

For the parameterization of the airfoil curves, a minimum of seven control points are needed, and the maximum number of control points implemented in the reconstruction program was ten. Six of the control points represent the start and end points of the morphing surface plus

two extra control points on each side to ensure smoothness in the passage between reconstructed and existing airfoil curves.

The cubic spline method was used because it was fast to implement and is widely used for curve interpolation. The method was also successfully used for the reconstruction of the aileron upper and lower curves in the first method of morphing of the aileron.

0.3.2 Genetic algorithm optimization procedure

Genetic algorithms are numerical optimization algorithms inspired by natural selection and genetics of living organisms. These algorithms are initialized with a population of guessed individuals, and use three operators, namely *selection*, *crossover* and *mutation*, to direct the population towards its convergence to the global optimum, over a series of generations (Coley, 1999).

In order to evaluate all individuals in the population, an objective function, called the fitness function, must be defined. This fitness function is calculated for all individuals of a given generation. The higher the values of the fitness function are, the higher are the chances of the individual to be selected for the creation of the next generation.

The general outline of the method and all the steps of the genetic algorithm are presented in Figure 0.5, in the way which they were applied for the CRIAQ MDO 505 wing airfoil optimization. The process of evaluation of the fitness function, selection of the best individuals to become parents, crossover and mutation of the new individuals continues in an iterative manner, until the maximum number of generations is reached. Tournament selection, simulated binary crossover (Herrera, Lozano and Verdegay, 1998) and polynomial mutation (Herrera, Lozano and Verdegay, 1998) were used. The termination criterion used was the achievement of the maximum number of generations.

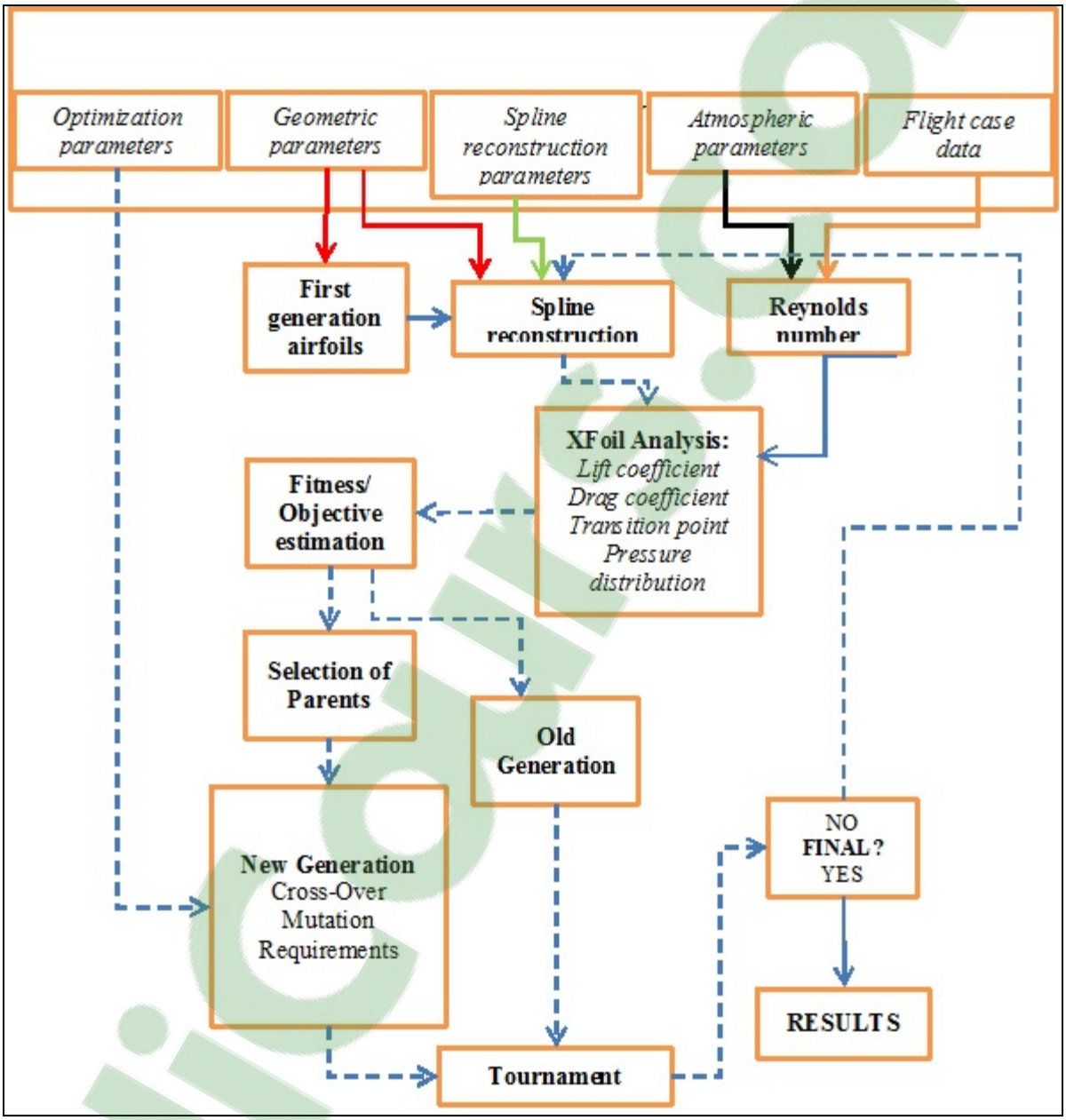

Figure 0.5 Diagram of the Genetic Algorithm software process
(Retrieved from (Koreanschi et al., 2016))

0.3.3 The Artificial Bee Colony optimization procedure

The *ABC algorithm* is an optimization algorithm based on the intelligent behaviour of a *honeybee swarm*. Karaboga and Basturk conceived the original algorithm in 2007 (Karaboga and Basturk, 2007a), that was applicable only for the unconstrained optimization of linear and nonlinear problems. Other authors have proposed methods for enhancing the algorithm's capabilities, such as the handling of constrained optimization problems (Karaboga and Basturk, 2007b) or the significant improvement of the algorithm convergence properties. Because the *ABC algorithm* simultaneously performed a global search throughout the entire definition domain of the objective function and a local search around the more promising solutions already found, it had efficiently avoided converging towards a local minimum point of the objective function, and thus it was able to approximate the global optimum point.

The general configuration of the ABC algorithm as it was applied for the morphing wing optimization procedure is presented in Figure 0.6.

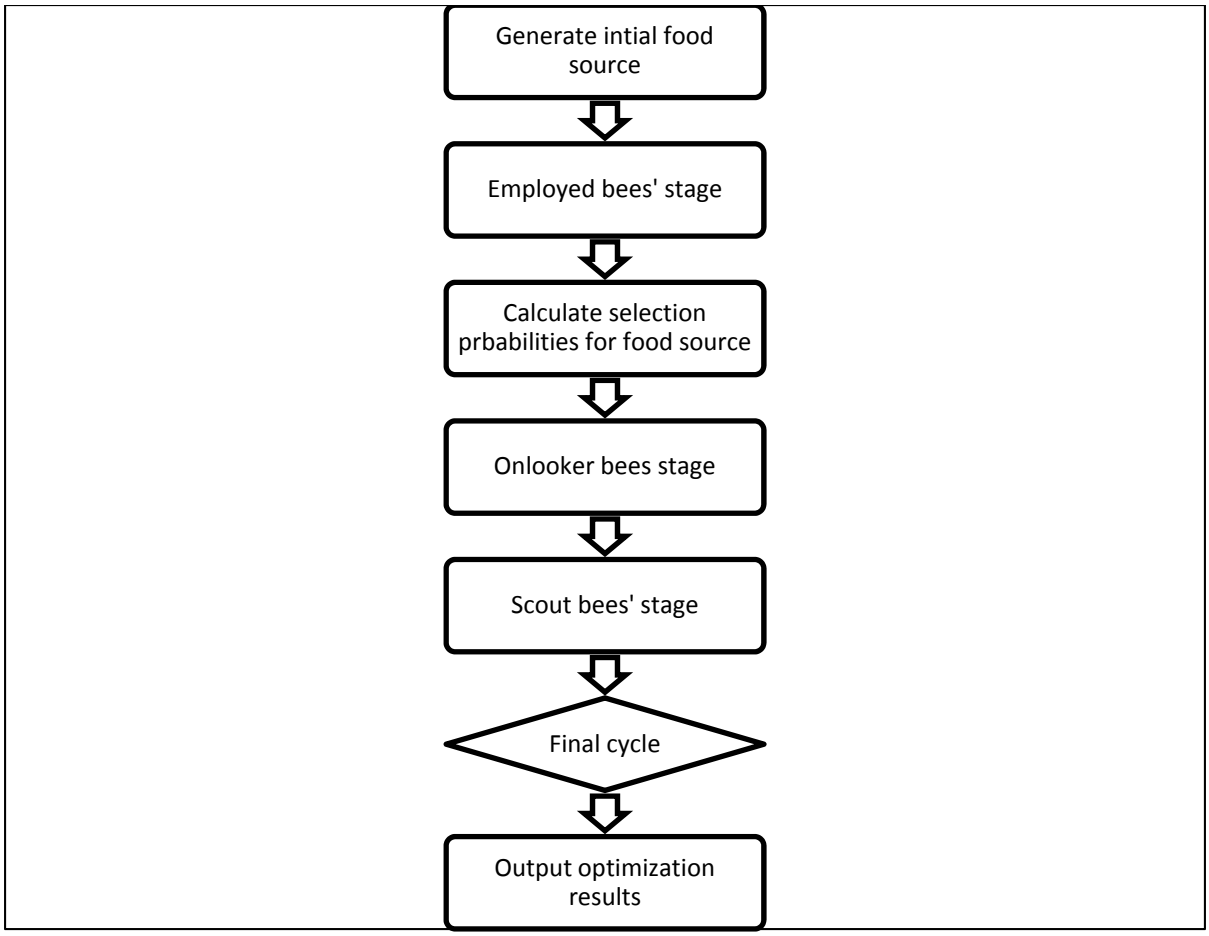

Figure 0.6 Outline of the ABC algorithm

0.3.4 The Gradient Descent Optimization Method

The *Gradient Descent method* is a first-order optimization algorithm. To find a local minimum of a function using this method, steps proportional to the negative value of the *gradient* (or of the approximate gradient) of that function at its current point in time are taken. When steps proportional to the positive of the gradient are taken, a local maximum of that function is approached; the procedure is known as *Gradient Ascent* (Snyman, 2005), (Yuan, 2008).

The search starts from the un-morphed airfoil, with (0 mm, 0 mm) displacements. At this point, the gradient is calculated using *finite differences approximations*. These finite

differences are calculated in order to give the direction to find the maximum of the objective function. If the problem has two distinct objective functions – for example, minimization of the drag coefficient and delay of the transition point towards the trailing edge – basically a minimization and a maximization problem, the algorithm was designed to switch between the two types of gradients (objective functions) without stopping for user input.

In addition, for direction tracking, a step is needed to find new displacements. To solve the morphing wing problem, a step of 1E-06 was chosen in addition to the gradient's value. The displacements are then modified according to equation (0.6) :

$$Displacement_{new} = Displacement_{old} \mp step \times gradient \tag{0.6}$$

The method converges very fast, but its disadvantage was that it covers a small search area. The algorithm stoped when a local minimum was found, thus the quality of the results was very random and depended upon each individual flight cases that was studied. This method is also very sensitive to aerodynamic solver convergence, as its results were improved in an iterative fashion. Therefore, if the solver does not converge during the iterative procedure, the calculation of the new gradient value is not possible, with consequences on the optimization process convergence.

0.3.5 Morphing aileron shape optimization methods

For the conventional aileron, the main problem resides with rotating the entire control surface around its hinge point, which creates a discontinuity of the slope of the airfoil camber line. This discontinuity is also reflected over the upper and lower surfaces. At high deflection angles, this discontinuity can lead to premature boundary layer separation and a loss of efficiency of the control surface. Therefore, two methods for morphing the aileron shape were developed and each method used the genetic algorithm presented in section 0.3.2.

Only one of the methods was chosen for implementation in the CRIAQ MDO 505 project after consultations with the Italian teams who were tasked with the design and manufacturing of the morphing aileron. Based on these consultations and on the performance comparison between the two methods, the second method for morphing the aileron was chosen. In this section, both researched methods will be presented, with focus on the second method of morphing the aileron.

Both methods for morphing the aileron were required to respect a set of constraints. One of the main constrains was to keep the airfoil thickness constant. This condition had arisen from one of the main objectives of the project, which was the manufacturing of a fully functional wing model equipped with an aileron using existing technologies.

Consistence between the conventional and the morphed aileron deflection angles was another constraint that was taken into account. The overall aileron deflection angle, calculated as the angle between the horizontal (which is defined as the position of the aileron at zero degree deflection) and the tip of the trailing edge of the morphed aileron shape, must remain consistent to the overall deflection angle of a conventional aileron.

A third constraint was related to the camber line of the aileron. The curvature of the camber line must maintain a constant slope direction from the articulation point to the tip of the aileron.

First aileron morphing method

The first method developed for the morphing aileron was inspired from the method used to morph the upper surface skin of the wing airfoil. The method uses vertically displaced control points, affording a fast understanding and numerical implementation of the method.

This method must take into account the conditions expressed in the beginning of this section, thus it was found necessary to use control points on both the upper and lower surface of the

aileron, due to the difficulties of maintaining the thickness constant. Two control points were found to be sufficient for the upper surface and another two control points were selected for the lower surface. The number of control points was decided based on the necessity of respecting the space inside the aileron where the mechanism should reside.

The shape of the aileron was kept by allowing only vertical movements. The control points on the lower surface were not allowed to move independently from the control points on the upper surface. The displacement of the control points (for all four of them) was limited to two-time the maximum displacement allowed for the control points on the upper surface of the airfoil. This limit was chosen after convergence tests and shape analyses were done, with the aim to avoid the apparition of unrealistic shapes of the aileron. These types of shapes would raise problems during manufacturing or would produce aerodynamic and convergence problems, thus the need to avoid their apparition.

In order to respect the third constraint and avoid the change in the curvature slope, the control points were set at the leading and trailing edge sections of the aileron. The resulted aileron shapes retain the allure of the conventional aileron, a smoother curvature but does not completely eliminate the discontinuity problem discussed in the beginning of section 0.4, as seen in Figure 0.7.

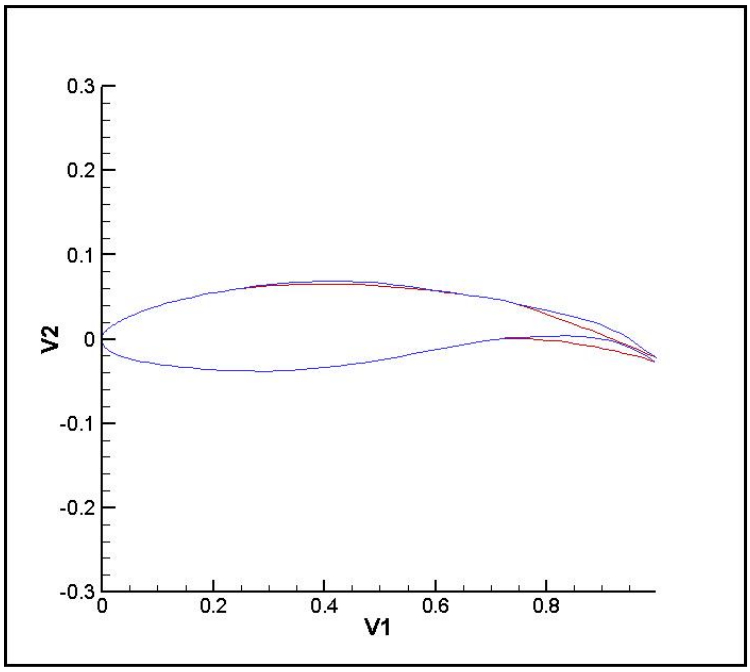

Figure 0.7 Example of a morphed aileron using the 1st method of morphing

Second aileron morphing method

In order to avoid the discontinuity problem mentioned in the beginning of this section, a second method was developed for obtaining any desired deflection angle while preserving the smoothness of the airfoil camber line. The method should also be easy to implement from a manufacturing point of view, since it implied only rotations around specified points, keeping the same basic control principles as for conventional control surfaces.

The aileron camber line has been divided into several chord-wise sections, each defined by a starting and an ending point. The starting point of the first section coincides with the original hinge point, while the ending point of the last section coincided with the tip of the trailing edge. For each point along the camber line two corresponding points on the upper and lower surfaces were defined based on the local thickness of the airfoil section. In addition, for each section we calculate the coordinates of a hinge point so that the rotation of any section with respect to the previous section preserves the continuity of the camber line. Using this method,

the deflection of any chord-wise section, with respect to the section directly upstream of it, preserves both the local thickness of the airfoil and the length of the segment, since rotation does not modify any other geometrical characteristic. If all segments are rotated in the same direction the overall deflection of the aileron, as measured at the trailing edge and using the original hinge point as reference, is simply the sum of all segment rotations, each segment being rotated with reference to the segment immediately upstream of it.

By controlling the number of chord-wise segments, as well as the local rotation angles for each individual segment, we can obtain a great flexibility in the shape changing of the aileron. All these degrees of freedom could be adjusted to match the technological limitations associated to the fabrication process of such an aileron.

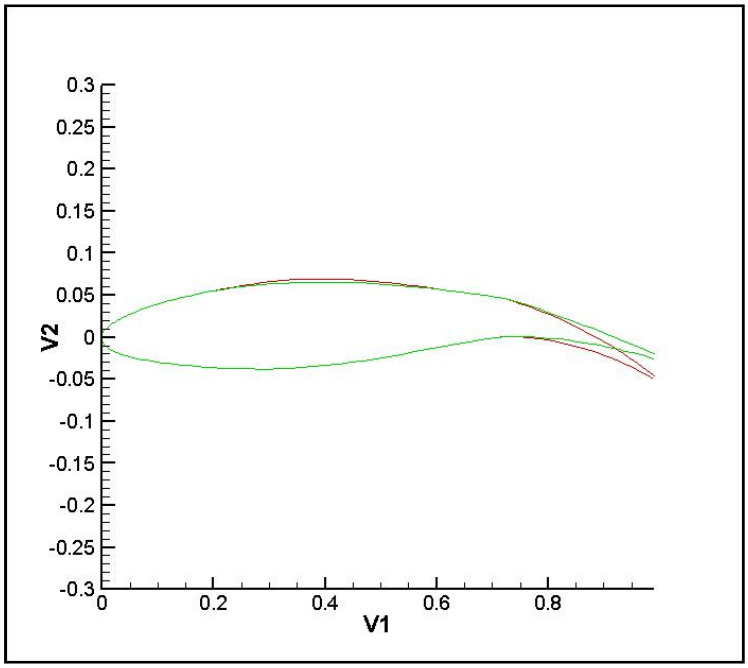

Figure 0.8 Example of a morphed aileron using the 2nd method of morphing

Based on the analysis and decisions of the Italian team that designed and manufactured the aileron, the second method of morphing the aileron was considered as closest to their design

for the morphing aileron and therefore chosen to be used for the wind tunnel cases optimizations.

0.3.6 XFoil aerodynamic solver

XFoil is an open source aerodynamic solver developed by Mark Drela (Drela and Youngren, 2001) that allows it to perform both inviscid and viscous calculations. It also includes the estimation of the boundary layer parameters, including the transition position, and the functions the airfoil geometry modification, such as curvature change and flap deflection.

In *XFoil*, the inviscid calculations are performed using a *linear vorticity stream function panel method.* A *Karman-Tsien compressibility correction* (Drela, 1989b) was added to the Panel Method, and thus allowed it to obtain more accurate predictions in subsonic flow. For the viscous flow calculations, *XFoil* uses a *two-equation lagged dissipation integral boundary layer formulation* (Drela, 1989a) and incorporates the e^N *transition criterion* (Drela, 2003). The flow in the boundary layer and in the wake interacts with the inviscid potential flow by using the *surface transpiration model*.

The *XFoil* code was chosen because of its precision and effectiveness for rapid design and assessment that have proven to be acceptable, and because of the code's rapid convergence. The latter attribute is especially important in an optimization using the genetic algorithm, where a large number of individuals and generations are analyzed simultaneously.

0.3.7 XFLR 5 aerodynamic code

XFLR5 is an analysis tool for airfoils, wings and airplanes operating at low Reynolds numbers (Deperrois, 2015). It includes *XFoil*'s direct and inverse analysis capabilities, as well as wing design and analysis capabilities based on the *Lifting Line Theory* (Sivells and Neely, 1947), the *Vortex Lattice Method* (Katz and Plotkin, 1991) and the *3D Panel Method* (Maskew, 1987).

For the *XFLR5* analysis of a wing, three steps need to be followed:

- Analysis of the airfoil(s) composing the wing using a *multi-threaded batch analysis*, which allows the code to analyse multiple airfoils at a specific speed over a range of Reynolds numbers and angles of attack, by using *XFLR5*'s *XFoil* section;
- Construction of the wing model, based on the airfoil(s) analysed in the previous step. This step requires the number of sections (minimum two: root and tip sections), the span and chord dimensions for each section and, if present, the offset, dihedral and twist angles. Finally, the wing model needs the total number of panels required for the calculations in each direction for each section;
- Analysis of the wing model using one of the following methods: the Lifting Line Theory, the Horse-shoe Vortex Lattice Method, the Ring Vortex Lattice Method or the 3D Panel Method;

The wing model example presented in Figure 0.9 is a representation of the CRIAQ MDO 505 wing demonstrator, and it was created from four sections: sections 1 and 4, representing the root and the tip of the wing model, where the corresponding airfoil is the base airfoil; and sections 2 and 3, which represent the actuator lines along the span length, where the airfoils corresponding to them are the optimized airfoils, which are specific for each studied flight case.

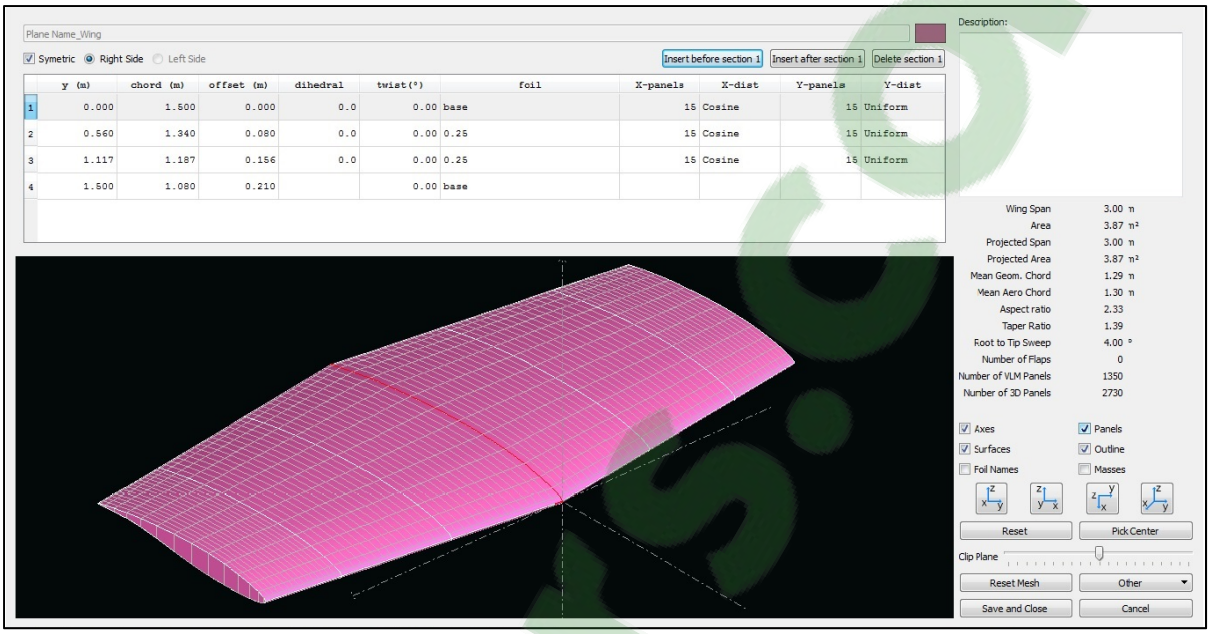

Figure 0.9 Wing modeling in XFLR5 for Mach number of 0.15 and angle of attack of 0.25°

Analyses can be run for a range of speeds up to Mach number of 0.5 (for accuracy purposes) and over a range of global angles of attack using any of the methods incorporated. For the morphing wing research, the *3D Panel Method* was chosen because the other methods were considered as insufficiently accurate for the analysis. The *Lifting Line Method* (LLM) works only for wings with aspect ratio greater than 4, while the CRIAQ MDO 505 wing demonstrator has an aspect ratio of 2.9.

The *Vortex Lattice Method* (VLM) reduces the wing to a middle surface with zero thickness, which eliminates the notions of upper and lower surfaces and gives only the difference between upper and lower surfaces pressure coefficients.

The *3D Panel Method* takes into account the three-dimensional geometry surface, and gives more detailed and accurate results for the studied geometry in comparison with the VLM. The principle of the *3D Panel Method* resides in modelling the perturbation generated by the wing by a sum of doublets and sources distributed over the wing's top and bottom surfaces. The strength of the doublets and sources is calculated to satisfy the appropriate boundary conditions, which may be of the Dirichlet or Neumann type. A comprehensive description of

the principles of such a method is outside the scope of this research. The 3D method implemented in the XFLR5 code is essentially based on the method presented by (Maskew, 1987).

0.3.8 Hypermesh Finite Element Modelling code

The design and development of the *Finite Element Models* (FEM) necessary for the run of aeroelastic studies was done using *Hypermesh* software, which is part of *Hyperworks* software package.

Hypermesh is a multi-disciplinary *FEM* pre-processor which manages the generation of large and complex models from importing the CAD geometry to exporting ready-to-run files.

Hypermesh provides a large database of elements for creating general or detailed *FEMs* from zero dimension (0D) elements, such as mass points, 1D element, such as beams, rods or springs to 2D and 3D elements, such as shells, plates, hexahedral or tetrahedral elements.

The *Finite Element Models* developed during this research were designed using a combination of surface and solid meshing capabilities of *Hypermesh*, which included the abilities to interactively adjust a variety of mesh parameters, create a mesh using a wide range of advanced techniques and optimize a mesh based on a set of user-defined quality criteria, (HyperWorks, 2016). An example of the FEM for the CRIAQ MDO 505 wing is shown in Figure 0.10.

Several refining, correction and manipulation tools provided by *Hypermesh* were used to develop the *FEM*, as well as the interfaces for the most common solvers such as *MSC/Nastran* and *Optistruct.*

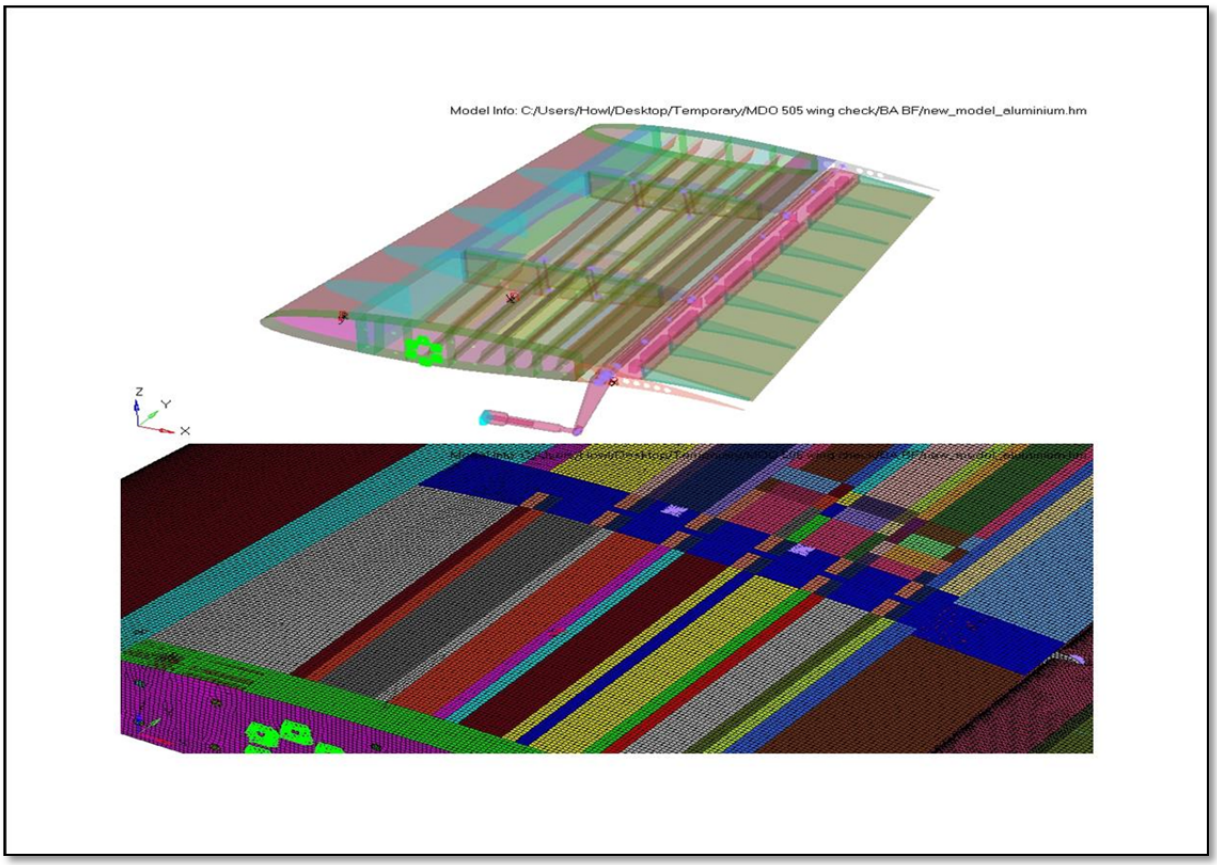

Figure 0.10 The Finite Element Model of the MDO 505 wing – global view and close-up

0.3.9 Optistruct Structural solver

For the preliminary *Normal Modes* analysis of the MDO 505 wing *FEM*, the *Optistruct* solver was used. *Optistruct* is a structural solver, from *Hyperworks* software package, based on finite-element and multi-body dynamics technology.

A *normal mode* of an oscillating system is a pattern of motion in which all parts of the system move sinusoidallly, with the same frequency and a fixed phase relationship. The motion described by the normal modes is called *resonance*. The frequencies of the normal modes of a system are known as *natural frequencies* or *resonant frequencies* (Blevins and Plunkett, 1980). It is important to know these frequencies; if cyclic loads are applied at these frequencies, the structure enters into resonance, which will lead to structural failure. It is also

important to know the modal shapes in order to ensure that loads are not applied at points that will cause the resonance condition. The calculation of these frequencies and vibration shapes is known as *eigenvalues analysis* or *normal modes analysis*.

In *Optistruct*, the normal modes analysis was done using the *Lanczos method*. It has the advantage that the eigenvalues and their associated mode shapes are calculated exactly. This method is efficient for calculations in which the number of modes is small and the full shape of each mode is required. Its disadvantage lies in the large amount of calculation time, for example the problem may have millions of degrees of freedom for which hundreds of modes are required.

A short mathematical description of the way in which the normal modes are calculated in a general form is presented below.

The equilibrium equation for a structure performing free vibrations appears under the form of the eigenvalue problem:

$$[K - \lambda M]\{x\} = 0. \tag{0.7}$$

where K and M are the stiffness and mass matrices, respectively. The damping matrix is neglected. The solution of the system is given by the eigenvalues λ_n, where n is the number of degrees of freedom. A space of vector $\Phi(i)$ is defined as the eigenvectors corresponding to the eigenvalues. Finally, the natural frequency f_i is calculated directly from the eigenvalue λ_i.

$$f_i = \frac{\sqrt{\lambda_i}}{2\pi} \tag{0.8}$$

0.3.10 MSC/Patran Finite Element Modelling code

The pre-processing of the *FE* model, after its transfer from *Hypermesh,* was done using the *MSC/Patran* software.

MSC/Patran is one of the most widely used pre/post-processing software for *Finite Element Analysis* (FEA), and provides solid modeling, meshing, analysis setup and post-processing for multiple solvers including *MSC/Nastran*, *Marc*, *Abaqus*, *LS-DYNA*, *ANSYS*, and *Pam-Crash* (Patran/Nastran, 2016).

MSC/Patran was used for correcting the *FEM* transfer errors. The multi and single constraint points that were lost during transfer from *Hypermesh* were redefined; nodes and elements were renumbered in preparation of the model for the aeroelastic analysis pre-processing with the *MSC/Flight Loads and Dynamics*.

0.3.11 MSC/Flight Loads and Dynamics Solutions solver

'*MSC/Flight Loads and Dynamics*' provides the ability to start with either a native *CAD* geometry or a *Finite Element Model,* and to define an aeroelastic environment using coupled structural and aerodynamic models. This code facilitates the definition and evaluation of the appropriate rigid aerodynamic pressure distributions and aeroelastic influence coefficients to generate the external loads on the vehicle (Patran/Nastran, 2016).

Each major step in aeroelastic modeling and analysis is supported through unique modules. These main modules include:

- Aero Modeling
- Aeroelasticity.

Aero Modelling Module

The basic aerodynamic modeling capabilities include the definition of aerodynamic lifting surfaces, bodies, components (collections of surfaces and bodies) and control surfaces. Modeling error detection is implemented to provide on-the-spot corrections so aerodynamic models adhere to *MSC/NASTRAN* rules. Multiple aerodynamic mesh representations are described through the use of *SuperGroups*. Each *SuperGroup* represents a complete aerodynamic model. For aeroelastic analysis, a *SuperGroup* must be selected and coupled to a structural model. Extensive tools are provided to manage the individual aerodynamic groups (surfaces and bodies), and the *SuperGroups*. These SuperGroups are located under *Model Management* in the *Aero Modeling Module*.

Aeroelasticity Module

The aeroelastic features of *MSC/Flight Loads and Dynamics* couples the aerodynamic and structural data to perform aeroelastic response analyses. The *Aeroelasticity* user interface module supports static aeroelastic analyses for flexible trim, rigid trim, the computation of flexible increments, and the dynamic aeroelastic analysis for flutter phenomena.

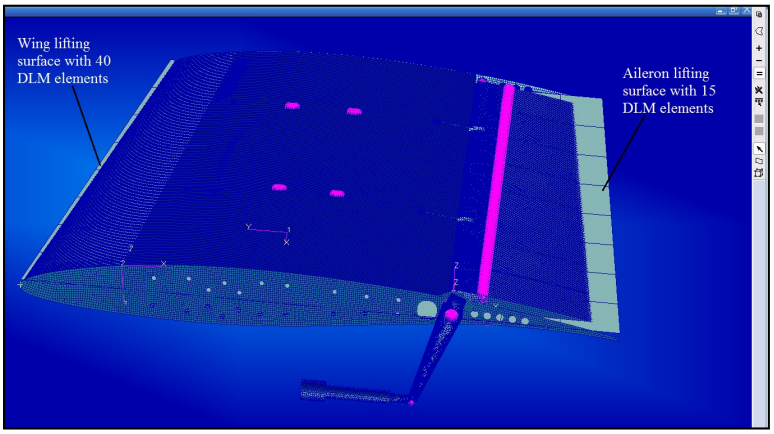

Figure 0.11 The CRIAQ MDO 505 wing model ready for starting the flutter analysis

The *FLDS* software is the final step before performing aeroelastic analysis using MSC/Nastran

0.3.12 MSC/Nastran solver

The aeroelastic flutter analysis of the CRIAQ MDO 50 wing demonstrator finite element models with and without composite upper surface was done using the MSC/Nastran solver.

MSC/Nastran is a multidisciplinary structural analysis application used to perform static, dynamic, and thermal analyses across the linear and nonlinear domains, complemented with automated structural optimization and embedded fatigue analysis technologies.

The MSC/Nastran Aeroelasticity product modules enable the analysis of structural performance in the presence of an air stream for the cost-effective design of airplanes, helicopters, missiles, suspension bridges, as well as tall chimneys, exhaust stacks, power lines, and other structures exposed to aerodynamic loads (Patran/Nastran, 2016).

Industry standard methods such as the *p-k* analysis, the *k*-method and their derivative algorithms provide a comprehensive set of tools to model flutter behavior of damped, linear systems including flutter analysis methods applicable across a range of Mach numbers:

- K, KE, PK.
- *PKS* (K-Range Sweep).
- *PKNL* (No Looping).
- *PKNLS* (No Looping, K-Range Sweep).

During the flutter studies conducted for the CRIAQ MDO 505 wing demonstrator the *PK* method was used for calculating the displacements and frequencies for a range of speeds.

This method was chosen due to its pertinence in the results it offers, especially at low speeds regimes, where the test speeds selected for the IAR-NRC wind tunnel testing were also

considered (Baxevanou et al., 2008), (van Zyl and Maserumule, 2001). The test speeds considered for the aeroelastic analysis were up to 120 m/s, where the maximum speed of the IAR_NRC wind tunnel is 113 m/s, and the maximum speed used during tests was 85 m/s.

The fundamental equation describing the *PK* method is given by equation (0.9):

$$\left[\frac{V^2}{L^2}Mp^2 + K - \frac{1}{2}\rho V^2 Q(ik)\right]\{q\} = 0. \tag{0.9}$$

For simplification purposes, equation (0.9) excludes the structural damping matrix *C*. *M* and *K* represent the mass and stiffness matrixes, *V* is the speed and *Q(ik)* the vector of external forces. In equation (0.9), *p* is the Laplace non-dimensional parameter that is defined by equation (0.10):

$$p = g + ik \tag{0.10}$$

$$g = \gamma k \tag{0.11}$$

where *g* represents the damping coefficient, calculated using the reduced frequency *k* and an under-relaxation coefficient γ, as shown in equation (0.11).

The *PK* equation was modified by adding an aerodynamic damping matrix to it (Rodden and Bellinger, 1982), thus in *MSC/Nastran* solver, the *PK* equation is expressed as shown in equation (0.12):

$$\left[\frac{V^2}{L^2}Mp^2 + k - \frac{1}{2}\rho V^2\frac{Q^I}{K}p - \frac{1}{2}\rho V^2\frac{Q^R}{K}\right]\{q\} = 0. \tag{0.12}$$

Where Q^I and Q^R are the imaginary and real parts of the force matrix Q(ik). Equation (0.12) can also be expressed in the following state space formulation:

$$[A - pI]\{q\} = 0. \tag{0.13}$$

where p represents the specter of all eigenvalues. Its solution is expressed by the eigenvalues of matrix A:

$$A = \begin{bmatrix} 0 & 1 \\ -M^{-1}\left[k - \frac{1}{2}\rho V^2 \frac{Q^R}{K}\right] & -M^{-1}\left[-\frac{1}{2}\rho V^2 \frac{Q^I}{K}\right] \end{bmatrix} \tag{0.14}$$

where A and q, from equations (0.13) and (0.14), include the speeds and modal displacements. For this nonlinear system, the solution is found through an iterative process.

CHAPTER 1

LITERATURE REVIEW

From the moment it was discovered that heavier-than-air machines can fly, a challenging race started for finding the most performing aircrafts in terms of aerodynamic, structure, power and control efficiency. For this purpose, thousands of aircraft concepts were developed and tested, concepts of the most variable design possible; subsonic, transonic, supersonic or hypersonic aircrafts, all have their specific characteristics, and inside each category, several designs are available to accomplish the most various flight envelopes. But, with such a diversity of aircrafts, comes the challenge: how many aircrafts can be sent for a flight mission where perhaps several manoeuvres overlap and a single aircraft cannot perform them all? Therein lays the answer, researching and developing aircrafts that were capable of adapting to their mission profiles, even if that mission changes during flight. The solution, in the beginning, was to research for an aircraft with fixed configuration capable of doing all types of missions, but the aerodynamic, structural, power and control characteristics needed for different kinds of manoeuvres are most of the times in contradiction: e.g. the configurations that were found to work best for subsonic flights were not sufficiently performing in transonic flight and even less in supersonic or hypersonic conditions or high manoeuvrability during high speed flights was not compatible with high stability during low speed flights; therefore the idea of a single configuration aircraft capable of managing a multitude of flight missions seemed impossible, until the concept of morphing took flight.

1.1 Morphing Aircrafts

The concept of morphing does not have a stable definition, other than it refers to modifications of shapes - multi-purpose or stand-alone - for the purpose of improving the performances of the object to be morphed. The Defense Advanced Research Projects Agency or DARPA attempts to offer a definition for morphing by which researchers can be guided. According to DRAPA (McGowan et al., 2002), a morphing aircraft is one that:

- Changes its state substantially to adapt to changing mission environments;
- Provides superior system capability not possible without reconfiguration;
- Uses a design that integrates innovative combinations of advanced materials, actuators, flow controllers, and mechanisms to achieve the state change.

For most aircrafts, morphing usually applies to wings, high-lift devices such as ailerons and flaps and more rarely for tails (Nir and Abramovich, 2010), (Good, 2004) or helicopter blades (Kota, Hetrick and Osborn Jr, 2006). But morphing is not limited to these devices, it can also be present at engine level, for example in altering the engine outlet nozzle positions and geometry to achieve thrust vectoring as seen on the Harrier, Eurofighter and Joint Strike Fighter or on the rotation of the entire engine as in the V-22 Osprey.

Since the research developed in the present thesis pertains to the aspect of morphing wings and trailing edges, in this chapter only a review of morphing concepts applied to wing and wing components is addressed.

1.1.1 Morphing Wings

Historically, many concepts were developed as the idea of morphing by varying the wing component of an aircraft appeared in the first decades after the Second World War, as the first supersonic aircrafts were developed. An example is the variation in sweep angle for the Messerschmidtt P1101 (on ground) or for the Bell X-5 (in flight) in 1951. Other aircrafts were equipped with morphing wings to increase their performances in either sub- or supersonic flights: e.g. MiG-23 in 1967, Grumman F14 Tomcat in 1970 and the Rockwell B1-B Lancer 1983.

Wing morphing can be classified as function of the type of modification produced and the level of component at which it is produced. There is planform morphing characterised by changes in span, chord or sweep dimensions, out-of-plane morphing such as changes in twist or dihedral angles and airfoil morphing, which refers to the modification of the camber or

thickness of the airfoil component of the wing, although there is no consensus on whether camber morphing is airfoil morphing or out-of-plane wing morphing and most authors consider it both.

1.1.1.1 Planform Wing Morphing

As mentioned above, in-plane or planform morphing of the wing refers to changes in the structure of the wing that lead to modifications of the span, chord or sweep angle. In a NASA study for a NextGen-type of morphing aircraft, the wing was capable of increasing its root chord dimension and changed its sweep angle value in function of the mission leg proposed: take-off, ascent, cruise, loitering, dash, etc. Practically the wing shape was optimized as function of the behaviour desired for a specific mission leg; e.g if take-off was considered then an increase of the root chord would lead to an increase in the wing's area which would lead to an increase in the lift force needed for the aircraft to take-off (Skillen and Crossley, 2008).

For span length modification two main designs were used: a first design was based on telescopic structures for dramatic changes in span length and the second design was based on scissor like mechanism for the wing box.

A wing was designed that was capable of changing its span with 38% more than its original length by using a telescopic pneumatic actuator made of thin-walled stainless steel cylinder and a carbon steel rod. Wind tunnel tests showed that the change in span length had an important impact on the wing performances by allowing a low drag to be maintained for a range of lift coefficients (Neal et al., 2004).

A reconfigurable wing box was developed using a four-bar mechanism with rigid links and with which the optimal location of a distributed network of actuators within the scissor wing box mechanism was studied (Joo et al., 2006).

A scissor-like mechanism was designed and manufactured to alter the wing's span and sweep angle. This prototype, when tested, achieved a 55% span change using a spooling screw actuated by a DC motor (Bharti et al., 2007).

For chord changes along the span, an interpenetrating rib mechanism actuated by means of miniature DC motors and lead screws was designed and manufactured by (Reed Jr et al., 2005). Partial rib structures that could slide through a central slotted box and alter the chord wise position of the leading and trailing edges were used. The mechanism design allowed the camber bending due to aerodynamic loads to be supported by the ribs. The smooth operation of the lead and screw mechanism under transversal aerodynamic loads was studied. Other challenges were encountered for maintaining the chord wise bending stiffness. The mechanism had its disadvantages as well, the main being its weight and complexity, for which more optimization research was needed.

1.1.1.2 Out-of-Plane Wing Morphing

Dihedral angle change and change in gull configuration of the wing was also considered by researchers for shape morphing of aircraft. In gull designs, the wing was divided into two hinged segments that rotate with respect to each other and at the wing root. The most innovative was, perhaps, Lockheed Martin's folding wing concept, which included a variation in span and sweep for the wing. For this concept, shape-memory polymer that softens and morphs was used to create the skin material. The polymer was heated using small, flexible heaters embedded in the material. The advantage of this concept was that after the morphing action stopped, the shape was fixed without necessitating further heat input, until the next command was given, thus giving the wing the capability to maintain its smooth shape under high strains (Love et al., 2007).

Another innovative concept was the 'belt-rib' concept for compliant structures. The belt-rib frame was consisted of a closed shell (belt) reinforced by in-plane stiffeners (spokes). The stiffeners were then connected to the belt by means of flexible hinges, which provided

rotational freedom at the joints. An internal actuator system consisted of Bowden cables and a spindle mechanism deformed a prototype carrying a 335 kg distributed load (Campanile and Sachau, 2000).

In the DARPA Smart Wing program, shape memory alloys were studied as candidates for actuating materials for their out-of-plane wing morphing concept. In this concept, two SMA linear actuators were connected to the tip of a flexible trailing edge. The other ends were connected to the top and bottom of the trailing edge spar in extended position. By contracting the actuators, the trailing edge was bent and its shape morphed. The ability of the actuator to displace the trailing edge tip was reduced because of wasting of the shape memory recovery force due to the undesired in-plane compression of the center sheet; therefore the gained deformations were not satisfactory for the desired objective (Wang et al., 2001).

A wing that consisted of an elastic wing box structure (ABS plastic material), which was covered with an elastomeric skin, was studied (Majji and Junkins, 2006). This concept showed that, by twisting the wing, the angle of attack envelope of the twisted wing has increased. The design was based on rigidly coupling the wing box to four concentric tubes, which were independently attached to the wing at four locations along the span. The outer tubes passed through the inner ones and were connected to servomotors at the wing root. The wing was twisted by the arbitrary rotation of the tubes.

1.1.1.3 Airfoil Morphing

Airfoil morphing refers to the modification produced in the camber of the airfoil for local wing morphing or in the thickness of the airfoil to improve the boundary layer behaviour during flight.

There are many ways in which airfoil morphing can be achieved: inflating devices, smart materials, piezoelectric and electric actuators, etc. Several concepts implemented by various research projects are described below.

In the DARPA Smart Wing program, shape memory alloys were studied as candidates for actuating materials for their out-of-plane wing morphing concept. In this concept, two SMA linear actuators were connected to the tip of a flexible trailing edge. The other ends were connected to the top and bottom of the trailing edge spar in extended position. By contracting the actuators, the trailing edge was bent and its shape morphed. The ability of the actuator to displace the trailing edge tip was reduced because of wasting of the shape memory recovery force due to the undesired in-plane compression of the center sheet; therefore the gained deformations were not satisfactory for the desired objective (Wang et al., 2001).

Various concepts for deforming the airfoil shape by using bi-stable laminate structures were studied (Diaconu, Weaver and Mattioni, 2008). The objective was to identify geometries and lay-ups of candidate configurations that offer multiple stable shapes for the airfoil section. Three concepts that focused on morphing a flap-like structure, the camber and the chord of an airfoil section were proposed. Several geometries and laminate configurations were investigated and analysed. Carbon-fiber laminated composites with non-symmetric laminate configurations were used for morphing the airfoil section.

Inflatable wings have been in existence for decades and have found application in manned aircraft and unmanned aircraft vehicles UAVs. Recent system design challenges have given advances in the areas of materials, manufacturing, and configuration. These advances have given inflatable wing technologies a practical form for near term application. Inflatable wings can be packed into volumes tens of times smaller than their deployed volume without damaging the structural integrity of the wing. Deployment can occur on the ground or in flight in less than one second depending on the size of the wing and the type of inflation system used. The efforts needed in morphing the inflatable wing to provide roll control through wing warping were studied (Cadogan et al., 2004). Several approaches were developed that lend themselves to camber control via locally altering the geometry of the wing. Apart from use as a stand-alone aerodynamic surface on a small UAV, the inflatable assemblies could be used as an aspect ratio increasing device on a larger aircraft, enabling a more radical change in the wing configuration. This approach serves to improve system

efficiencies across flight regimes changes, allowing aircrafts to transition from high speed target approach to low speed loitering.

The possibility of using variable length trusses to reshape an airfoil was investigated (Austin et al., 1994). Linear displacement actuators were attached inside the wing section in a diagonal manner. The airfoil shape modification occurred by expansion or contraction of these actuators. A model of an adaptive rib with 14 mechanical ball-screw actuators was constructed to demonstrate the shape control concept. A theoretical model was developed, and validated, which was implemented to determine the optimal airfoil shape for various flight conditions.

Another concept that made use of SMA springs was developed, where the SMA springs were implemented between the wing skin and its supporting wing-box (Dong, Boming and Jun, 2008). In this design, the wing-box consisted of rigid steel ribs and spars. The covering skin was allowed to slide over a cushion at the leading edge spar. By controlling the temperature, the length of the SMA spring was controlled, which in turn changed the airfoil thickness.

A morphing wing concept where SMA linear actuators were connected to a flexible skin through a cam based transmission system was investigated (Coutu et al., 2007). Contraction of the SMA wire upon heating rotated the cam and transferred the displacement of the SMA wire to a flexible skin by means of a crank. A prototype of an actuated wing was manufactured and the performance properties of SMA actuators were studied during bench test experiments.

An adaptive wing for a small unmanned aircraft (UAV), entirely actuated by shape memory alloy devices was developed (Icardi and Ferrero, 2009). This wing concept consisted of a sandwich box sub-structure with laminated faces, flexible ribs and a flexible skin. The optimization of the shape was carried at airfoil level with local wing shape adjustments. For the camber morphing of the wing counter rotating, concentric torsion SMA tubes were used, while for the local adjustments levers powered by SMA wires were installed. The direction

of the morphing, for upward or downward motions, was controlled by external and internal tubes. The tubes were connected to the flexible ribs through an electro-mechanical clutch and a positioning piezoelectric motor. By limiting the deformation to 4% of the original shape, small stresses and a smooth wing shape were achieved. The design was capable of obtaining trailing edge deformations corresponding to 30° of a conventional aileron or flap. A variation in camber of at least 10° from root to tip, an increase of the airfoil chord by 4.5% at 55% of the chord, coupled with a reduction of the airfoil thickness by 3.9% at 40% of the chord, were also observed.

Other information on the state of the art in conceptual design, prototype fabrication, and evaluation of shape morphing wing, as well as more details on some of the concepts already presented, can be found (Sofla et al., 2010). In their review, concepts that included smart materials such as shape memory alloys (SMA), piezoelectric actuators (PZT), and shape memory polymers (SMP) were considered of special interest.

The morphing wings were studied from three different perspectives, by questions related to what to morph, why morph and how to morph (Vasista, Tong and Wong, 2012). Therefore, an integrated approach for the overview of the morphing field was used and the focus was given to morphing of conventional fixed-wing aircraft, and to their structural system in particular.

Although many morphing aircraft concepts have been elaborated, only few concepts dealt with the problems related to the design and manufacturing of a smooth and continuous skin that simultaneously deforms and carries loads (Thill et al., 2008). Therefore, the concepts presented in this review of morphing wings designs have focused on those structures where primary loads were transmitted in the span wise direction, and a morphing function was achieved via chord wise flexibility.

1.1.2 Morphing Trailing Edge

Trailing edge morphing represents modifications such as aileron or flaps morphing. Most of the projects in which morphing trailing edges were developed, as stand-alone projects or as part of wing and aileron system, were focused on camber modification.

The modification of the camber line of an airfoil, whether for trailing edge or for wing, was particularly effective for improvement of the lift performances. For the trailing edge devices, achieving a smoother slope when they are deflected represented a benefit for the behaviour of the boundary layer Therefore, many concepts were designed and prototypes were further developed to achieve this type of morphing.

An aerodynamic optimization for a wing equipped with a morphing trailing edge system was (Lyu and Martins, 2014). The computations were performed with a high-fidelity computational fluid dynamics solver, coupled with an optimization routine. The wing base geometry was designed with a multipoint approach, while the optimal shape of the morphing trailing edge was determined for each different flight condition. Drag reduction of 1% for the on-design conditions, and of over 5% for the off-design conditions were obtained, with respect to the base multipoint optimized wing.

In the ADIF Adaptive Wing project, carried out by EADS (European Aeronautic Defence and Space Company), Daimler and DLR (German Aerospace Research Center), a compliant structure wing was developed (Monner, Hanselka and Breitbach, 1998). This structure was able to redistribute external aerodynamic forces, so that it could be morphed in certain predetermined areas, while it remained rigid to deformations in other areas. The trailing edge part of the wing was composed of a flexible structure made of several rigid plate elements connected with a cinematic type mechanism. Each rib was actuated at a single, predetermined point. The desired rotation was transferred to the other plates of the rib via the cinematic mechanism in order to obtain the desired wing shape.

The applicability of a finger-like configuration for shape changing high lift devices was applied on a regional aircraft (Pecora et al., 2013). Their aeroelastic studies have shown definite improvement in the behaviour of the wing when fitted with a morphing flap. They also have successfully demonstrated the capabilities of a high lift device prototype (Pecora et al., 2011).

Three cases of design and application of compliant mechanisms for morphing aircraft structures were studied (Kota et al., 2003). The first case refered to a variable geometry leading edge flap, with the aim to challenge compliant mechanism technology to create a camber morphing design for maintaining structural integrity under sever loads. These types of wing loadings are most commonly encountered by modern fighter aircrafts. The second case presented a trailing edge flap with variable geometry. The purpose of this design was to create a seamless, hinge-less flap that could change the wing camber and minimize drag over a wide range of lift values. For a conventional flap, such a demand would produce flow separation and increased drag. A wind tunnel prototype was developed and tested for this concept, and the results validated the expectations. The third design was developed for high-frequency vortex generators and the purpose was to design and demonstrate a mechanical control device that could achieve flow separation control characteristics competitive with other systems already developed.

1.2 Morphing Wing Objectives

The morphing projects presented in section 1.1 treated the ‘what’ and ‘how’ aspects of morphing, but there is another aspect just as important and which can determine the answer to the other two questions: ‘why’ to morph an aircraft.

There are many reasons why morphing represents an advantage for aviation. As mentioned in the Introduction of the present thesis, a morphing aircraft would be capable of extending its flight envelope for missions for which it was not originally designed, but what does this mean in more detail? The answer is, that, individually or as a combination, the structural,

aerodynamic and control performances of the aircraft would be improved. The reasons for which morphing would be adopted, are mostly related to aerodynamic performances: increase of lift, minimisation of drag, control of the shockwaves in transonic or supersonic flight, and other optimization objectives of certain aerodynamic or aeroelastic characteristics: transition, friction coefficient, angle of attack, aileron or flap deflection, speed, frequency of vibration, etc.

The possible benefits of conformal trailing edges versus conventional ones were investigated (Sanders, Eastep and Forster, 2003). It has been discovered that the conformal trailing edge showed an increase in lift and pitching moment with respect to conventional trailing edges. It has also been observed that the maximum roll rate was greater and the reversal dynamic pressure was lower for a wing with conformal control surfaces than for wings with conventional control surfaces. The conclusion of the authors was that wings with conformal control surfaces presented some distinct aerodynamic benefits when compared with wings equipped with conventional control surfaces. The concept of conformal control surface could work well for take-off or landing configurations.

Research on developing an integrated systematic approach to design compliant structures to carry out required shape changes under distributed pressure loads was conducted (Shili, Wenjie and Shujun, 2008). A structural analysis solver, ANSYS, was coupled with a genetic optimization routine from MATLAB, and using air loads, input displacements and geometric nonlinearities, the compliant structure had successfully changed its shape from 0° to 9°.

The modifications that occur in the boundary layer when an airfoil/wing morphs was investigated (Sainmont et al., 2009). The objective was to reduce aerodynamic drag through laminar-turbulent transition location delay to promote a large laminar region on the wing's surface. Two optimization approaches were used to obtain the new airfoil shapes. Firstly, a classical approach used mathematical functions to model the morphing of the flexible skin parts of the airfoil. Then, a multidisciplinary approach integrated the finite element model of the adaptable wing structure into the aerodynamic optimization. This combination of classic

and multidisciplinary approach permitted to avoid the task of reconstructing the airfoil geometry. The numerical and experimental results have shown a delay of the transition region of up to 30% of the chord and a minimization of the airfoil drag of up to 22%.

Another project focused on the optimization of the laminar flow for a wing was developed (Pagès, Trifu and Paraschivoiu, 2007). The effect that morphing a large surface of an airfoil has on the behaviour of the flow was studied. Aerodynamic optimization coupled with genetic algorithm Genial V1.1 and XFOIL code was used to determine the best airfoil shapes for a range of speeds, Reynolds numbers and angles of attack. Using the optimization technique applied to a laminar airfoil, the transition point was moved backward by up to 10% of the chord and the friction drag was reduced by up to 9%.

The aeroelastic control of a wing using impeded piezoelectric actuators was improved (Rocha, Moniz and Suleman, 2007). Both the numerical and experimental testing proved that the active wing exhibited significant aeroelastic control with respect to the corresponding passive wing. Optimization methods were applied for morphing the shape of the wing.

1.3 Optimization Methods Applied to Morphing Wings

For all the morphing concepts presented above, one or more new shapes were required for each of the objectives pursued. To obtain these shapes, while taking into account compromises between structures, aerodynamic, control and constraints imposed by the desired or actual performance, various optimization methods were employed. Some optimization methods were derived from pure mathematical methods, while others were inspired from the natural world. The following paragraphs present some the optimization methods employed for solving morphing problems for aircraft wings.

The use of the Newton-Krylov Algorithm for aerodynamic shape optimization for an adaptive airfoil concept for drag reduction at transonic speeds was investigated (Zingg, Diosady and Billing, 2006). The objective was to quantify the improvements in drag that

could be achieved and the magnitudes of the shape changes needed. Firstly, a base airfoil was optimized for multiple flight points – range of speeds at a fixed lift. The comparison between the optimization results and a series of airfoils considered optimal for a single operating point showed that for shape changes occurring for less than 2% of the chord, the drag was reduced with up to 4-6%. For changes of the upper surface only, occurring for less than 1% of the chord, the drag was reduced by up to 3-5%.

The optimization of an active upper surface structure using genetic algorithm was studied, with the aim to create a database of possible shapes (Coutu, Brailovski and Terriault, 2010). The ANSYS code was used to model the finite element model of the flexible skin concept for optimization and structural analysis. By using the number of plies in the composite laminate and the number of actuators as design parameters and by adding aerodynamic and mechanical performance criteria, a multi-objective optimization analysis was performed that showed that a 4-ply 2 actuator configuration was best for the adaptive upper surface structure of the morphing concept.

The use of evolutionary algorithms for the optimization of aeroelastic composite structures was studied (Manan et al., 2010). Four biologically inspired optimization algorithms were used. The chosen algorithms were: binary genetic algorithm, continuous genetic algorithm, particle swarm optimization and ant colony optimization. Also a meta-modelling approach for the same problem set was implemented. The analysis has shown that the type of optimization method did not matter for improving the flutter speed as all have obtained similar results. It has been observed that the continuous methods gave slightly better results that the discrete ones.

The Direct Numerical Optimization (DNO) methodology for airfoil optimization was investigated and the method used PARSEC shape function for the airfoil geometry parameterisation (Khurana, 2008). For higher convergence rate, it was coupled with a low-fidelity solver and Particle Swarm Optimization. For the single point optimization of the airfoil an Artificial Neural Networks (ANN) was added to address the problem of

computational demand. It was found that a hybrid method PSO/ANN gave the best results both in terms of optimized shapes and computation and that it also was applicable for multi-point optimization.

Research on how to balance the goal for performance optimization over a range of on-design operating conditions with the need to meet design constraints at various off-design operation conditions was studied (Buckley, Zhou and Zingg, 2010). This type of problem was studied as a multi-point optimization problem, where the off-design and the on-design operating conditions were represented as design points with corresponding objective/constraints functions. Two methods were presented. The first method was an unconstrained optimization algorithm where the optimal design was achieved by minimizing a weighted sum of the objective function at each of the operating conditions. The second method used the constrained optimization algorithm SNOPT, which allowed the aerodynamic constraints imposed at the off-design operating conditions to be treated explicitly. Both methods were applied to the design of an airfoil for which the problem was formulated as an 18-point multi-point optimization.

1.4 Multi-Disciplinary Optimization

In this section, attention is given to the multi-disciplinary optimization, as the research proposed in this thesis is related to it. Many projects related to morphing wings focus either on how to structurally obtain a morphing configuration or what kind of aerodynamic or aeroelastic performances can be obtained using the morphing concepts. The subject of morphing wings is primarily a multi-disciplinary effort where various disciplines interact and compromise to obtain a new structural wing configuration that would be more performing than the original one. The projects presented in the next paragraphs describe multi-disciplinary procedures and results for morphing wings related to optimization achievements of aeroelastic or aerodynamic objectives.

An integrated multidisciplinary procedure for structural and aeroelastic optimization of composite wings was developed (Jha and Chattopadhyay, 1999). The objective of this optimization was to minimize wing structural weight with constraints on flutter/divergence speed and stresses at wing root due to the static loads. For the structural analysis of the wing box, the wing was modeled as a composite box beam, which represented the load carrying element of the wing, and analysed it using refined higher-order theory. The unsteady aerodynamic analysis was performed using a panel code based on constant pressure lifting surface method. The Laplace domain method using rotational function approximation for unsteady aerodynamic loads was used to compute the flutter/divergence dynamic pressure. To efficiently integrate the objective function and the constraints into a single enveloping function, a Kreisselmeier-Stteinhauser approach was used. The resulted unconstrained problem was solved using Davidon-Fletcher-Powell algorithm. The numerical results have shown significant improvements of the wing after optimization, compared to the reference design.

A multi-disciplinary optimization procedure for delaying the occurrence of store-induced flutter of an aircraft wing/tip store configuration was investigated (Janardhan and Grandhi, 2004). Automated Structural Optimization System and Computational Aeroelasticity Program – Transonic Small Disturbance were the computational tools employed to perform the structural optimization and subsequent aeroelastic analysis in the transonic regime. The results have shown that an improved store-induced flutter speed was obtained by increasing the separation between the first two natural frequencies of the wing structure.

A multi-disciplinary project which was focused on aerodynamic optimization was the CRIAQ 7.1 project which took place between 2006 and 2009 and was realized following a collaboration between teams from École de Technologie Supérieure (ÉTS), École Polytechnique de Montréal, Bombardier Aerospace, Thales Canada and the Institute for Aerospace Research-Canadian National Research Center (IAR-CNRC). The main objective of the project was to improve and control the laminarity of the flow past a morphing wing, in order to obtain important drag reductions (Botez, Molaret and Laurendeau, 2007). The two-

dimensional wing was designed considering and modifying the WTEA Natural Laminar Flow airfoil. The morphing wing active structure was composed of three main subsystems: 1) a flexible, composite material upper surface, stretching between 3% and 70% of the airfoil chord; 2) a rigid inner surface; 3) a Shape Memory Alloy (SMA) actuator group located inside the wing box, which would morph the flexible skin at two points, located at 25.3% and 47.6% of the chord (Brailovski et al., 2008). Numerical optimizations were performed on the airfoil prior to model manufacturing(Pagès, Trifu and Paraschivoiu, 2007), and promising results were obtained: the morphing system was able to delay the transition location downstream by up to 30% of the chord, and to reduce the airfoil drag by up to 22%. For each different flight condition, the optimal displacements for the SMA actuators, which were determined through the numerical optimization procedure, were provided using two different control approaches. In the open loop configuration, the desired displacements were directly imposed on the system (Popov et al., 2010b), while in the closed loop configuration, the displacements were automatically determined as function of the pressure readings from the wing upper surface (Popov et al., 2010a). The wind tunnel tests were performed in the 2 m by 3 m atmospheric closed circuit subsonic wind tunnel at IAR-NRC and validated the numerical wing optimisations (Sainmont et al., 2009) and designed control techniques (Grigorie, Botez and Popov, 2012).

CHAPTER 2

RESEARCH APPROACH AND THESIS ORGANIZATION

The research presented in the current thesis concerned the development of an optimization procedure for aerodynamic performances improvement, aeroelastic analysis and experimental aerodynamic validation of a wing tip equipped with aileron system. The research work was performed in several phases:

- Statement of the problem and design of the morphing wing upper surface and aileron concept;
- Development and validation of tools needed for the analysis;
- Two-dimensional shape optimization performed on the ATR-42 wing airfoil;
- Two-dimensional shape optimization performed on the CRIAQ MDO 505 wing airfoil;
- Two-dimensional shape optimization performed on the CRIAQ MDO 505 aileron;
- Three-dimensional optimization and high-fidelity analysis of the CRIAQ MDO 505 wing equipped with either conventional or morphing aileron;
- Aeroelastic flutter analysis of the CRIAQ MDO 505 wing;
- Experimental wind tunnel testing of the ATR-42 rigid wing models – one model with unmorphed airfoil shape and one model with optimized airfoil shape;
- Validation of the numerical predictions for the ATR-42 'Morphing Wing' project;
- Experimental wind tunnel testing of the CRIAQ MDO 505 morphing wing;
- Validation of the numerical predictions for the CRIAQ MDO 505 project.

The phases presented above were required for the development, understanding and successful achievement of the desired objectives and provide further knowledge on the performances, application range of the morphing wing concept.

2.1 Thesis Research Approach

The technology of morphing wings represents the breakthrough solution that aerospace engineers need for developing more performing aircrafts with less compromise on the aerodynamic and structural design.

A recurring objective for morphing wings is the possibility of reducing the drag of the aircraft at each flight condition with the aim of reducing the fuel consumption. Drag reduction can be achieved by manipulating the behaviour of the flow in the boundary layer region by extending the laminar region, and by contracting the turbulent region of the boundary layer as much as possible. For a given Reynolds number value, laminar flow exhibits less viscous friction than a turbulent flow, and thus generates lower drag per unit of surface. Modifications of the transition between the laminar and turbulent regions of the boundary layer is made by modifying the pressure distribution on the wing's surface so that the recompression occurring after the leading edge suction peak would be gradual, and the adverse pressure gradient would become less strong.

Another objective of morphing wings was the improvement of the high-lift devices performance through the use of morphing trailing edges such as ailerons and flaps. The smooth change in camber that is usually used for morphing trailing edge devices affects the pressure distribution over the wing at the trailing edge area by making the peak of the adverse pressure gradient due to changing of deflection less strong, thus minimizing the possibility of boundary layer detachment.

2.1.1 The ATR-42 'Morphing Wing' Project

The ATR-42 morphing wing is an ongoing LARCASE internal project that started two years after the end of the CRIAQ 7.1 project. The purpose of the ATR-42 morphing wing project was the development of the necessary 'know how' for the CRIAQ MDO 505 project that started one year later. The project provided the necessary framework for developing

optimization, aerodynamic, composite and control skills that represented the basis for the work done during the CRIAQ MDO 505 project.

The ATR-42 morphing wing continued the idea of research on morphing upper surface from the CRIAQ 7.1 project. Because of the collaboration on this project with an Italian team specialized on the ATR-42, the subsonic airfoil of the ATR-42 wing was selected to be optimized, manufactured and tested in the Price-Païdoussis blow down subsonic wind tunnel. A description of the Price-Païdoussis wind tunnel is provided in first journal paper presented in this thesis.

Three wind tunnel models were manufactured for this project. Two of the models were rigid and had no morphing capabilities. One of these two rigid models represented the original airfoil shape and the second rigid model represented an optimized version of the ATR-42 wing airfoil. The optimization for the second rigid wing model was carried for 30 m/s and angle of attack of 0°.

The third model was designed with morphing capabilities for its upper surface during wind tunnel tests. Morphing the wing model from its original zero deformation shape to any other positions needed higher forces than the fibre glass composite was capable of sustaining, especially when tested at the highest speed in the test case matrix. These forces risked affecting the integrity of the wing model; therefore, the original shape of the morphing wing was changed for the un-morphed ATR-42 wing airfoil to an already optimized version of it, thus minimizing the forces needed to deform the material.

All three models were manufactured from composite fibre glass and epoxy resin, with the active morphing wing having its upper surface portion optimized in terms of fiber distribution, number and thickness of plies.

For both numerical and experimental research conducted on this project, the upper surface of the airfoil was considered to be flexible, limited between 10% and 70% of the chord, and

constrained in length of the morphing surface. The shape of the surface was changed using an actuation system composed of two electrical brushless motors situated outside the wing model that rotated two steel shafts. The shafts had a variable diameter along the span of the model, with their maximum diameter being 8 mm. The shafts were designed to attain their maximum diameter between 20% and 60% of their total length, where their length equals the span of the wing models. The two shafts were installed at 30% and 50% of the chord, which corresponds to the optimization control points used by the algorithm. These positions were chosen following an analysis of multiple positions possibilities along the chord and after a sensitivity analysis of the optimization process to them.

For the optimization of the airfoil, a genetic algorithm optimization tool was developed and coupled with the bi-dimensional aerodynamic solver Xfoil developed by M. Drela. The genetic algorithm used cross-over, mutation and tournament techniques to perform fast and to avoid the divergence of the optimization.

The genetic algorithm method searched and combined solutions in a pool of genes represented by the vertical displacements of the control points. Based on the selected displacements, the airfoil upper surface was reconstructed using cubic splines with ‘natural boundary conditions’. The evolution of the solution, from the first generation towards the last, was made by evaluating the fitness of each reconstructed airfoil in accordance with the desired objective. The best airfoil found at the end of the optimization was compared with the original airfoil before considering it as the final optimal solution for the studied case.

The optimization objective was the extension of the laminar region on the upper surface of the wing for speeds up to 30 m/s and angles of attack between -5° and 5°. The optimization of the ATR-42 wing airfoil was carried for a wide range of cases, based on the speed capabilities of the Price-Païdoussis wind tunnel and the composite material optimization.

The research for the ATR-42 wing airfoil was carried in the following several phases: 1) preliminary optimization of the ATR-42 wing airfoil, which revealed the potential of

aerodynamic optimization for a large number of cases, 2) selection and preliminary optimization of the fibre glass-epoxy composite, 3) manufacturing and testing in the wind tunnel of two rigid ATR-42 wing models – one original and one optimized shape; 4) final optimization of the composite material for the upper surface region, manufacturing and testing of the morphing ATR-42 wing.

The rigid and the morphing wing were designed respecting the criteria presented by (Rae and Pope, 1984) for wind tunnel testing for bi-dimensional flow. A testing chamber of 0.31 m by 0.61 m by 1.22 m (H x W x L) was chosen. Following their indications and using the chambers' dimensions, the span and chord of the wing models were calculated. All three wind tunnel models were equipped with 20 pressure taps mounted on their upper and lower surfaces. The number of pressure taps on the upper surface varied slightly from model to model and was always higher than the number of pressure taps on the lower surface. The pressure taps positions on the upper surface were selected based on the Xfoil transition predictions. These pressure taps were installed with a varying step on one of the rigid models, with constant step on the second rigid model and again with varying step on the morphing model. This variation was included to allow studying the influence the distance between pressure taps would have on detecting the transition positions, when the pressure taps positions were selected based on numerical predictions. For the transition position detection a method developed by (Popov, Botez and Labib, 2008) was used, which was based on the second derivative of the pressure distribution on the upper surface.

2.1.2 The CRIAQ MDO 505 Morphing Architectures and Related Technologies for Wing Efficiency Improvement

The CRIAQ MDO 505 project is a direct continuation of the CRIAQ 7.1 project. Whereas the CRIAQ 7.1 project developed the design and manufacturing of a wind tunnel wing model with bi-dimensional flow based on a laminar airfoil that has an active upper-surface from carbon-kevlar composite and an actuation system using smart material actuators (SMA), the CRIAQ MDO 505 project took the active upper surface idea and further developed it for a full scale real structure wing tip demonstrator equipped with aileron. During wind tunnel

tests, the flow around the morphing wing demonstrator would have tridimensional properties due to the wing geometry.

The wing tip that featured in the CRIAQ MDO 505 project is a representation of a commercial aircraft wing tip without winglet. The wing tip was slightly scaled down in dimensions to fit the NRC subsonic wind tunnel in Ottawa and had the structural properties and geometry of a real wing tip. The upper surface skin was designed not only to be able to morph but also to sustain the structural loads the skin of a wing needs to support during 1g flight conditions.

The wing tip is a 1.5 m span by 1.5 m root chord structure with two spars by four ribs design and a full span aileron. The spars, situated at 20% and 65% of the chord, represent the boundaries for the morphing skin. The four ribs have an equilibrated distribution, with two of the ribs separating the span in three almost equal parts while the other two form the root and tip boundaries of the model. The whole structure, excluding the upper surface skin and the stiffness stringers, was made from aluminium and steel. The upper surface and the stringers were made from carbon composite. The electrical actuators used for morphing the upper surface were installed on the two center ribs, two on each rib, and were designed and manufactured specifically for this project.

The composite skin was designed and optimized using aerospace industry constraints and aerodynamic optimization results to determine the best combination of carbon fibre direction and number, distribution and thickness of plies along the span and the chord of the wing. The purpose of the optimization of the skin was to match the numerical shapes provided by the aerodynamic optimization with an error of less than 0.5 mm. The weight of the skin was also optimized, and after manufacturing, a gain of 1.2 kg was obtained with respect to the original aluminium skin. The skin was fixed on all four sides of the wing box, that was different different from the skin attachments in CRIAQ 7.1 project where one end was kept free. The elasticity of the skin was introduced as required constrained in the aerodynamic optimization,

and the strains developed by the skin when pushed or retracted during morphing imposed several displacement constraints for the control points during optimization.

The aerodynamic optimization was done using a perfected version of the genetic algorithm optimization tool developed in the ATR-42 morphing wing project. The optimization tool was further developed to include the analysis of cases with classic aileron deflection, cases with morphing aileron deflection, analysis using lift coefficient as input parameter instead of angle of attack, user defined input on the fitness function such as the weigths of the fitness function components, two morphing aileron methods and the possibility of user defined temperature, air dynamic viscosity and density for Reynolds number calculation. The optimization tool also allowed various combinations of optimizations between upper-surface skin, morphing or classic aileron, lift coefficient or angle of attack analysis and free or constrained aileron morphing.

Further improvements were included in the method by upgrading the cross-over function from one step to two steps, a modified version of binary cross-over was used as the second step of the cross-over. The mutation process was kept similar as the one in the original version of the method and it was further applied for the morphing aileron methods. Constraints were related to the maximum allowed displacements of the control points, displacement differences between control points situated on the same chord line, aileron thickness and elastic length, as well as to the relationships between conventional and morphing aileron angles of deflection.

The optimization algorithm was used to determine the type of cases to be used further in the wind tunnel tests and the obtained results were needed for the development of the controllers used during these tests.

Before wind tunnel testing took place, an aeroelastic analysis was done on the wing tip model equipped with aileron to ensure the safety of the model testing. For the aeroelastic analysis a Finite Element Model (FEM) was developed for the wing and the conventional aileron. The

FEM was done using Hypermesh and used uni-, bi- and tridimensional elements to represent the main components of the model. To avoid charging the model and delaying the analysis, most of the model was realised using 2D elements called *shell*s and the connections between structural components were modeled using 0D elements. The flutter analysis was considered as the most representative phenomenon that could pose a danger to the wind tunnel model during testing and it was performed using the MSC Nastran solver.

Before the first wind tunnel series of tests took place, the wing model without leading edge and aileron was subjected to 1g loads bench testing to ensure that its internal structure rigidity respected the Bombardier requirements. A bench test model was designed and manufactured specifically for the structural tests. These static tests were done to ensure the behaviour of the structure under various structural loadings while controlling the actuator displacements and morphing the upper surface. The electrical actuators were designed and manufactured specifically for the wing tip model based on the specifications extracted from structural analysis through which maximum allowed forces were determined when the composite skin was morphed.

The wind tunnel testing took place in three rounds at the NRC subsonic wind tunnel in Ottawa. A description of the wind tunnel is provided in Annex II. For the wind tunnel tests, the model was equipped with 32 kulite pressure sensors installed on the upper surface of the model on two parallel staggered lines near the first actuation line. The kulite sensors were installed next to the first line of actuation, which was installed on the first rib at approximately 0.6 m from the wing root. The data collected from the kulites was used for calculation of the transition region position and upper surface pressure distribution. 60 pressure taps were installed in the same manner as the kulite sensors at the leading and trailing edges and the lower surface, providing a complete pressure distribution profile.

Infrared thermography photography was used for each wind tunnel test case to determine the laminar, transition and turbulent regions of the upper surface of the wing. Balance readings

were added for comparisons of these results with 3D aerodynamic analysis performed with ANSYS Fluent.

The first round of experiments was concentrated on testing 38 cases that were optimized using a preliminary scan of the manufactured wing model's airfoil at the region where the Kulite sensor lines were situated. The objective of the optimization was the extension of the laminar region towards the trailing edge for the first nine cases and the contraction of the laminar region towards leading edge for 29 cases. The results were used to validate numerical 2D and 3D transition predictions and the pressure distribution.

A second round of scans using high precision tools was done on the wing ad provided data for validating the shapes of the airfoil for non-morphed and morphed situations. The data from the first series of wind tunnel tests was used to fine tune the aerodynamic optimization codes, the control system and the infrared methodology. The infrared and kulite transition regions were used to calibrate the Xfoil and Fluent analysis. Based on the experimental results, the possibility of introducing the critical amplification factor, Ncrit, as a variable of the analysis was evaluated due to the nature of the flow observed over the upper surface of the wing. The morphing upper surface was designed to have bi-dimensional flow characteristics between the two actuation lines. During the wind tunnel testing, it was observed that the flow behaviours was neither fully 2D nor completely 3D in nature, thus this behaviour introduced a new level of complexity in the analysis. A post processing procedure was developed for the comparison of the experimental with the numerical aerodynamic data.

The second series of wind tunnel tests was conducted for 97 cases, from which, 38 represented a repetition of the previous series of cases for comparison and verification purposes. The other 59 cases regarded the optimization of the shape of the scanned non-morphed wing airfoil for two objectives: delay of transition region towards the leading edge for 30 cases and advancement of the turbulent region towards the leading edge for the other 29 cases. The second objective was chosen because, in the case of a wing with conventional aileron deflection, it was of interest to observe whether boundary layer detachment could be

observed over the trailing edge and whether would it be affected by the deformation of the upper surface. Another reason to consider the objective of turbulence region advancement, was to determine whether a more turbulent flow over the wing, which means a higher drag, could be useful for minimising the descending or landing angle of attack seen by the wing or for minimizing the high-lift device upward deflection.

The infrared and kulite transition results from the second series of tests were used to validate the numerical predictions using the post-processing procedure developed during the first tests. In addition, the pressure measurements, infrared transition and balance data were used for comparison with the 3D analysis results produced with ANSYS Fluent.

Based on the results from the second series of tests a test matrix was developed for the third series of tests were the morphing wing was equipped with a morphing aileron. The initial constraints for the morphing aileron were a maximum deflection of 6° in the upward or downward direction, for the wing demonstrator tested at a maximum speed of 85 m/s in the wind tunnel and a maximum wing angle of attack of 3°.

Two objectives were pursued for the optimization of the morphing wing equipped with morphing aileron: 1) improvement of the lift coefficient through the morphing aileron coupled with minimization of the drag coefficient through morphing of the upper surface of the wing and 2) minimization of the morphing-wing-equipped-with-morphing-ailerons flexible deflection angle when tested at the same lift coefficient as the morphing-wing-equipped-with-conventional-aileron.

49 cases were tested at two speeds, 51 m/s and 70 m/s, angles of attack between -3° and 3° and flexible deflections between 2° upward and 6° downward. A mix was considered between cases from the second series of tests where good transition region delay results were obtained, and cases with flight conditions similar to some from the second series of tests, but optimized with coupled morphing upper-surface and morphing aileron. Therefore, the cases were grouped based on the optimization objective as follows:

Table 2.1 Optimization objectives used during the third set of wind tunnel tests

Number of cases considered for optimization	Type of optimization objective
16	Lift and drag coefficient improvement using coupled wing upper-surface morphing and aileron morphiing optimization
18	Lift and drag coefficient improvement using morphing aileron optimization and the upper-surface wing morphing from the previous series of tests
8	Minimization of the morphing aileron deflection at constant lift using cases from the previous series of tests
9	Lift coefficient improvement through aileron morphing without wing upper-surface morphing

The Infrared transition experimental results from the third series were analysed. A comparison was made between the morphed and un-morphed transition regions behaviour as a result of the aerodynamic optimization.

2.2 Thesis Organization

As main author, the research performed and included in the thesis was presented in five peer-review journal papers and four conference papers. Three of the journal papers have been published and two are currently under review for publication. These scientific papers are presented in the thesis from Chapter 3 to Chapter 7.

Dr. Ruxandra Mihaela Botez, as co-author for all journal and conference papers, supervised the realization and the progress of the performed research. In the first paper, Mr. Oliviu Sugar Gabor, PhD student, worked as co-author by contributing to the development of the genetic algorithm and the aerodynamic analysis using the XFLR solver. In the second paper, Mr. Oliviu Sugar Gabor, PhD student, worked as co-author by contributing to the experimental set-up of the ATR-42 rigid models in the Price-Païdoussis wind tunnel and to

the post-processing of the pressure measurements. In the third paper, Mr. Francois Michaude, Master student, and Mr. Olivier Guillemet, Internship student, worked as co-authors by contributing to the development of the FEM of the wing and of the conventional aileron. Mr. Mehdi ben Henia, Master student, worked as co-author by contributing to the transfer of the FEM model from the Hypermesh software to the MSC Patran/Nastran solvers, while Master students, Mr. Yvan Tondji and Mr. Manuel Flores-Salinas, worked as co-authors by contributing to the post-processing of the experimental data collected from the accelerometers during wind tunnel tests and Mr. Oliviu Sugar Gabor, PhD student, worked as co-author by contribution to the flutter analysis setup. In the fourth and fifth papers, Mr.Oliviu Sugar Gabor, PhD student, worked as co-author by contributing to the development of the artificial bee colony algorithm, while Mr. Joran Acotto, Internship student, worked as co-author by contributing to the development of the gradient descent optimization method. Mr. Guillaume Brianchon and Mr. Gregoire Portier, Internship students, worked as co-authors by contributing to the post-processing of aerodynamic experimental data, while NRC senior research officers Dr. Mamou Mahmoud and Dr. Youssef Mebarki worked as co-authors by contributing to the experimental set-up and testing of the morphing wing demonstrator at the NRC subsonic wind tunnel facility.

2.2.1 First journal paper

In Chapter 3, the research paper entitled “Numerical and Experimental Validation of a Morphed Wing Geometry Using Price-Païdoussis Wind Tunnel Testing” is included, that was accepted for publication in The Aeronautical Journal in November 2015. In this paper, the numerical and experimental results obtained for the two rigid ATR-42 wing models are presented.

The paper presents the multi disciplinary framework for developing two rigid wing models based on an original and morphed shape of the ATR-42 wing airfoil. The morphing shape was obtained using the genetic algorithm optimization for changing the upper surface between leading edge and trailing edge – 10% and 70% of the chord – for an angle of attack

of 0° and speed of 30 m/s with the aim of improving its aerodynamic performances. The description of the wind tunnel and of how the wing models were designed and manufactured specifically for the Price-Païdoussis wind tunnel was given. The design of the models respected the requirements needed for obtaining a bi-dimensional flow around the wings during tests. Finally, a method was presented for determining the transition region on the upper surface based on the second derivative of the pressure distribution recorded using pressure taps installed at special positions. The pressure taps positions were selected based on the numerical prediction of the transition positions obtained during optimization procedures. The numerical transition results were compared with the experimental results for 15 cases that were tested at three speeds and angles of attack between -2 and 2 degrees.

2.2.2 Second journal paper

In Chapter 4, the journal paper “Drag Optimization of a Wing Equipped with a Morphing Upper Surface” is presented. This paper was published in The Aeronautical Journal in March 2016. The focus of this paper was the optimization of the airfoil shape of the CRIAQ MDO 505 wing tip and how a bi-dimensional optimization affected the performances of the wing tip in a three-dimensional analysis.

In this paper, a genetic algorithm coupled with cubic splines and Xfoil aerodynamic solver was used to create optimized shapes of the original CRIAQ MDO 505 wing airfoil for various speeds, angles of attack and conventional aileron deflections. The genetic algorithm used was described, and details on the optimization process were given. The optimization objective was the improvement of the boundary layer flow over the upper surface of the airfoil by delaying the transition from laminar to turbulent regions of the flow, and thus decreasing the drag coefficient value.

The shapes obtained through optimization were used to reconstruct the wing tip using XFLR 5 capabilities, and to analyze the resulted wing using the 3D Panel Method incorporated in XFLR 5 software. The results were presented for one Reynolds number and speed for various

angles of attack, corresponding to cases that were later tested in the NRC subsonic wind tunnel.

2.2.3 Third journal paper

In Chapter 5, the research paper entitled “Flutter Analysis of a Morphing Wing Technology Demonstrator: Numerical Simulation and Wind Tunnel Testing” is included. The paper was published in the INCAS Bulletin in March 2016. The paper focused on the development of the finite element model of the wing tip demonstrator, its flutter analysis using MSC/Nastran and the experimental results obtained from the accelerometers installed inside the model during the wind tunnel tests.

A description of the CRIAQ MDO 505 project was included in the paper. A detailed presentation was made of the constituent elements, and the manner in which the wing tip was modeled using Hypermesh software. Then, the procedure used to create an aerodynamic surface and couple it with the structural model using the MSC/FLDS software was presented. Further, tests were conducted to determine the best compromise between number of nodes for splinning and the most efficient calculation time. The results of the flutter analysis were presented, both in terms of frequency versus speed, and damping versus speed as well as a presentation of the first four modes. Finally, the accelerometers used during the wind tunnel test and their positions on the wing were described, as well as the method employed for determining the experimental frequencies and their interpretation with respect with their numerical values obtained using the MSC/Natran solver.

2.2.4 Fourth journal paper

In Chapter 6, the research paper entitled “Optimization of a Morphing Wing Tip Aircraft Demonstrator for Drag Reduction at Low Speeds, Part I – Numerical Analysis using 3 Algorithms: Genetic, Artificial Bee Colony and Gradient Descent” is included. The paper was submitted and is under review in the Chinese Journal of Aeronautics since March 2016.

This paper was focused on the optimization of the upper surface of the CRIAQ MDO 505 wing airfoil under strict constraints using three optimization algorithms - genetic, artificial bee colony and gradient descent – and demonstrated the robustness and performance of the genetic algorithm that was used for obtaining the final shapes of the wing airfoils.

The paper described in detail the genetic algorithm used for the optimization of the CRIAQ MDO 505 wing airfoil and its performances, presented in terms of convergence as number of individuals and generations, that were obtained by varying its mutation and tournament parameters. The results of the Genetic Algorithm optimization were then compared with the results obtained with the Artificial Bee Colony algorithm and the Gradient Descent method by plotting their optimization results on Monte Carlo (MP) maps. The MP maps show the aerodynamic performances of the airfoil as function of all possible actuators displacement combinations.

For the comparison between the three algorithms, two objectives functions were tested: 1) delay of the transition point on the upper surface and 2) minimization of the total drag coefficient. All three algorithms were coupled with cubic spline interpolation for geometry reconstruction, and with Xfoil code for aerodynamic analysis. Because different computation machines were used for the optimization and the aerodynamic analysis, an analysis was presented on the impact of the machine errors on the obtained results.

2.2.5 Fifth journal paper

In Chapter 7, the research paper entitled “Optimization Morphing Wing Tip Aircraft Demonstrator for Drag Reduction at Low Speeds, Part II – Experimental Validation using Infra-Red Transition Measurements during Wind Tunnel Tests” is included. The paper was submitted and is under review in the Chinese Journal of Aeronautics since March 2016. This paper was focused on the experimental validation of the numerical predictions obtained using the genetic algorithms in the previous chapter. For validation purpose, the infrared thermography results were considered.

In this paper, the CRIAQ MDO 505 project was described in detail, and a presentation was made for the NRC subsonic wind tunnel and of the infrared thermography technique used for determining the transition region on the upper surface of the wing during wind tunnel testing. The experimental results were analyzed, by introducing two parameters, λ and τ, to describe the laminar to turbulent flow transition. A convention was presented for interpreting the differences between numerical predictions and experimental transition results that were obtained for all the 16 cases presented in the paper. The experimental results were extracted from the second series of tests. Eight cases were presented on the accomplishment of the objective of transition region delay towards the trailing edge. The other eight cases were chosen for the objective of transition region advancement towards the leading edge. The results were presented both in terms of optimization success between experimental morphed and un-morphed states of the wing tip demonstrator and of numerical prediction versus experimental results for all cases.

2.3 Concluding Remarks

Following the aforementioned research steps, it was observed that the aerodynamic performances of the ATR-42 and CRIAQ MDO 505 wing airfoils were improved in terms of manipulation of the boundary layer behavior using a multidisciplinary approach. Using this type of approach, in which constrained aerodynamic optimization was combined with design and optimization of composite materials, various experimental set ups were tested. The obtained experimental results were used to validate and demonstrate the concepts proposed and designed. Optimization methods were researched and tested demonstrating the capabilities of obtaining two-dimensional and tri-dimensional morphed shapes according to the desired objectives. Aeroelastic analyses were performed on optimized wing structures showing that destructive phenomena would not take place. Finally, experimental testing was performed in two subsonic wind tunnels using various methods for determining the degree of optimization on real models based on numerical optimization.

CHAPTER 3

NUMERICAL AND EXPERIMENTAL VALIDATION OF A MORPHED GEOMETRY USING PRICE – PAÏDOUSSIS WIND TUNNEL TESTING

Andreea Koreanschi, Oliviu Şugar Gabor and Ruxandra Mihaela Botez
LARCASE Laboratory of Applied Reasearch in Active Controls,
Avionics and Aeroservoelasticity
École de Technologie Supérieure, 1100 rue Notre Dame Ouest,
Montréal, H3C1K3, Québec, Canada

This article was published in *The Aeronautical Journal, Vol 120, Issue 1227, pg. 757-795, 18th May, http://dx.doi.org/10.1017/aer.2016.30*

Résumé

Une validation expérimentale d'une géométrie de l'aile optimisée dans la soufflerie subsonique Price-Païdoussis est présentée. Deux modèles d'ailes ont été fabriqués en utilisant des matériaux composites à base de fibres de verre et testés à trois vitesses et à des angles d'attaque différents. Ces modèles d'ailes ont été construites sur la base du profil aérodynamique original de l'aile d'avion ATR 42 et sur une version optimisée du même profil pour une condition de vol à nombre de Mach égal à 0,1 et l'angle d'attaque de 0 °. L'optimisation aérodynamique a été réalisée en utilisant un algorithme génétique "in house" couplée avec une routine de reconstruction de spline cubique, et a été analysé à l'aide du solveur aérodynamique XFoil. L'optimisation a été concentrée sur l'amélioration de l'écoulement laminaire sur la surface supérieure de l'aile, entre 10% et 70% de la corde. Les distributions de pressions prédites par XFoil ont été comparées avec les données expérimentales obtenues dans la soufflerie. La position de transition a été estimée à partir des données de pression expérimentales en utilisant une méthode base sur seconde dérivée de la distribution de pression et est comparée à la transition prévue par le code XFoil. Les résultats ont montré la concordance entre les données numériques et expérimentales. Les essais en

soufflerie ont montré que l'amélioration de l'écoulement laminaire de l'aile optimisée est supérieure à la valeur prédite numériquement.

Abstract

An experimental validation of an optimized wing geometry[1] in the Price-Païdoussis subsonic wind tunnel is presented. Two wing models were manufactured using optimized glass fiber composite and tested at three speeds and various angles of attack. These wing models were constructed based on the original aerofoil shape of the ATR 42 aircraft and an optimized version of the same aerofoil for a flight condition of Mach number equal to 0.1 and angle of attack of 0°. The aerofoil's optimization was realized using an 'in-house' genetic algorithm coupled with a cubic spline reconstruction routine, and was analyzed using XFoil aerodynamic solver. The optimization was concentrated on improving the laminar flow on the upper surface of the wing, between 10% and 70% of the chord. XFoil-predicted pressure distributions were compared with experimental data obtained in the wind tunnel. The transition position was estimated from the experimental pressure data using a second derivative methodology and was compared with the transition predicted by XFoil code. The results have shown the agreement between numerical and experimental data. The wind tunnel tests have shown that the improvement of the laminar flow of the optimized wing is higher than the value predicted numerically.

3.1 Introduction

In the context of a world in continuous change, the aerospace industry has to develop greener and more efficient airplanes, which consume less fuel and have a smaller CO_2 footprint. The aerospace industry has therefore developed methods to improve the aerodynamical properties of airplanes. A number of international collaborations and projects were established to tackle this problem.

[1] Wing models or wing geometries tested in the Price-Païdoussis Wind Tunnel refer to bidimentional wing models.

One research direction regards the development of new methods for flight trajectories optimization. Several methods are underway at various academic laboratories, mostly in collaboration with industrial partners. One such collaboration takes place between the teams in the LARCASE laboratory and CMC Electronics-Esterline in the GARDN project. The main objective of the collaboration was to optimize the vertical and horizontal path of the aircraft within the Flight Management System by taking into account the Required Time of Arrival, the wind grids and meteorological conditions. The main motivation of the project was to reduce overall carbon emissions and flight costs. This project was funded by the Green Aviation Research Development Business Led Network GARDN in its second round (Patron, Botez and Labour, 2013; Patrón, Kessaci and Botez, 2014).

Another research direction regards the optimization of the aircraft itself, which can be achieved by modifying any or all of its parts: wing, fuselage, nose, tail, etc. The most common area, and the one with the greatest impact, is the aircraft wing. There are several ways in which a wing can be modified: in-plane modifications, which can be done by optimizing the span or chord for example, out-of-plane modifications, which refers to modifying the twist and bending of the wing, and optimization of the aerofoil or aerofoils that compose the wing. Also, adaptive, morphing wings can be effectively used to replace conventional high-lift devices (Pecora et al., 2011), (Diodati et al., 2013), or the conventional control surfaces (Pecora, Amoroso and Lecce, 2012).

In-plane and out-of-plane wing modifications are radical types of optimization that require complete reconstruction of the wing and, thus, cannot be introduced directly onto an existing aircraft due to certification considerations and high costs. In addition, their aerodynamic properties were not completely demonstrated, with the exception of projects dedicated to UAV developments. (Gamboa et al., 2009) designed an UAV wing capable of independent span and chord changes, using a telescopic spar and a rib system. The numerical analysis demonstrated drag reductions of up to 23% when compared to the non-morphing geometry. (Falcão, Gomes and Suleman, 2011) designed and tested a morphing winglet for a military

UAV, achieving important performance improvement by simply changing the winglet cant and toe angles. Another research on UAV wing morphing was done by (Sugar Gabor, Koreanschi and Botez, 2013a; Sugar Gabor et al., 2014), where the upper-surface of the wing was optimized between the leading edge and 55% of the chord and they also explored morphing of the full wing's geometry.

For further references on these types of optimization, (Sofla et al., 2010) and (Vasista, Tong and Wong, 2012) have presented an exhaustive state of the art list of wing geometry modifications.

'Aerofoil optimization' is a much more accessible method of modifying wing geometry. It is a branch of the wing modification domain that has been well studied; as attested by the large number of different aerofoils that represent compromises to obtain specific performance levels. The aerofoil geometry (e.g. symmetric shape, more cambered aerofoil, thicker aerofoil) was manipulated to improve its performances for subsonic, transonic or supersonic flight or across a range of speeds passing from one regime to another (Eppler, 1990), (Mueller, 2013).

The purpose of the 'in-flight modification' of the aerofoil shape was to enable the aircraft to improve its wing parameters as a function of the flight conditions in which it flies (speed, global or local angle of attack, aileron deflection, flap deflection, etc.). This approach enables the aircraft to extend its flight envelope and to become more flexible during flight without having to radically change its wing shape. The climbing and descending phases of the flight are two practical situations in which the optimization of the wing shape can improve the performances of the aircraft and could also lead to further improvements in the design of the landing gear. Another practical situation would be the minimization of the shock wave or "buffet" on the wing for the transonic flight regime by modifications to the upper-surface of the wing. The minimization of the shockwave could lead to important reductions in drag.

Several experiments were conducted in the area of ‘active aerofoil optimization’. One of the most recent experiments was performed in the CRIAQ 7.1 project, in which collaboration took place between aerospace industrial teams at Bombardier and Thales, and academic partners from the École de Téchnologie Supérieure (ETS) and École Polytéchnique, and the National Aerospace Research Center (NRC). The purpose of the project was to demonstrate the capabilities of morphing wings for developing the flow transition from laminar to turbulent (Popov et al., 2009), (Botez, Molaret and Laurendeau, 2007). Morphing was achieved by replacing the upper surface of the wing between 7% and 70% of the wing chord with a flexible carbon-Kevlar composite and by morphing it using two SMA actuation lines to obtain an optimized shape for each flight condition studied in a wind tunnel (Grigorie et al., 2012a). The optimization was done using a genetic algorithm method coupled with the aerodynamic solver XFoil. The wind tunnel tests have proven that the concept of upper surface morphing was viable, controllable, and gave good results, confirming the delay of the transition from laminar to turbulent flow as well as a reduction of the drag coefficient (Sainmont et al., 2009). PID (Grigorie, Botez and Popov, 2012) and neuro-fuzzy controllers (Grigorie et al., 2011a) were tested to prove that the ability to control the shape of the morphing system to determine the delay of the transition. They gave excellent results in both open (Popov et al., 2010b) and closed loops (Popov et al., 2010a).

Based on the CRIAQ 7.1 experience, another project was developed at the LARCASE laboratory. Its purpose was to develop a wind tunnel active morphing model[2] using electrical actuators, optimized epoxy-glass fiber composite skin, a PID controller and an 'in-house' genetic algorithm coupled with the XFoil aerodynamic solver. Another goal of this project was to demonstrate the morphing-aerofoil concept on a different wing, and therefore with different lengths of morphing upper-surface skin (10%c to 70%c). In this project, the ATR 42 wing model was manufactured totally from composite, instead of a combination of an upper-surface composite and aluminium wing body.

---

[2] Wing models or wing geometries tested in the Price-Païdoussis Wind Tunnel refer to bidimentional wing models.

The project described in the paragraph above was a multi-disciplinary project, in which aerodynamic optimization and analysis, composite material optimization and manufacturing and active control of the morphing structure work together to obtain an active morphing wing.

This project was developed in two phases. **The first phase of the project, presented in this paper**, concentrated on several aspects: development of the aerodynamic shape optimization algorithm, optimization of the composite material and the manufacturing of two rigid wing models[3]. The rigid wing models were based on the original ATR-42 aerofoil and one optimized version of the same aerofoil at a specific flight condition (angle of attack 0° and speed 34.6 m/s). The two rigid wing models were designed and developed with the purpose of validating the optimization algorithm and the wind tunnel experimental set-up. In addition, another purpose was to determine the necessity of wind tunnel corrections and to test the composite material in wind tunnel conditions.

The second phase of the project, which is not described in the present paper, treated the design and development of the morphing mechanism, numerical optimization results for multiple flight conditions, control of the morphing upper surface and wind tunnel experimental results for the active morphing wing.

The present paper is concentrating on the presentation of the general aspects of the project for three of the disciplines involved (aerodynamic optimization, manufacturing, experimental testing) and on the results that validate the aerodynamic optimization for two aerofoil shapes (original and one optimized shape) and on the validation of the method of post-processing the experimental data for obtaining information that can be successfully compared with the numeric results.

---

[3] Wing models or wing geometries tested in the Price-Païdoussis Wind Tunnel refer to bidimentional wing models.

3.2 Methodology

3.2.1 Problem description

Aerofoil shape changing can refer to the whole aerofoil or to just one section of it; for example the aerofoil's upper surface, aileron section or leading edge, etc. The geometric characteristics of an aerofoil are its coordinates, chord length, thickness and camber. Based on these, the wing aerofoil is also described by its aerodynamical parameters, such as lift, drag, aerodynamic moment and pressure coefficients, and the region where the flow passes from laminar to turbulent, also known as transition regime. The purpose of the optimization depends on the flow conditions for which the wing will be deployed. For an aircraft, and implicitly for a wing, these conditions are related to flight maneuvers: take-off, cruise, landing, stall, etc. For example, in a take-off configuration the purpose would be to increase the maximum lift while keeping the drag constant, while for landing the purpose would be to maintain the lift and increase the drag at the same time. In both cases, the results could lead to the development of an aircraft that can safely operate with a shorter take-off or landing strip.

For the ATR 42 wing aerofoil the morphing region was situated on the upper surface of the aerofoil and the objective was to obtain delay of the transition onset with the purpose of reducing the drag coefficient.

3.2.2 Genetic algorithm general description

For the optimization of the aerofoil, an 'in-house' genetic algorithm was developed and verified with the Monte Carlo method. The aerodynamic analysis was done using the XFoil aerodynamic solver; a brief description of this solver is given section 3.2.4.

The genetic algorithm is a meta-heuristic method of optimization inspired from nature, which uses various characteristics of the object to be optimized as 'genes'. The genes were used to

create new objects or individuals, based on the initial ones but having different characteristics. The creation of new individuals was done using two processes found in nature: ‘cross-over’ and ‘mutation’. The cross-over is a process where the genes of two individuals are mixed in various proportions, usually equal, but more complicated functions can be used. While the mutation process affects a percentage of the individuals resulted from the cross-over function(s), and changes the values of the genes using a percentage of mutation.

A fitness function was used to evaluate the optimization level of the new individuals with respect to the original ones. This fitness function is a representation of the purpose of the optimization and describes the ideal characteristics of the optimized individual.

The genetic algorithm method was well studied and validated in various problems; it uses different combinations of cross-over and mutation functions as well as problem-dependent fitness functions (Mitchell, 1998), (Coley, 1999).

3.2.3 Application of the genetic algorithm to the airfoil optimization problem

This algorithm was applied, in this paper, to the geometric optimization of the ATR 42 wing aerofoil upper surface.

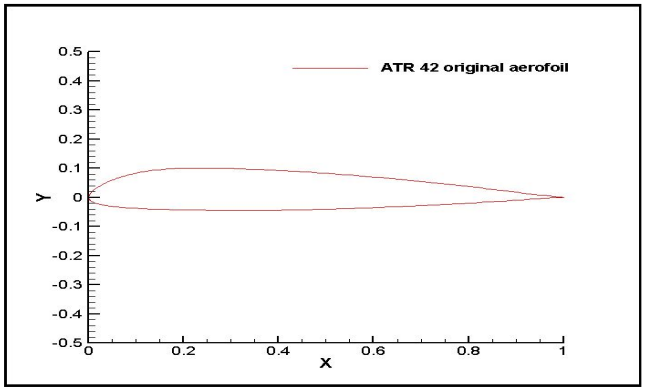

Figure 3.1 Shape of the ATR-42 wing aerfoil

In this project, the upper surface of the aerofoil was optimized between 10% and 70 % of the chord, and no aileron was considered for the wing models. The length of the upper surface to be modified was chosen based on the fact that the leading edge part of a wing is manufactured separately for most civil aircraft, and thus from a morphing point of view it would be extremely difficult to introduce continuous modifications between a leading edge and the rest of the wing. The 70% end limit was chosen because most aircraft have an aileron or flap starting near this point

The area to be optimized was modified using two actuation points situated at 30% and 50% of the chord. Several other positions and number of actuators were tested: a) one actuator situated at 30% of the chord; b) one actuator situated at 50% of the chord; c) two actuators situated at 30% and 50% of the chord; d) two actuators situated at 25% and 40% of the chord; e) three actuators situated at 20%, 35% and 50% of the chord and f) four actuators situated at 20%, 35%, 45% and 60% of the chord. From all these combinations only version c) has given the best results in terms of compromise between aerodynamic optimization, structural forces need to push the skin, shape of the skin obtained after actuator deployment and coupled with the small space inside the wing box and actuator system design.

For the ATR 42 aerofoil, the optimization objective was to obtain a reduction of the aerofoil's drag coefficient at constant angle of attack by delaying the position where the flow passes from laminar to turbulent, for small variations of speed and angles of attack. Because only small variations in speed were studied, only one optimized shape was considered for the first phase of the project and then analyzed and tested over a range of angles of attack to observe its performances.

From the various geometrical characteristics that describe an aerofoil (the geometric characteristics of an aerofoil are its coordinates, chord length, thickness and camber), the authors have chosen to use the *coordinates of the actuation points as 'genes'*, thus reducing the number of unknowns to two – the two vertical displacements of the 'genes'. The upper

surface of the aerofoil, between 10% and 70% of the chord, was reconstructed using ***cubic splines***, which proved to be a sufficiently accurate method (Kulfan and Bussoletti, 2006).

As mentioned before, for the aerofoil reconstruction of the upper surface cubic splines were used. The cubic splines give sufficient accuracy in reconstructing small curvatures. The spline functions are characterized by their shape on subintervals, between two control points. They are also known as piece-wise polynomial real functions. In interpolating problems, spline interpolation is often referred to as polynomial interpolation, due to the fact that it yields similar results; when using lower degree splines (e.g bi-splines or cubic splines) the resulted curve is just as well traced as if interpolated with high degree polynomials, but with the benefit of avoiding instability due to Runge's phenomenon.

The most used spline interpolation is the cubic spline, which insures continuity up to, and including, the second order derivatives, which allows the calculation of the curvature radius. For the reconstruction of the aerofoil using cubic splines, the coordinates for the morphing skin which starts at 10%c and ends at 70%c and the 'genes' (actuation points), which are now defined as control points, were used.

As mentioned above, the optimization method was coupled with the aerodynamic solver XFoil to calculate the aerodynamic characteristics of each new aerofoil that resulted from the optimization process. The solver calculated the lift, drag, moment and pressure coefficients as well as the transition position based on the shape of the aerofoil and the flight conditions introduced. The methods employed by XFoil for the calculation of the aerodynamic parameters are presented in section 3.2.4 of the Methodology. Given that the purpose of the optimization was to reduce the drag coefficient by delaying the transition on the upper surface, the *fitness function,* F_f, was developed as a sum of multiple single objective functions based on the aerodynamic parameters calculated with the XFoil solver:

$$F_f = w_1 \cdot C_l + w_2 \cdot \frac{1}{C_d} + w_3 \cdot Up_{Tr} + w_4 \cdot \frac{1}{Up_{Tr}} + w_5 \cdot \frac{C_l}{C_d} + w_6 \cdot \frac{Up_{Tr}}{C_d} \qquad (3.1)$$

, where w_i represent weights given by the user as natural numbers, positive or negative, depending on the purpose of the optimization, U_{pTr} represents the transition point and F_f represents the *fitness function*.

The fitness function presented din equation (3.1) is a multi-objective single point optimization function. Its purpose was to show that by using all the aerodynamic characteristics provided by the XFoil analysis, and that, based on the particular objective of the optimization, the fitness function used for the actual optimization could be reduced to one of the functions presented in equation (3.2).

Thus, in the particular case of optimizing for drag coefficient reduction at constant angle of attack, the *fitness function Ff* was reduced to any of these expressions:

$$F_f = w_2 \cdot \frac{1}{C_d} \text{ or } F_f = w_3 \cdot Up_{Tr} \text{ or } F_f = w_6 \cdot \frac{Up_{Tr}}{C_d} \tag{3.2}$$

Using any of the fitness functions presented in equation (3.2), the optimization results, in terms of the aerodynamic performances (lift and drag coefficient and upper surface transition) of the aerfoils, were similar.

In this genetic algorithm the final value of the fitness function it was not imposed, because the optimization was considered free – no fixed value was associated to the objective, for example there was no specific percentage of reduction that was demanded to be achieved – it was preferred to limit the number of generations and individuals. Based on convergence tests, 20 generations and 40 individual aerofoils were considered sufficient, as changes in results were not obtained with higher values:

Because a maximum value for the fitness function was not imposed, a method for evaluating the performances of the aerofoils was developed based on the values of the fitness function the aerofoils obtained.

Thus, the maximum and minimum values of the fitness function were calculated for each generation. Then an interval was determined by using equation (3.3)

$$Interval = \frac{Fitness_{\max} + Fitness_{\min}}{10} \tag{3.3}$$

Based on the fitness function values and the 'intervals', groups of fitness values were created. Each group was awarded a grade. The highest the fitness function values in a group the higher the grade, with the maximum grade awarded being 10. The group that contained the lowest values of fitness function was awarded grade 1.

New aerofoils were created using the genes of the analyzed ones, and all of the aerofoils in a generation had at least one chance of being used as providers of genes for the next generation of aerofoils. The likelihood of each aerofoil to be used as a gene provider or parent was established based on its grade. A function to represent this probability was developed and is presented below:

$$P_s = 11 - x; x \in \mathbb{N}, P_s \in \mathbb{N} \tag{3.4}$$

$$x = \begin{cases} y, y \geq 1 \\ 1, y \leq 1 \end{cases}; x, y \in \mathbb{N} \tag{3.5}$$

$$y = \begin{cases} z^{A_f}, z^{A_f} \leq 10 \\ 10\ , z^{A_f} \geq 10 \end{cases}; y, z \in \mathbb{N} \tag{3.6}$$

$$z = \begin{cases} \underline{\lambda}, \lambda \geq 0 \\ \overline{\lambda}, \lambda \leq 0 \end{cases}, z \in \mathbb{N}, \lambda \in \mathbb{R}$$
$$\lambda = \delta \cdot 10^{A_f}, random\ \delta \in [0,1] \tag{3.7}$$

, where P_S is the *probability of selection* and A_f represents the attraction factor given by the user, which is set at 2, for the present case. The attraction factor shows with how much an

individual with a high grade is more attractive to become a parent. The P_S function returned values between 1 and 10, corresponding to the grades associated to the aerofoils. The value of P_S was compared to the grades allocated to each aerofoil based on the fitness function. All aerofoils whose grades were equal to the P_S value were grouped and one of them was selected at random to play the role of parent. The process was repeated until all the required parents were chosen. In order to solve the problem of aerofoil shape modification, two parents were considered sufficient for each new individual aerofoil.

The new set of aerofoils was created using *cross-over* and *mutation* functions applied to the randomly chosen parents. Two *cross-over* functions were used, depending on the number of aerofoil generations deemed necessary to achieve the optimum in drag reduction. It was observed that, for this algorithm, the optimum region was reached after the analysis of ten generations of aerofoils using a simple *cross-over* function, which mixed equal shares of the genes. To avoid finding a local optimum instead of a global one, another *cross-over* function was added and it affects the generations beyond the tenth. This function was based on the simulated binary *cross-solver* technique (Deb and Agrawal, 1994) and used a random number in the following manner:

$$child = \begin{cases} child_{equalshare}, generation \le 10 \\ child_{\neq equalshare}, generation > 10 \end{cases} \tag{3.8}$$

$$\begin{aligned} &child_{equalshare}(gene_i) = gene_{i\_parent_j}; \\ &i \in [1, number\_of\_genes], j \in [2, number\_of\_parents] \end{aligned} \tag{3.9}$$

$$\begin{aligned} &child_{\neq equalshare} = \begin{cases} \frac{1}{2} \cdot (1+\delta) \cdot gene_{i\_parent_j}, \delta \ge 0.5 \\ \frac{1}{2} \cdot (1+\delta) \cdot gene_{i\_parent_{j+1}}, \delta < 0.5 \end{cases}; \\ &random\ \delta \in [0,1]; i \in [1, number\_of\_genes], j \in [2, number\_of\_parents] \end{aligned} \tag{3.10}$$

The *mutation* affected a percentage of the aerofoils resulted from the *cross-over* function(s), and changed the values of the genes with a percentage of *mutation*. Two variables were used to achieve *mutation*. One variable gave the 'chance of mutation', which gave a percentage of the number of aerofoils in a generation that would be affected by the mutation process and was always a very small value (in percentage) that did not lead to a degeneration of the optimization. For our problem, the chance of mutation was set at 0.01 % of the number of aerofoils in a set. The second variable was the 'percentages of mutation' that gives the amount of genes, which were to be modified. This variable must always be sufficiently small, so that the modified value of the gene does not surpass the upper or lower limits, if there are any imposed. In our case, the percentage of mutation was set at a maximum of 2% of the value of the genes it affected.

A final step in the genetic algorithm that ensures a rapid convergence towards the optimum was the *tournament*. The *tournament* is a process in which some of the worst members of the current generation of aerofoils are replaced with some of the best members from the previous aerofoil generation. This process gives more chances to those aerofoils that are close to the optimum to contribute with their genes to the next set of aerofoils. For our problem, the maximum number of aerofoils and generations used was 40 aerofoils per generation for a total of 20 generations. The maximum number of generations was imposed after convergence tests have shown that for more than 20 generations and 40 aerofoils no extraordinary modifications in the shape of the optimal aerofoil occur.

Figure 3.2 presents the 'step by step' process of optimization from input, which contains the original aerofoil coordinates, the flight and optimization conditions, to the result, which contains the optimized aerofoil coordinates and its pressure and aerodynamic characteristics.

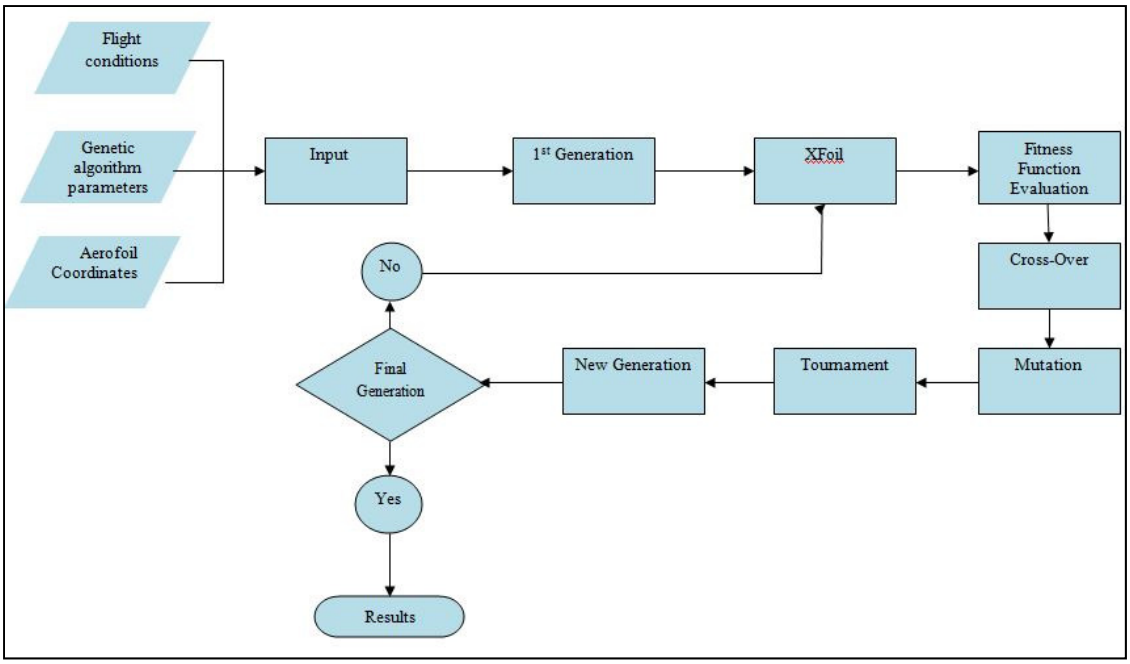

Figure 3.2 Schematic of the Genetic Algorithm/XFoil coupled software

3.2.4 XFoil code description

The code used for the calculation of the two-dimensional aerodynamic characteristics of the wing's control sections is XFoil, version 6.96, developed by (Drela and Youngren, 2001). The XFoil code was chosen because it has proven its precision and effectiveness over time, and because of its rapid convergence. In XFoil, inviscid calculations were performed using a *linear vorticity stream function panel method,* to which a Karman-Tsien compressibility correction, (Drela, 1989b), was added, allowing for the obtaining of good predictions of subsonic flow. For the viscous flow calculations, XFoil uses a two-equation lagged dissipation integral boundary layer formulation (Drela, 1989a) and incorporates the e^n transition criterion (Drela, 2003). The flow in the boundary layer and in the wake interacts with the inviscid potential flow by using the *surface transpiration model*.

3.3 Price-Païdoussis Subsonic Wind tunnel

Before the presentation of the wing model design and manufacturing in the following section, a short presentation of the Price-Païdoussis wind tunnel is given, as the dimensions of the test chamber and some of the characteristics of the wind tunnel have an impact on both models dimensions

The Price-Païdoussis wind tunnel is an experimental facility at the École de Téchnologie Supérieure under the supervision of Professor Ruxandra M. Botez, head of the LARCASE laboratory (Aeronautical Research Laboratory in Active Control, Avionics and Aeroservoelasticity) and the Canada Research Chair for Aircraft Modeling and Simulation Technologies. The Price - Païdoussis facility is a twelve-meter blow down subsonic wind tunnel. The main components of the wind tunnel are represented in Figure 3.3 and its dimensions in Figure 3.4

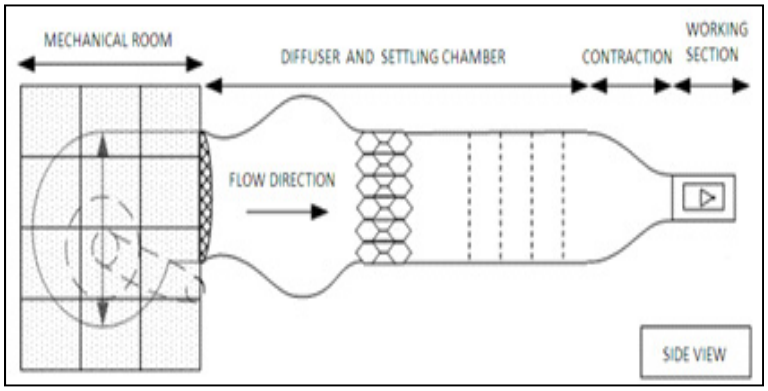

Figure 3.3 Components of the Price- Païdoussis wind tunnel retrieved from (Mosbah et al., 2013)

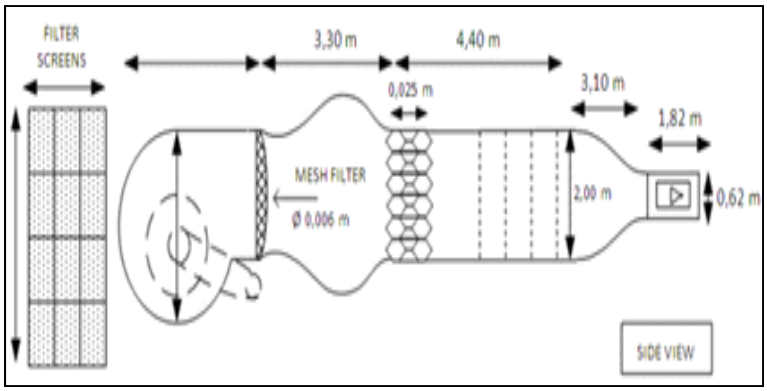

Figure 3.4 Dimenssions of the Price- Païdoussis wind tunnel retrieved from (Mosbah et al., 2013)

Figure 3.5 Wing model[4] installed in the wind tunnel chamber

[4] Wing models or wing geometries tested in the Price-Païdoussis Wind Tunnel refer to bidimentional wing models.

The wind tunnel is powered by a 40 HP, 67 Amps electrical engine, from North Western Electric Co and is fitted with a double impeller centrifugal fan. The maximum speed it can reach is approximately 61 m/s or 0.18 Mach in the smaller of the two test chambers that complete the wind tunnel. The chambers are made of wood, with Plexiglas removable doors on each side, for greater accessibility to the models installed inside. The main test chamber has dimensions of 0.62 x 0.91 x 1.83 m (H x W x L) and the speeds that can be sustained in it are around 40 m/s, equivalent to 0.12 Mach, with a maximum Reynolds number of 2.4 million. The smaller of the two chambers is 0.31 x 0.61 x 1.22 m (H x W x L) and can sustain the maximum speed of the wind tunnel and a Reynolds number of 3.5 million. Reynolds numbers were calculated using a chord of 0.8 m, which is the maximum chord that a model can have, in order to be tested in either of the test chambers.

The wind tunnel's turbulence level is approximately 0.3, corresponding to a critical amplification factor of 5.5 for the XFoil analysis. The correspondence between the flow turbulence level (T) and the critical amplification factor (N), used in the 'e^n' transition estimation method, was given by Mack's formula (Van Ingen, 2008):

$$N = -8.43 - 2.4\ln(T) \tag{3.11}$$

A. Ben Mosbah and M.F. Salinas, (Mosbah et al., 2013), presented a detailed description of the wind tunnel components and flow measurements, for ISO certification.

In order to decide which one of the test chambers should be used, it was necessary to determine the dimensions of the models. The requirements for the models dimensions were determined by the requirements for a bi-dimensional wing model, as recommended by J. Borlow, W. Rae Jr. and A. Pope (Rae and Pope, 1984). In addition, the models dimensions were determined by the requirements of the active morphing wing model developed in the second phase of the project. The active morphing model included a morphing mechanism and pressure sensor cables installed inside the model, which indicates the need for a model large enough to house them.

Based on these considerations, the larger testing chamber was chosen. The final dimensions of the models were calculated using the testing chamber length and width, the thickness of the aerofoil and the formulas indicated in (Rae and Pope, 1984). Thus, the wing models have a span of 0.6 m and a chord of 0.244 m, and their thickness is 35 mm. This thickness was considered more than enough to house the pressure taps used for pressure measurement on the rigid wing models in the first phase of the project, presented in this paper, and sufficiently large to house most of the morphing mechanism of the active morphing wing developed in the second phase of the project.

3.4 Manufacturing of the rigid wing models[5]

As mentioned in the first section, the wings were manufactured from fiberglass-epoxy resin composite material, which was selected because it meets several of the requirements for the morphing area material. The proposed materials were aluminum, carbon-Kevlar and unidirectional TG-18_U glass fiber combined with epoxy resin (fiberglass). The criteria, on which the material was chosen, were based on mechanical properties as well as on the financial and technological availabilities. The Carbon-Kevlar material was successfully used during the CRIAQ 7.1 project and it was considered as a possible candidate, but it was not chosen because it was not easily available and reproducible and also because it was considered more beneficial to explore other materials and optimization techniques. The aluminums' intrinsic mechanical properties makes it an unlikely choice for a flexible skin that needs to change shape while minimizing the forces needed for the actuation system, therefore it is difficult to optimise aluminium and the amount of time needed for such a process was considered too high. The final weight of the model was also one of the parameters considered in the choice of materials.

The final decision was to create an optimized unidirectional TG-18_U fiber-epoxy resin composite best-suited to the project's needs. The fibers used were JB Martin's UD TG-9U

[5] Wing models or wing geometries tested in the Price-Païdoussis Wind Tunnel refer to bidimentional wing models.

fibers infused with epoxy at a fiber volume fraction of 50%. The optimization, of the number of plies along the span and chord of the wing and the direction of the glass fibers, was carried out using the Hyperworks software. The optimization process and the evaluations of the resulted composite are presented by (Michaud, Joncas and Botez, 2013).
Table 3.1 presents several characteristics of the composite material that was used for the manufacturing of the wing models.

Table 3.1 Properties of the composite components
retrieved from (Michaud, Joncas and Botez, 2013)

Property	Unit (SI)	Epoxy/Glass UD	Bonding Paste
E_1	GPa	48	4
E2	GPa	13	-
G12	GPa	4.75	1.2
S1T	MPa	848	62
S2T	MPa	62	-
S1C	MPa	579	100
S2C	MPa	239	-
S12	MPa	76	13.35
ν12	-	0.26	0.31

The composite optimization process took into account the deformations obtained with the aerodynamic optimization software in a multidisciplinary loop between the aerodynamic and structural parts of the project.

The goal of the material optimization process was to match the structural shape to the theoretical shape provided by the aerodynamic optimization.

The composite material for the rigid models was found to have a constant thickness of 0.25 mm per ply, four plies in both the span and the chord lengths, while the glass fibers were

oriented at 0° and 90° to insure sufficient rigidity in both directions of the chord and span. The composite material was stiffened with an epoxy-based bonding paste.

Initially, it was planned to use the composite material only for the region between 10% and 70 % of the chord on the upper-surface. Due to the complications in manufacturing a small model from two different materials and in the interest of observing the behavior of the composite material, it was decided to use it for the full surface of the wing models.

Several materials (metal, wood, composite, etc.) were proposed for the manufacturing of the wing models moulds. Since the models were made one after another and the moulds were to be used for the manufacturing of the morphing wing in the second phase of the project, the material from which the moulds were made must provide precision and reliability for the manufacturing process without deteriorating. Thus, the moulds were machined from aluminum blocks and the base of the wing models was made from solid steel that was cut to shape with laser tools.

Two molds were created for each wing model – one for the upper surface part and one for the lower surface part of the wing – and after the installation of the pressure tap's cables, the two parts were assembled together using EPIKOTE Resin MGS BPR 135G.

The manufacturing process, the assembly and the finishing of the models was done at ETS in our LARCASE laboratory.

The wings were placed in the wind tunnel testing chamber with tufts (small wool fibers) placed on the upper surface and were tested to verify that the effects of the wing model edges were attenuated and disappeared at the center of the wing. This meant that the flow around the wing had bi-dimensional characteristics in the region where the pressure sensors were installed.

A detailed description of the realization of the rigid wing models for the Price-Païdoussis wind tunnel was given in R. Caléstreme's Master's thesis (Caléstreme, 2012).

The testing of the wing models in the Price-Païdoussis wind tunnel confirms that the simple optimization of the composite was sufficient for this phase of the project. The material has resisted to the aerodynamic forces developed by the wind tunnel at the highest speed and angle of attack without any visible deterioration.

3.5 Pressure measurement system

As mentioned earlier, the pressure in the wind tunnel was measured using pressure taps connected to an AeroLab PTA (pressure transducer array) measurement system. These pressure taps were chosen because, they are used in experimental setups and represent an economical solution (Bastedo and Mueller, 1986), (Storms, Takahashi and Ross, 1995).

The AeroLab PTA system was chosen to record the data without the inaccuracies of interpretation inherent to traditional fluid-filled multi-tube manometers, which need manual recording. The PTA is an adaptable and configurable system that comes completely fitted with pressure sensors that allows the measurement of the absolute atmospheric pressure between 800 and 1200 mbar and absolute pressure between 0 to 10 bar with an accuracy of +/- 0.05% of the basic range and a resolution of 0.002% of the basic range. The connecting vinyl tubes, from the taps on the upper and lower surfaces of the wing, needed to be connected to the 24 pressure fittings installed on the PTA system box, which was equipped with its own, easy to use, executable program, LabView. More details on this PTA system can be found on the AeroLab site (Aerolab, 2015).

The most convenient method of installing the pressure sensors was to integrate them, using flexible connecting vinyl tubes connected to a cavity on the model surface at one end and the pressure measurement system at the other end. This method was chosen because it eliminated the need to disassemble the models after manufacturing, and to assemble them again in order to change a pressure sensor without damaging other sensors in the process.

The holes in the upper and lower model skins had to respect a number of constraints. The literature in this domain, (Shaw, 1960), (Tavoularis, 2005) , (Vercauteren et al., 2010), states that the dimensions of the holes should be between 0.5 and 3 mm in diameter, the ratio between their lengths and diameters must be between 5 and 15, and the cavity for the connecting vinyl tubes should have a greater diameter than the hole. The last condition, when respected, will minimize the length of the hole's channel. These three conditions were necessary to obtain good precision in measurements and to avoid parasitic effects, for example turbulence in the cavity, which would change the measured values. In our case, the holes had a diameter smaller than 1mm; thus, it was not necessary to respect all of the above conditions, because for a hole with a very small diameter the geometry and inclination of the hole's channel would have no effect on the measurements, thereby facilitating the process of puncturing the holes during the skin manufacturing process.

Twenty pressure taps were installed on the upper and lower surfaces of the original wing model. Eighteen were installed on the upper and lower surfaces of the optimized wing model. The wing reproducing the original shape of the ATR 42 aerofoil has fourteen taps on the upper surface and six taps on the lower surface, while the model reproducing the optimized shape has sixteen taps on the upper surface and only four on the lower. Fewer pressure taps were used for the lower surface because the upper surface was considered of more importance because of the morphed region. Table 3.2 and Table 3.3 present the distribution of the pressure taps on both wings. In Table 3.2, it can be observed that the distribution of the pressure taps on the upper surface of the rigid wing model has a variable step in the chord direction. The variable step was chosen after analyzing the numerically calculated transition point positions. On the optimized model (Table 3.3), the step between pressure taps is maintained constant in order to observe how much the position of the pressure taps, determined in function of the numerical transition, influences the accuracy of determining the experimental transition. Figure 3.6 and Figure 3.7 present the wind tunnel setup for the wing models.

Table 3.2 Pressure taps positions on the upper and lower surfaces of the rigid original model

Original Rigid Wing model upper-surface														
Chord position (%)	5	10	15	20	25	30	32.5	35	37.5	40	45	50	60	70
Chord position (mm)	12.2	24.4	36.6	48.8	61	73.2	79.3	85.4	91.5	97.6	109.8	122	146.4	183
Original Rigid Wing model lower-surface														
Chord position (%)	2.77	10	20	40	60	80								
Chord position (mm)	6.8	24.4	48.8	97.6	146.4	195.2								

Table 3.3 Pressure taps positions on the upper and lower surfaces of the rigid optimized model

Optimized Rigid Wing model upper-surface														
Chord position (%)	5	10	15	20	25	30	35	40	45	50	55	60	65	70
Chord position (mm)	12.2	24.4	36.6	48.8	61	73.2	85.4	97.6	109.8	122	134.2	146.4	158.6	170.8
Optimized Rigid Wing model lower-surface														
Chord position (%)	3.1	10	20	30										
Chord position (mm)	7.6	24.4	48.8	73.2										

Figure 3.6 Optimized wing model installed inside
the test chamber ready for testing

Figure 3.7 Original rigid model installed in the wind tunnel test
chamber and connected to the AEROLAB measurement system

Before the installation of both models in the wind tunnel, the positions of the pressure taps and the dimensions of the holes were measured and compared with the theoretical values from the CAD files. The measurements were done using a ‘contour gauge’ with a precision of 0.1 mm and an ‘electronic caliper’, and the results show small, negligible differences between the theoretical and the actual values.

3.6 Results

The numerical analysis results were compared with the experimental data, for the two rigid models discussed above, for the pressure distributions along the chord and for the second derivative of the pressure coefficient. One of the objectives of the first phase of the project, presented in this paper, was to ascertain whether wind tunnel corrections were needed. From the analysis of the experimental data and comparison with the numerical results no wind tunnel corrections (wall effects) were needed for the pressures or the angles of attack used for the experiment; as the validation of numerical versus experimental data gave very good results for the subsonic Price-Païdoussis wind tunnel.

Wind tunnel test cases

As mentioned in the previous sections, two rigid wing models were manufactured. The first model was a representation of the original aerofoil, while the second was the reproduction of an optimized version of the original aerofoil. The aerofoil was optimized for Mach number of 0.1 and angle of attack of 0˚ using two control points situated at 30% and 50% of the chord. Figure 3.8 shows the shapes of the two aerofoils used for the development of the wing models.

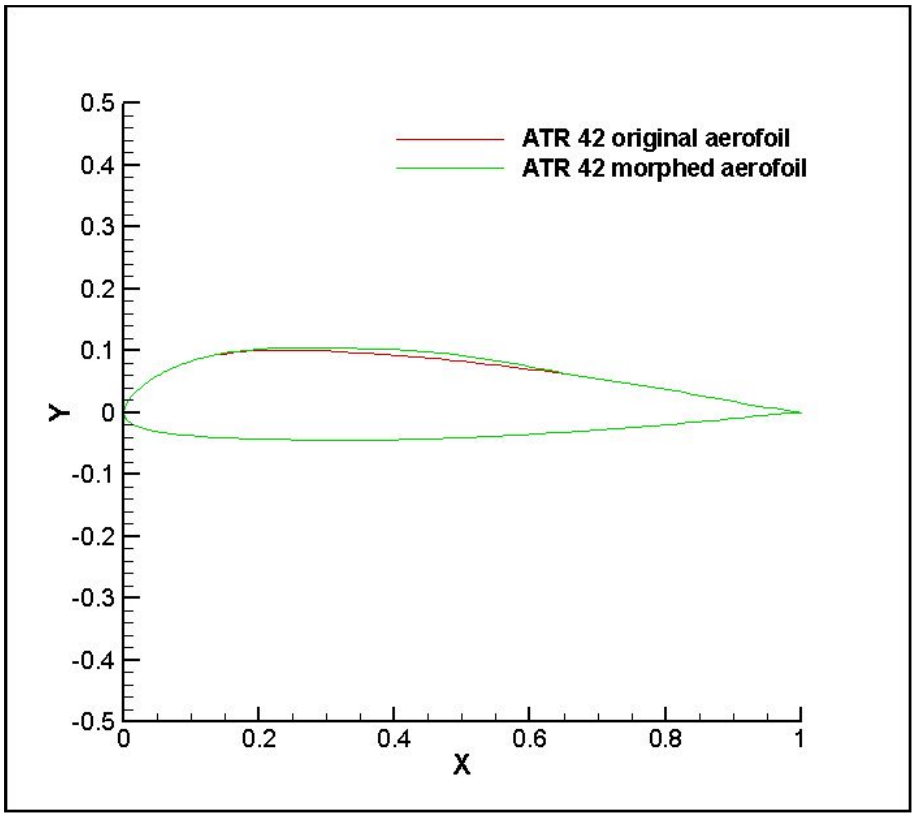

Figure 3.8 Optimized ATR 42 aerofoil shape vs. Original ATR 42 aerofoil shape

The optimization function used was described in Section 3.2.3 on optimization (equation.3.2). Forty randomly modified aerofoils based on the original ATR 42 aerofoil and twenty generations were needed to obtain the final aerofoil shape that was used for manufacturing.

The numerical and experimental tests were done to validate the aerodynamic and composite material optimization procedures and to prove that the modification of the upper surface of the ATR-42 aerofoil (one aerofoil shape presented as optimized wing model) produces improvements in the transition location, and implicitly in the value of the drag coefficient.

Table 3.4 presents a complete list of the tests performed for both the experimental setup in the Price-Païdoussis wind tunnel and the numerical analysis with XFoil.

Table 3.4 Numerical and experimental test cases for both rigid models

Case	Speed(m/s)	Mach	Angle of attack(°)	Reynolds No.
1	27.2	0.08	-2	4.30E+05
2			-1	
3			0	
4			1	
5			2	
6	30.6	0.09	-2	4.85E+05
7			-1	
8			0	
9			1	
10			2	
11	34	0.1	-2	5.40E+05
12			-1	
13			0	
14			1	
15			2	

In this section, only the results obtained for three test cases, 2, 8 and 15 (Table 3.4), are presented and discussed, for different speeds and angles of attack, because of the similarity of the results obtained for the group of cases. In the final part of the results section, the numerical results for all test cases are given in Tables 3.7 to 3.10.

Figure 3.9 to Figure 3.17 show a comparison between the pressure distribution calculated with XFoil and the pressure distribution determined from wind tunnel experimental data for each of the rigid models. In each set of three figures, corresponding to each of the three cases presented in this paper, the first figure represents the comparison between the experimental and numerical data for the original model, the second figure represents the comparison between the experimental and numerical data for the optimized model, and the third figure represents the comparison between the experimental data for both models.

3.6.1 Analysis of the pressure distribution

Case 2 – Analysis and testing for Mach number of 0.08 and angle of attack of -1°

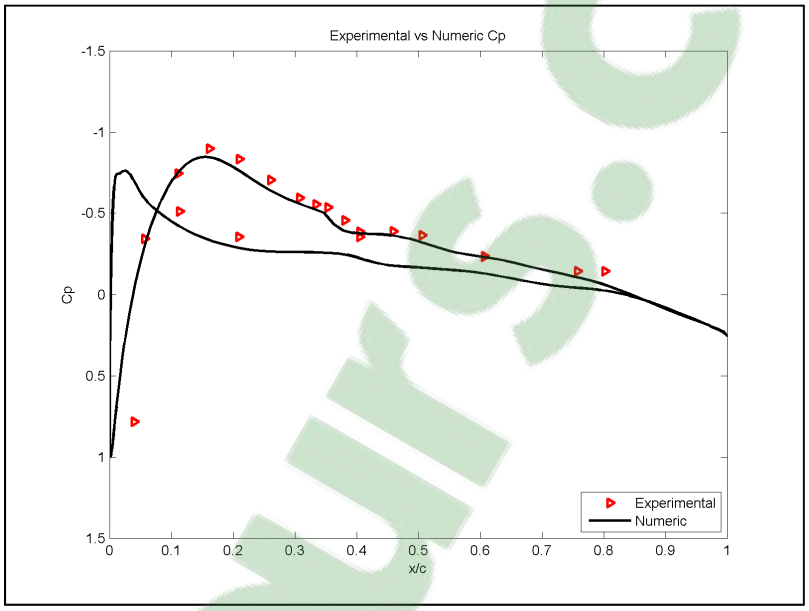

Figure 3.9 Comparison, for the original model, of the pressure distribution calculated with XFoil vs experimental pressure distribution

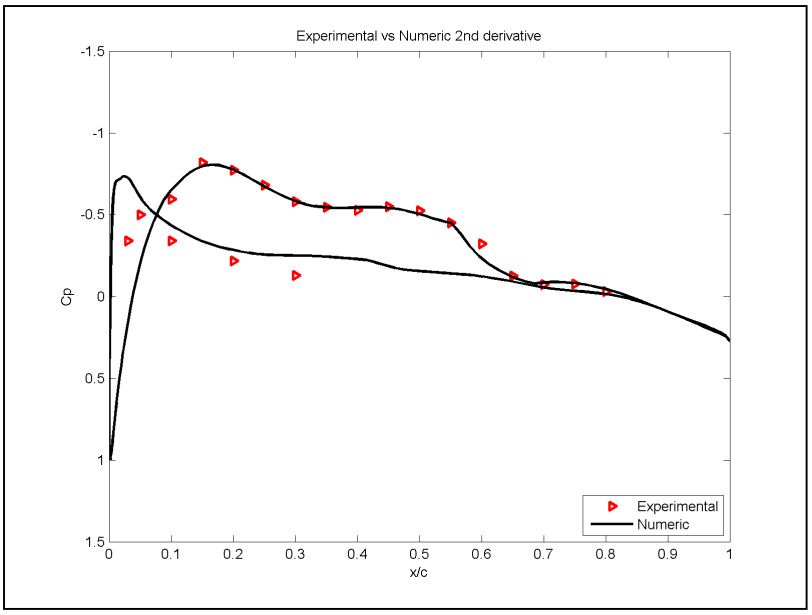

Figure 3.10 Comparison, for the optimized model, of the pressure distribution calculate with XFoil vs experimental pressure distribution

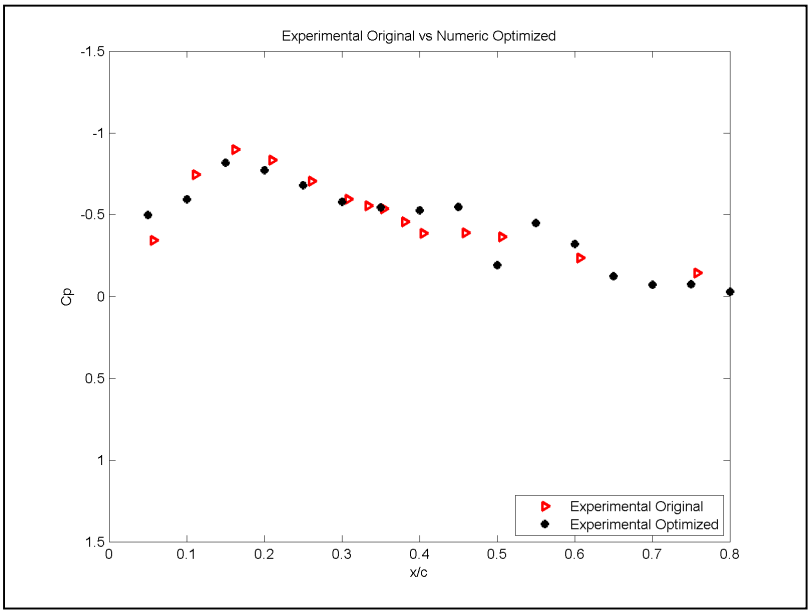

Figure 3.11 Comparison of the experimental pressure distribution for the optimized model vs experimental pressure distribution for the original model[6]

[6] The 10th pressure sensors for the Experimental Optimmized data in Figures 3.11, 3.14 and 3.17 has suffered air leaks during the wind tunnel experiment.

Case 8 – Analysis and testing for Mach number of 0.08 and angle of attack of -1°

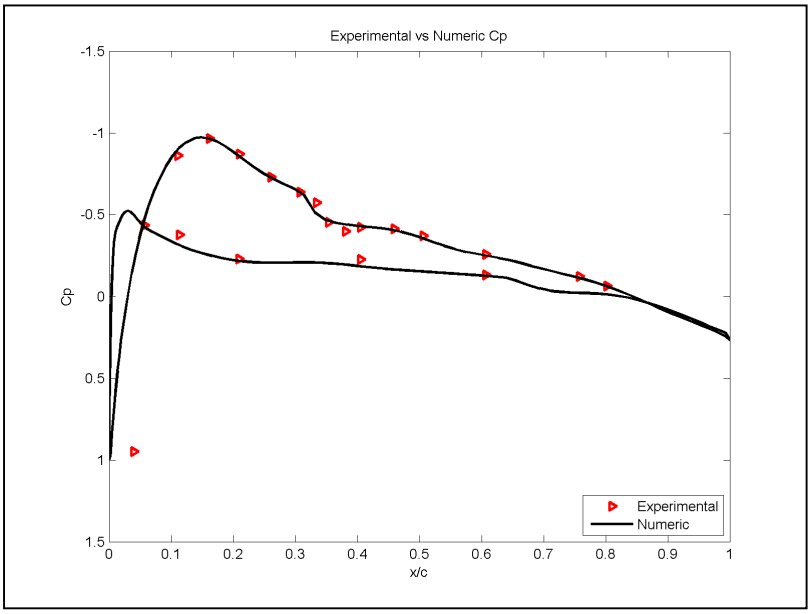

Figure 3.12 Comparison, for the original model, of the pressure distribution calculated with XFoil vs experimental pressure distribution

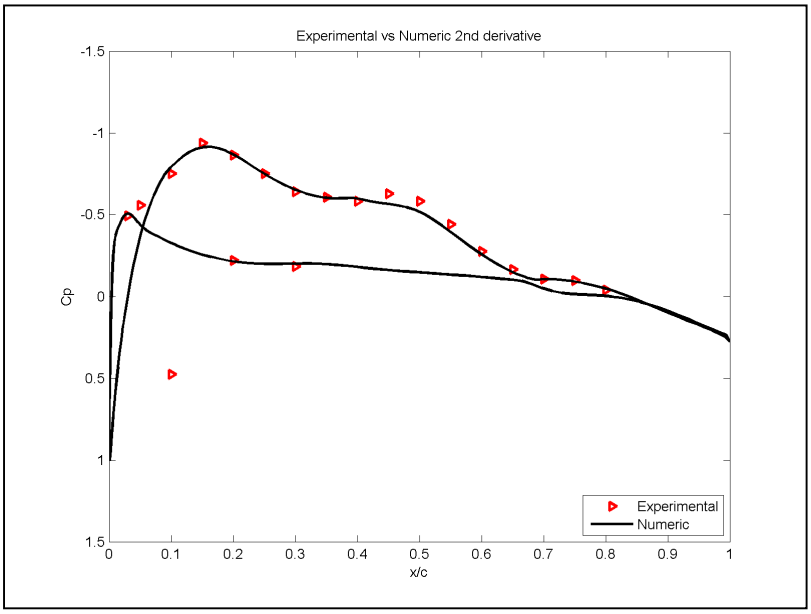

Figure 3.13 Comparison, for the optimized model, of the the pressure distribution calculated with XFoil vs experimental pressure distribution

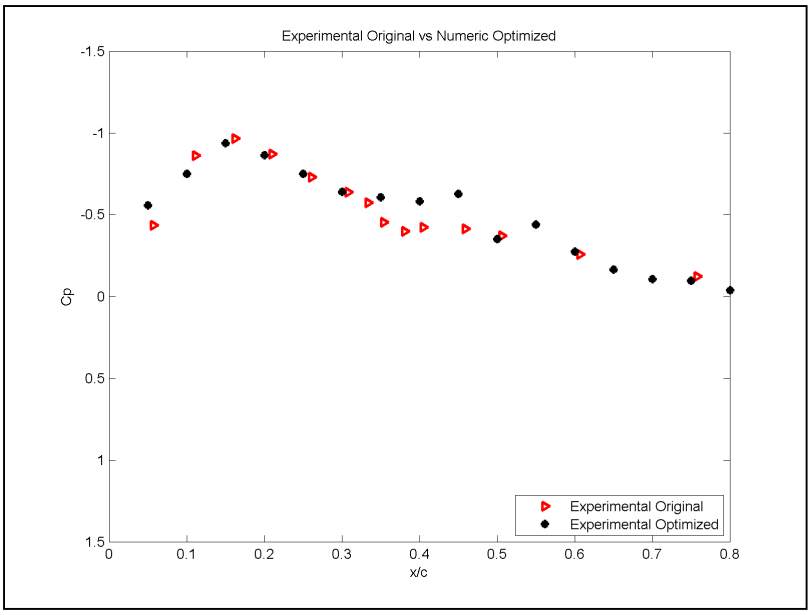

Figure 3.14 Comparison of the experimental pressure measurements for the optimized model vs the experimental pressure measurements for the original model[7]

[7] The 10th pressure sensors for the Experimental Optimmized data in Figures 3.11, 3.14 and 3.17 has suffered air leaks during the wind tunnel experiment.

Case 15 – Analysis and testing for Mach number of 0.08 and angle of attack of -1°

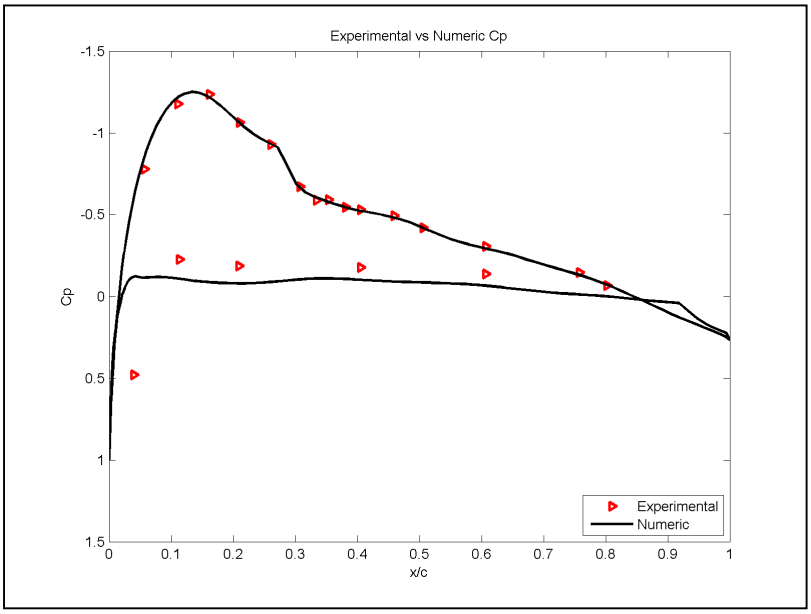

Figure 3.15 Comparison, for the original model, of the pressure distribution calculated with XFoil code versus experimental pressure

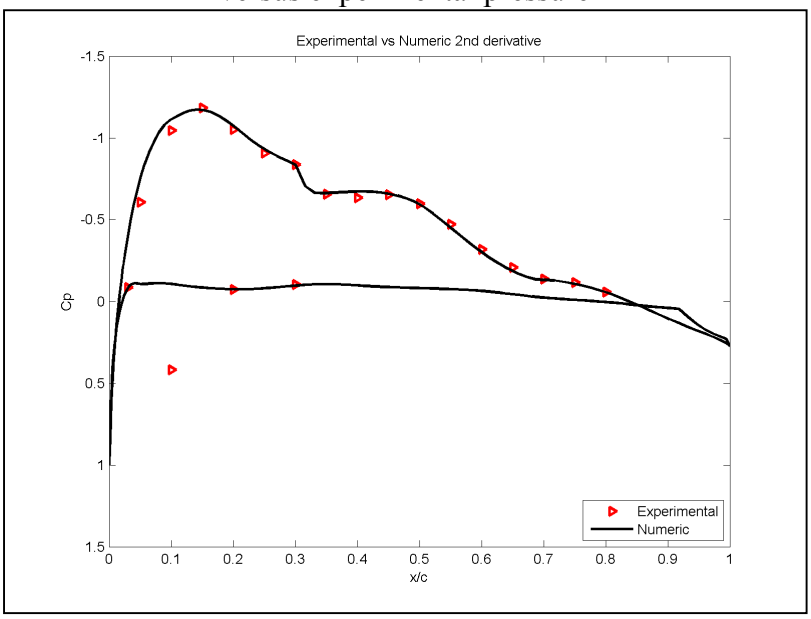

Figure 3.16 Comparison, for the optimized model, of the pressure distribution calculated with XFoil code versus experimental pressure distribution

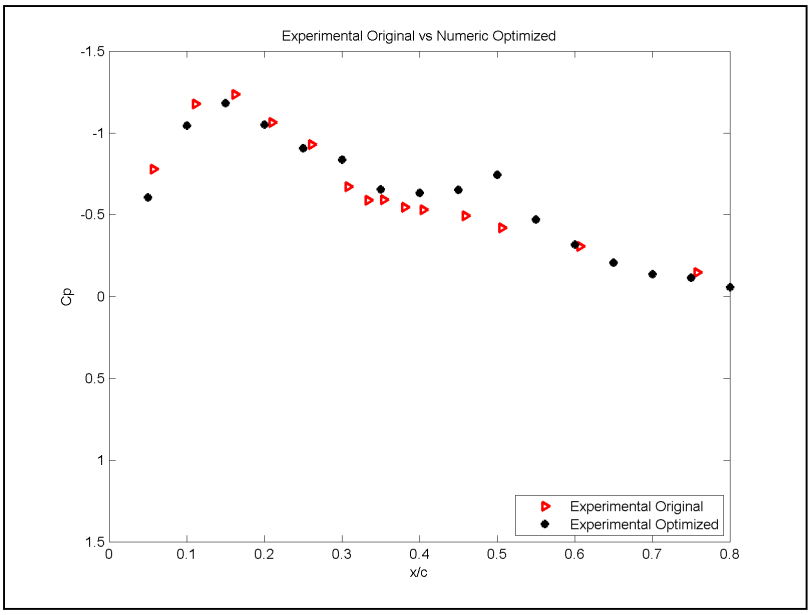

Figure 3.17 Comparison of the experimental pressure measurements for the optimized model versus the experimental pressure measurements for the original model[8]

From the results presented in the three set of figures, in the first and second figures from each set it was observed that the experimental data agrees with the XFoil predictions without applying any wind tunnel corrections, which confirms that at very small speeds and angles of attack, 2D wind tunnel corrections are not necessary. On the upper surface, the good agreement between the experiment and the numerical prediction was due to the sufficiently high number of pressure taps installed, and it was observed that the pressure taps' readings closely follows the XFoil predicted curve. On the lower surface, the pressure taps' readings do not follow the shape of the numerical curve as closely. This was due to the small number of sensors installed, to a blocking of the second pressure sensor on the lower surface, but, since the most accurate readings were needed on the upper surface, where the optimization took place, the experimental data obtained for the lower surface was considered sufficient.

[8] The 10th pressure sensors for the Experimental Optimmized data in Figures 3.11, 3.14 and 3.17 has suffered air leaks during the wind tunnel experiment.

The third figure, from each of the three sets of figures, shows the comparison between the experimental results of the original shape model and the optimized shape model for each of the cases. It can be seen that even a small difference in shape induced a visible change in the pressure distributions. Numerical percentages of the improvements of the transition position for each of the cases are presented in Tables 3.7 to 3.10.

3.6.2 Second derivative analysis of the pressure data for transition estimation

Figures 3.18 to 3.23 present the analysis of the second derivative of the pressure coefficient measurements, which allowed us to predict the transition position from the experimental data without requiring expensive or complicated equipment.

The transition of the boundary layer from laminar to turbulent has been an important topic in aerodynamics since (Reynolds, 1883) publication on this subject. Today there is still no complete transition theory; instead, empirical or semi-empirical correlations and expensive wind tunnel measurements are used to determine transition.

The classical approach for determining transition in numerical aerodynamic calculations is based on iterative methodology, by combining a panel code with a boundary layer code. To be able to simulate the transition region, the boundary layer code needs to be coupled with a stability code based either on linear stability theory or on wind tunnel-derived correlations. However, this approach only works for cases where classical boundary layer theory (Schlichting and Gersten, 2003) holds true, which restricts it to cases with attached flow. More recently, codes such as ANSYS Fluent (Menter et al., 2006) have introduced transition calculation in conjunction with modern aerodynamic methods, but, even here, the methods used to determine transition are actually empirical correlations. A different way of determining transition was proposed by (Silisteanu and Botez, 2010). He uses the refining of the grid as the starting point to obtain accurate information on the boundary layer.

The most commonly known empirical correlations are the 'Granville' method (Granville, 1953), the 'one step' method of (Michel, 1951), the Wazzan method (Wazzan, Gazley and Smith, 1979), and the e^n method implemented in XFoil solver that was used for our numerical calculations.

Practically, even if no general transition theory exists, as of yet, there are a number of methods that can be used to numerically determine the transition position with very good accuracy (Khrabrov and Ol, 2004; Langtry et al., 2006; Mamou et al., 2006; Menter et al., 2006).

From an experimental point of view, the detection of the transition region on a wing in a wind tunnel needs expensive equipment during the tests, e.g. an infrared scanner, highly sensitive optical sensors, Kulite pressure sensors, etc., as well as post processing equipment for the resulted experimental data. In an experimental setup, such as the one presented in this article, in which a reduced scale wing model was fitted with pressure taps, it was not possible to have all that equipment, but the estimation the transition position on the upper surface with a reasonable degree of accuracy was necessary and it was done. Thus, pressure data was collected during our experiment, and this data was used to determine, with a certain degree of accuracy, the region on the upper surface where transition occurs.

The flow transition can be detected on an XFoil pressure distribution plot by a point with a high gradient in the local pressure. This detection is shown analytically in the equation of motion (3.12) of the boundary layer to which wall conditions are applied.

$$\begin{aligned} &\rho\left(\frac{\partial u}{\partial t}+\frac{u\partial u}{\partial x}+\frac{v\partial u}{\partial y}\right)=\frac{-\partial p}{\partial x}+\frac{\partial}{\partial y}\left(\mu\frac{\partial u}{\partial y}\right) \\ &\textit{wall conditions} \\ &u=v=0 \text{ at } y=0 \end{aligned} \tag{3.12}$$

By applying the wall conditions above, equation (3.12) becomes equation (3.13):

$$\frac{\partial p}{\partial x} = \mu \left. \frac{\partial^2 u}{\partial y^2} \right|_{y=0} \tag{3.13}$$

When the pressure gradient is positive, a deceleration of the flow occurs until it becomes reversed.

The transition onset is associated with the maximum of the velocity streamline curvature and the maximum curvature in the pressure plot. To determine the maximum velocity streamline curvature, it is sufficient to derive equation (3.13) one time with respect to x and equation (3.14) will be obtained.

$$\frac{\partial}{\partial x}\left(\frac{\partial p}{\partial x}\right) = \frac{\partial}{\partial x}\left(\mu \left. \frac{\partial^2 u}{\partial y^2} \right|_{y=0} \right) \tag{3.14}$$

It was observed that the result corresponds to the second derivative of the pressure, which, in turn, corresponds to the ‘maximum of the pressure curvature’.
The laminar separation point was defined at the point where:

$$\left. \left(\frac{\partial u}{\partial y}\right) \right|_{y=0} = 0 \tag{3.15}$$

By considering equations (3.14) and (3.15), it results that at the laminar separation point the second derivative of the pressure must also be zero. Immediately downstream from this point, the boundary layer may reattach itself, forming a turbulent boundary layer, or it may remain detached, creating a highly unsteady shear layer. The ‘transition zone’ is the region situated between the detachment point of the laminar boundary layer and its reattachment point as a turbulent one.

Further details, demonstrations and comparisons on this method are presented in (Popov, Botez and Labib, 2008). Other active control methods for the transition detection on a morphing wing are given (Grigorie and Botez, 2010; Grigorie et al., 2012b).

Based on the above formulations, an approximation of the transition position can be computed from the pressure data. This method was successfully applied to the experimental pressure data collected during the Price-Païdoussis wind tunnel tests to determine the transition point on the upper surface of the two rigid models. The comparison of the numerical transition prediction versus experimental transition estimated using the second derivative method on the pressure distribution was presented in Figures 3.18 to 3.23. The second derivative method was applied on the raw experimental pressure data without the use of spline interpolations.

The derivative from the pressure distribution was calculated by using the second derivative as shown in equation (3.16)[9].

$$\left.\begin{aligned} \frac{\partial^2 p}{\partial x^2} &= \frac{\partial}{\partial x}\left(\left.\frac{\partial p}{\partial x}\right|_{iR}\right)\Bigg|_{iL} \\ \left.\frac{\partial p}{\partial x}\right|_{iR} &= \frac{p_{i+1}-p_i}{x_{i+1}-x_i} \end{aligned}\right| \Rightarrow \frac{\partial^2 p}{\partial x^2} = \frac{p_{i+1}\cdot(x_i - x_{i-1}) - 2\cdot p_i\cdot(x_{i+1}-x_{i-1}) + p_{i-1}\cdot(x_{i+1}-x_i)}{(x_{i+1}-x_i)\cdot(x_i-x_{i-1})^2} \tag{3.16}$$

This formulation was chosen because of the non-uniformity of the steps between two consecutive pressure taps. For the XFoil pressure distribution, the classic second derivative approximation, expressed by equation (3.17), and obtained from the Taylor series, was used:

$$\frac{\partial^2 p}{\partial x^2} = \frac{p_{i+1} - 2\cdot p_i + p_{i-1}}{\Delta x^2} \tag{3.17}$$

[9] The formulation presented in equation (3.16) was developed by the author, but any other formulation for the second derivative can be used with similar success.

Case 2 – Analysis and testing for Mach number of 0.08 and angle of attack of -1°

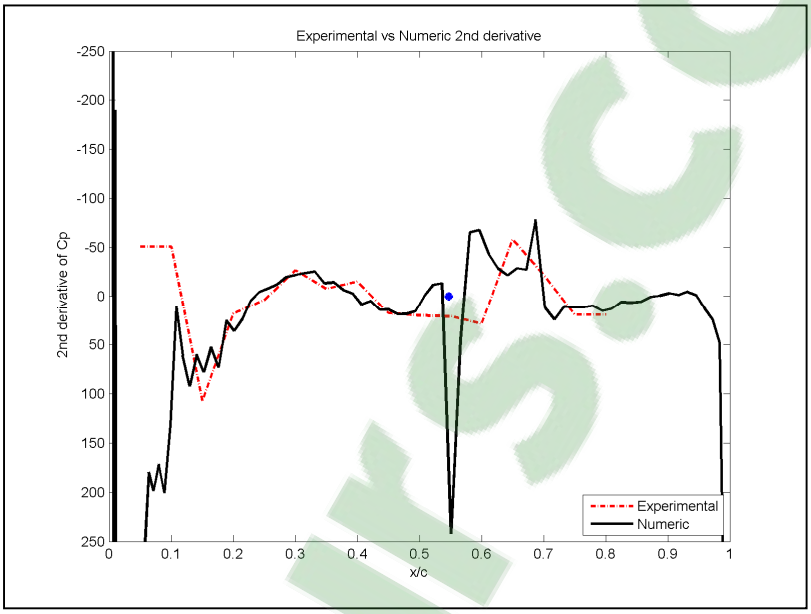

Figure 3.18 Variation of the second pressure derivative using XFoil pressure distribution, experimental distribution and the XFoil predicted transition point, for the optimized model

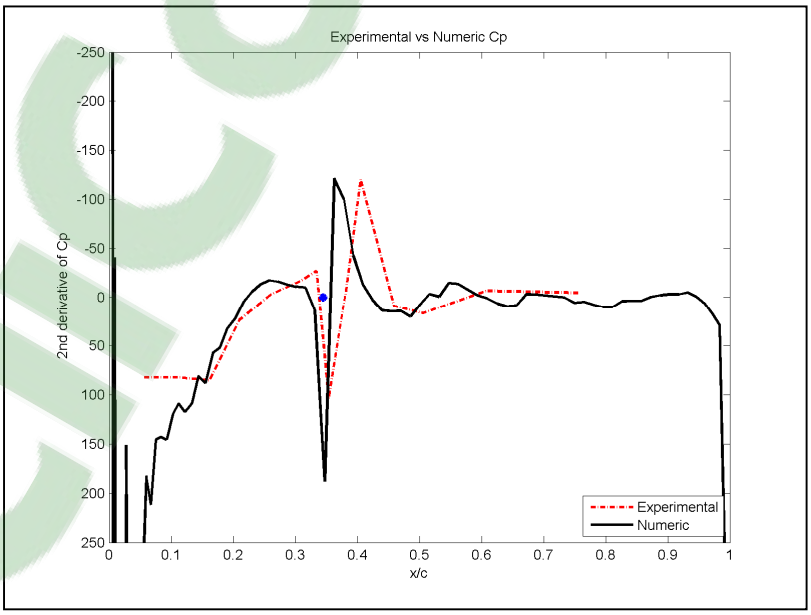

Figure 3.19 Variation of the second pressure derivative using XFoil pressure distribution, experimental distribution and the XFoil predicted transition point, for the original model

Case 8 – Analysis and testing for Mach number of 0.08 and angle of attack of -1°

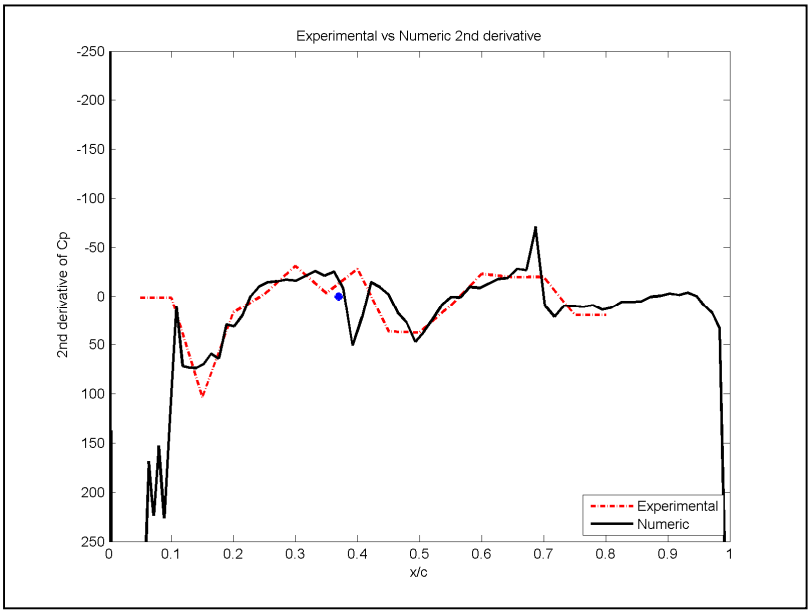

Figure 3.20 Variation of the second pressure derivative using XFoil pressure distribution, experimental distribution and the XFoil predicted transition point, for the optimized model

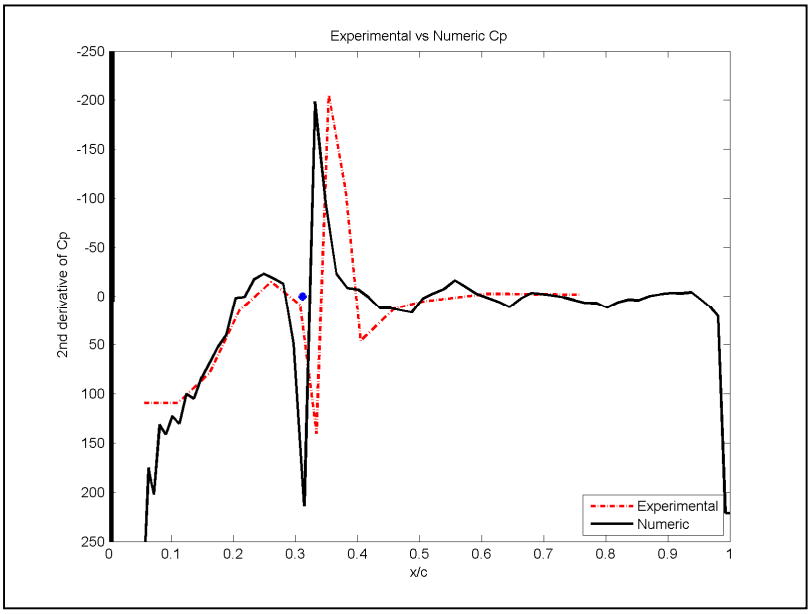

Figure 3.21 Variation of the second pressure derivative using XFoil pressure distribution, experimental distribution and the XFoil predicted transition point, for the original model

Case 15 – Analysis and testing for Mach number of 0.08 and angle of attack of -1°

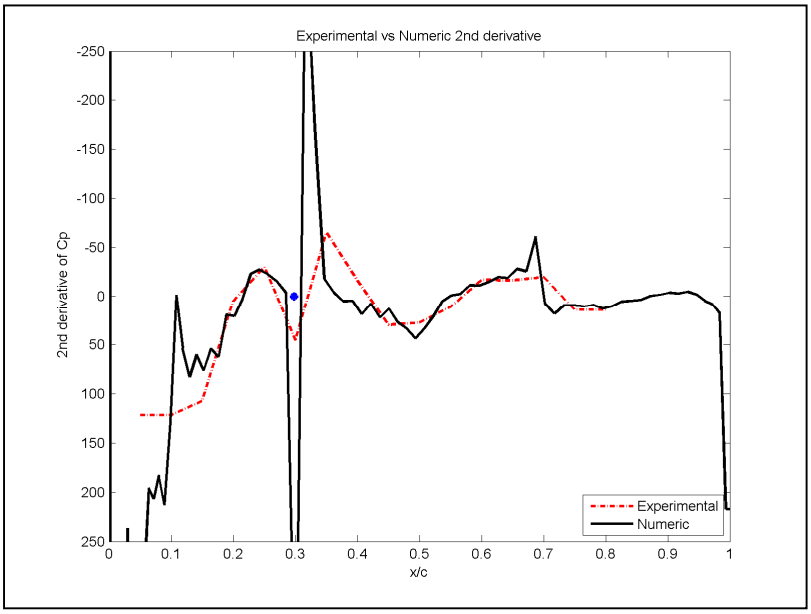

Figure 3.22 Variation of the second pressure derivative using XFoil pressure distribution, experimental distribution and the XFoil predicted transition point, for the optimized model

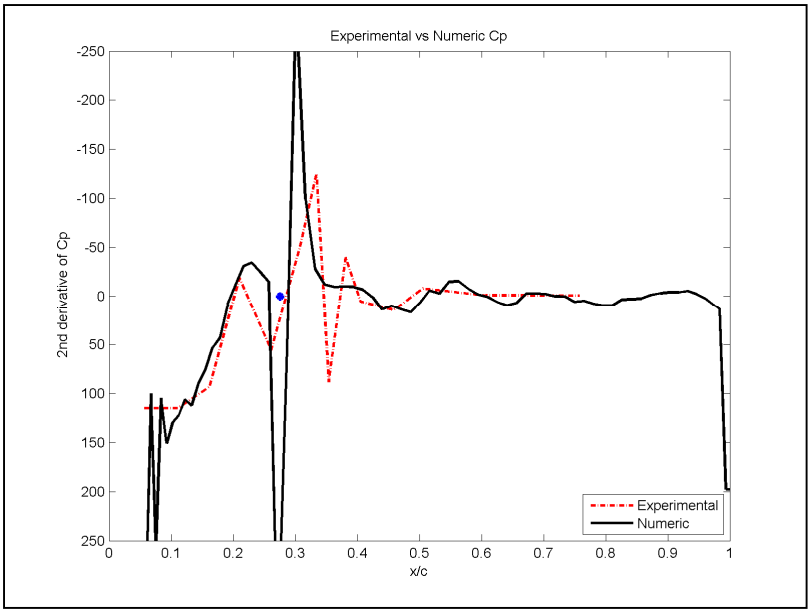

Figure 3.23 Variation of the second pressure derivative using XFoil pressure distribution, experimental distribution and the XFoil predicted transition point, for the original model

Numerically, XFoil gives a single point for the transition, experimentally it is impossible to extract a discreet value for the transition on the upper surface; normally, there is a transition region for which an average can be calculated with an uncertainty value. Thus, the results were presented in terms of the most probable minimum, maximum and average transition and the numerical prediction. Given that the speed interval is small, the transition interval variation from one speed to another at the same angle of attack is also small. This means that the pressure sensors show the transition is approximately in the same area for cases at the same angles of attack and small variation of the speed. This does not apply if the speed variation is high.

For the original wing model, Figures 3.19, 3.21 and 3.23 show the comparison of the variation of the second derivative of pressure for experimental and numerically calculated data.

Table 3.5 presents the interval of the experimental transition and the numerical prediction for the cases presented in Figures 3.19, 3.21 and 3.23. The transitions were presented in percentage of chord.

The uncertainty values were determined manually for each case, based on the pressure measurements, and were calculated as half the distance between the transition point's maximum and minimum possible locations.

Table 3.5 Transition results for Numerical and Experimental pressure data – Original wing model

Angle of Attack (°)	Mach	Numerical Original (%c)	Experiment Original min (%c)	Experiment Original average (%c)	Experiment Original max (%c)	+/- Experimental Uncertainty (% c)
-1	0.08	34.50	33.00	36.50	40.00	3.50
0	0.09	31.13	31.00	32.50	34.00	1.50
2	0.1	27.58	20.00	27.00	34.00	7.00

Table 3.6 presents the interval of the experimental transition and the numerical prediction for the cases presented in Figures 3.18, 3.20 and 3.22, which are for the optimized rigid wing model.

Table 3.6 Transition results for Numerical and Experimental pressure data – Optimized wing model

Angle of Attack (°)	Mach	Numerical Original (%c)	Experiment Original min (%c)	Experiment Original average (%c)	Experiment Original max (%c)	+/- Experimental Uncertainty (% c)
-1	0.08	54.70	55.00	60.00	65.00	5.00
0	0.09	37.01	30.00	35.00	40.00	5.00
2	0.1	29.78	23.00	29.00	35.00	6.00

For the cases presented above, on average, the error between the numerical and experimental transition is between 0.5 and 2% for the original wing model and between 0.7 and 5% for the optimized wing model. However, the error can drop to less than 0.5% or go as high as 10% if the uncertainty interval is taken into account. The large interval in the experimental transition, especially in the case of the optimized wing model, is partially given by the position of the pressure sensors. In Section 3.5, it was mentioned that a different step was used when installing the pressure taps on the original and optimized wings. These results show that the original wing model, on which the sensors were installed using a variable step based on the numerical transition predictions, the uncertainty interval is much smaller than for the optimized wing on which the sensors were installed at a constant step. The previous observation confirms the attention that needs to be taken when installing the pressure sensors. An analysis of the number and positions of the sensors should be done, while taking into account numerical predictions, before tests are done in wind tunnel.

The differences between numerical and experimental transition were also dues to other factors, the precision of the aerodynamic solver XFoil, an insufficient number of sensors in regions where transition is expected to appear, the manner in which the experimental data

was interpolated, human error. By improving any of the above differences, the error between the experimental readings and the theoretic prediction should decrease.

The results presented in Figure 3.18 to Figure 3.23 show that using a reasonable number of sensors installed on the upper surface, and even in the absence of an interpolation method for the pressure data, preliminary results were obtained for the transition onset without the need of more complex measurement systems. The following Tables, 3.7 to 3.10, present the numerical and the experimental transition results for all the cases tested in the wind tunnel for the two wing models and the transition improvement obtained both numerically and experimental. The Reynolds numbers range from 430000 for Mach number 0.08 to 540000 for Mach 0.1.

Table 3.7 Numerical transition results for all wind tunnel cases

Angle of attack (°)	**Mach**	**Original (%c)**	**Optimized (%c)**	**Numerical improvement (Original – Optimized) (%c)**
-2	0.08	37.82	57.75	19.93
	0.09	36.62	57.10	20.48
	0.1	35.73	56.47	20.74
-1	0.08	34.50	54.70	20.20
	0.09	33.34	53.67	20.33
	0.1	32.75	52.43	19.68
0	0.08	31.67	40.75	9.08
	0.09	31.13	37.01	5.88
	0.1	30.64	35.17	4.53
1	0.08	29.91	33.22	3.31
	0.09	29.44	32.43	2.99
	0.1	28.99	31.73	2.74
2	0.08	28.34	30.82	2.48
	0.09	27.93	30.27	2.34
	0.1	27.58	29.78	2.20

Table 3.8 Estimated experimental transition results with uncertainty for all wind tunnel cases for the original wing model

Angle of attack (°)	Mach	Experimental Original_min (%c)	Experimental Original_average (%c)	Experimental Original_max (%c)	+/- Uncertainty (%c)
-2	0.08	40.00	45.00	50.00	5.00
	0.09	35.00	38.50	42.00	3.50
	0.1	35.00	37.50	40.00	2.50
-1	0.08	33.00	36.50	40.00	3.50
	0.09	33.00	35.00	37.00	2.00
	0.1	31.00	33.50	36.00	2.50
0	0.08	31.00	33.00	35.00	2.00
	0.09	31.00	32.50	34.00	1.50
	0.1	27.00	31.00	35.00	4.00
1	0.08	29.00	30.50	32.00	1.50
	0.09	28.00	30.00	32.00	2.00
	0.1	26.00	29.00	32.00	3.00
2	0.08	23.00	28.00	33.00	5.00
	0.09	23.00	28.00	33.00	5.00
	0.1	20.00	27.00	34.00	7.00

Table 3.9 Estimated experimental transition results with uncertainty for all wind tunnel cases for the optimized wing model

Angle of attack (°)	Mach	Experimental Optimized min (%c)	Experimental Optimized average (%c)	Experimental Optimized max (%c)	+/- Uncertainty (%c)
-2	0.08	55.00	61.00	67.00	6.00
	0.09	55.00	61.00	67.00	6.00
	0.1	55.00	60.00	65.00	5.00
-1	0.08	55.00	60.00	65.00	5.00
	0.09	50.00	55.00	60.00	5.00
	0.1	50.00	55.00	60.00	5.00
0	0.08	30.00	35.00	40.00	5.00
	0.09	30.00	35.00	40.00	5.00
	0.1	30.00	35.00	40.00	5.00
1	0.08	No estimation	No estimation	No estimation	No estimation
	0.09	30.0	35.00	40.00	5.00
	0.1	30.00	35.00	40.00	5.00
2	0.08	23.00	29.50	36.00	6.50
	0.09	23.00	28.50	34.00	5.50
	0.1	23.00	29.00	35.00	6.00

Table 3.10 Estimated experimental vs numerical transition improvement for all wind tunnel cases

Angle of attack (°)	Mach	Numerical improvement (%c)	Experimental Improvement (%c)
-2	0.08	19.93	16.00
	0.09	20.48	22.50
	0.1	20.74	22.50
-1	0.08	20.20	23.50
	0.09	20.33	20.00
	0.1	19.68	21.50
0	0.08	9.08	2.00
	0.09	5.88	2.50
	0.1	4.53	4.00
1	0.08	3.31	No estimation
	0.09	2.99	5.00
	0.1	2.74	6.00
2	0.08	2.48	1.50
	0.09	2.34	0.50
	0.1	2.20	2.00

Figure 3.24 to Figure 3.27 present, for each speed, the comparison between the predicted and the estimated improvement.

As seen in Tables 3.7 to 3.10 and in Figures 3.24 to 3.26, the experimental data showed greater improvement of the transition position than the numerical predictions for some of the

cases, while for others it obtains similar results. The exceptions were at angle of attack 2° where the improvement percentage was smaller than what was numerically predicted.

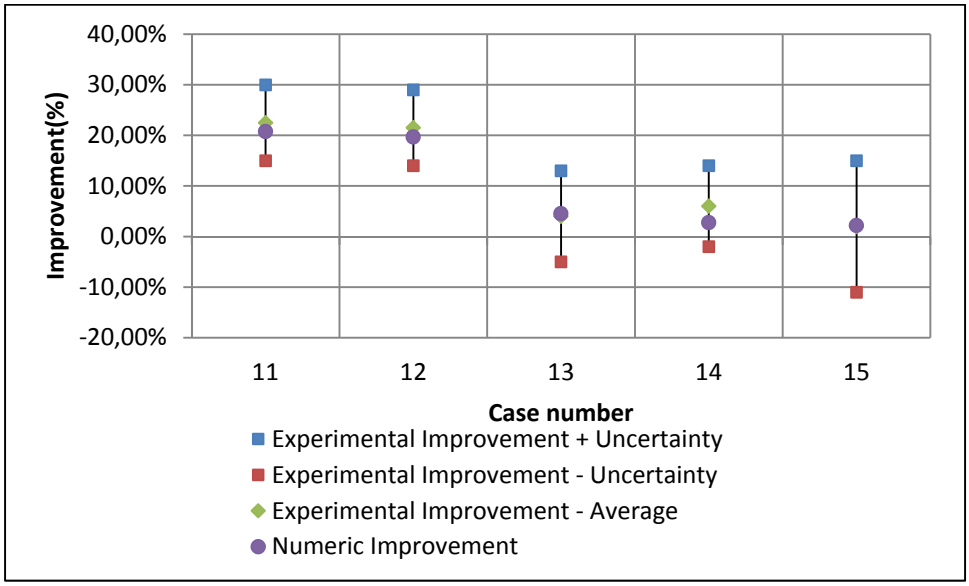

Figure 3.24 Transition improvement numerical vs experimental with uncertainty margins for cases at Mach number = 0.1

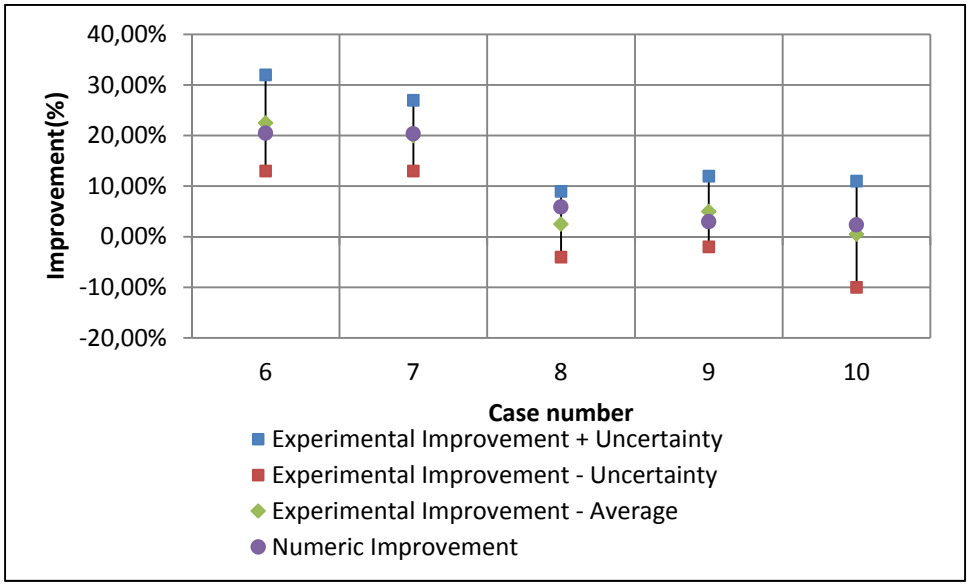

Figure 3.25 Transition improvement numerical vs experimental with uncertainty margins for cases at Mach number = 0.09

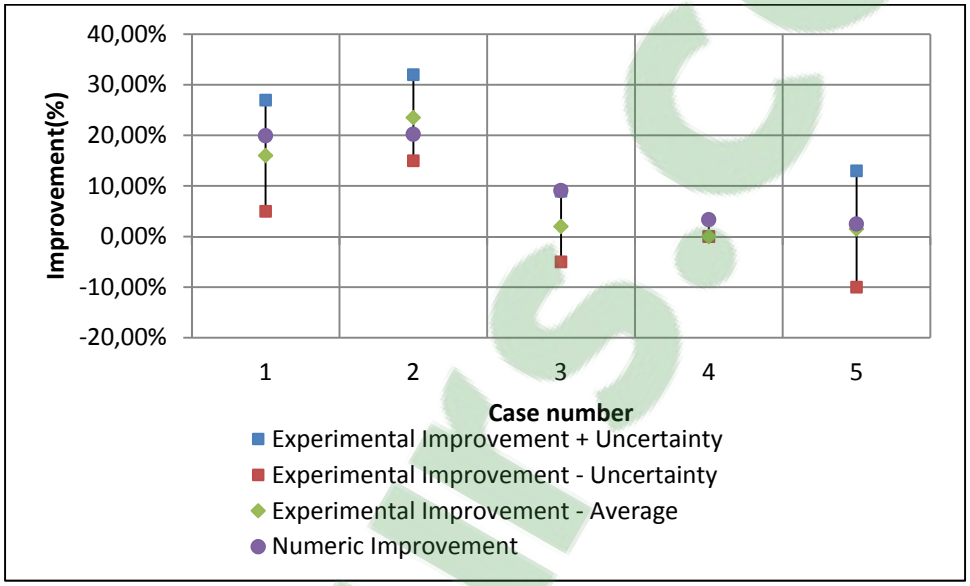

Figure 3.26 Transition improvement numerical vs experimental with uncertainty margins for cases at Mach number = 0.08

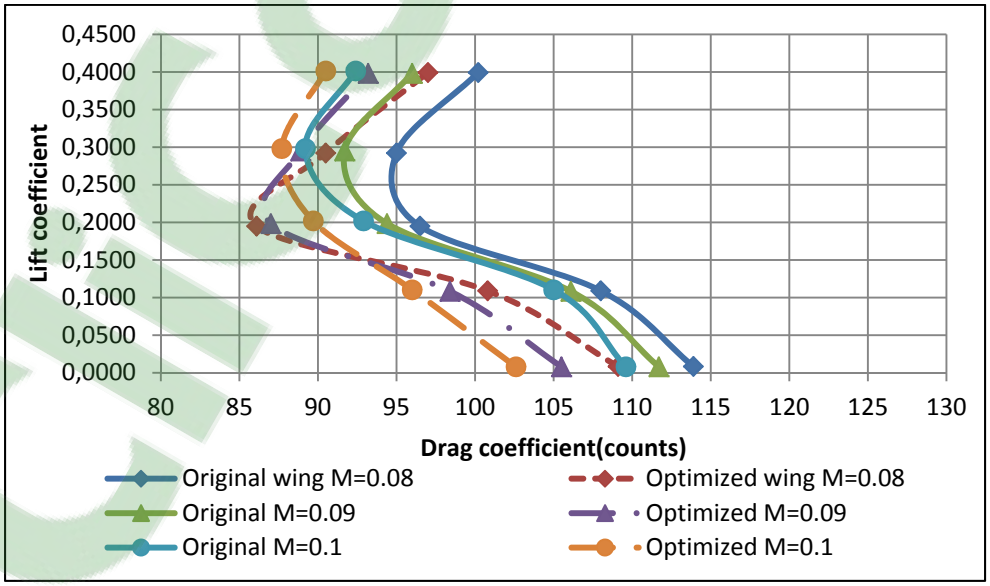

Figure 3.27 Transition improvement numerical vs experimental with uncertainty margins for cases at Mach number = 0.1

Figure 3.27 represents the Lift versus Drag coefficient curve comparison between original and optimized wing models. It is evident that at Mach 0.08 the optimized shape is particularly performing, also that in all cases there is a marked reduction in the drag coefficient. Numerically, the drag reduction varies between 3 and 10% between original and optimized shape, with higher reductions at negative angles of attack.

Finally, for a better understanding of the optimization results, both numerical and experimental, the performances of the original aerofoil were compared with the performances of the optimized shape (obtained from the optimization at a single flight case, Mach number 0.1 and angle of attack 0°). The purpose of this comparison was to show that the optimized shape, although very efficient outside its optimization condition, was not sufficiently performing in order to replace the original aerofoil; and that based on the observed performances of the optimized aerofoil, other optimal shapes should be researched to improve the original aerofoil for as many flight conditions as possible.

It can be seen in Figure 3.28 that the lift coefficient is not affected by the new optimized shape, since the objective was concentrated on the drag and transition and curvature of the aerofoil was not modified.

Figure 3.29 presents the Lift to Drag curve and Figure 3.30 presents the Transition to Drag curves for both original and optimized aerofoils. Both figures were drawn for a range of angles of attack between -5° and 10°. It was observed that the optimized aerofoil has improvements outside the design range at negative angles of attack up to -3° and small improvements at 2° and 3° angles of attack. Above and below these thresholds the optimized shape differs in no way from the original aerofoil performances, with the exception of the negative (-4° and -5°) and very high positive angles of attack (9° and 10°).

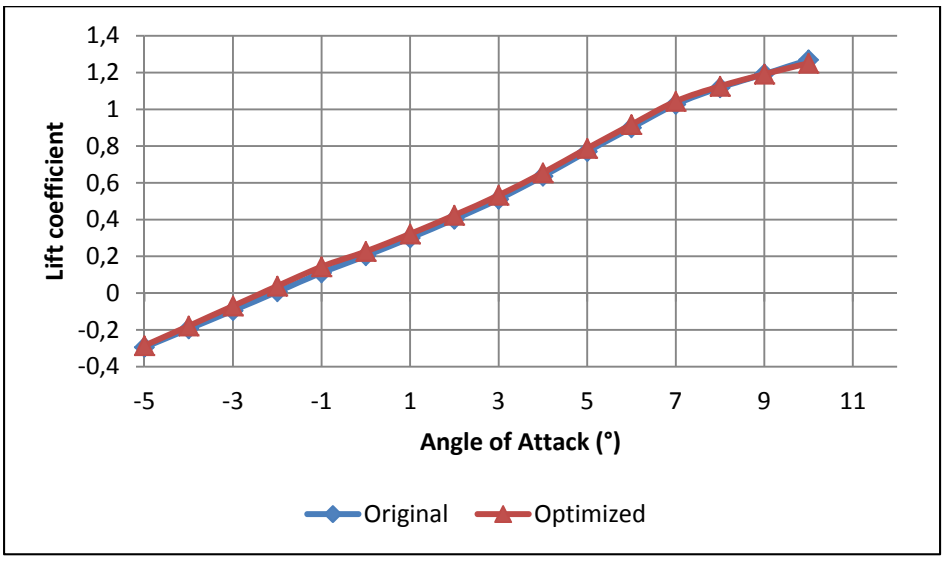

Figure 3.28 Lift coefficient curve comparison between original and optimized wing models for a large range of angles of attack and Mach number 0.1

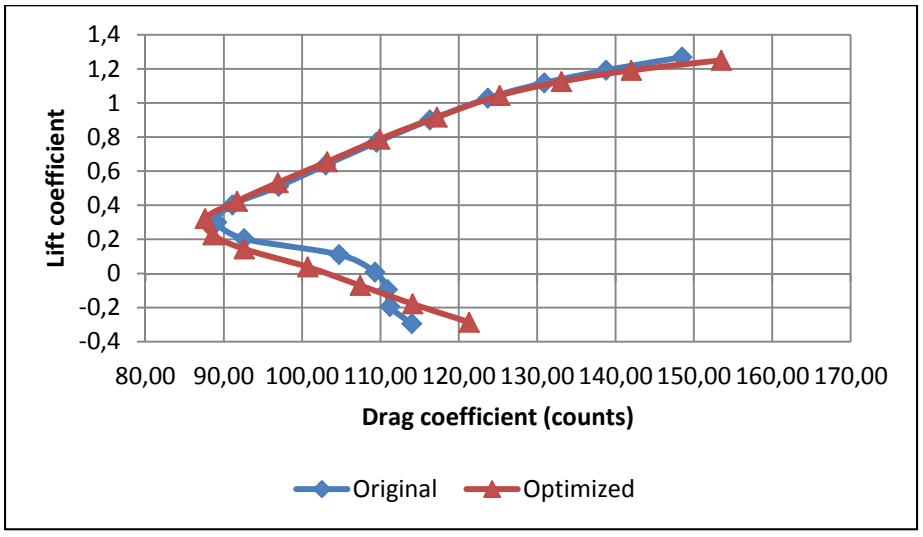

Figure 3.29 Lift-Drag curve comparisons between original and optimized wing models for a large range of angles of attack and Mach number 0.1

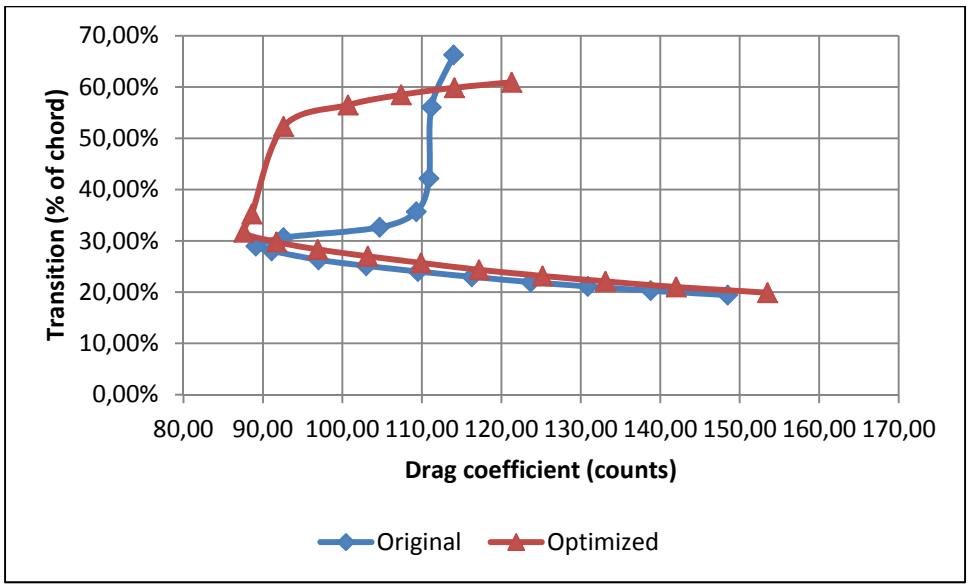

Figure 3.30 Transition-Drag curve comparisons between original and optimized wing models for a large range of angles of attack (-5° to 10°) and Mach number 0.1

These results confirmed that the shape obtained with the genetic algorithm optimization software for Mach number of 0.1 and angle of attack of 0° can be successfully used as an optimal shape for speeds and angles of attack situated in the immediate vicinity of the speed and angle of attack at which the optimization took place. This aspect could be particularly useful when successive maneuvers are done in a short period at small variations of speed and angle of attack values (as for example in the presented cases where the speeds vary between 20m/s and 34 m/s). In these cases, it is sufficient to use a single optimal shape and to morph the wing to another optimal shape when the range of speeds or angles of attack increases beyond a problem-dependent value.

In this case, the optimized aerofoil has obtained improvements for both the angle of attack and speed variation. It is evident from the results presented above, that for the higher angles of attack (more than 1°) the original ATR 42 aerofoil should be optimized for each flight case instead of grouping them in order to maximize the chances of having a high improvement of the transition region and by consequence of the drag coefficient for all flight cases.

3.7 Conclusions

In the present paper, the first phase of a multi-disciplinary project for the development of a reduced scale morphing wing was presented. This first phase concerned the development, testing and validation of an optimization genetic algorithm coupled with the XFoil aerodynamic solver, the development of a composite material and manufacturing of two rigid wing models for wind tunnel testing. The objectives of the paper were to validate, over a range of angles of attack and speeds, the optimized shape of the ATR42 aerofoil for Mach 0.1 angle of attack 0°, to validate the composite material choice for these models in the wind tunnel, to analyse the relationship between the pressure sensors positions and numbers and the accuracy of the readings, and to validate a method for estimating the transition improvement from the pressure data collected during these tests.

The results, presented in Section 3.6.1, have shown that from an aerodynamic point of view an agreement was obtained between the numerical pressure distribution and the pressure distribution measured in the wind tunnel. On the lower surface of the models the agreement was not as good as on the upper surface due to the loss of one of the pressure taps and to the low number of sensors installed. Figures 3.9 to 3.17, which presented a comparison between the pressure distribution for the original shape and the pressure distribution of the optimized shape, demonstrated that the pressure distribution was visibly affected by the skin's small vertical displacements, as the ones used for the optimized shape (less than 3mm).

The results presented in Section 3.6.2 showed the estimation of the transition from experimental data using the second derivative of the pressure coefficient and its comparison with the numerically estimated transition. The results showed that the efficiency of the method depends on the number of sensors on the upper surface and on the step with which they were installed. Better results in the estimation of the transition were obtained for the original shape wing model where the step was varied as function of the numerical prediction (of the transition) compared with the estimations for the optimized shape model for which a

constant step was used. These results have shown that more care should be taken when determining the number and positions of the sensors for a wind tunnel model.

Regardless of these shortcomes, the method was useful for preliminary estimation of the transition region within a certain degree of accuracy, especially when no complex methods and tools are available, where the estimation time is an important variable or the collected data consists to pressure measurements.

The results presented in Tables 3.7 to 3.10 validated the second derivative estimation method of the experimental transition and the optimization of the aerofoil shape used for the optimized wing model. For almost all cases a significant transition improvement was obtained. The average transition improvement was estimated to be at more than 10% of the chord with the maximum achieved being 20% of the chord. The numerically predicted improvement of the drag coefficient was also indirectly validated and the reductions were predicted to be up to 10% of the original values, with the average reduction of the drag coefficient being approximately 3 to 5 %.

The present paper brings a multidisciplinary perspective on the upper surface morphing technique by applying it to a different aerofoil, using an in-house developed genetic algorithm, different from the algorithm that was used in the previous CRIAQ 7.1 project. The optimization technique was validated with experimental testing in the Price-Païdoussis wind tunnel on two rigid wing models with the aim to apply it on an active morphing wing in the second phase of the project. In addition, this paper validates a method for determining the transition region on the upper surface from experimental pressure data and discusses the importance of the pressure sensors positions and numbers for obtaining accurate readings and results. A composite material was optimized, used for the complete manufacturing of each of the wing models and, was validated through wind tunnel testing.

Acknowledgments

We would like to thank Professors Stuart Price and Michael Païdoussis from McGill University for the donation of their blow down subsonic wind tunnel, and Mr. Oscar Carranza and Master's student Manuel Flores Salinas for their dedicated work related to its functioning at the LARCASE laboratory at ETS. We would also like to indicate our appreciation of the work on the composite wing model conducted by Professor Simon Joncas, Master student François Michaud and internship student Robin Calestreme. Thanks are due to the Natural Sciences and Engineering Research Council NSERC for the funds received in the frame of the Canada Research Chair in Aircraft Modeling and Simulation.

CHAPTER 4

DRAG OPTIMIZATION OF A WING EQUIPPED WITH A MORPHING UPPER SURFACE

Andreea Koreanschi Oliviu Şugar Gabor and Ruxandra Mihaela Botez
LARCASE Laboratory of Applied Reasearch in Active Controls,
Avionics and Aeroservoelasticity
École de Technologie Supérieure, 1100 rue Notre Dame Ouest,
Montréal, H3C1K3, Québec, Canada

This article was published in *The Aeronautical Journal,*
March 2016, Vol. 120, No. 1225, pp.473-493, doi: 10.1017/aer.2016.6

Résumé

Le coefficient de traînée et la transition du laminaire à turbulent pour le profil d'un modèle d'aile sont optimisées grâce à un concept de surface supérieure d'aile déformable avec deux points d'actionnement. Les effets de nouvelles formes du profil sur le coefficient global de traînée du modèle d'aile sont également étudiés. Le profil aérodynamique a été optimisé avec un programme `` in-house`` d'algorithme génétique couplé avec une reconstruction de la forme du profil avec la méthode cubique spline et avec XFoil 6.96 solveur aérodynamique open source. L'analyse du modèle de l'aile a été réalisée avec le solveur open source XFLR5, en utilisant une méthode Panel 3D pour le calcul aérodynamique. Les résultats de l'optimisation du profil aérodynamique indiquent des améliorations du coefficient de la traînée et une retard de la transition de 2% à 4% de leurs valeurs initiales. Ces améliorations des caractéristiques aerodynamiques, affectent la traînée globale du modèle d'aile, en la réduisant jusqu'à 2% de la valeur initiale. Les analyses ont été réalisées pour un seul nombre de Reynolds et de la vitesse, sur une plage d'angles d'attaque. Les mêmes cas seront également utilisés dans les tests de soufflerie faite sur le modèle fabriqué d'aile déformable.

Abstract

The drag coefficient and the laminar-to-turbulent transition for the airfoil component of a wing model are optimized using an adaptive upper-surface with two actuation points. The effects of the new shaped airfoils on the global drag coefficient of the wing model are also studied. The airfoil was optimized with an ``in-house`` genetic algorithm program coupled with a cubic spline airfoil shape reconstruction and XFoil 6.96 open source aerodynamic solver. The wing model analysis was performed with the open source solver XFLR5, and using a 3D Panel Method for the aerodynamic calculation. The results of the airfoil optimization indicate improvements of both the drag coefficient and transition delay of 2% to 4% of their original values. These improvements in the airfoil characteristics affect the global drag of the wing model, reducing it by up to 2% of the original value. The analyses were conducted for a single Reynolds number and speed over a range of angles of attack. The same cases will also be used in the experimental testing of the manufactured morphing wing model.

4.1 Introduction

Reducing fuel consumption has become a central concern around the world, due to the detrimental environmental effects as well as the significant costs involved in fuel extraction, transport and consumption (Kwan, Rutherford and Zeinali, 2014; Okamoto, Rhee and Mourtos, 2005). The search for the best solutions to reduce aircraft fuel consumption has therefore captured the attention of industry, academia and government institutions.

Most of the major research projects in the aerospace industry were undertaken by research consortiums, for example the CRIAQ (Consortium for Research and Innovation in Quebec) and the GARDN (Green Aviation Research and Development Network) in Canada, and the Clean Sky project in Europe. There are a high number of other collaborations between aerospace companies and universities throughout the world.

The active modification of the wing geometry, or “wing morphing”, is an example of Green Aircraft Technology. Previously, the only projects that investigated active wing morphing to improve aerodynamic performance (ex., in STOL) were (mostly) limited to military aviation. Some of these projects were applied on the Grumann F-14, which has a varying sweep angle wing design (Navy, 2003), the North American Aviation XB-70 Valkyrie prototype, which uses a 'drooping' wing tip that helped trap the shock wave under the wing between the downturned wing tips and also added more vertical surface to the aircraft to improve directional stability at high speeds (Talay, 1975), and the AFTI/F-111 'Mission Adaptive Wing', which has an advanced supercritical wing design that uses a smooth variable wing camber to change the wing shape (Bonnema and Smith, 1988; Smith and Nelson, 1990).

An extensive bibliographical review of morphing wing projects is presented in (Sofla et al., 2010) and in (Barbarino et al., 2011). Many morphing wing projects, such as those presented by (Bharti et al., 2007; Blondeau, Richeson and Pines, 2003; Shili, Wenjie and Shujun, 2008) in their articles, focused more on the mechanical – structural capabilities of their morphing configurations and less on the aerodynamic gains that can be obtained from these configurations. However, several projects have used numerical analysis, wind tunnel tests or even flight tests to demonstrate the validity of the morphing wing concept from an aerodynamic point of view as well (Diodati et al., 2013; Falcao, Gomes and Suleman, 2011; Gamboa et al., 2009; Secanell, Suleman and Gamboa, 2005). (Pecora, Amoroso and Amendola, 2014; Pecora, Amoroso and Lecce, 2012; Pecora et al., 2011) also discusses, proposes and validates several concepts for morphing trailing edges for future development of wings with adaptive high lift devices.

Due to the time involved in developing and testing morphing wing concepts, some projects have concentrated on UAV wing modifications, as unmanned aerial vehicles started to play a more important role in military and agricultural operations. They are considered safer to research different configurations and the results can be implemented faster than on civil aircrafts (Sugar Gabor, Koreanschi and Botez; Sugar Gabor, Koreanschi and Botez, 2013a; 2013b; Sugar Gabor et al., 2014).

In 2002, the Aerospace Industry Association of Canada, the government of Quebec and key university research centers formed the CRIAQ to encourage mostly civil aviation research. One of their recent projects, called CRIAQ 7.1, was focused on shape changing wings and was realised between Canadian aerospace industry companies, such as Bombardier and Thales, the IAR-NRC Research Center and two universities, the École de Téchnologie Supérieure and École Polytechnique (Botez, Molaret and Laurendeau, 2007; Grigorie et al., 2010a; 2010b).

The purpose of project CRIAQ 7.1 was to prove that controlling the position of the transition point and pushing it towards the trailing edge using shape-changing techniques can reduce the drag coefficient, and implicitly, the fuel consumption (Coutu, Brailovski and Terriault, 2009; Popov, Botez and Labib, 2008; Silisteanu and Botez, 2012). As shown in the obtained results, it is possible to obtain up to 40% laminar flow improvement on a laminar airfoil-based wing model, and at the same time to achieve up to 20% drag coefficient reduction by using active control with smart material alloy actuators (SMA). A subsequent aeroelastic study proved that the morphing technique would not induce flutter phenomena during wind tunnel testing (Courchesne, Popov and Botez, 2010). In addition, many breakthroughs were achieved in active open-loop and closed-loop control using Proportional Integration PI, (Grigorie et al., 2011b; Popov et al., 2010a), and fuzzy logic based controllers in wind tunnel testing, (Grigorie and Botez, 2009; Grigorie, Botez and Popov, 2009; Popov et al., 2010b), under the auspices of this same project.

The research presented here was completed in the frame of the CRIAQ MDO 505 project, an international collaboration between Canadian and Italian industries, universities and research centers. The collaboration is between Bombardier Aerospace, Thales and Alenia Aeronautica on the industry side and École de Téechnologie Supérieure (ETS), École Polytechnique, CNRC, the University of Naples and CIRA on the academic and research institutes side. This project is a continuation of the CRIAQ 7.1 project.

The purpose of the project is to demonstrate the structural, aerodynamic and control abilities of a wing tip equipped with an adaptive upper surface and an adaptive aileron during low speed (subsonic) wind tunnel tests. The novelty of the project consists in the design, analysis and manufacturing of an aerodynamically and structurally optimized real wing tip. For all performed research, the wing tip was isolated from the rest of the wing and therefore it will be named the wing model in the present paper.

The wing model was tested for structural 1g loads, and, during these tests, the composite upper surface and the adaptive aileron were controlled with electrical actuators situated in the wing model and in the aileron boxes.

The present paper addresses the aerodynamic optimization of the airfoil component of the wing model using the adaptive upper surface. The purpose of this optimization is the reduction of the drag coefficient and, for control and visualization purposes in future wind tunnel testing, the extension of the laminar flow regime on the upper surface of the wing model.

The paper is divided into six parts: a review of the CRIAQ MDO 505 project concept, a review of the base airfoil performances, description of the ‘in-house’ developed genetic algorithm method, presentation and discussion of the optimization results for the base airfoil, presentation and discussion of the airfoil’s optimization impact on the wing model’s performances, and conclusions.

4.2 Review of the CRIAQ MDO 505 project concept

The CRIAQ MDO 505 project continues the CRIAQ 7.1 project’s adaptive upper-surface wing concept and adds a real wing-tip structure, structural optimization, new aerodynamic optimization constraints, new control challenges, electrical actuation system and classic and adaptive ailerons.

The full-scale wing model is an optimized structure with a 1.5 m span and a 1.5 m root chord, including its aileron, with a taper ratio of 0.72 and a leading edge sweep of 8°.

The wing model box and internal structure is manufactured from aluminium with the composite adaptive upper surface extending from 20% to 65% of the wing model chord. The adaptive upper surface (skin) is specifically designed and optimised for this project as a carbon composite skin. The actuators are also specifically designed and manufactured to the project requirements. Four electric actuators are installed on two actuation lines, fixed to the center ribs and to the composite skin. Each actuator is capable of independent action. On each line the actuators are situated at 32% and 48% of the chord. These actuator positions were selected after analysing several other possibilities. From the analysis it was observed that positioning the actuators at equal distances from the ends of the composite skin returned the best results in term of airfoil optimization. These actuator positions also represent the optimization points used during aerodynamic optimization. The aileron's articulation is situated at 72% of the chord. Figure 4.1 presents a sketch of the wing model concept.

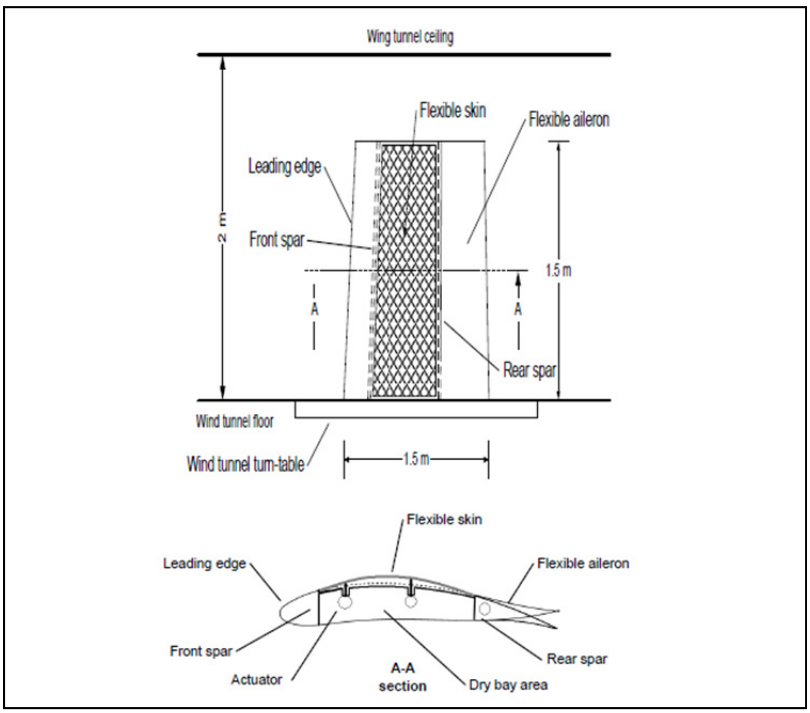

Figure 4.1 CRIAQ MDO 505 Wing-tip concept sketch

4.2.1 Base airfoil performances

The airfoil (base airfoil), on which the wing model is based, was provided by one of the industrial partners and is a modified version of a supercritical airfoil. Figure 4.2 presents the base airfoil in non-dimensional coordinates.

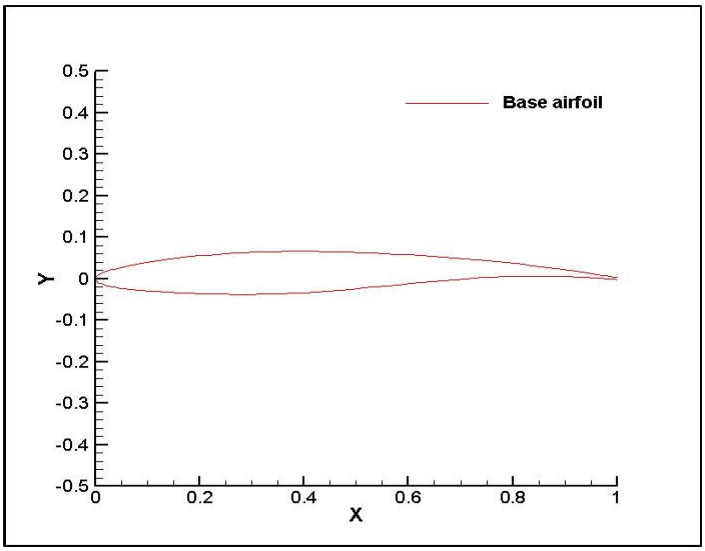

Figure 4.2 Base airfoil

The base airfoil performance was evaluated with XFoil 6.96, an aerodynamic solver that is used for all airfoil analyses throughout this paper. XFoil was developed by (Drela and Youngren, 2001) and was chosen to be used in this paper because of its precision, effectiveness and rapid convergence. It is a solver that permits both inviscid and viscous analyses as well as geometrical modification of the airfoil. The inviscid calculation is performed with a linear vorticity stream function panel method (Drela, 1989b), to which a Karman-Tsien compressibility correction is added, allowing for good subsonic flow prediction. For its viscous calculations a two-equation lagged dissipation integral boundary layer formulation (Drela, 1989a) is used, which incorporates the e^n transition criterion (Drela, 2003). The flow in the boundary layer and in the wake interacts with the inviscid potential flow by means of a surface transpiration model.

Figure 4.3 presents the pressure distribution results for the base airfoil, for an angle of attack range between -3 and 3 deg, at Mach 0.15 and a Reynolds number of 2.15E+06.

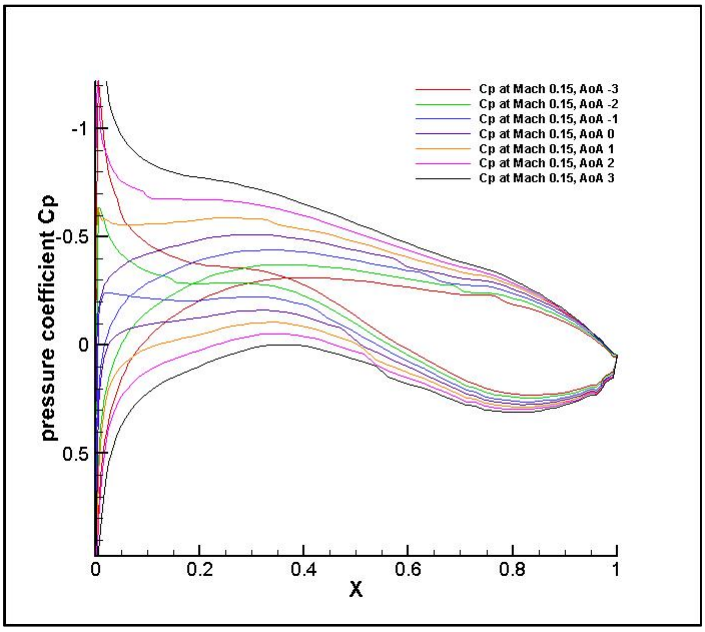

Figure 4.3 Pressure distributions for Reynolds number of 2.15E+06

4.3 Optimization algorithm

An 'in-house' genetic algorithm software was developed to optimize the base airfoil's drag and transition. The genetic algorithm was chosen because of its ability to give a great number of possible solutions and obtain a global optimum in each case.

A genetic algorithm is a meta-heuristic method inspired from the process of natural selection. It is an iterative method that necessitates a high number of individuals and several generations to achieve its convergence; both the number of individuals and the number of generations are problem-dependent.

In a simple version of a genetic algorithm, a first generation of individuals, represented by their genes, is created randomly. The genes that represent each of the individuals are chosen

based on their abilities to change at each generation, towards attaining the proposed objective. The first random generation is evaluated, and then a fitness value is associated with each individual. The fitness value is based on the results obtained from comparison with the objective requirements. Random individuals are then chosen as parents based on their fitness values. Through a simple mixing of their genes (with the simplest method being that of associating 50% of the genes from each parent to the children) new individuals are created. The sum of the new individuals forms a new generation. The process is repeated until a certain number of generations have passed or until the fitness value has reached a user-imposed limit (Coley, 1999; Mitchell, 1998; Whitley, 1994).

In the 'in-house' version of the algorithm, the individuals are represented by airfoils and the genes that characterise them are the vertical displacements of the actuators situated at 32% and 48% of the chord. The fitness value of each individual airfoil is calculated from a fitness function based on its aerodynamic performances. A first version of this 'in-house' genetic algorithm was used in (Sugar Gabor, Koreanschi and Botez, 2012).

Figure 4.4 presents the logic flow diagram of the genetic algorithm used for the airfoil optimization.

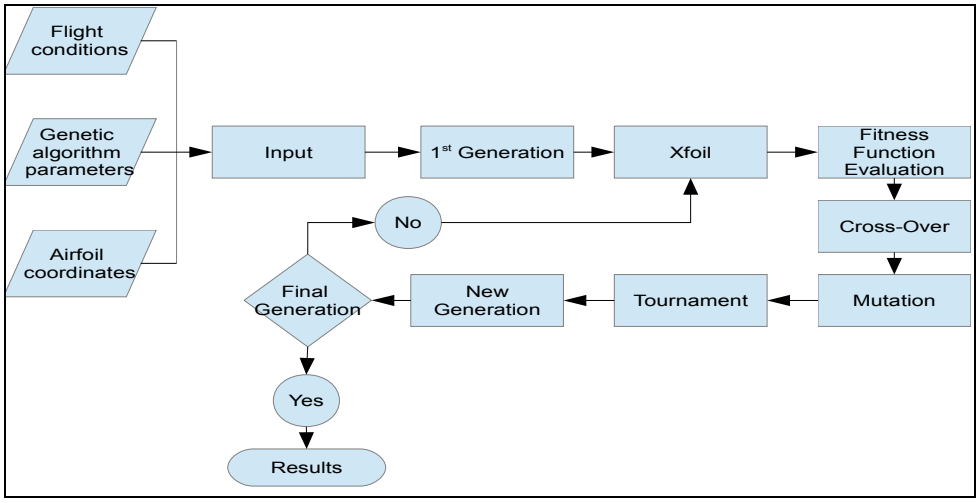

Figure 4.4 Logic flow diagram of the genetic algorithm coupled with XFoil

The aerodynamic performances are evaluated with XFoil 6.96 and are represented by the lift coefficient, C_l, the drag coefficient, C_d, the transition position and the skin friction coefficient variation with the chord, C_f. Based on these characteristics and the behaviour to be improved, single objective functions were developed and grouped in a fitness function to allow the selection of more than one objective if desired. The functions were developed on the most desired objectives encountered for airfoil optimization, for example: delaying transition for a more laminar flow on the upper surface, minimization of the drag coefficient or maximizing or minimizing the lift in case of optimization of a multi element airfoil:

$$F_f = w_1(C_{l\_m} - C_{l\_o}) + w_2 \frac{C_{l\_m}}{C_{l\_o}} + w_3 C_l + w_4 \frac{C_l}{C_d} + w_5 \frac{1}{C_d^{\,2}} + w_6 \frac{Tr}{C_d} + w_7 Tr + w_8 \frac{1}{Tr} + w_9 C_f \tag{4.1}$$

where the values of w_i represent the weight associated with the searched-for aerodynamic characteristic. The weights are chosen by the user based on the importance attached to each aerodynamic characteristic it wants to optimize. The weights can have positive or negative values, but the sum of all the weights in the fitness function should not exceed the absolute value of 100, which corresponds to attaching 100% importance to an objective in detriment of the others.

Although, some of the objective functions might seem to be redundant, actually they explore different behaviour combination. For example, if a double objective of maximizing lift and minimizing drag is searched, one can either work with two objective function, giving them weight based on the importance attached to both lift and drag or the user could choose one objective function that contains both terms, thus giving them equal value or letting the optimization program to find the best combination of lift and drag.

To analyze, XFoil needs the airfoil coordinates, but the optimization algorithm only returns the vertical displacements of the points where the actuators are situated. As such, a

reconstruction method that enforces a tangency condition as well as an iso arc-length condition is necessary for the upper surface of the airfoil (between 20% and 65% of the chord, corresponding to the flexible skin); the other coordinates are kept identical to those of the base airfoil. The reconstruction is incorporated in the optimization algorithm.

Several different parameterization techniques have been developed and applied over the years for airfoil design, such as the polynomial representation (Abbott and Von Doenhoff, 1959), the CST method created by (Kulfan and Bussoletti, 2006), and Non-Uniform Rational B-Splines (Piegl and Tiller, 2012). However, these methods, either parameterize the complete airfoil, thus are not able to represent only a limited part of it, or they are difficult to implement when only the reconstruction of a specific part is required, and they are not judged sufficiently time-efficient to solve our problem here presented. Therefore, spline functions, (Berbente, Mitran and Zancu, 1997; McKinley and Levine, 1998) were selected for the reconstruction of the upper surface of the wing model airfoil.

The most-known spline interpolation is the "cubic spline", which ensures continuity up to and including second-order derivatives, and which allows for the calculation of the curvature radius. (Fincham and Friswell, 2015) use a cubic spline interpolation for their morphing trailing edge system in their paper.

The cubic spline is represented by the third-degree polynomial:

$$P_{3,i}(x) = y_i + m_i(x - x_i) + b_i(x - x_i)^2 + a_i(x - x_i)^3 \tag{4.2}$$

which describes the behavior of the splines at each interval h_i (eq.4.2).

The parameters a_i and b_i are functions of the slope m_i calculated in each node i. The slope is the solution to the tri-diagonal linear system:

$$\rho_i m_{i-1} + 2m_i + \lambda_i m_{i+1} = d_i,\ i \in \overline{2,(N-2)} \tag{4.3}$$

where,

$$\rho_i = \frac{h_i}{h_{i-1}+h_i},\ \lambda_i = 1-\rho_i,\ d_i = \frac{3\lambda_i(y_{i+1}-y_i)}{h_i} + \frac{\rho_i(y_i-y_{i-1})}{h_{i-1}} \tag{4.4}$$
$$h_i = x_{i+1} - x_i;$$

to which we add relations that replace the continuity conditions for the first and second derivatives that cannot be imposed on x_N. These conditions could either be imposed as values for the end slopes m_1 and m_N, or they could be given in a more general form, through relations with their neighboring slopes.

For our problem, we have chosen to add the continuity conditions in a more general form, through relations with their neighboring slopes, using a particular case of the cubic spline interpolation, that is the "natural cubic spline interpolation", and which is defined by the following conditions at the ends xi:.

$$P''(x_1) = P''(x_N) = 0; \tag{4.5}$$

By replacing eq. (4.5) in eq. (4.3) we obtain the following linear system for the end slopes, m_1 and m_N:

$$\begin{cases} 2m_1 + m_2 = 3\dfrac{y_2 - y_1}{h_1} \\ m_{N-1} + m_N = 3\dfrac{y_N - y_{N-1}}{h_{N-1}} \end{cases} \tag{4.6}$$

By imposing these conditions, the following integral is minimized:

$$I = \int_{x_1}^{x_N} [\, f''(x)\,]^2 \, dx \tag{4.7}$$

where *f(x)* is the exact function that is approximated by the spline interpolation. Minimizing the above integral by imposing the natural conditions (eq. 4.5) produces the smoothest cubic spline interpolation; therefore, this type of interpolation is chosen to reconstruct the airfoil shapes.

After the reconstruction of the airfoils, based on the vertical displacements of the actuation points and analysed with XFoil, they (the airfoils) are evaluated with the fitness function. Based on their results, they are graded between 1 and 10, where 10 is the grade given to the best airfoil.

The next generation of airfoils is created from the present one, with each airfoil in the current generation having at least one chance at being selected as parent.

To ensure that the choice of the parents is random, and thus to give the most chances to those airfoils with higher grades, a probability function[10] was created, which returns values between 1 and 10.

$$P_S = 11 - \max(\min((\mathrm{int}(random(0) \cdot 10^{\frac{1}{A_t}}))^{A_t}, 10), 1) \tag{4.8}$$

The obtained value is then compared with the grades of each airfoil, and those grades that match it are grouped. From this group one airfoil is randomly chosen as 'parent'. The process is repeated for a number of times that is equal to the number of parents used to create the new airfoil. In our case, we used the classical approach of one 'mother' and one 'father'.

---

[10] The Probability of Selection function uses a random function, which permits the alleatoar choice of a number in the [0,1] range.

When all the parents are chosen, they are passed through the cross-over and mutation processes (Herrera, Lozano and Verdegay, 1998). The ‘cross-over routine’ used has a two-steps approach. For the first 10 generations, the genes of the parents are mixed in equal proportions. This first step hastens the convergence process and leads the optimization towards the global optimum area. The second step, applied for the remaining number of generations, is a cross-over function derived from a simulated binary cross-over technique (Deb and Agrawal, 1994) coupled with a ‘random number generator’ function.

$$
\begin{aligned}
&random(0)\\
&if\,(random(0) >= 0.5)then\\
&child = 0.5\cdot(1+random(0))\cdot parent1\\
&else\\
&child = 0.5\cdot(1+random(0))\cdot parent2\\
&endif
\end{aligned}
\tag{4.9}
$$

This second step is used to pinpoint, as accurately as possible, the best solution from the multitude of solutions found in the global optimum area.

Each new airfoil in each generation is passed through a ‘mutation routine’ in which, based on the probability of occurrence (which is a value introduced by the user – 0.1% from the individuals in a generation in our case), is affected by gene mutation.

The mutation process, if it occurs, depends on the amplitude of mutation (also user-dependent) which in turn depends on the value to be mutated. The amplitude of mutation is usually a small percentage (2% in this case) of the gene’s values, resulted after cross-over.

From mutation, the new airfoils are passed through a verification process. Here, are verified the conditions related to actuator’s maximum and minimum displacements and delta values between the actuator displacements. The conditions are derived from multidisciplinary work, as they are provided from aerodynamic, structural and control calculations and limitations.

If an airfoil fails the requirements, the selection, cross-over and mutation processes are reiterated until a valid airfoil is obtained. If a certain number of iterations (10000 is the value imposed for this specific problem) have passed without yielding valid results the optimization process stops.

Under normal conditions, the processes of selection, cross-over, mutation and verification are repeated for each pair of parents until a fixed number of airfoils in a generation is reached. This number of airfoils (also referred as generation) is set by the user at the beginning of the optimization process.

The complete process of reconstruction, analysis and evaluation is repeated until the maximum number of generation is reached.

To improve the overall convergence of the optimization process a tournament is introduced. A tournament takes place after the current generation is analysed and graded and before the creation of the new generation. The tournament compares the worst airfoils from the current generation with the best ones from the previous generation and replaces the former with some of the latter, thus favoring the propagation of good genes from the older generation to the current and then on to the future generations.

This tournament process hastens the convergence of the optimization and for our problem of optimizing a specific part of the airfoil it reduces the number of generations from 40 to 20 and the number of airfoils in a generation from 50 to 40.

4.4 Optimization results for the base airfoil

The concept of an adaptive upper-surface wing model and the optimization program were described in sections 4.2 and 4.3. The adaptive upper surface extends from 20% to 65% of the chord and its length remains unchanged. The actuators are situated at 32% and 48% of

the chord and their displacements are limited to +/- 5 mm each, while the difference between the displacements of the actuators is limited to 6 mm.

The aerodynamic analysis was carried out for a speed of 51 m/s, equivalent to Mach 0.15 at sea level, and Reynolds number of 2.1E+06 with the airfoil chord as the reference length. The angles of attack analysed with XFoil are local angles of attack, which are calculated for the specific area of the wing model where the actuator line is situated.

In this optimization, the delay of the transition on the upper surface is chosen, in order to obtain a more laminar flow, and only one objective function was used– transition. It was chosen because a side effect of delaying transition and creating a more laminar flow is the reduction of the drag value. Of course, any of the three objective functions that contain either drag, transition or both could have been chosen, as all will return an optimized airfoil that is in the global optimum area, but since the main objective was transition delay, the transition function was chosen as the fittest for the problem

$$F_f = w_7 Tr \tag{4.10}$$

where all other weights from eq.(1) are considered 0.

The optimization process is done for each flight case, and for each case a different optimized shape is obtained.

Table 4.1 presents the cases analysed for Mach number equal to 0.15 and the optimum actuators displacements obtained with the optimization algorithm for each case (local angle of attack and corresponding global wing model angle of attack).

Table 4.1 Analysed cases – actuator displacements

Local AoA (°)	Wing model global AOA (°)	D1 (mm)	D2 (mm)
-1.6	-0.5	-2.13E+00	-1.61E+00
-1.5	-0.25	-1.26E+00	-3.33E-01
-1.3	0	-2.23E+00	-1.96E+00
-1.2	0.25	-2.17E+00	-1.84E+00
-1	0.5	-1.48E+00	-1.05E+00
-0.9	0.75	-2.19E+00	-1.90E+00
-0.7	1	-2.11E+00	-1.74E+00
-0.5	1.25	-1.63E+00	-1.40E+00
-0.4	1.5	-1.88E+00	-2.06E+00

Figure 4.5 presents the comparison between the shapes obtained with the optimization algorithm for 4 generations (5th, 10th, 15th and 20th which is also the final) and the base airfoil.

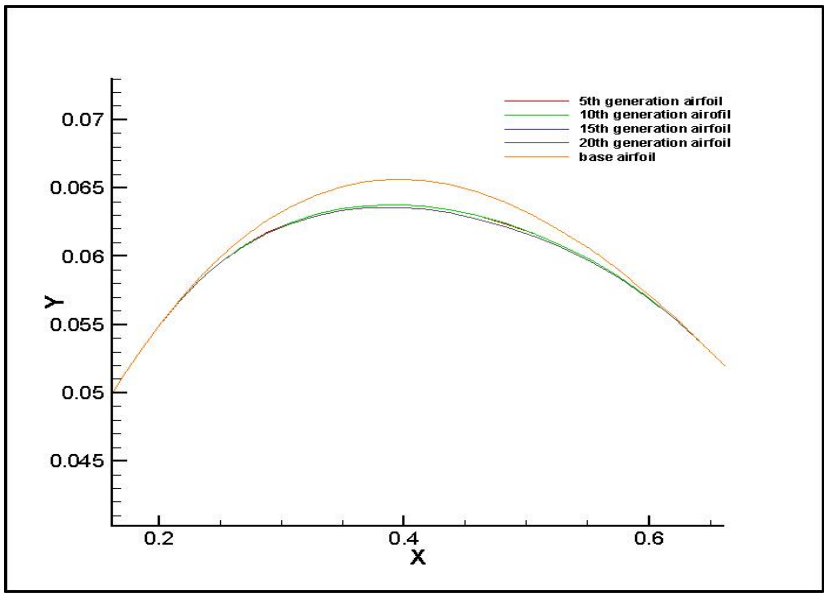

Figure 4.5 Comparison between the optimized airfoil shapes and base airfoil at Mach number of 0.15 and wing model global angle of attack α= 0°

Figures 4.6 to 4.9 present the results expressed in terms of lift coefficient (Cl) vs global angle of attack, drag coefficient (Cd) versus lift coefficient, transition point versus global angle of attack and transition point versus drag coefficient (Cd), respectively, as comparisons between the base and optimized airfoil results.

For the angles of attack where the flow is completely attached the weight w_1 was set to one, w_2 was set to zero and the constraint on the lift is ignored. For angles of attack with detached boundary layer, the weight w_1 was set to zero, w_2 was set to one, and all constraints are considered active.

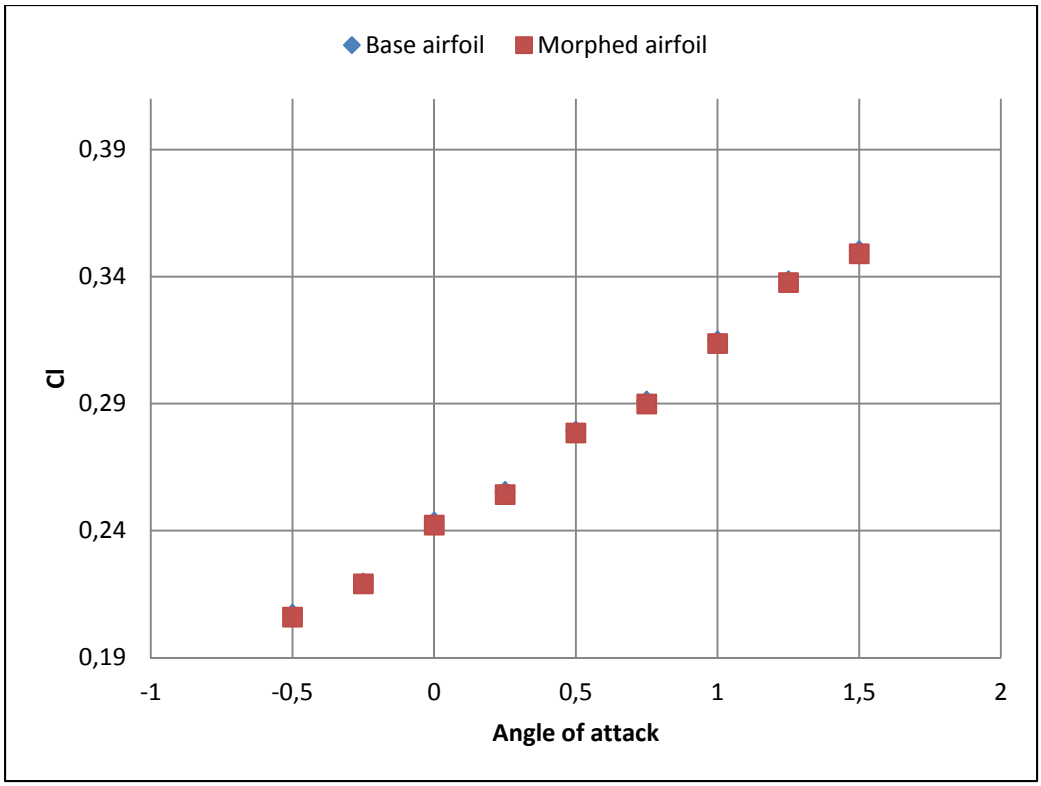

Figure 4.6 Lift coefficient vs global angle of attack

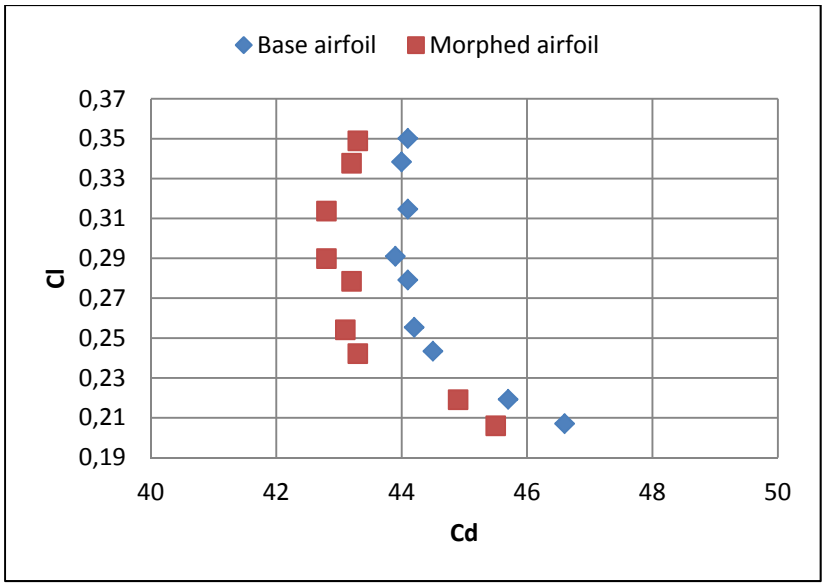

Figure 4.7 Drag coefficient vs lift coefficient

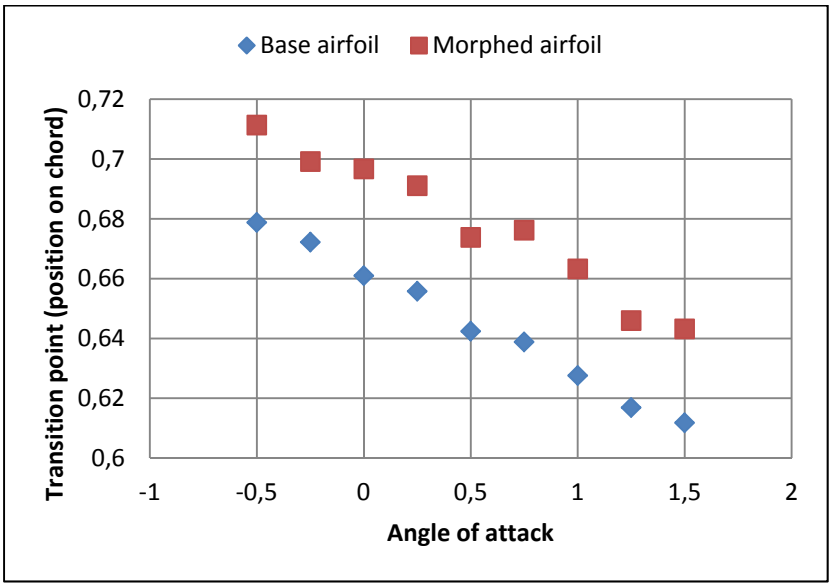

Figure 4.8 Transition point vs global angle of attack

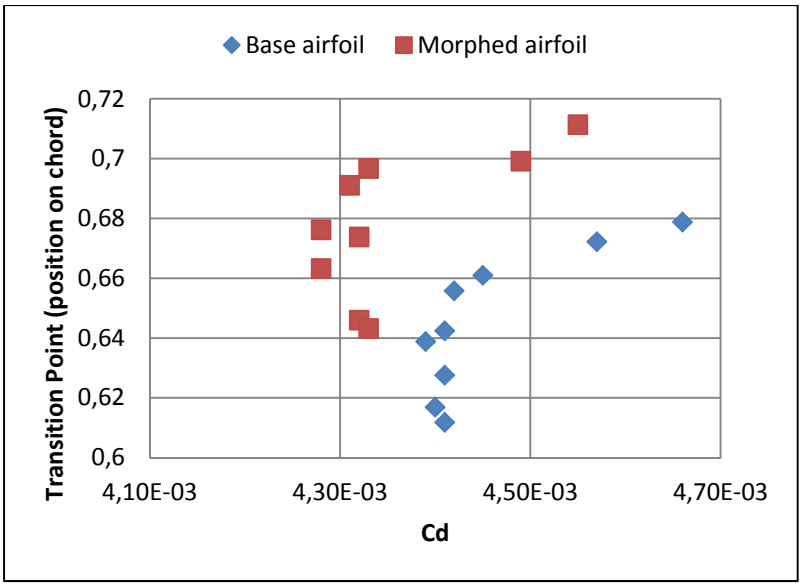

Figure 4.9 Transition point vs drag coefficient

Since the objective of the optimization was not the improvement of the lift coefficient and the modifications did not affect the overall curvature of the airfoil, figure 4.6 confirms that there is no change in the values of the lift coefficients for any of the morphed results. From figures 4.7 to 4.9, it can be deduced that the objective of optimizing the airfoil for drag coefficient and delay of the laminar flow transition was attained, and figure 4.10 shows the drag reduction versus the global angle of attack. The average drag coefficient reduction is approximately 2.3% for the nine cases here presented, while the average transition delay is approximately 3.3% for the same cases.

The reduction is calculated as the relative error between the morphed and the base airfoils:

$$\varepsilon = \frac{(C_{d\_m} - C_{d\_o})}{C_{d\_o}} \cdot 100 \tag{4.11}$$

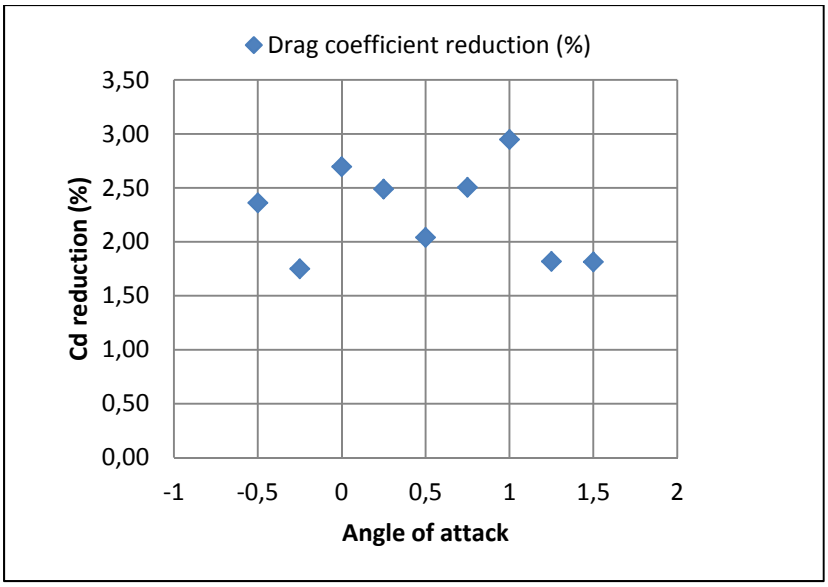

Figure 4.10 Drag coefficient improvements

4.5 Airfoil optimization impact on wing model performances

To fully understand the impact of the results obtained on the airfoil optimization, an analysis of the wing model, with its geometry based on the optimized airfoils, is done using the XFLR5 code, (Deperrois, 2015). XFLR5 is an analysis tool for airfoils, wings and airplanes operating at low Reynolds numbers. It includes XFoil's direct and inverse analysis capabilities, as well as wing design and analysis capabilities based on Lifting Line Theory (Sivells and Neely, 1947), the Vortex Lattice Method (Maskew, 1987) and the 3D Panel Method (Katz and Plotkin, 1991).

For the XFLR5 analysis of a wing there are three steps to be followed:

1. Analysis of the airfoil(s) composing the wing using a multi-threaded batch analysis, which allows the analysis of multiple airfoils at a specific speed over a range of Reynolds Numbers, ranges of angles of attack, using XFLR5's XFoil section.
2. Construction of the wing model, based on the airfoil(s) analysed in the previous step. This step requires the number of sections (minimum 2 – root and tip sections), the span and chord dimensions for each section and, if present, the offset (m), dihedral

and twist angles. Finally, the wing model needs the total number of panels required for the calculations in each direction for each section.

3. Analysis of the wing model using one of the following methods: Lifting Line Theory, the Horse-shoe Vortex Lattice Method, the Ring Vortex Lattice Method or the 3D Panel Method.

For the present analysis, the airfoils are the base airfoil and the airfoils resulted from the optimization process for each case. The wing model is created from four sections: sections 1 and 4, representing the root and the tip of the wing model -- the corresponding airfoil is the base airfoil; and sections 2 and 3, which represent the actuator lines in the span length -- the airfoils corresponding to them are the optimized airfoils, specific for each studied flight case. Figure 4.11 presents the wing model for one flight case as it is created using XFLR5.

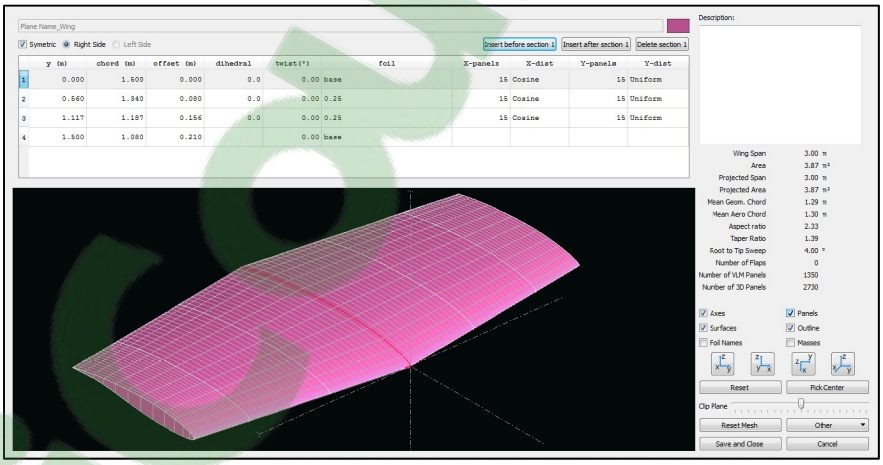

Figure 4.11 Wing model definition in XFLR5 for Mach 0.15 and angle of attack 0.25°

The analysis was done at the Mach number of 0.15 over the same range of global angles of attack as the optimized airfoils, using the 3D Panels Method option for aerodynamic analysis. The 3D Panel Method was chosen because the other methods were considered as insufficiently accurate for the analysis. The Lifting Line Method works only for wings with aspect ratio greater than 4, while this wing model has an aspect ratio of 2.9. The Vortex Lattice Method reduces the body to a middle surface with zero thickness, which eliminates

the notions of upper and lower surfaces and returns only the difference between upper and lower surfaces pressure coefficients. The 3D Panel Method takes into account the three-dimensional geometry surface, and gives more detailed results for the studied geometry.

Figures 4.12 to 4.14 present the global reduction of the drag coefficient as indicated in the global CD versus lift coefficient, viscous CD versus lift coefficient and inviscid CD versus lift coefficient graphs, for the original and morphed (optimized) wing model.

$$C_{D\_total} = C_{D\_viscous} + C_{D\_inviscid} \tag{4.12}$$

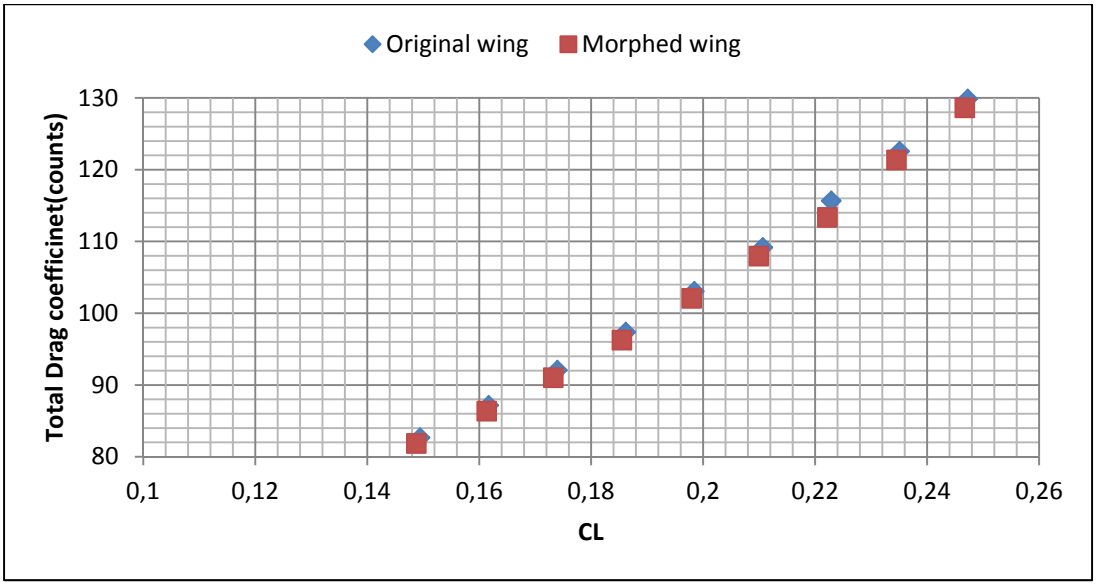

Figure 4.12 Wing model total drag coefficient versus Lift coefficient for Mach 0.15

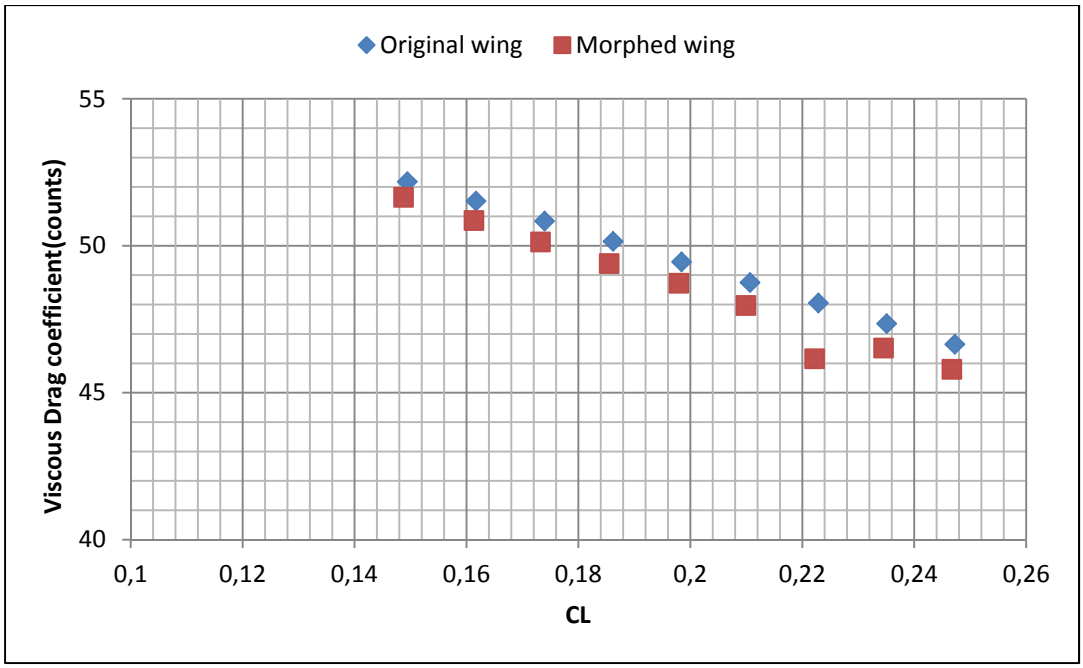

Figure 4.13 Wing model viscous drag coefficient vs Lift coefficient for Mach 0.15

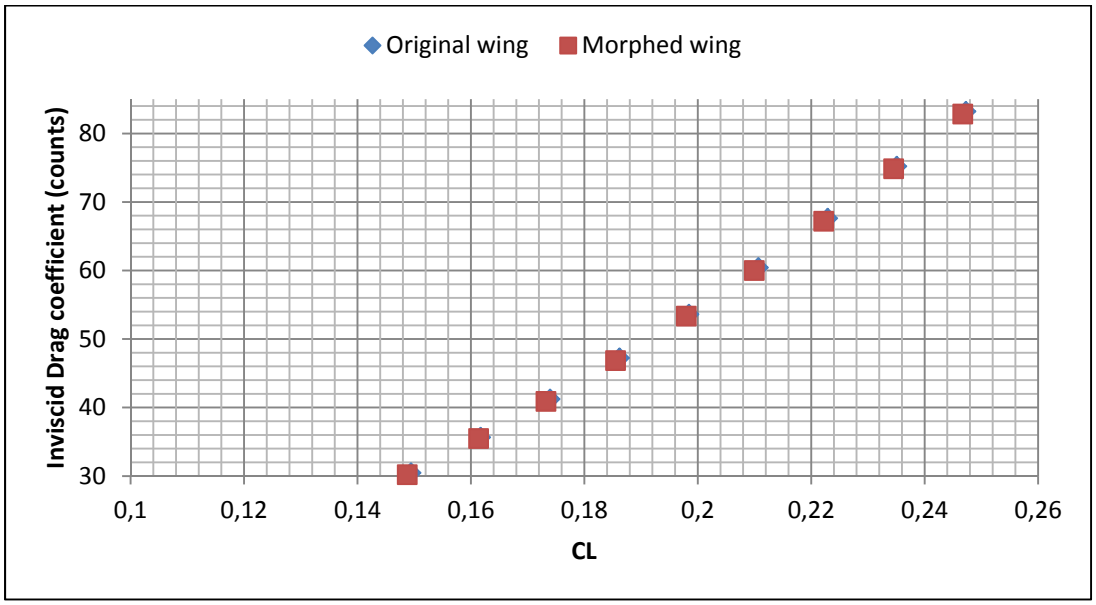

Figure 4.14 Wing model inviscid drag coefficient versus Lift coefficient for Mach number = 0.15

Table 4.2 shows the values of the global and viscous drag and the global drag reduction for Mach number of 0.15 and each angle of attack. The drag is presented in counts, where one drag count is equal to 10^{-4}.

Table 4.2 Total wing model's drag coefficient improvement

AoA (°)	Base wing model		Morphed wing model		Reduction = [(Cd_m - Cd_o)/Cd_o]*100
	C_d viscous	C_d total	C_d viscous	C_d total	
-0.5	52.18	82.66	51.65	81.87	-0.95
-0.25	51.52	87.18	50.86	86.37	-0.92
0	50.84	92.08	50.13	91.03	-1.14
0.25	50.15	97.38	49.4	96.27	-1.13
0.5	49.45	103.07	48.73	102.09	-0.95
0.75	48.75	109.17	47.97	107.97	-1.09
1	48.05	115.67	46.16	113.36	-1.99
1.25	47.35	122.57	46.52	121.38	-0.97
1.5	46.65	129.87	45.8	128.64	-0.94

Figures 4.15 to 4.17 present the span distribution of the profile drag for each case analysed, showing the difference between the original and the morphed wing model's. The profile drag is the most affected by any modification in the airfoil shape. Here, it is presented in counts, where one count represents 10^{-4}.

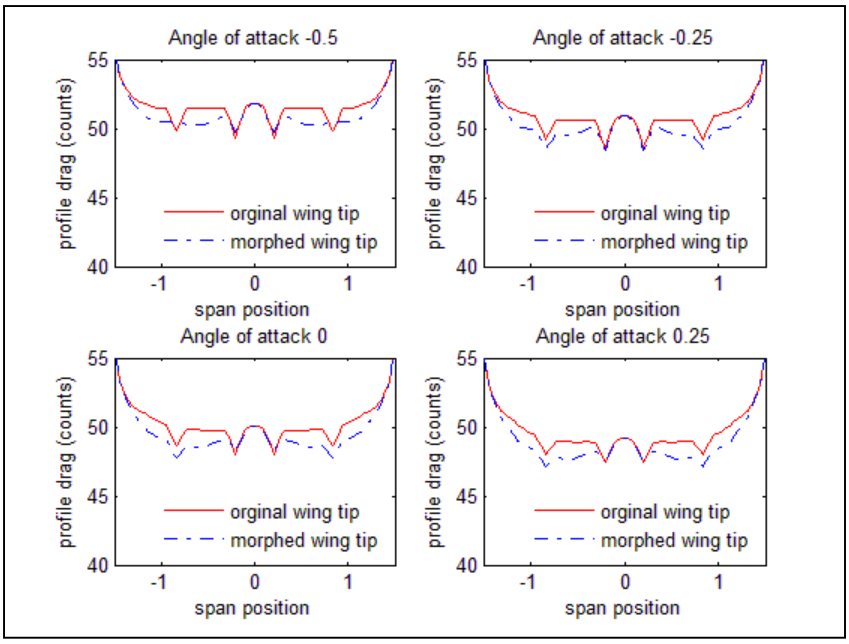

Figure 4.15 Profile shape drag vs wing model span – Angles of attack -0.5 to 0.25

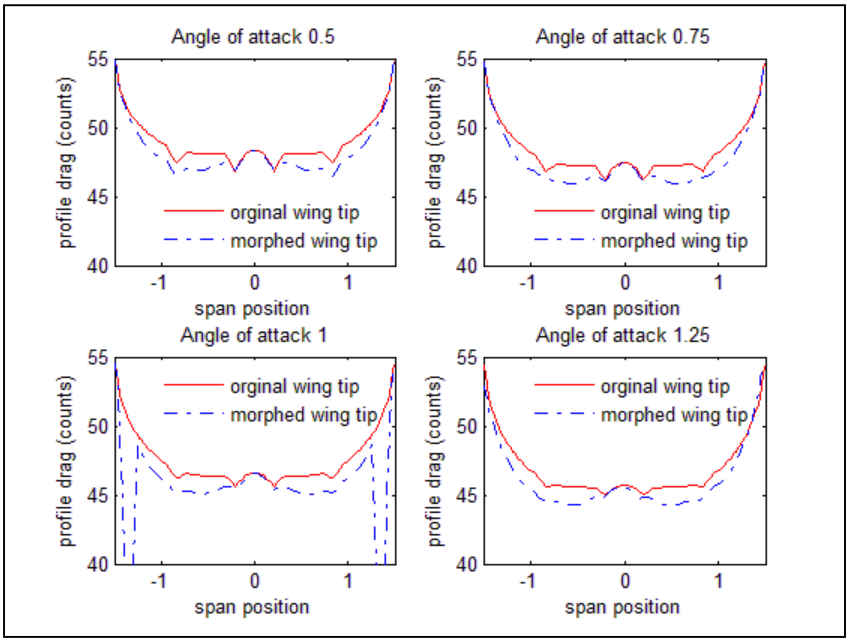

Figure 4.16 Profile shape drag vs wing model span – Angles of attack 0.5 to 1.25

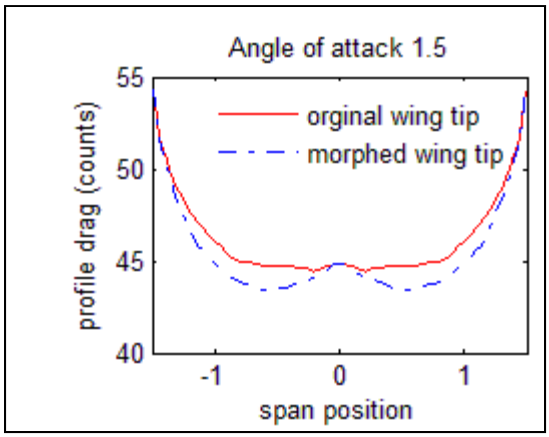

Figure 4.17 Profile shape drag vs wing model span – Angle of attack 1.5

The figures presented above show that even though the morphing area is situated only in the space between the spars of the wing model and the displacements are quite small, an overall wing model drag improvement takes place for all of the studied cases.

Each case shows that the main reduction is concentrated in the region between the actuation lines, which are situated at 0.56 m and 1.117 m along the span as presented in section 4.2 of this paper.

An exception is the case corresponding to Mach number of 0.15 angle of attack α equal to 1° where a numerical error appears which affects the value of the drag coefficient in small measure. Most probably the reduction is less than 2%, but as the trend shown in Figure 4.16 left lower corner is similar to the others it can be assumed that there is an approximately 1% reduction for it as well.

4.6 Conclusions

This paper has indicated how the shape optimization of the airfoil component of a wing model can be achieved using an adaptive upper surface approach. The goal was to conduct single-point optimization of the drag characteristics of the airfoil and to analyze its effects on

the overall wing model drag characteristics. To achieve this objective, an optimization routine was developed, based on a genetic algorithm and coupled with the XFoil 6.96 solver for the aerodynamic analysis of the resulted optimized airfoils. Several constraints were taken into account, based on an aerodynamic – structural – control multidisciplinary optimization approach.

The results revealed that a delay in the transition of the laminar flow over the airfoil upper surface can be achieved with small displacements of -2 mm, as well as the reduction of the drag coefficient of the airfoil component. To evaluate the impact of these improvements on the wing model, the wing model performance was analyzed using the open-source solver XFLR5, utilizing the 3D Panel Method incorporated in XFLR5. The results show a reduction of the drag coefficient of up to 2% from the original wing model shape, and figures 18 to 26 show that this improvement mainly comes from and is concentrated in the morphing region of the wing model, between the two actuation lines. Overall, airfoil optimization has proven its utility, and in particular, the laminar flow behaviour of the boundary layer is improved, as shown in figures 4.8 and 4.9. Further studies of the morphing wing model will include the introduction of an adaptive aileron and the combined optimization of adaptive upper surfaces and adaptive aileron for various objectives.

Acknowledgments

We would like to indicate our appreciation for the financial support obtained in the framework of the CRIAQ MDO-505 project and for the implication of our industrial partners Bombardier Aerospace and Thales Canada. We also wish to thank NSERC for their support.

Special thanks are dues to our collaborators and leaders in this project: Mr. Patrick Germain and Mr. Fassi Kafyeke from Bombardier Aerospace, Mr. Philippe Molaret from Thalès Canada and Mr. Eric Laurendeau from École Polytechnique.

CHAPTER 5

FLUTTER ANALYSIS OF A MORPHING WING TECHNOLOGY DEMONSTRATOR: NUMERICAL SIMULATION AND WIND TUNNEL TESTING

Andreea Koreanschi, Mehdi ben Henia, Olivier Guillemette, Francois Michaud, Yvan Tondji, Oliviu Şugar Gabor, Ruxandra Mihaela Botez and Manuel Flores Salinas
LARCASE Laboratory of Applied Reasearch in Active Controls,
Avionics and Aeroservoelasticity
École de Technologie Supérieure, 1100 rue Notre Dame Ouest,
Montréal, H3C1K3, Québec, Canada

This article was published in *INCAS Bulletin Vol. 8, Issue 1, pp 99-124*
DOI: 10.13111/2066-8201.2016.8.1

Résumé

Dans le cadre d'un projet de développement des technologies d'aile déformable, l'analyse de flottement de deux modèles d'éléments finis et les résultats expérimentaux d'un démonstrateur d'aile déformable équipé avec un aileron sont présentés. Les modèles d'éléments finis représentent une section de l'aile située au bout de l'aile; le premier modèle correspond à une aile avec peau supérieure en aluminium d'une épaisseur constante et le second modèle correspond à une aile avec surface supérieure en composite optimise pour être déformable. Les deux modèles ont été analysés pour l'occurrence du flottement et les effets du remplacement de la peau en aluminium avec celui en composite, spécialement conçu pour sa capacité de déformation, sur le comportement aéroélastique de l'aile. Le modèle d'aile déformable avec surface supérieure en composite a été fabriqué et équipé de trois accéléromètres pour enregistrer les amplitudes et les fréquences au cours des essais dans la soufflerie subsonique au Conseil National de Recherches. Les résultats présentés ont montré qu'aucune phénomène aéroélastique ne se sont produits aux vitesses, angles d'attaque

et déflections d'ailerons étudiés dans la soufflerie et ils ont confirmé la prédiction de l'analyse de flottement sur les fréquences et les déplacements modaux.

Abstract

As part of a morphing wing technology project, the flutter analysis of two finite element models and the experimental results of a morphing wing demonstrator equipped with aileron are presented. The finite element models are representing a wing section situated at the tip of the wing; the first model corresponds to a traditional aluminium upper surface skin of constant thickness and the second model corresponds to a composite optimized upper surface skin for morphing capabilities. The two models were analyzed for flutter occurrence and effects on the aeroelastic behaviour of the wing were studied by replacing the aluminium upper surface skin of the wing with a specially developed composite version. The morphing wing model with composite upper surface was manufactured and fitted with three accelerometers to record the amplitudes and frequencies during tests at the subsonic wind tunnel facility at the National Research Council. The results presented showed that no aeroelastic phenomenon occurred at the speeds, angles of attack and aileron deflections studied in the wind tunnel and confirmed the prediction of the flutter analysis on the frequencies and modal displacements.

5.1 Introduction

Today's aircrafts are not just flying machines; their design relies on a compromise between aerodynamic efficiency, structural optimization, fuel consumption minimization and environment requirements. This compromise asked for new methods in flight management, in aircraft design, structure, aerodynamics and controls. Many types of answers were found depending on the objective problem; for the minimization of fuel consumption or for the improvement of the aircraft flight envelope, the morphing methods are considered the most promising solutions. Morphing consists in changing the structure or appearance of an aircraft during flight by modifying the wing sweep (Joo et al., 2006), span (Neal et al., 2004), chord

(Reed Jr et al., 2005) or camber (Monner, Hanselka and Breitbach, 1998; Poonsong, 2004), by the high lift devices (Pecora et al., 2011; Pecora et al., 2013) or the fuselage, for small aircraft and for UAV's (Sugar Gabor, Koreanschi and Botez, 2013a; Sugar Gabor et al., 2015b). A state of the art in aircraft morphing, particularly on wing morphing, were given by (Sofla et al., 2010), (Vasista, Tong and Wong, 2012) and (Barbarino et al., 2011). The common features of all morphing configurations are a flexible structure, or skin. and free or unconventional structural elements, e.g. actuators or morphing mechanisms. These configurations need aero-elastic studies (Liauzun, 2010) to prove that they meet safety requirements demanded in aircraft industry and therefore flutter or divergence phenomena would not occur at certain flight conditions (speeds, angles of attack or aileron deflection angles). For example, many of the morphing structures use composite materials, for example (Huo et al., 2013) have studied the aero-elastic effects of composite wings using Nastran-Fluent coupling with implications for engineering applications. Many other aero-elastic studies were performed to prove the excellent qualities of the morphing structures with regards to their static and dynamic aero-elastic effects. Pecora R, Magnifico M, Amoroso F and Monaco E. have proposed the study of wing twist morphing on the aircraft roll control (Pecora, Amoroso and Lecce, 2012) and also they explored the flutter effects of a morphing wing trailing edge (Pecora et al., 2014). (Xie, Liu and Yang, 2012) have explored methods to realize aero-elastic static and flutter analysis using lifting –line theory for very flexible wings, which were encountered at high-altitude long-endurance aircrafts with high-aspect-ration wings. Also, (Murua, Palacios and Peiró, 2010) investigated the effects of chord-wise flexibility on the dynamic stability of compliant airfoils using a classical two-dimensional aero-elastic model expanded with an additional degree of freedom to capture time-varying camber deformations. A review of the progress made in aerodynamic and aero-elastic analysis of flapping wings was presented by (Shyy et al., 2010). In 2002, the Aerospace Industry Association of Canada, the Government of Quebec and key university research centers formed the Consortium for Research and Innovation in Aerospace Quebec (CRIAQ) to encourage mostly Civil Aviation research. One of their projects, called CRIAQ 7.1, was focused on shape changing wings and was realized between teams from Canadian aerospace industry companies, such as Bombardier and Thales, the IAR-NRC Research Center and two

universities, the École de Téchnologie Supérieure and École Polytechnique (Botez, Molaret and Laurendeau, 2007; Grigorie et al., 2010a; 2011b). The purpose of the CRIAQ 7.1 project was to prove that controlling the position of the transition point and pushing it towards the trailing edge using shape-changing techniques can reduce the drag coefficient, and implicitly, the fuel consumption (Coutu, Brailovski and Terriault, 2009; Popov, Botez and Labib, 2008; Silisteanu and Botez, 2012). As shown in the obtained results, it was possible to obtain up to 40% laminar flow improvement on a laminar airfoil-based wing model, and at the same time to achieve up to 20% drag coefficient reduction by using active control with smart material alloy actuators (SMA). A subsequent aeroelastic study proved that the morphing technique would not induce flutter phenomena during wind tunnel testing (Courchesne, Popov and Botez, 2010; 2012). In addition, many breakthroughs were achieved in active open-loop and closed-loop control using Proportional – Integrate (PI), (Grigorie et al., 2012c; Popov et al., 2010a), and Fuzzy Logic based controllers in wind tunnel testing, (Grigorie and Botez, 2009; Grigorie, Botez and Popov, 2009; Popov et al., 2010b), under the auspices of this same project. The research presented in this paper was completed in the frame of the CRIAQ MDO 505 project realized as an international collaboration between Canadian and Italian industries, universities and research centers. The purpose of this project was to demonstrate the structural, aerodynamic and control abilities of a real aircraft wing tip equipped with an adaptive upper surface and an adaptive aileron during subsonic wind tunnel tests. The novelty of the project consists in the design, analysis and manufacturing of an aerodynamically and structurally optimized real wing tip. The wing tip was tested for structural 1g loads, and, during these tests, the composite upper surface and the adaptive aileron were controlled with electrical actuators situated in the wing and in the aileron boxes. The present paper is concerned with the aero-elastic behavior, specifically flutter phenomenon, of the wing tip during wind tunnel testing, especially at the Mach number of 0.25 which was the highest speed to be tested in the wind tunnel. The behavior of the wing was of outmost concern due to the composite flexible skin attached on all four sides of the wing box and of the electrical actuation system installed inside. For this purpose, a comparison of the flutter behavior was made between the wing model with flexible composite upper surface and its version with classic aluminium upper surface. To these

configurations, a rigid aileron was added, actuated by an external actuator rigidly fixed to the wing mounting support under the wind tunnel floor. Finally, acceleration results obtained over a range of 1 second from the accelerometers installed on the wing were presented to show that the wing demonstrator suffered no aero-elastic phenomena during wind tunnel tests.

5.2 Presentation of the Research Context

The research presented in this present paper was done within the framework of the international CRIAQ MDO505 Morphing Wing project. The participants in this project were the Ecole de Technologie Supérieure (ETS), Ecole Polytehnique of Montreal and University of Naples 'Federico II' as academia research partners, the Canadian National Research Council (CNRC) and the Italian Aerospace Research Center (CIRA) as research center partners, and Bombardier Aerospace, Thales Canada and Alenia Aermacchi as industrial partners. The objectives of the project were to design, manufacture and control a wing demonstrator based on a real aircraft wing tip equipped with both a conventional and an adaptive aileron. The CRIAQ MDO 505 project was a continuation of the earlier research project CRIAQ 7.1, and was aimed at a higher Technical Readiness Level (TRL) by considering a real wing internal structure, a certifiable electric control system and controllers. The objectives of the active morphing wing tip project were mainly: (1) an improvement of the aerodynamic performance of the wing, through the active control of the boundary layer transition from laminar to turbulent states, (2) the design and manufacturing of a morphing wing model that withstand gust loads of up to 1g, and (3) the design, implementation and integration of control systems and a morphing mechanism to control the shape of the wing in wind tunnel experiments. The morphing wing demonstrator represents a wing section situated between the fuel tank section and the winglet. Figure 5.1 presents the position of the wing section under discussion.

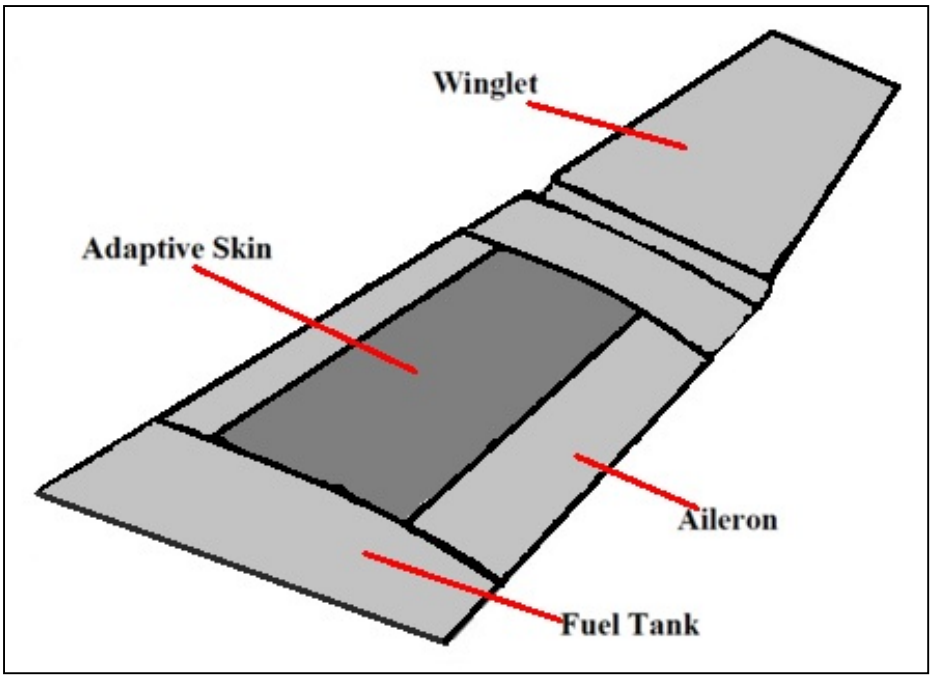

Figure 5.1 Layout and position of the morphing skin
on the aircraft wing

Unlike a full wing, the demonstrator does not display a sweep angle, this aspect being eliminated to reduce the tridimensional effects of the flow on the wing. In addition, at this section of the wing the aileron would occupy half of the wing section's span, but for the demonstrator, the span of the aileron was chosen to equal that of the wing.

The wing demonstrator internal structure contains the same components as a real wing: ribs, spars, stiffeners, etc, which was designed in accordance with the designs and positions of such structural elements on a real wing. Figure 5.2 shows the structural elements of the CRIAQ MDO 505 project morphing wing concept, where the morphing skin is not shown.

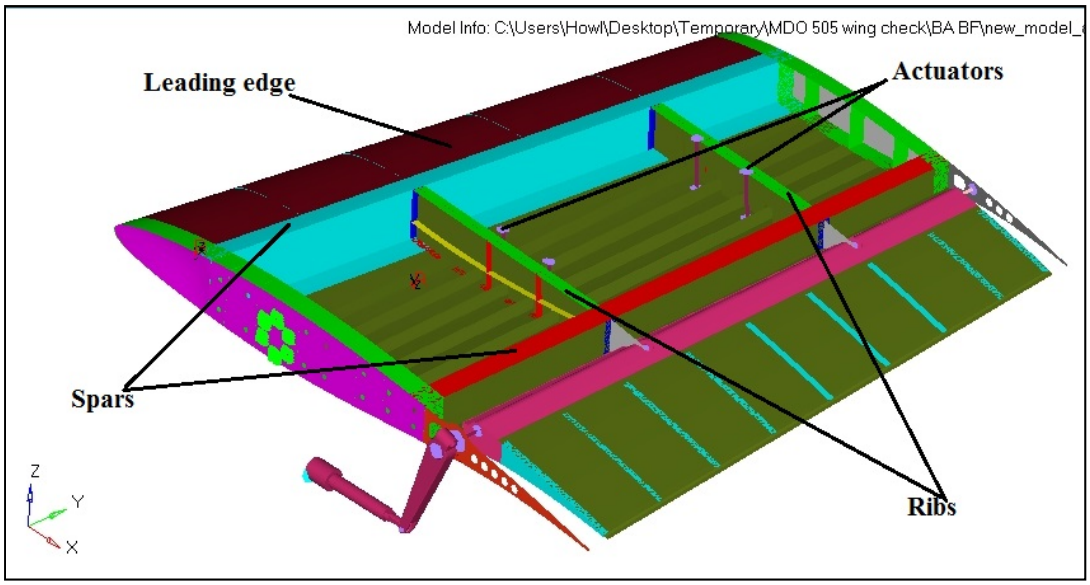

Figure 5.2 Structural elements of the CRIAQ MDO 505 morphing wing concept

However, the leading edge was simplified by using a thin aluminium skin supported by ribs. The dimensions of the wing demonstrator were slightly adapted to respect the dimensions of the IAR-NRC subsonic wind tunnel chamber which has a section of 2m x 3m. Therefore, the wing demonstrator has a span of 1.5 m and a root chord of 1.5 m. Despite the modifications that were made to the structure of the demonstrator, its trapezoidal shape was conserved (tapered wing), with a taper angle of 8° on both leading and trailing edge sides. The chord varies progressively between 1.5m at its root to 1.08m at its tip and has a maximum thickness of 143 mm at the root section. Figure 5.3 presents the geometrical design of the wing demonstrator and its main dimensions.

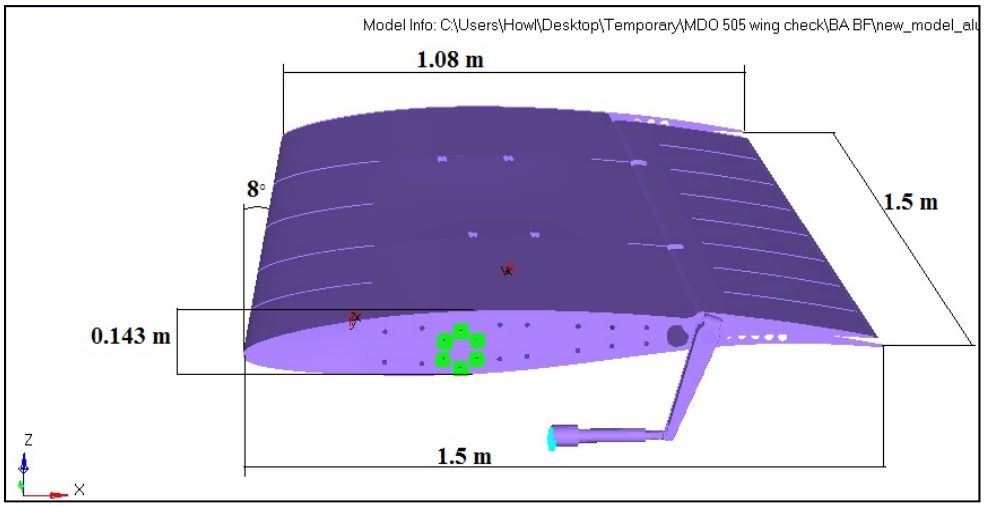

Figure 5.3 View of the wing demonstrator with its dimensions

The aileron's hinge was located at 72% of the chord. Two types of ailerons were designed and manufactured. One aileron was structurally rigid, while the other was a new morphing aileron. Both ailerons were designed to be attached to the same hinge axis on the wing box, and both were able to undergo a controlled deflection between -7° and +7°.

In order to ensure the best multidisciplinary optimization of the wing-tip, structural constraints were, in a first step, discussed and imposed. The multidisciplinary optimization was a combination of integrated aerodynamic, structural and control optimization processes. The aerodynamic optimization was carried at airfoil level, and was done by controlling four points situated on the upper surface of the airfoil. These four points corresponded to the leading and trailing edge fixation points of the skin defining the morphing region, and to two vertically mobile points, situated at 32% and 48% of the chord, which represent the actuator's displacements. The four points were used in conjunction with cubic splines method (Piegl and Tiller, 2012) to retrace the upper surface of the airfoil and obtain a new shape. For a specific combination of angles of attack, speeds and aileron deflection angle, the mobile points were displaced with values between -3.5 mm and 3.5 mm during the optimization iteration process until it was achieved the objective of delaying the transition from laminar to turbulent flow. Further information on the aerodynamic optimization process and its results, obtained both numerically and experimentally, was presented by (Koreanschi,

Sugar-Gabor and Botez, 2016a; 2016b; Koreanschi et al., 2016) and (Sugar Gabor, Koreanschi and Botez, 2012).

In order to maintain the structural integrity of the demonstrator, the aerodynamic optimization was constraint by geometry and skin deformation limitations. The positions of the leading and trailing edge spars represented the main geometric constraint. They were situated at 20% and 65% of the chord, and these positions represent the actual delimitation of the morphing skin. In return, to better comply with the aerodynamic spline reconstruction, the skin was fixed to the spar caps, and it remained continuously tangent to them at all moments.

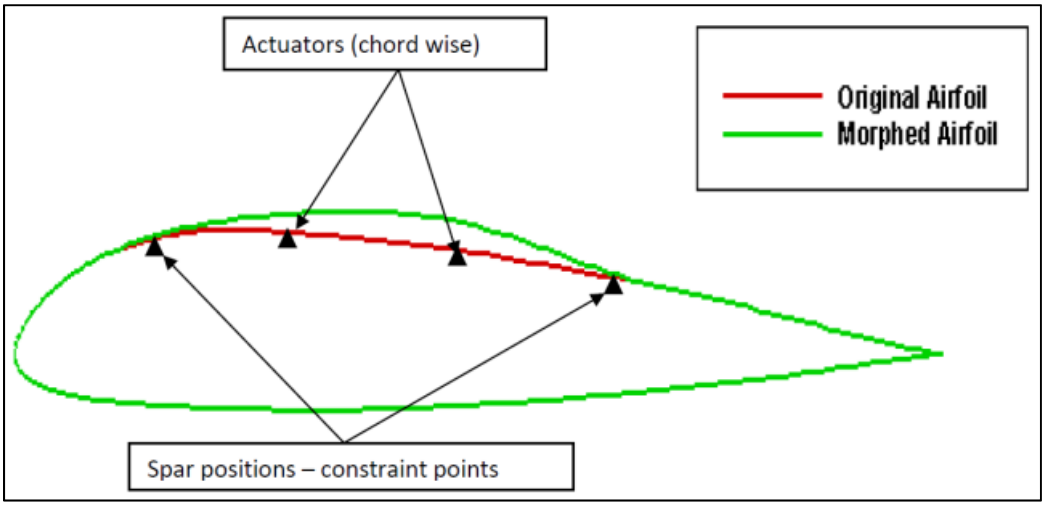

Figure 5.4 Example of the morphed versus original airfoil shape with spar optimization constraint

Another structural constraint for the aerodynamic optimization was the imposition of a maximum allowable skin length deformation. Such a constraint was imposed because without it the skin would have been submitted to high elastic deformations which would have affected the quality and quantity of structural optimization process needed for the composite skin. The maximum allowable deformation was set at +/- 0.03% of the original spline length which was equivalent to the chord-wise skin length. Further details on the structural

optimization of the wing and on the composite skin optimization process can be found in (Michaud, 2014).

5.3 Detailed Finite Element Model Presentation

The model used for the flutter analysis was a Detailed Finite Element Model or DFEM. The morphing wing demonstrator was constituted of several structural elements: two spars, four ribs, 12 stiffeners (six for each surface), six leading edge ribs, nine trailing edge ribs, five skins (two skins for the wing box, one for the leading edge and two for the trailing edge), four internal actuators and one external aileron actuator. The finite element model or FEM was designed using Altair Hypermesh software (HyperWorks, 2016). Two FEM models were created, one model was equipped with a traditional aluminium upper surface skin of 3mm constant thickness, and another model with carbon fiber composite upper surface optimized for morphing behavior, this latter model corresponded to the wing demonstrator that was tested in the wind tunnel. The purpose of this research was to determine whether the replacement of the aluminium skin with constant thickness by a composite skin with variable number of plies and thickness per ply would affect the dynamic aero-elastic behavior of the wing demonstrator.

The FEM model has used of a mixture of 3D, 2D and 1D elements, where the 1D elements were used to represent the connectors, the aileron shaft and the four internal actuators. The 1D elements used for connectors to model the connections between the skins, spars and ribs were of the type SPRING, and were associated to PBUSH properties which defined the material and type of connections used. The four internal actuators were modeled using BEAM elements; Figure 5.5 presents an example of the modeled actuators installed inside the wing box. A BEAM element is a 1D representation of a simple beam with its associated physical and geometrical properties. This type of element is capable of sustaining all efforts in translation and rotation at its extremities. The cross-section for this type of element was defined by the menu Hyperbeam where the dimensions are defined by the user. For the four actuators, the diameter of the BEAM was chosen to be 25 mm which was representative of

the real actuator diameter, while the material associated with the actuators was aluminium. RBE2 rigid elements were added to the extremes of the BEAM to ensure a representative contact surface with the upper and lower skins. The RBE2 defines a rigid body whose independent degree of freedom was specified at a single 'master' node, while the dependent degrees of freedom were specified at a number of 'slave' nodes chosen by the user. The aileron shaft was also modeled using BEAM elements of circular area with a variable diameter along the span – the diameter of the shaft varies between 25 mm at the root to 12.5 mm at the tip of the wing – and steel material properties were assigned to it.

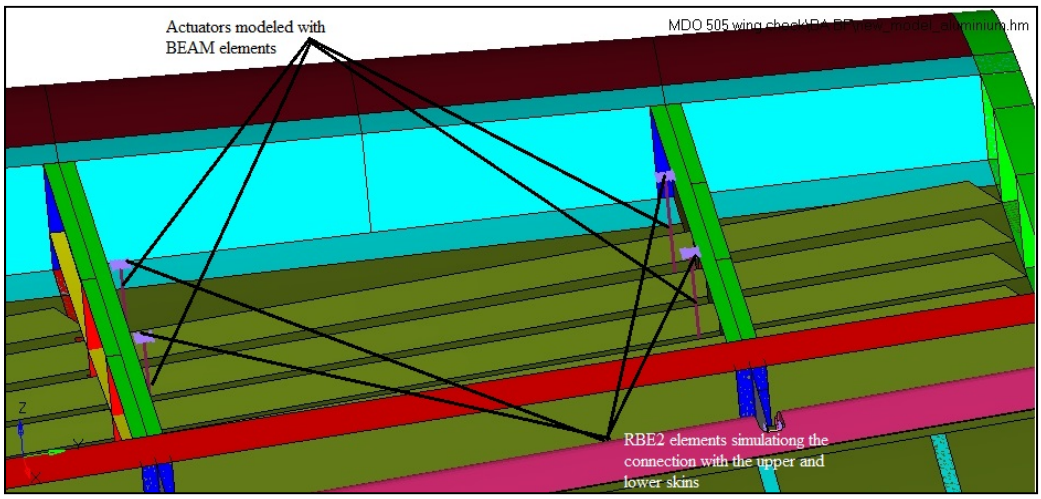

Figure 5.5 View of the BEAM elements modeling the actuators and their connections to flexible skin

The rigid fixation of the wing demonstrator to a steel mount, as it was installed in the wind tunnel, was done using rigid elements called RBE3, Figure 6 shows a representation of the rigid fixation and constrains applied. The RBE3 elements define a rigid body similar to the RBE2 element described in the previous paragraph with the difference that the RBE3 element allows the natural deformation of the rigidly fixed structure which minimizes the stress concentration that usually were associated with RBE2 elements. The RBE3 were constrained in all directions and similar constraints were used for the area surrounding the mounting holes.

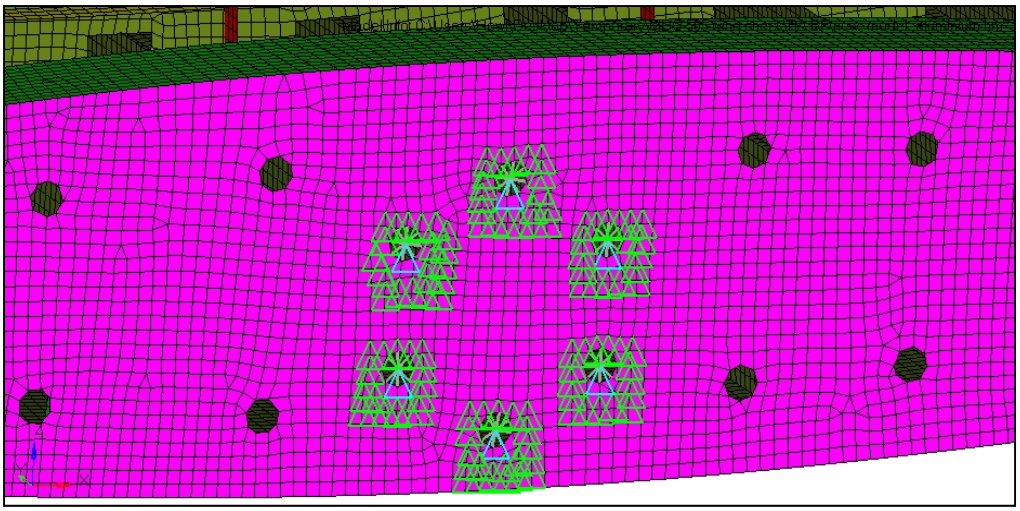

Figure 5.6 RBE3 rigid elements and constraints simulating
the mounting of the wing in the subsonic wind tunnel

All structural components of the wing, with the exception of the aileron leading edge, aileron shaft and external actuator were defined as surfaces and were meshed using a combination of quadrilateral CQUAD4 and triangular CTRIA3 elements in order to ensure the optimal progression of the mesh on the trapezoidal shape of the wing. All surface elements were of the type SHELL to which either PSHEL or PCOMP properties were assigned in function of the section of the wing.

The PSHELL or PCOMP properties ensured a thickness and a material was associated to each element. The PCOMP property characterized the composite skin section of the wing and it allowed the user to indicate the number of plies and the direction of the carbon composite fibers in both chord- and span-wise directions, as well as the thickness for each individual ply.

The PCOMP property was given to all elements that meshed the upper surface skin and stringers of the wing demonstrator. All other surfaces of the wing, that were not composite, were assigned PSHELL property with aluminium as associated material (E = 71GPa, G = 27GPa and $\nu = 0.33$).

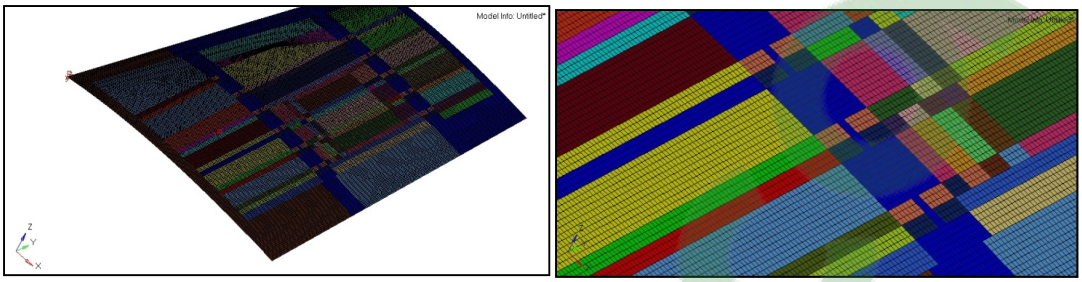

Figure 5.7 Left – View of the upper surface skin designed in composite material;
Right – Close-up view of the upper-surface skin

The different colors, shown in Figure 5.7, represent various sections of the upper surface skin that have different number of plies, different thickness per ply and different orientations of the carbon fibers.

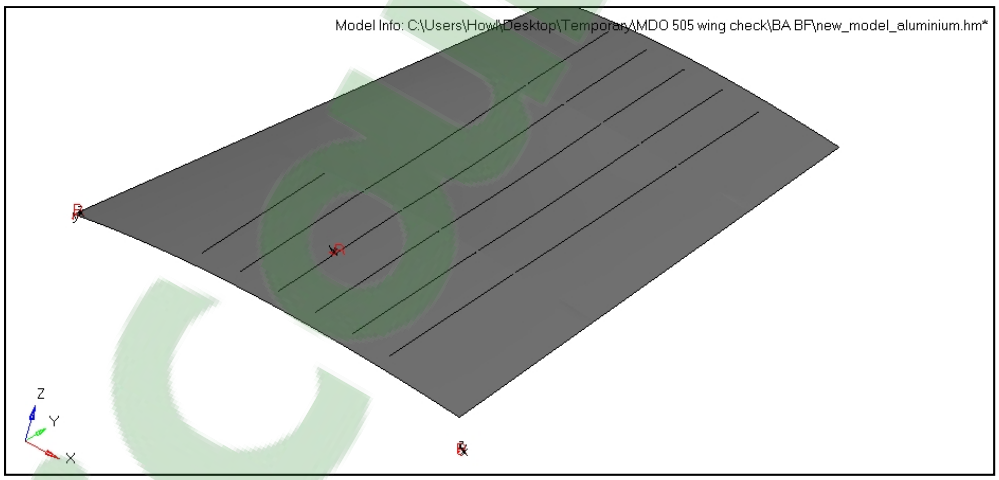

Figure 5.8 View of the upper surface skin of the wing in aluminium

The aileron's external actuator was meshed using 3D tetrahedral elements of the CTETRA type to which PSOLID and steel properties were associated. The PSOLID properties associate a number and a reference system for each CTETREA element. The aileron leading edge was also meshed using CTETRA elements but the material associated to it was aluminium.

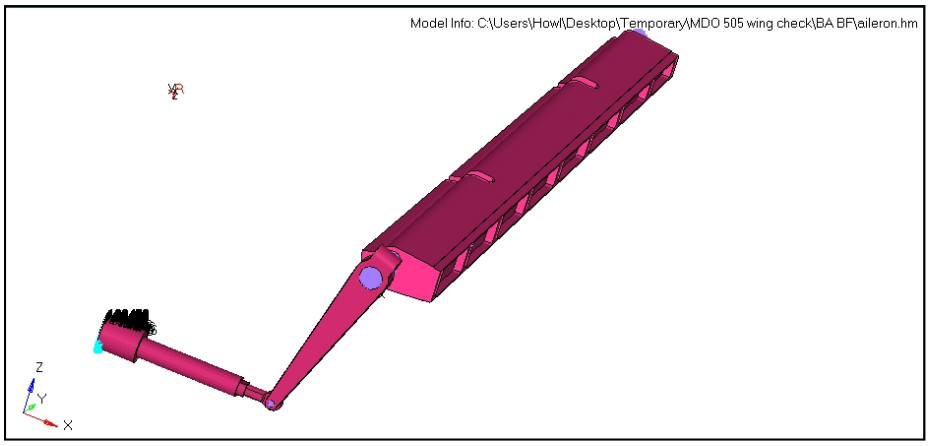

Figure 5.9 View of the aileron leading edge, shaft and actuator

5.4 Flutter Analysis

The FEM models used during the flutter analysis were described in section III above. The Hyperworks software Hypermesh was used for the development of the FEM model and to export all information as a Nastran deck file,'.bdf', for MSC Patran/Nastran, (Patran/Nastran, 2016), aero-elastic flutter analysis. MSC Patran was used to correct errors that were obtained from importing a model from a platform to another, from Hypermesh to Patran in this case. Most of the errors encountered concerned nodes duplication, errors in the definition of the boundary conditions, and different definitions for the multi- point constraint (MPC) – the multi-point constraint have a different name associated in each of the software used.

Figure 5.10 presents the workflow diagram for the aero-elastic analysis of the wing demonstrator.

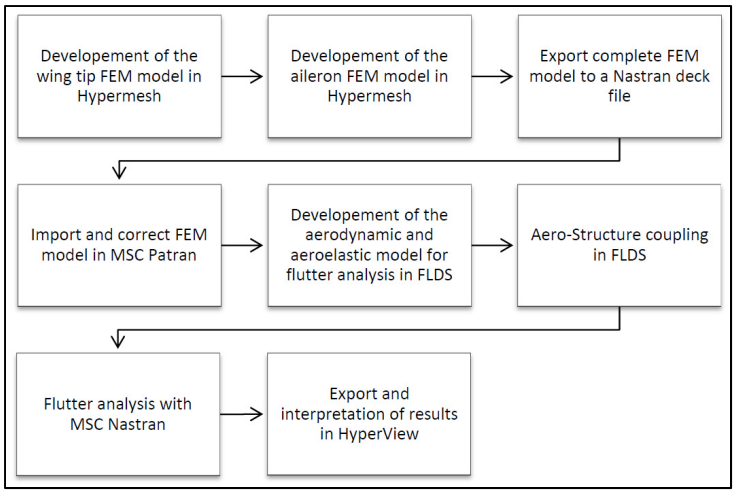

Figure 5.10 Workflow diagram of the aeroelastic flutter analysis of the CRIAQ MDO wing tip

5.4.1 Aero-Struture modeling

For the flutter analysis a definition of the aerodynamic model and its coupling with the structural FEM model was needed, and MSC's Flight and Loads Dynamics (FLDS) software was used to create them. The aerodynamic model was defined through reference lifting surfaces or flat plates. For the FEM wing model, two lifting surfaces were created: one for the wing box and another for the aileron. The reference lifting surfaces were defined by a reference chord (mean aerodynamic chord), span and sweep angle (for the model presented in this paper no sweep angle was considered). To minimize the time needed for doing mesh convergence, MSC Nastran recommendations, (Rodden and Erwin, 1994), were used to establish the number of aerodynamic elements or DLM boxes needed to obtain the best results:

$$\frac{DLM_{boxes}}{\frac{v}{fc}} > 15 \tag{5.1}$$

where v is the reference speed, f is the reduced frequency of the flow and c is the reference chord of the wing. In this case, eight boxes in the span directions with 5 boxes in the chord

direction, for a total of 40 DLM boxes, were used to model the wing body lifting surface, and eight boxes in span direction with three boxes in chord direction were used to model the aileron lifting surface. Figure 5.11 presents the wing tip demonstrator FEM model with lifting surfaces for the wing body and aileron.

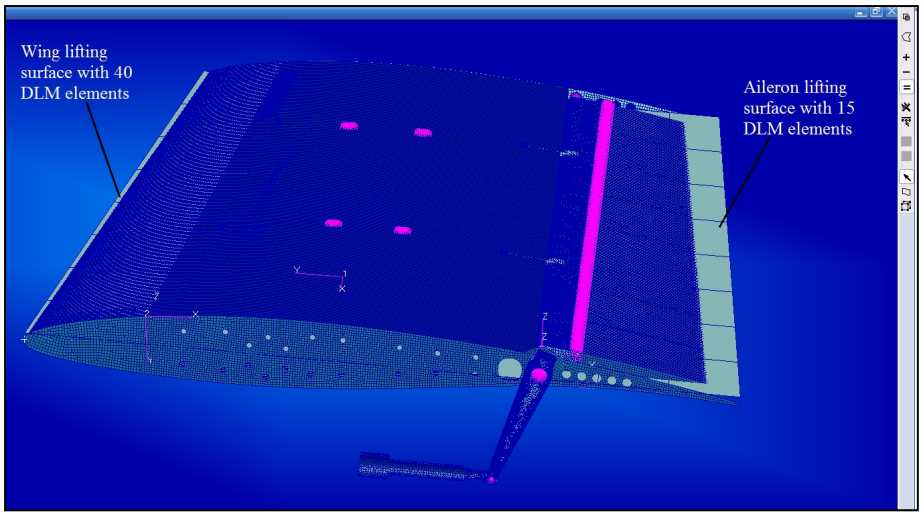

Figure 5.11 View of the model with lifting surfaces

The flow properties are described by the Mach - reduced frequencies (Mk), the velocity and densities list. All three are requirements of the PK method used for the flutter analysis.

The coupling of the structural and aerodynamic models was realized through splining or interpolation between the structural and aerodynamic grids. The Thin Plate Spline (TPS) method that was provided by the FLDS software was used. The ‘Thin Plate Spline’ is an interpolation method used for structures which have elements in the three-dimensional space (x, y, z), and it was developed from the Infinite Plate Spline (IPS) method which is used for structures developed in a bi-dimensional space (2D plates) (Zona_Technology, 2014). Due to lack of information for the treatment of the selection of the structure nodes or their location for the splining process, ‘two test procedures’ were proposed to find the optimal combination of the number and positions of nodes. The first test proposes a selection of all the nodes on the upper and lower surfaces. The test showed that such a high number of nodes made the

analysis almost impossible in terms of calculation time; thus, some of the resulted files – e.g. the '.DBALL' file hosting the splining matrix or the '.F06' file hosting the analysis results - attained prohibitive dimensions – several Gb of data which were difficult to manage. In the second test, several combinations of number of nodes and locations were used. Six groups were created, each group contained 137, 194, 266, 298, 330 and 391 nodes, respectively. The results of the second test made for finding the optimal number and positions of nodes are presented in Figures 5.12 and 5.13 for the first two modes in terms of frequency versus speed curves. It can be observed that regardless of the number of points (N) used or their location on the upper and lower surfaces, the results are close and the differences are negligible; still, a sufficient number of nodes, no less than the number of DLM boxes, and an even distribution of the nodes were desired.

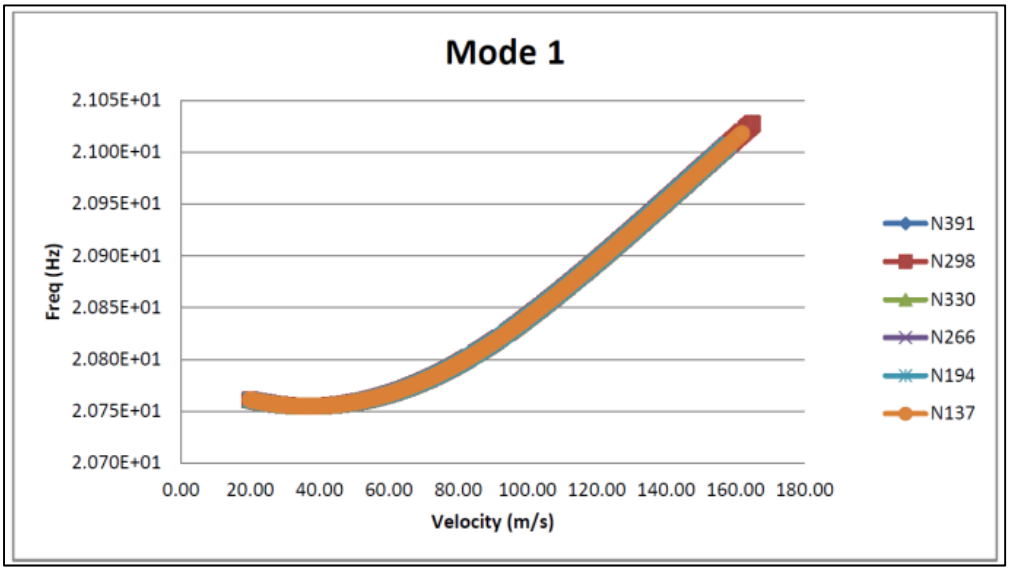

Figure 5.12 Frequency versus velocities for 1st Mode obtained by using six combinations of number of nodes

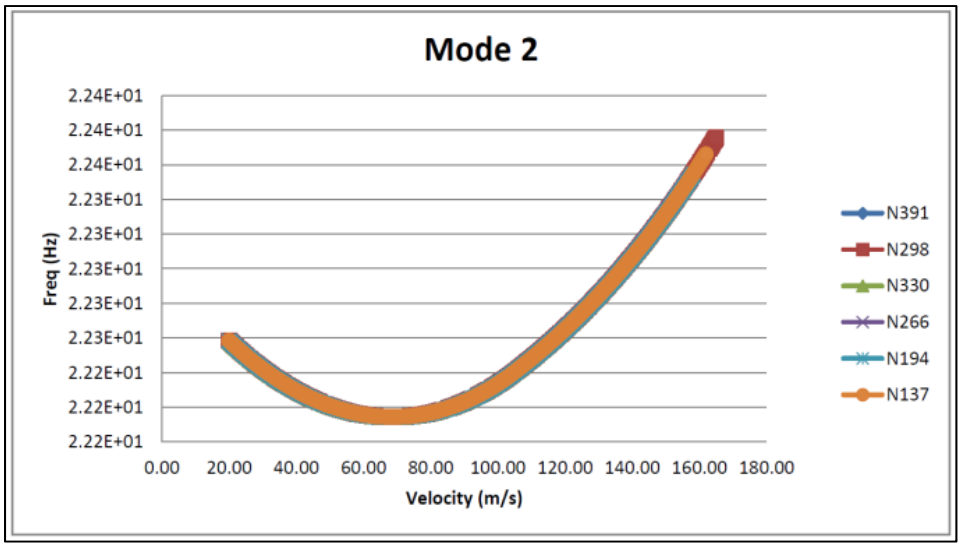

Figure 5.13 Frequency versus velocities for 2nd Mode obtained by using six combinations of number of nodes

For the finite element model of the wing equipped with flexible upper surface and an aileron, a number N of 110 nodes was used for the splining process.

5.4.2 P-K method

As mentioned before, the aeroelastic flutter analysis was done using the PK method offered by Nastran. This method was chosen due to its pertinence in the results it offers, especially at low speeds regimes, in which the presented test speeds were also considered(Baxevanou et al., 2008; van Zyl and Maserumule, 2001).

The fundamental equation describing the PK method is given by equation (5.2):

$$\left[\frac{V^2}{L^2}Mp^2 + K - \frac{1}{2}\rho V^2 Q(ik)\right]\{q\} = 0. \qquad (5.2)$$

For simplification purposes, equation (5.2) excludes the structural damping matrix C. M and K represent the mass and stiffness matrixes, V is the speed and Q(ik) the vector of external

forces. In equation (5.2), p is the Laplace non-dimensional parameter that is defined by equation (5.3).

$$p = g + ik \tag{5.3}$$

$$g = \gamma k \tag{5.4}$$

where, g represents the damping coefficient, calculated using the reduced frequency k and an under-relaxation coefficient γ, as shown in equation (5.4).

(Rodden and Bellinger, 1982) has modified the PK equation by adding an aerodynamic damping matrix to it, thus in Nastran solver the PK equation is expressed as shown in equation (5.5).

$$\left[\frac{V^2}{L^2}Mp^2 + k - \frac{1}{2}\rho V^2\frac{Q^I}{k}p - \frac{1}{2}\rho V^2\frac{Q^R}{k}\right]\{q\} = 0. \tag{5.5}$$

Where QI and QR are the imaginary and real parts of the force matrix Q(ik). Equation (5.5) can also be expressed in the following state space formulation.

$$[A - pI]\{q\} = 0. \tag{5.6}$$

where p represents the spectrum of all the eigenvalues. Its solution is expressed by the eigenvalues of matrix A:

$$A = \begin{matrix} 0 & 1 \end{matrix}\begin{bmatrix} -M^{-1}\left[k - \frac{1}{2}\rho V^2\frac{Q^R}{K}\right] & -M^{-1}\left[-\frac{1}{2}\rho V^2\frac{Q^I}{K}\right] \end{bmatrix} \tag{5.7}$$

where A and q, from equation (5.7), include the speeds and modal displacements. For this nonlinear system, the solution is found through an iterative process.

5.4.3 Flutter analysis results

As mention in the above section III, two FEM models were created; the first model had a traditional aluminium upper surface while the second model had an optimized flexible composite upper surface skin. The purpose of the analysis was to demonstrate that although the wing model with composite skin was designed and optimized for its morphing behavior, its aero-elastic behavior remained close to that of the wing normally equipped with an aluminium skin of constant thickness. Also, the analysis served to demonstrate that for the speeds used during the wind tunnel tests, no flutter phenomenon was expected to occur. The maximum speed at which the wing demonstrator was tested in the wind tunnel was 85 m/s or Mach number of 0.25.

Table 5.1 present the first five natural modes obtained for the wing models, as the natural frequencies of the structure were calculated first during the flutter analysis.

Table 5.1 Comparison between the natural frequencies of the wing models with upper surface aluminium skin and composite skin

Mode No.	**Frequency (Hz)**	
	Wing Model with aluminium upper surface skin	**Wing model with composite upper surface skin**
I	2.04E+01	2.08E+01
II	2.17E+01	2.22E+01
III	7.31E+01	7.37E+01
IV	1.28E+02	1.29E+02
V	1.38E+02	1.39E+02

From the table above, it can be summarized that there is almost no change in the values of the natural frequencies whether the upper surface of the wing demonstrator was made from aluminium and had a constant thickness or from optimized carbon composite material with variable thickness.

Table 5.2 presents the frequencies and damping values for the first 5 modes for the following three speeds used during wind tunnel tests: 50 m/s, 70 m/s and 90 m/s.

Table 5.2 Comparison of the frequencies and damping values for speeds of 50, 70 and 90 m/s

Mode No.	Speed (m/s)	Wing Model with aluminium upper surface skin		Wing model with composite upper surface skin	
		Frequency (Hz)	Damping	Frequency (Hz)	Damping
I	50	2.04E+01	-5.82E-03	2.08E+01	-4.02E-03
	70	2.04E+01	-8.26E-03	2.08E+01	-5.70E-03
	90	2.04E+01	-1.05E-02	2.08E+01	-7.23E-03
II	50	2.16E+01	-5.62E-03	2.21E+01	-7.23E-03
	70	2.16E+01	-7.84E-03	2.21E+01	-1.01E-02
	90	2.16E+01	-1.02E-02	2.21E+01	-1.32E-02
III	50	7.29E+01	-8.26E-03	7.35E+01	-8.12E-03
	70	7.29E+01	-1.32E-02	7.35E+01	-1.31E-02
	90	7.29E+01	-1.82E-02	7.35E+01	-1.81E-02
IV	50	1.28E+02	1.40E-04	1.29E+02	-6.27E-04
	70	1.28E+02	-7.90E-04	1.29E+02	-1.55E-03
	90	1.28E+02	-1.72E-03	1.29E+02	-2.48E-03
V	50	1.38E+02	-8.07E-03	1.39E+02	-7.02E-03
	70	1.38E+02	-9.29E-03	1.39E+02	-8.20E-03
	90	1.38E+02	-1.05E-02	1.39E+02	-9.36E-03

From Table 5.2 it can be observed that no flutter tendencies appear at any of the studied speeds. The analysis was performed up to a speed of 110 m/s which is the maximum speed of the IAR-NRC wind tunnel, and no flutter behavior was predicted. In Figures 5.14 and 5.15, the evolution of the frequency and damping with speed is presented for the five modes mentioned above.

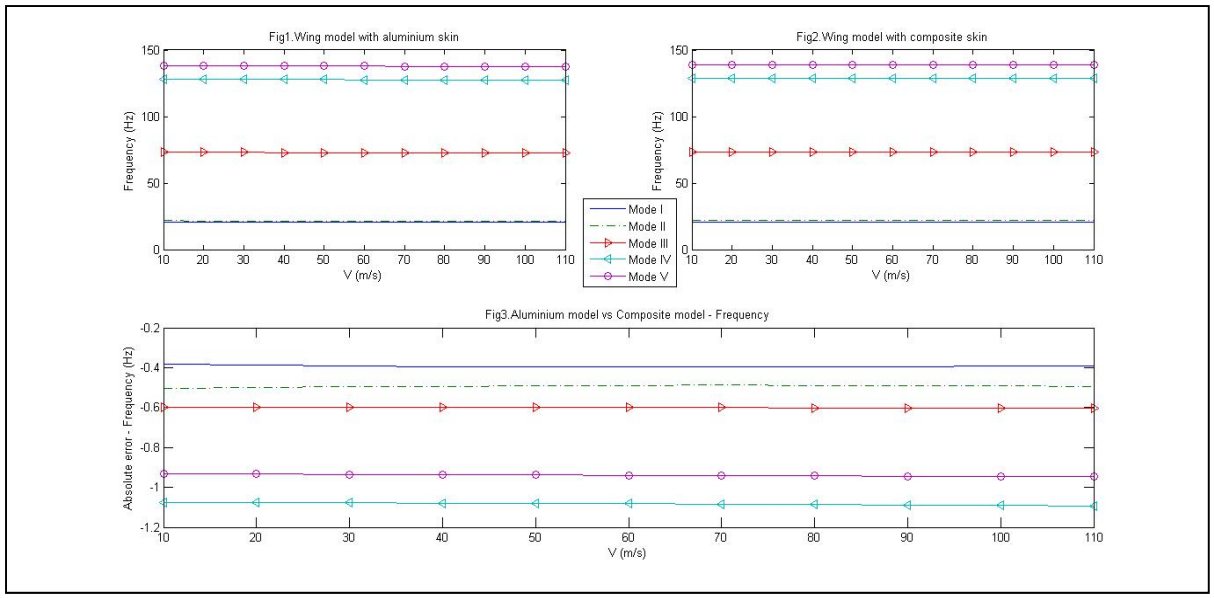

Figure 5.14 Frequencies of the first five modes over a range of speeds

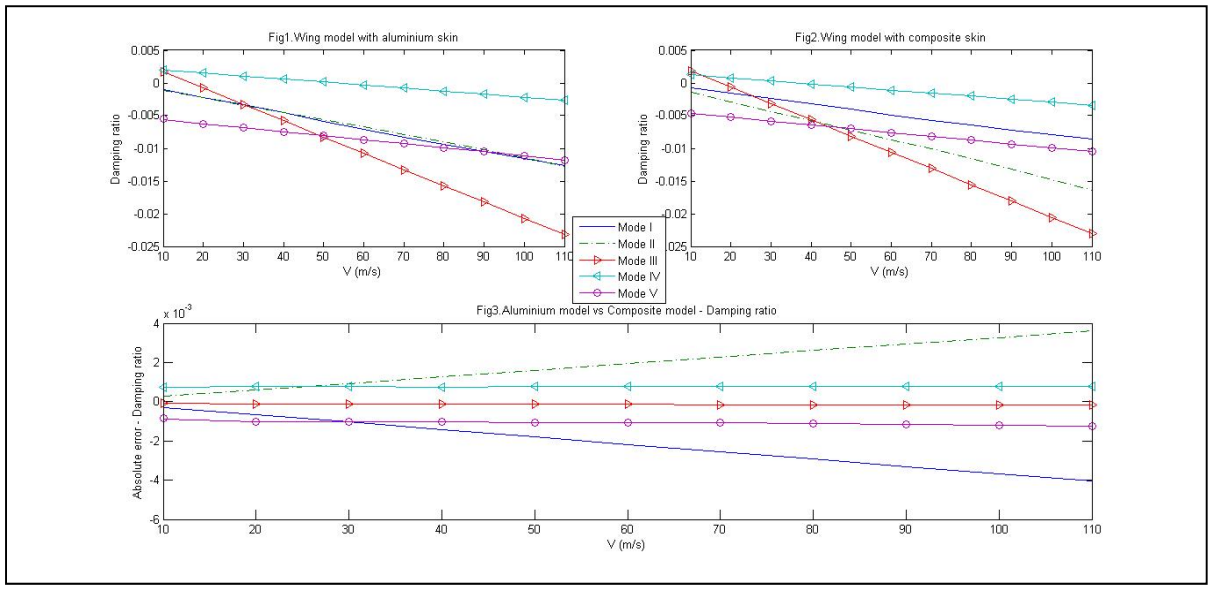

Figure 5.15 Damping behaviour of the first five modes over a range of speeds

From Figure 5.14 it is observable that the wing model with composite upper surface skin has close frequency to those obtained for the wing model equipped with aluminium upper surface skin, the average absolute error was less than 1Hz. From Figure 5.15, it can be deduced that

for the first and second mode the composite skin has some influence in the damping behavior of the model. For mode I, the vibrations of the wing model with composite skin are dampened slower than for the wing model with aluminium skin. For mode II, the vibrations of the wing model with composite skin are dampened faster than for the wing model with aluminium skin.

Also, from Figure 5.15.1 and 5.15.2, for the wing with composite skin, the first and second modes show a tendency to separate, whereas for the model with aluminium skin the two modes almost overlap. The behavior of the wing models for the last three modes is almost the same, the absolute error being approximately +/- 0.5*10-3.

Figures 5.16 to 5.19 present, in terms of modal displacements, the behaviour of each mode for both aluminium and composite upper surface wing models, with the first and second modes representing the bending behavior around the x, respectively the y axis; the third mode representing the torsion behavior while the 4th mode representing the coupling behavior between torsion and bending.

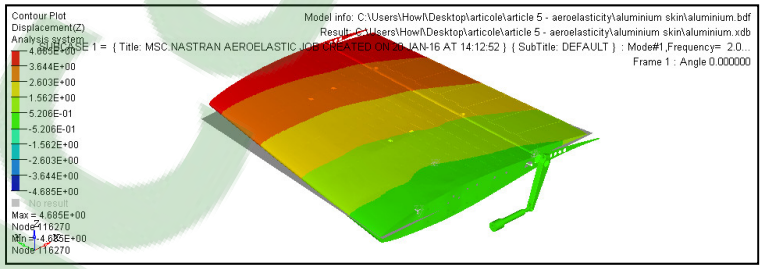

a)

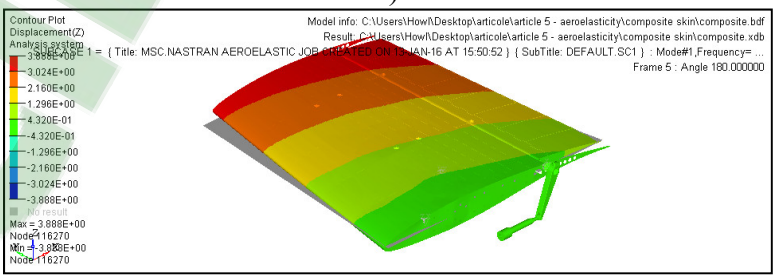

b)

Figure 5.16 First mode behavior – bending

Figure 5.16 a) presents the first mode behavior for the FEM model with upper surface aluminium skin, while Figure 5.16 b) presents the first mode for the FEM model with upper surface composite skin. The behavior is identical for both models but the displacement of the composite skin model is smaller than for the aluminium skin model, which shows that the model with composite skin was developed, through the optimization process, to be more rigid in the span direction.

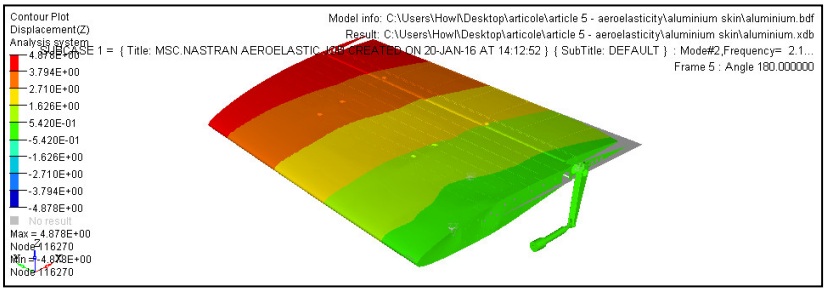

a)

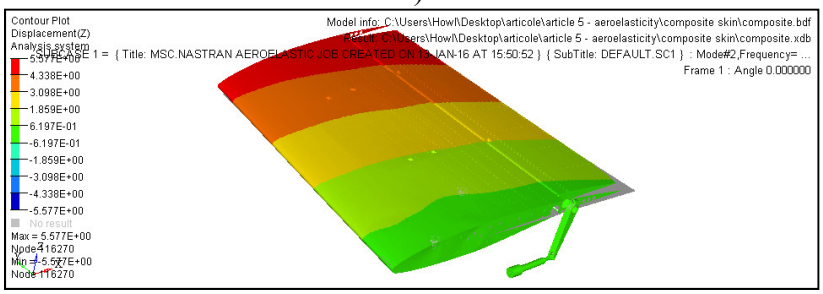

b)

Figure 5.17 Second mode behaviour – lateral bending

Figure 5.17 a) presents the second mode behavior for the FEM model with upper surface aluminium skin, while Figure 5.17 b) presents the second mode for the FEM model with upper surface composite skin. The behavior is identical for both models but the displacement of the composite skin model is higher than for the aluminium skin model because the model with composite skin was developed to be more flexible in the chord wise direction.

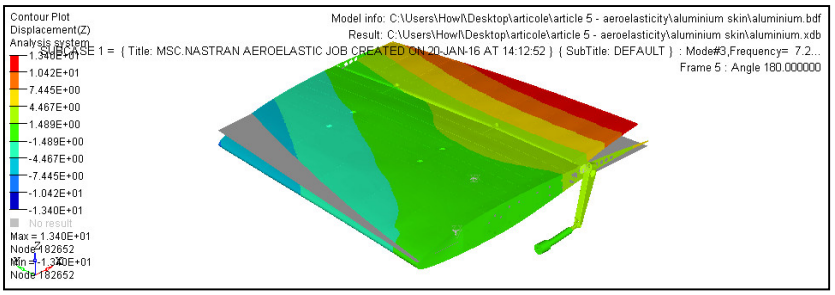

a)

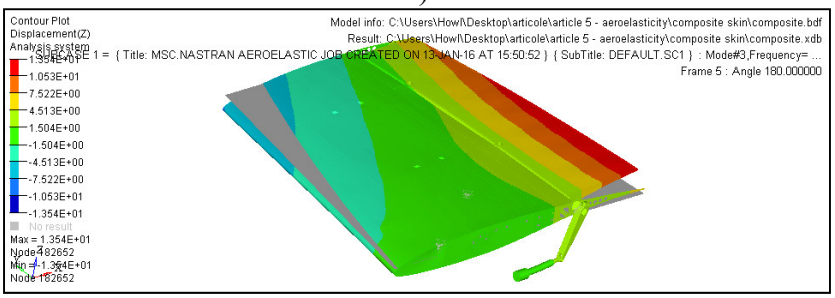

b)

Figure 5.18 Third mode behaviour – torsion

Figure 5.18 a) presents the third mode behavior for the FEM model with upper surface aluminium skin, while Figure 5.18 b) presents the third mode for the FEM model with upper surface composite skin. The behavior is torsion for both models, where the maximum and minimum displacements are almost identical. For this mode, the type of material and optimization of the upper surface skin seems to have no effect on the behavior of the models.

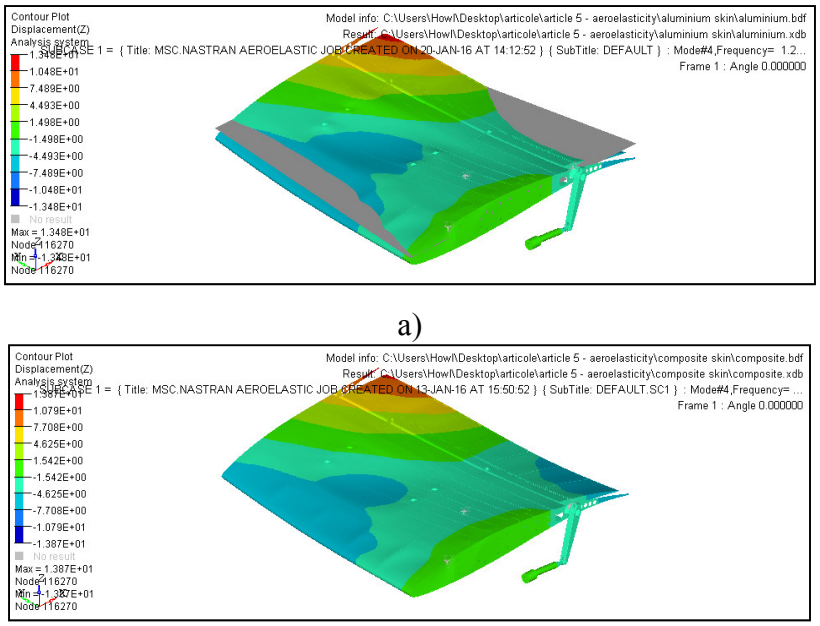

a)

b)

Figure 5.19 Fourth mode – Coupling between torsion and bending

Figure 5.19 a) presents the fourth mode behavior for the FEM model with upper surface aluminium skin, while Figure 5.19 b) presents the fourth mode for the FEM model with upper surface composite skin. The difference in the overall maximum displacement between the two FEM models is negligible, but the behavior of the aluminium upper surface skin model close to the leading edge is slightly different than the behavior of the composite skin model, which has a smaller displacement deformation in that area.

This difference is due to the bending component of the mode; in the fourth mode the bending deformation takes place in the span direction, and as shown in Figure 15, the composite upper surface wing model is more rigid in the span direction due to the constraint that the composite skin had to be capable of supporting the same type of loads as the aluminium upper surface skin would.

Based on the aero-elastic results presented above, the optimization process of the upper surface skin which includes the introduction of variable thickness in both span and chord

directions as well, and different material, has succeeded in obtaining a skin that has the same overall behavior as a traditional aluminium skin, but, is more rigid span-wise to account for the constraint of being capable of resisting to the same loads as the aluminium skin and more flexible chord-wise to permit deformation using two actuation points in the chord direction. The analysis has also shown that there was no possibility of flutter phenomena occurring for the speeds at which the wing demonstrator was tested and even for speeds beyond the capacity of the wind tunnel, which has shown that the model was structurally rigid for the tests that took place.

5.5 Wind Tunnel Testing

In this section the testing of the wing demonstrator and the results obtained from the accelerometers installed inside the wing are presented.

5.5.1 Wind Tunnel Description

The wind tunnel tests were performed at the 2 m x 3 m atmospheric closed circuit subsonic wind tunnel of the National Research Council Canada. This atmospheric wind tunnel can operate at a maximum Mach number of 0.33.

The upper surface flexible skin of the wing demonstrator was equipped with 32 high precision Kulite piezoelectric-type transducers, (Kulite, 2015), for pressure measurement on the flexible skin and the data was processed to determine the laminar-to-turbulent transition location. These sensors were installed in two staggered lines (with 16 Kulite sensors on each line), situated respectively at 0.600 m and 0.625 m from the wing root section. In addition to the Kulite piezoelectric sensors, at the same two span-wise stations, 60 static pressure taps were installed (30 taps on each line), on the wing leading edge, lower surface and aileron, thus providing complete experimental pressure distribution around the wing cross section at 40% of the wing span. The pressure sensors were installed in a staggered fashion to minimize the interference between them.

The experimental measurements also included the use of a wake rake pressure acquisition system, to measure the wing profile drag at different span-wise positions, and to use a wind tunnel balance for measuring the aerodynamic forces and moments.

Figure 5.20 presents the MDO 505 CRIAQ project morphing wing model installed in the tunnel test section, viewed from both the leading edge on the left) and the trailing edge (on the right).

(a) front view (b) rear view

Figure 5.20 MDO 505 wing model
setup in the wind tunnel test section;

To avoid the possibility of damaging the wing tip model during wind tunnel testing, and to be able to observe the first installments of the flutter vibrations, if such a case occurred despite the flutter analysis results, three accelerometers were installed on the wing. The accelerometer model used was the ADXL326, (Analog, 2015), which is a small, low power, complete 3-axis accelerometer with signal conditioned voltage outputs. The ADXL 328 card is an analog three axes accelerometer of ± 16g of full scale range, with a zero g voltage of 1.5 V and an output sensitivity of 57 mV/g, when it is powered at 3 V. It contains a poly-silicon surface micro-machined sensor and signal conditioning circuitry for the implementation of open-loop acceleration measurement architecture. The output signals are analog voltages that are proportional to the measured acceleration. The accelerometer can measure the static acceleration of gravity in tilt sensing applications, as well as dynamic acceleration, resulting

from motion, shock, or vibration. For the present case, the measurements were performed for wing vibration and motions resulted from the wind tunnel testing at various speeds.

The three accelerometers were installed in the wing box, aileron and wind tunnel balance respectively as shown in Figure 5.21.

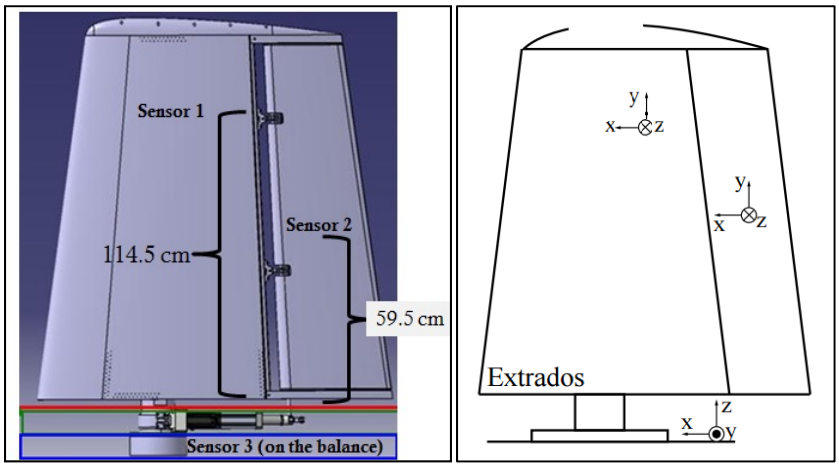

Figure 5.21 Positions and orientations of the accelerometers on the wing

5.5.2 Accelerometers results

The data recorded by the accelerometers is presented for several cases that were studied in the wind tunnel tests. The cases, for which graphical results are presented, are shown in Table 5.3.

Table 5.3 Wind tunnel test cases for which accelerometer results are presented

Case number	Speed (m/s)	Angle of attack (°)	Aileron deflection angle (°)
1	50	-3	-2
2	50	-1.4	4
3	85	-1.5	-4
4	85	-2	5
5	85	-3	1

To quantify the magnitude of the vibration of the wing and aileron, it is necessary to find to boundaries of the amplitude of the recorded acceleration points. Therefore, we suppose that the recorded waveform is the sum of sinusoids representing the vibration modes acceleration as shown in equation (5.8).

$$A(t) = \sum_i A_{X_i} \sin\left(2\pi f_{X_i} t + \phi_{X_i}\right) \vec{\imath} + \sum_i A_{Y_i} \sin\left(2\pi f_{Y_i} t + \phi_{Y_i}\right) \vec{\jmath} + \sum_i A_{z_i} \sin\left(2\pi f_{z_i} t + \phi_{z_i}\right) \vec{k} \tag{5.8}$$

where $A_{X_i}, A_{Y_i}, A_{Z_i}$ represent the acceleration amplitudes of the torsional mode on the X axis, lateral-bending mode on the Y-axis, and the bending mode on the Z-axis, respectively, and where $f_{X_i}, f_{Y_i}, f_{Z_i}$ are the frequencies, and $\phi_{X_i}, \phi_{Y_i}, \phi_{Z_i}$ are the phases.

The demonstration of the boundary is next shown only for the acceleration on the Z-axis, but is the same for the accelerations on the X and Y axes. By considering two sinusoids (vibration modes), so that the bending acceleration equals to the sum of that two sinusoids, we can write:

$$A_Z(t) = A_{z_1} \sin\left(2\pi f_{z_1} t + \phi_{z_1}\right) + A_{z_2} \sin\left(2\pi f_{z_2} t + \phi_{z_2}\right) \tag{5.9}$$

The associated root mean square value verifies equation (5.10):

$$\left(RMS_{Z_1+Z_2}\right)^2 = RMS_{Z_1}^2 + RMS_{Z_2}^2 \tag{5.10}$$

where

- $RMS_{Z_1+Z_2}$ is the root mean square of A_Z
- RMS_{Z_1} is the root mean square of the first sinusoid, and $RMS_{Z_1} = \frac{A_{Z_1}}{\sqrt{2}}$
- RMS_{Z_2} is the root mean square of the second sinusoid, and $RMS_{Z_2} = \frac{A_{Z_2}}{\sqrt{2}}$

Equation (5.10) gives:

$$\left(RMS_{Z_1+Z_2}\right)^2 = \frac{\mathrm{A}_{\mathrm{Z}_1}^2 + \mathrm{A}_{\mathrm{Z}_2}^2}{2} \tag{5.11}$$

$$\Rightarrow \; 4\left(RMS_{Z_1+Z_2}\right)^2 = 2\,(\mathrm{A}_{\mathrm{Z}_1}^2 + \mathrm{A}_{\mathrm{Z}_2}^2) \tag{5.12}$$

It can be shown that $2\,(\mathrm{A}_{\mathrm{Z}_1}^2 + \mathrm{A}_{\mathrm{Z}_2}^2) \geq \left(A_{Z_1} + A_{Z_2}\right)^2$ for all $A_{Z_1} \epsilon$ R and $A_{Z_1} \epsilon$ R:

$$A_Z \begin{cases} \left(A_{Z_1} - A_{Z_2}\right)^2 \geq 0 \\ => \; \mathrm{A}_{\mathrm{Z}_1}^2 + \mathrm{A}_{\mathrm{Z}_2}^2 \geq 2A_{Z_1}A_{Z_2} \\ => \; 2\,(\mathrm{A}_{\mathrm{Z}_1}^2 + \mathrm{A}_{\mathrm{Z}_2}^2) \geq 2A_{Z_1}A_{Z_2} + \; \mathrm{A}_{\mathrm{Z}_1}^2 + \mathrm{A}_{\mathrm{Z}_2}^2 \\ => 2\,(\mathrm{A}_{\mathrm{Z}_1}^2 + \mathrm{A}_{\mathrm{Z}_2}^2) \geq \left(A_{Z_1} + A_{Z_2}\right)^2 \end{cases} \tag{5.13}$$

It is evident that equation (5.12) leads to:

$$4\left(RMS_{Z_1+Z_2}\right)^2 \geq \left(A_{Z_1} + A_{Z_2}\right)^2 \tag{5.14}$$

$$\Rightarrow \; 2 * RMS_{Z_1+Z_2} \geq A_{Z_1} + A_{Z_2} \geq \left|A_{Z_1}\sin\left(2\pi f_{z_1}t + \phi_{z_1}\right) + A_{Z_2}\sin\left(2\pi f_{z_2}t + \phi_{z_2}\right)\right| \tag{5.15}$$

$$\left|A_{z_1}\sin\left(2\pi f_{z_1}t+\phi_{z_1}\right)+A_{z_2}\sin\left(2\pi f_{z_2}t+\phi_{z_2}\right)\right| \leq 2 * RMS_{Z_1+Z_2} \quad (5.16)$$

Equation (5.16) has been demonstrated for two sinusoids, but this inequality can be extended for *n* sinusoids, with $n \in \mathbb{N}$. It can be rewritten under the following form:

$$\left|\sum_{i=1}^{n} A_{z_i}\sin\left(2\pi f_{z_i}t+\phi_{z_i}\right)\right| \leq 2 * RMS_{Z_1+\cdots+Z_n} \quad (5.17)$$

Table 5.4 gives the boundaries of the recorded accelerations on the three axes X, Y and Z.

Table 5.4 Limits or boundaries of the recorded accelerations

Case number	X_max_ aileron (g)	Y_max_ aileron (g)	Z_max_ aileron (g)	X_max _wing (g)	Y_max _wing (g)	Z_max_ wing (g)
1	0.1201	0.1153	0.1659	0.0937	0.0924	0.0956
2	0.1086	0.1182	0.1913	0.0754	0.0777	0.0845
3	0.1283	0.1403	0.4247	0.0836	0.0994	0.1188
4	0.0864	0.1070	0.4287	0.0492	0.0709	0.1120
5	0.0990	0.1164	0.4533	0.0583	0.0860	0.1052

In Figures 5.22 to 5.26 (a) and (b), the post processed data from the accelerometers was presented as behavior of the acceleration (measured in *g*) with time for a time range of 1s and their correspondent power spectra density. The accelerations in time domain are presented only for the bending vibration (Z-axis) because it's much greater than for the other axis.

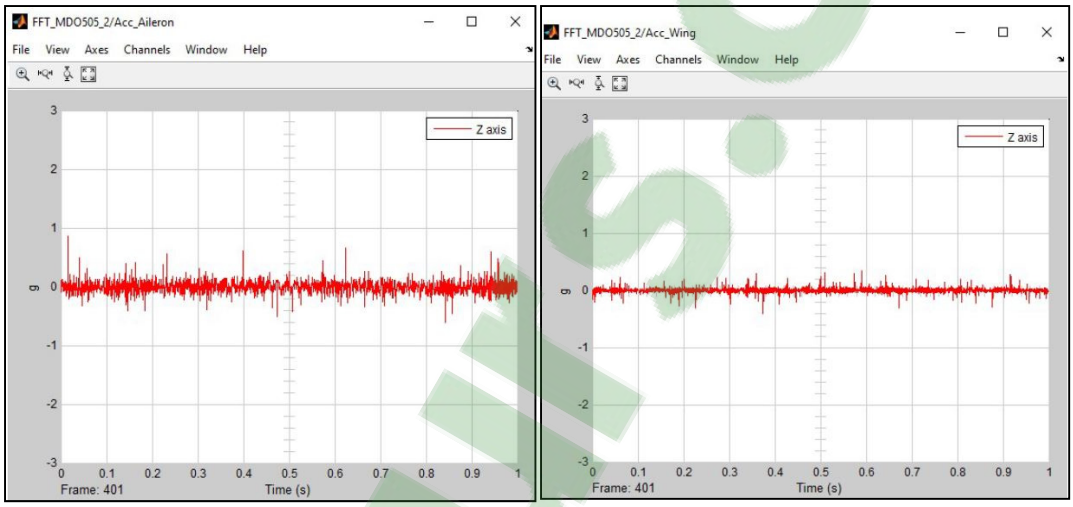

a)

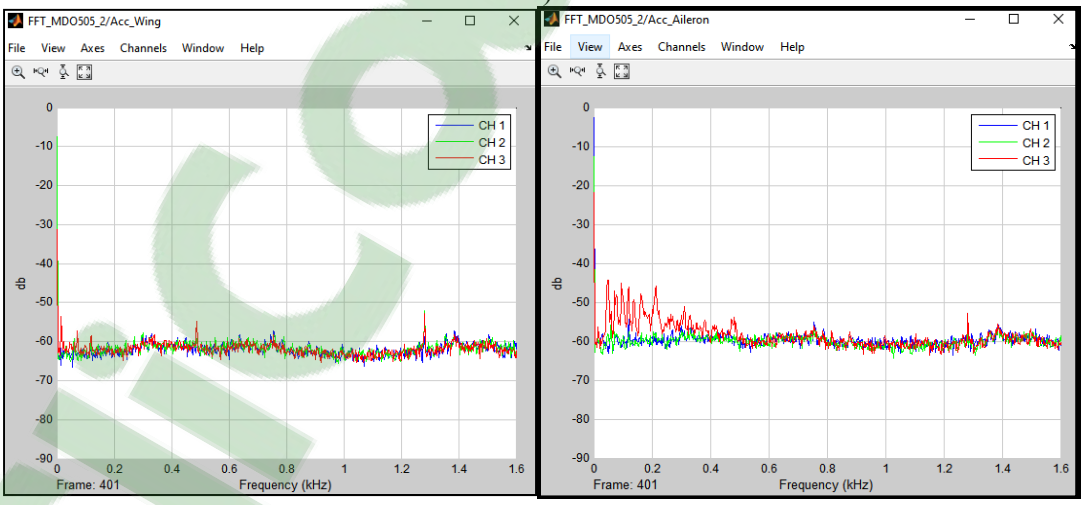

b)

Figure 5.22 Case 1 - Wing with aileron deflection 2° up at Mach 0.15

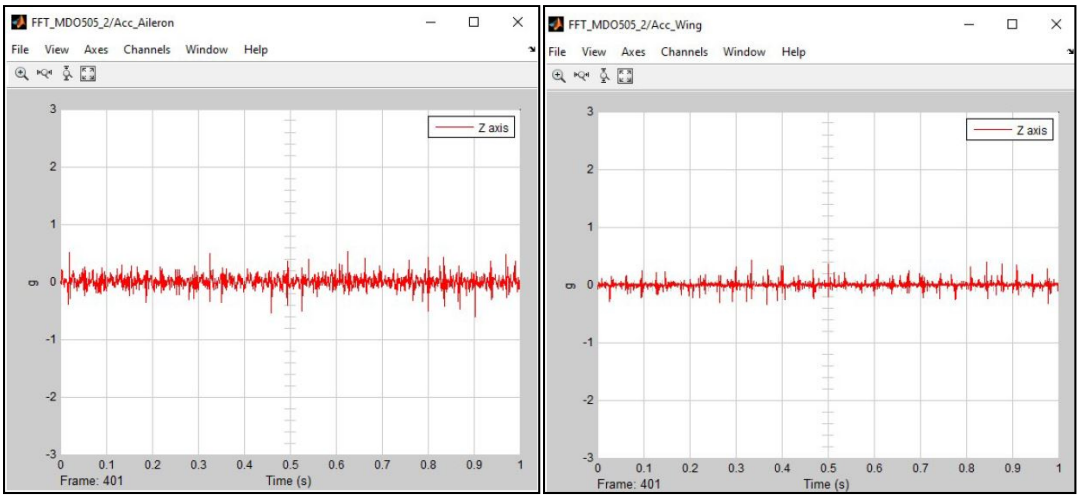

a)

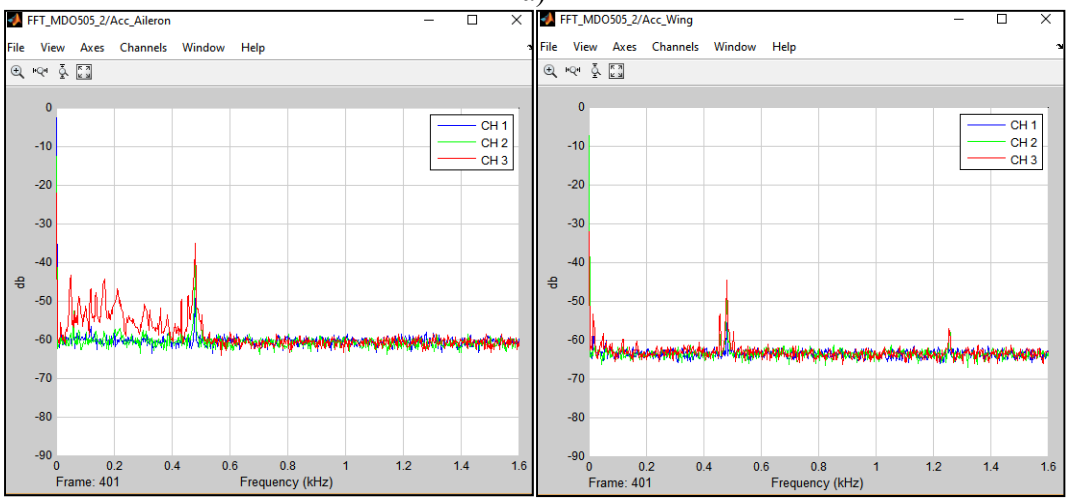

b)

Figure 5.23 Case 2 - Wing with aileron deflection 4° down at Mach 0.15

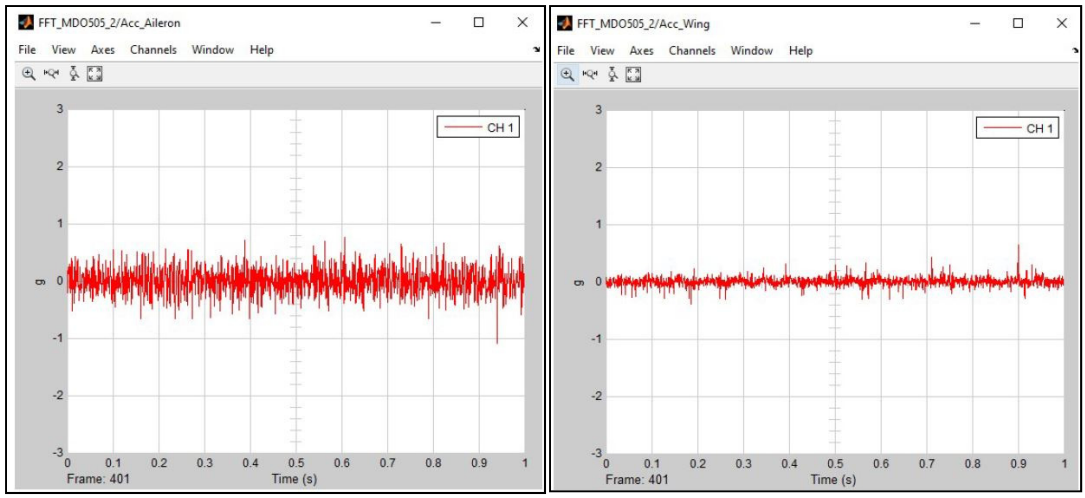

a)

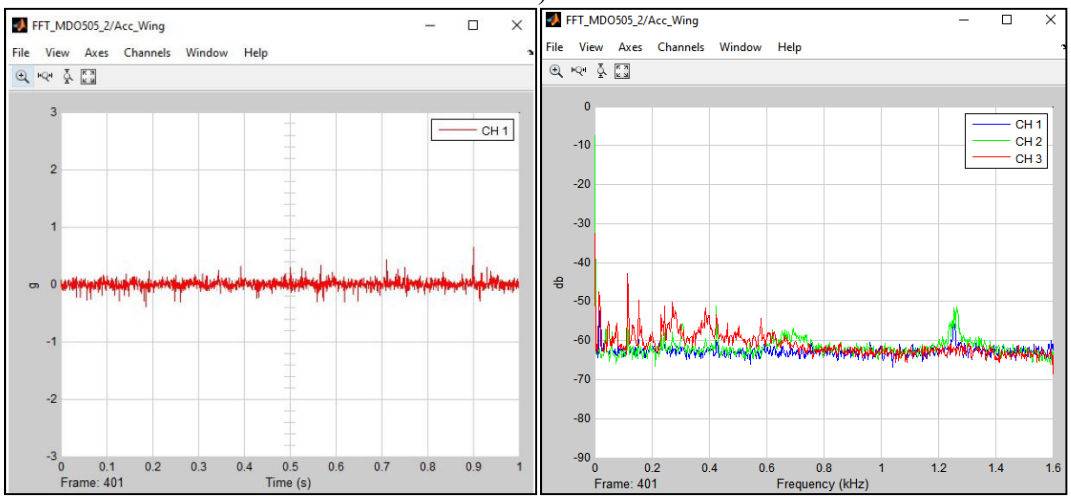

b)

Figure 5.24 Case 3 - Wing with aileron deflection -4° up at Mach 0.25

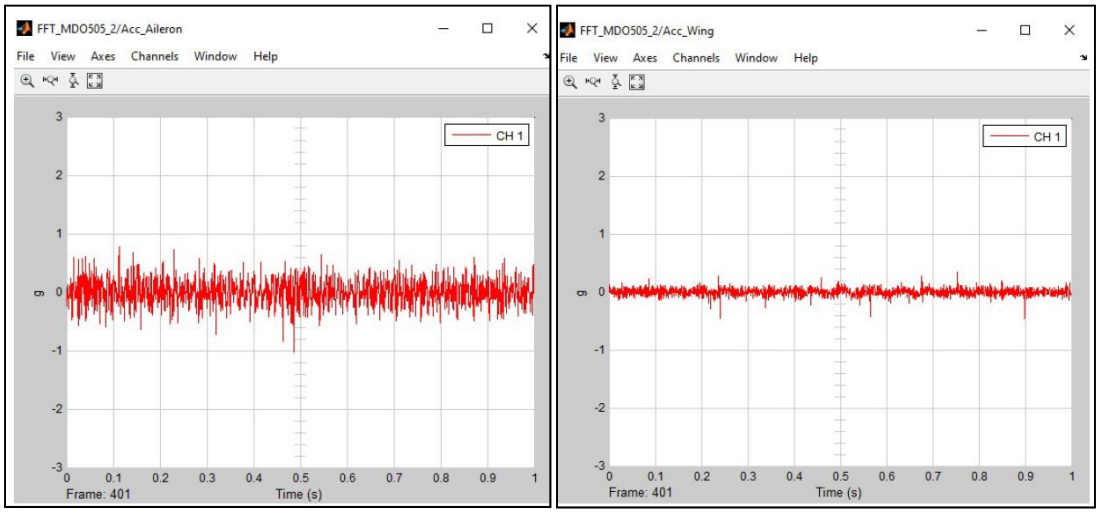

a)

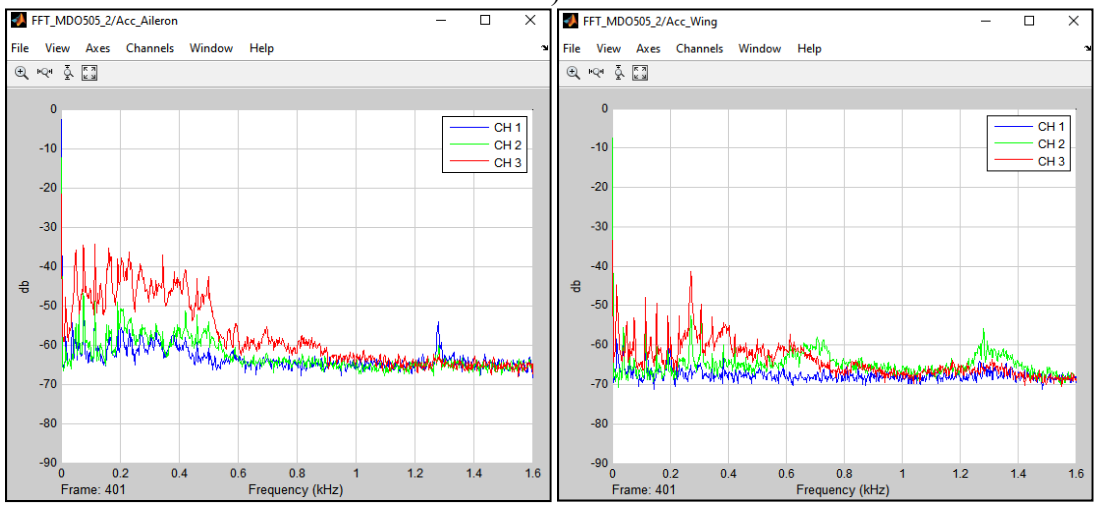

b)

Figure 5.25 Case 4 - Wing with aileron deflection 5° down at Mach 0.25

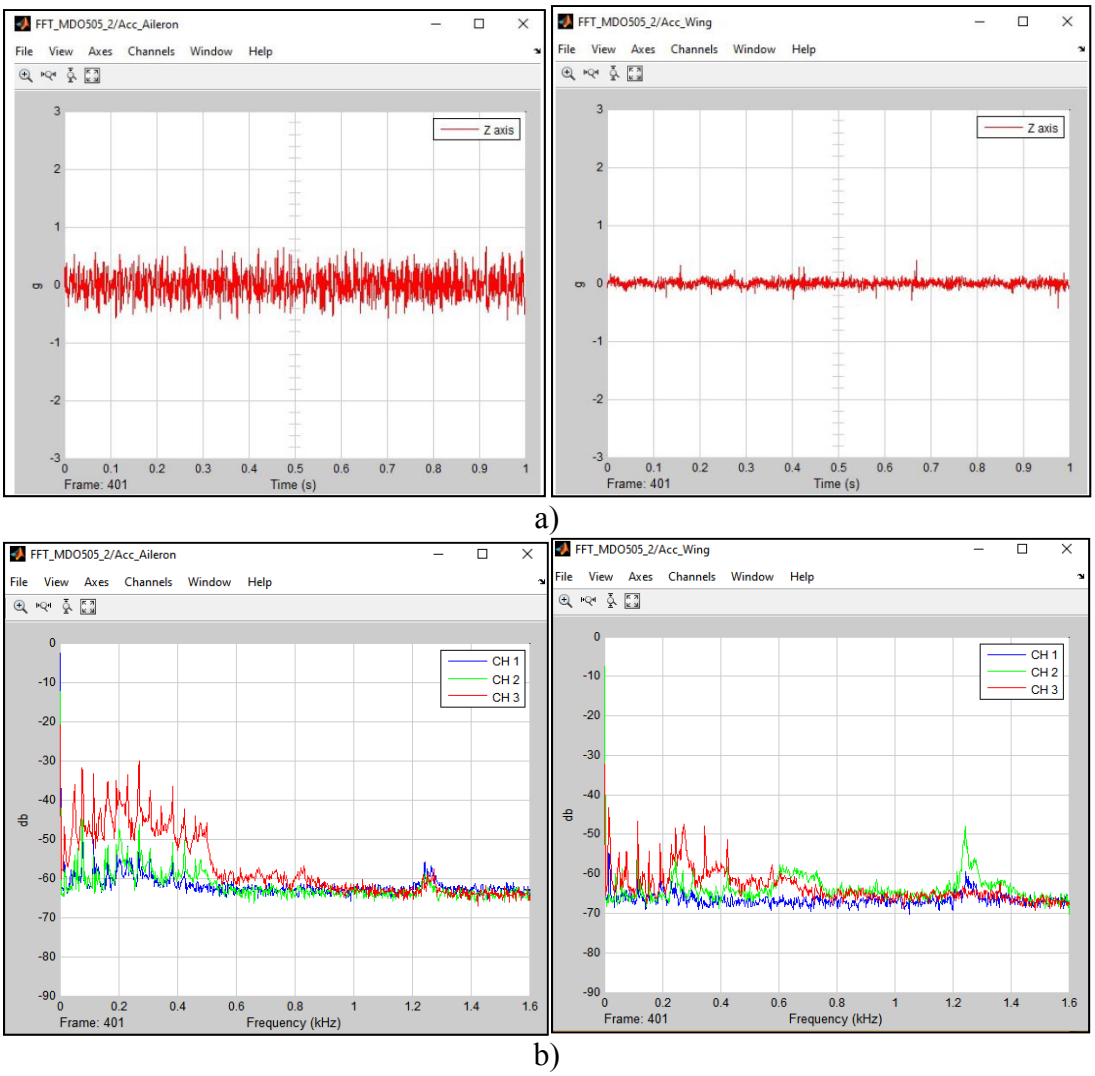

Figure 5.26 Case 5 - Wing with aileron deflection 1° down at Mach 0.25

From Figures 5.22 to 5.26 (a), the influence of the airspeed was observed on the accelerations; for the Mach number of 0.15 (50 m/s) the accelerations revolve around the 0.5 g for the accelerometer installed on the aileron, which is the accelerometer most sensitive to changes in amplitude due to the fact that the aileron is an almost free element (fixed by the external actuator), and therefore is the most flexible part of the wing demonstrator. The magnitude of the acceleration extracted for the Mach 0.25 (85 m/s) cases is three times the magnitude we have for Mach 0.15 (50 m/s) cases. Of course, these accelerations have small values which show small displacements as well, which confirms that the order of magnitude of the displacements predicted during the flutter analysis were correct.

In Figures 5.22 to 5.26 (b), the effect of the airspeed can also be seen, when passing from Mach number 0.15 to 0.25, but here the presence of the modes is also visible in the range 0 to 450 Hz, corresponding to first 10 modes. Channels 1, 2 and 3 represent the *x*, *y* and *z* axis. It can be observed that the axis on which the amplitude of vibrations is highest is the z axis, which is in fact oriented in the span direction of the model; it should also be noted that the amplitudes measured on the aileron are normally higher that those measured on the wing because the aileron is a flexible and movable part compared to the wing box and even to the morphing upper surface. But the magnitude of the amplitude of vibration remains less than 60dB, which for a rigid structure means that no aero-elastic effects, such as flutter, occurs at these speeds. From the wing's point of view, a mode appears at 1.3 kHz where a peak in amplitude occurs for the *y* axis, while at the same frequency the aileron has a peak in amplitude on the *x* axis (corresponding to the chord direction), but for both, the magnitude of the peak is smaller than the amplitude seen in the frequency range of 0 to 400 Hz, which means that this mode does not put in danger the structure of the wing demonstrator during tests. Overall, it can be said that by using the recorded accelerometers' data, it can be confirmed that the flutter analysis was correct in the assumption that for the speeds at which the wing demonstrator was tested, no aeroelastic dynamic or static phenomena occurred, and that the wing with aileron is a sufficiently rigid system that can safely be tested at similar or higher speeds (but remaining in the subsonic range) and no structural damages would occur.

5.6 Conclusions

In the present paper, the flutter analysis and the experimental accelerometer results were discussed for a wing demonstrator with a morphing composite upper surface. The research was part of multi- disciplinary project aimed at developing a safe morphing wing technology that would improve the performances of the wing and aircraft, and that could have a fast implementation on an already existing structure. The finite element model was discussed in detail, and presented the manner in which the structure was modeled as well as the differences that occurred between the composite upper surface skin and the traditional aluminium skin. For the flutter analysis, two models were developed. The difference between

the two FEM models was given by the material and properties of the upper surface between the two spar components. One model had a traditional aluminium upper surface with constant thickness, while the second model had a composite upper surface skin optimized for morphing capabilities and deformation performances, with variable thickness in both span and chord directions. The models were developed using Hypermesh software, part of the HyperWorks software package. The flutter analysis was conducted using the MSC Patran/Nastran software. For the flutter analysis the thin plate method was used to generate an aerodynamic plate with DLM boxes for the aerodynamic analysis and the coupling between structural and aerodynamic meshes was further done using thin plate splining method. The analysis was done using the p-k method for calculating the modal displacements and frequencies. The numerical results have shown small displacements corresponding to the first 5 modes, and the damping ratio curve for each mode calculated for a range of speeds has shown that not flutter phenomena was expected to take place for the speeds that were tested in the wind tunnel. The analysis of the two models has shown that the composite skin had a minimal influence on the aero-elastic behavior of the wing; the wing with composite upper-surface optimized for morphing capabilities performed in almost the same manner as the wing with traditional aluminium skin of constant thickness. This fact has shown that during the structural optimization and sizing, and through the composite skin optimization process, the structural criteria demanded by the industry partner was respected, and the results were successful in that the wing model equipped with composite upper surface has its rigidity properties close to those of the aluminium skin, while the flexibility needed for active controlled deformation was retained. The experimental data recorded by three accelerometers installed on the aileron, wing box and balance, have confirmed that analysis was correct in its prediction that flutter phenomenon would not occur and it had also shown that the small changes in speeds, as from 50 to 85 m/s, had a visible influence on the accelerations associated with the amplitudes of vibrations. Furthermore, on the frequency graphs, it was possible to visualize the main acting modes in the range of 0 to 450 Hz and to observe a mode that taking place at 1.3 kHz that was not predicted by the numerical analysis.

In conclusion, the analysis has shown that it was possible to develop a composite morphing skin that retains the behavior of an aluminium skin for a wing without endangering the structure of the wing. Both the analysis and the experimental data from accelerometers have shown that for an actively morphing wing demonstrator tested at subsonic speeds, at various angles of attack and aileron deflections, no aero-elastic effects could be observed.

Acknowledgments

We would like to indicate our appreciation for the financial support obtained in the framework of the CRIAQ MDO-505 project and for the implication of our industrial partners Bombardier Aerospace and Thales Canada. We also wish to thank NSERC for their support. Special thanks are dues to our collaborators and leaders in this project: Mr. Patrick Germain and Mr. Fassi Kafyeke from Bombardier Aerospace, Mr. Philippe Molaret from Thalès Canada and Mr. Eric Laurendeau from École Polytechnique.

CHAPTER 6

OPTIMIZATION AND DESIGN OF A MORPHING AIRCRAFT WING TIP DEMONSTRATOR FOR DRAG REDUCTION AT LOW SPEED, PART I – AERODYNAMIC OPTIMIZATION USING 3 ALGORITHMS: GENETIC, BEE COLONY AND GRADIENT DESCENT

Andreea Koreanschi, Oliviu Şugar Gabor, Joran Acotto, Guillaume Brianchon, Gregoire Portier and Ruxandra Mihaela Botez
LARCASE Laboratory of Applied Reasearch in Active Controls,
Avionics and Aeroservoelasticity
École de Technologie Supérieure, 1100 rue Notre Dame Ouest,
Montréal, H3C1K3, Québec, Canada

Mahmoud Mamou and Youssef Mebarki
Aerodynamic Laboratory
NRC Aerospace,
National Research Council Canada,
Ottawa, K1A0R6, Ontario, Canada

This article was accepted for publication in the *The Chinese Journal of Aeronautics*

Résumé

Dans cet article, un algorithme génétique « in-house» est décrit et appliqué à un problème d'optimisation pour améliorer les performances aérodynamiques d'un bout d'aile par la déformation de la surface supérieure. Les performances de l'algorithme ont été étudiées du point de vue de la convergence, en conformité avec les conditions de conception. L'algorithme a été comparé à deux autres méthodes d'optimisation, la colonie d'abeilles artificielles et une méthode de gradient, pour deux objectifs d'optimisation. Les résultats des optimisations avec chacune des trois méthodes ont été tracés sur les cartes obtenues avec la

méthode de Monte-Carlo, qui montrent qu'ils étaient situés dans la région d'optimum global. Les résultats d'optimisation pour 16 cas de test en soufflerie et 2 fonctions objectives ont été présentés. Les 16 cas utilisés pour les optimisations ont été inclus dans le plan d'essai expérimental pour le bout d'aile déformable, et les résultats obtenus en utilisant les déplacements donnés par les optimisations ont été évaluées.

Abstract

In this paper, an 'in-house' genetic algorithm is described and applied to an optimization problem for improving the aerodynamic performances of an aircraft wing-tip through upper surface morphing. The algorithm's performances were studied from the convergence point of view, in accordance with design conditions. The algorithm was compared to two other optimization methods, namely the Artificial Bee Colony and a Gradient Method, for two optimization objectives, and the results of the optimizations with each of the three methods were plotted on response surfaces obtained with the Monte Carlo method, to show that they were situated in the global optimum region. The optimization results for 16 wind tunnel test cases and 2 objective functions were presented. The 16 cases used for the optimizations were included in the experimental test plan for the morphing wing-tip demonstrator, and the results obtained using the displacements given by the optimizations were evaluated.

6.1 Introduction

In the context of a world in continuous change, the aerospace industry must develop greener and more efficient airplanes that will consume less fuel and have a lower CO_2 footprint. Therefore, new methods must be developed for improving the flight behavior of airplanes through the optimization of their existing properties.

Many optimization methods have been developed and could be used in the aerospace research. (Xing and Gao, 2014) provide an exhaustive presentation of various optimization algorithms inspired from the natural world's behavior[2], physical[3] and chemical[4] properties,

and also algorithms based only on abstract mathematical theory (Chen, Wang and Li, 2012; Irizarry, 2005; Maniezzo, Stützle and Voß, 2010; Xie and Zeng, 2009).

Applications of optimization algorithms can now be found in almost all industrial and academic research venues, from electric circuitry[6] to stock market predictions[7], image quality problems[8] and software implementation problems[9] (Bacanin, 2012; Cui et al., 2013; Majhi et al., 2009; Zhang and Ye, 2012).

In aerospace, many research projects and collaborations include the successful implementation of the more traditional metaheuristic optimization algorithms such as genetic algorithms, bee colony algorithms, artificial neural networks or ant colony optimization in their research for new optimized flight trajectories, wing shapes and control techniques. One such collaboration took place between the teams of the LARCASE laboratory and CMC Electronics-Esterline for their project, which was funded by the Green Aviation Research Development Business Led Network (GARDN) in its second round (Patron, Botez and Labour, 2013; Patrón, Kessaci and Botez, 2014). The main objective of the collaboration was to optimize the vertical and horizontal paths of an aircraft within the Flight Management System by taking into account the Required Time of Arrival, the wind grids and meteorological conditions. The main motivation of the project was to reduce overall carbon emissions and costs associated to aircraft flight.

Applications of optimization techniques for small aircraft were described by (Gamboa et al., 2009) in their design of an Unmanned Aerial Vehicle (UAV) morphing wing capable of independent span and chord changes, using a telescopic spar and a rib system. The numerical analysis demonstrated a drag reduction of up to 23% when compared to the non-morphing geometry. (Falcao, Gomes and Suleman, 2011) designed and tested a morphing winglet for a military UAV, achieving important performance improvements by simply changing the winglet cant and toe angles. Other research on UAV wing morphing was done by (Sugar Gabor, Koreanschi and Botez, 2013a; Sugar Gabor et al., 2015b), where the upper-surface of the wing was optimized on a segment between the leading edge and 55% of the chord, and in

which the morphing of the full wing's geometry was also explored; and by (Tianyuan and Xiongqing, 2009) who studied a multi-disciplinary optimization for improving aerodynamic, stealth and structural performances of an unmanned aerial combat vehicle. (Peifeng et al., 2012) developed a methodology for aerodynamic optimization aimed at demonstrating the performances of a blended wing body transport, while (Xie et al., 2013) studied the effects of static aeroelastic phenomena on very flexible wings.

Other experiments were conducted in the area of 'active airfoil optimization'. One of these experiments was performed in the CRIAQ 7.1 project, in which collaboration took place between aerospace industrial teams at Bombardier Aerospace and Thales Canada, academic partners from the École de Téchnologie Supérieure (ETS) and École Polytéchnique of Montreal, and researchers at the Canadian National Research Council (NRC). The purpose of this project was to demonstrate the capabilities of morphing wings in a wind tunnel for developing the flow transition from laminar to turbulent (Botez, Molaret and Laurendeau, 2007; Popov et al., 2009). Morphing was achieved by replacing the upper surface of the wing, spanned between 7% and 70% of the wing chord, with a flexible carbon-Kevlar composite skin. The skin morphing was achieved using two Shape Memory Alloy (SMA) actuation lines to obtain an optimized shape for each flight condition tested in the wind tunnel (Grigorie et al., 2012a). The optimization was done using a genetic algorithm method coupled with the aerodynamic solver XFoil. The wind tunnel tests had proven that the concept of upper surface morphing was viable, controllable, and provided tangible results confirming the delay of the transition from laminar to turbulent flow, thereby inducing a substantial reduction in the drag coefficient (Sainmont et al., 2009). Proportional – Integrator – Derivative (PID), (Grigorie, Botez and Popov, 2012), and neuro-fuzzy controllers, (Grigorie et al., 2011a), were tested to prove the ability of the flexible upper surface and the morphing mechanisms towards the transition delay. The controllers demonstrated an excellent performance in both open[25] and closed loops[26] (Popov et al., 2010a; 2010b).

Exhaustive state of the art listings of wing geometry optimization research are presented by (Sofla et al., 2010; Vasista, Tong and Wong, 2012).

The research presented in this paper concentrates on the practical application of an ‘in-house’ developed genetic algorithm to determine the optimum shape of the wing upper-surface that leads to improvements in the flow behavior on the upper-surface of the wing. The paper is focused on the design aspects of the optimization algorithm, depending on the imposed constraints, and on the practical aspects of a multi-disciplinary optimization applied to the aerodynamic improvement of an airfoil shape. The optimization concentrated on the improvement of the upper-surface behavior of the flow by changing the position of the transition from fully laminar to fully turbulent flow. The optimization was carried out at the airfoil level and, in practice, was applied to a full-scale wing tip with an aircraft-type internal structure. Comparisons were performed between the results obtained with this ‘in-house’ genetic algorithm and two other methods: Bee Colony algorithm and Gradient Descent. These comparisons led to the conclusion that the ‘in-house’ algorithm could be used for the experimental validation using wind tunnel testing for all test cases

6.2 Presentation of the research context

The research presented in this present paper was done within the framework of the international CRIAQ MDO505 Morphing Wing project. The participants in this project were teams from Ecole de Technologie Supérieure (ETS), Ecole Polytehnique of Montreal and University of Naples ‘Federico II’ as academia research partners, the Canadian National Research Council (CNRC) and the Italian Aerospace Research Center (CIRA) as research center partners, and Bombardier Aerospace, Thales Canada and Alenia Aermacchi as industrial partners.

The objectives of the project were to design, manufacture and control a wing demonstrator based on an aircraft wing tip equipped with both a conventional and an adaptive aileron. The novelty of the CRIAQ MDO 505 project was the multidisciplinary approach of the project, in which structure, aerodynamics, control and experimental design were combined to design and manufacture an active morphing wing demonstrator and then to test it under subsonic wind tunnel conditions.

Figure 6.1 presents the layout and the position of the morphing upper skin on a typical aircraft wing, while Figure 6.2 presents the structural elements of the morphing wing model.

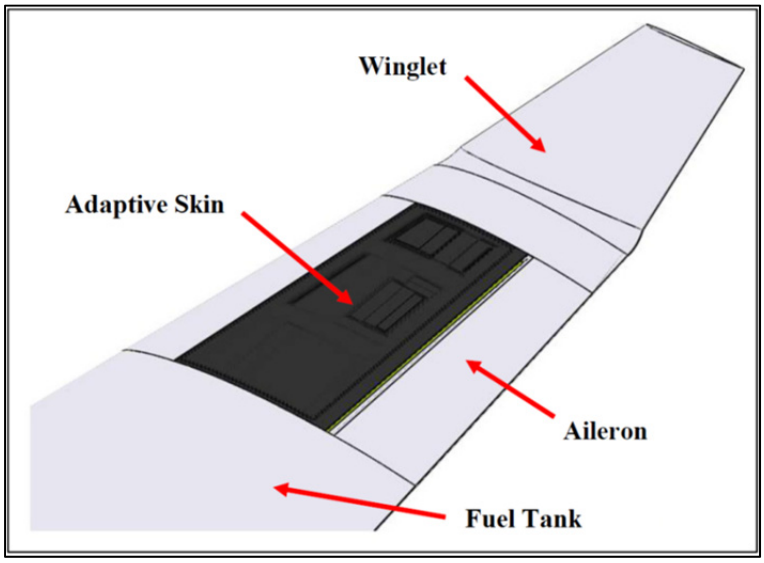

Figure 6.1 Layout and position of the morphing skin on the aircraft wing

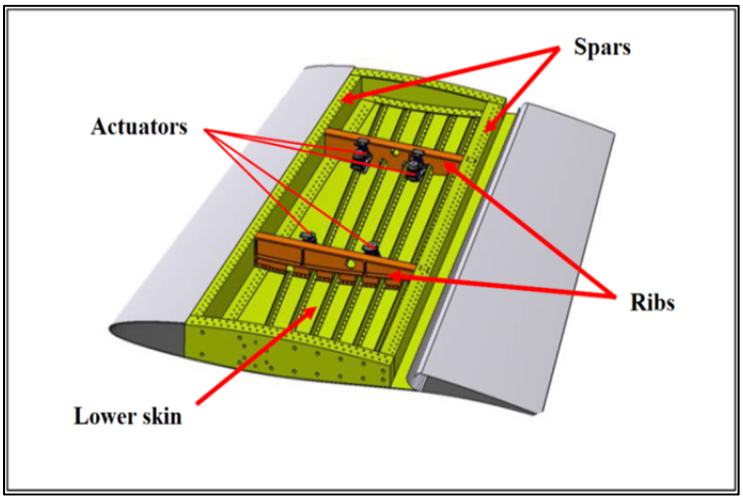

Figure 6.2 Structural elements of the CRIAQ MDO 505 morphing wing concept with morphing skin not shown

The CRIAQ MDO 505 project was a continuation of the former research project CRIAQ 7.1, and aimed at a higher level of technical readiness by considering a real aircraft wing internal

structure, a certifiable electric control system and controllers. The objectives of the active morphing wing tip project were mainly: (a) the design and manufacturing of a morphing wing model that withstands gust loads of up to 1g; (b) an improvement of the aerodynamic performance of the wing, through the active control of the boundary layer transition from laminar to turbulent states; (c) the design, implementation and integration of control systems and a morphing mechanism to control the shape of the wing in wind tunnel experiments.

The full-scale morphing wing model had an optimized structure with a 1.5 m span, a 1.5 m root chord, a taper ratio of 0.72, and leading and trailing edges sweep angles of 8°. The wing box and its internal structure (spars, ribs, and lower skin) were manufactured from aluminum alloy material, and the adaptive upper surface was positioned between 20% and 65% of the wing chord. The adaptive upper surface skin was specifically designed and optimized to meet the industry partners' requirements. The adaptive skin was manufactured using carbon fiber composite materials, (Michaud, 2014).

The deformation of the skin shape, driven by actuators placed inside the wing box structure, was a function of the flight conditions (defined in terms of Mach numbers, Reynolds numbers and angles of attack). These actuators were specifically designed and manufactured to meet wind tunnel test requirements. Four electric actuators were fixed to the ribs and to the composite skin and were installed on two actuation lines, each line placed at 37% and 75% of the wing span. The actuators were positioned at 32% and 48% of the local wing chord on each of the two actuation lines. Each actuator has the ability to operate independently from the others.

The aileron's hinge was located at 72% of the chord. Two types of ailerons were designed and manufactured. One aileron was structurally rigid, while the other one represented a new morphing aileron concept. Both ailerons were designed to be attached to the same hinge axis on the wing box, and both were able to undergo a maximum controlled deflection between -7° and +7°. Figure 6.3 presents a sketch of the morphing wing model concept that indicates how this model was mounted and tested in the NRC subsonic wind tunnel.

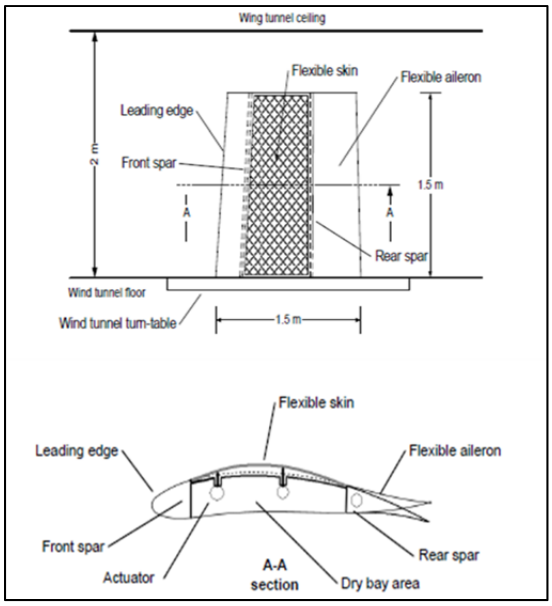

Figure 6.3 CRIAQ MDO 505 morphing wing concept

6.3 Optimization Algorithm

6.3.1 Genetic Algorithm

The Genetic Algorithm is a meta-heuristic method of optimization inspired from nature. It uses various characteristics of the object to be optimized as ‘genes’, and searches for the best combination of genes in an iterative fashion. The genes are used to create new objects or individuals, based on the original form (shape) of the object being optimized, but with different characteristics. The creation of new individuals is done using two processes inspired by natural genetic reproduction: ‘cross-over’ and ‘mutation’(Herrera, Lozano and Verdegay, 1998). The cross-over process is the one in which the genes of two individuals are mixed in various proportions to obtain new genes that form a new individual. Various types of functions can be used to determine how to assign and combine the parents’ genes, with the most simple being the assignment of genes in equal proportions. Mutation is a process that affects a percentage of the individuals resulted from the cross-over process, changing the

values of the genes using a mutation percentage, which allows a variation of the gene pool, so as not devolve into degeneration.

A fitness function is used to evaluate the optimization level of the new individuals with respect to the original ones. The fitness function is a representation of the objective of the optimization and describes the ideal characteristics of the optimized individual.

The genetic algorithm method has been studied and validated in various problems; it uses different combinations of cross-over and mutation functions as well as problem-dependent fitness functions (Engelbrecht, 2007; Marwala, 2010).

6.3.2 Description of the problem

The genetic algorithm approach was applied to solve the problem of airfoil upper-surface morphing. The problem objective was the search of the optimum shapes for an airfoil through local thickness modifications, with the aim of improving the upper surface laminar flow and thus the aerodynamic performance.

The local wing thickness modification was obtained through four actuations points, as described in the previous section. The shape of the flexible upper surface was obtained by an optimized combination of the four vertical displacements. These displacements were obtained by the local 'pushing and pulling' actions of four electric actuators installed inside the wing box. The vertical displacements were determined by use of the genetic algorithm optimization for the wing's airfoil.

The morphing upper surface problem was studied for two different airfoils: the ATR42 airfoil, designed for subsonic flight, and the theoretical supercritical airfoil provided by the aerospace industry partner. Figures 6.4 and 6.5 present the two airfoils considered in this study.

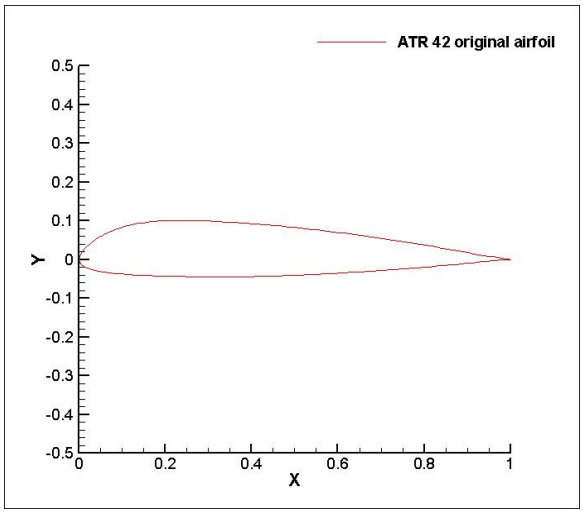

Figure 6.4 The ATR42 wing airfoil

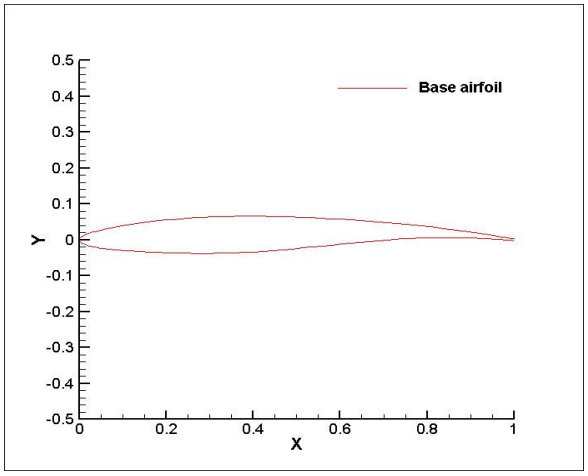

Figure 6.5 The theoretical supercritical airfoil

The variables to be determined for the morphing upper-surface problem were the actuator chord-wise positions, the actuator displacements, the number of actuators, and the length of the morphing surface. To obtain the solutions in terms of these variables, a multidisciplinary approach involving aerodynamics, structure and control was needed.

For each of the airfoils, slightly different solutions were found for the above mentioned variables. For the ATR42 airfoil, the lower number of constraints permitted the development of morphing surface that extended between 10% and 70% of the chord, while the maximum

vertical displacements of 3 mm were constrained by the actuation system and the composite material used for the model manufacturing. Table 6.1 presents the variable values used for the ATR 42 model: LE and TE refer to the leading and trailing edge parts of the airfoil, respectively.

Table 6.1 Morphing problem variable values for the ATR-42 wing airfoil

Morphing skin start point (%c)	Morphing skin end point (%c)	No. of actuators/ chord	LE actuator (%c)	TE actuator (%c)	Maximum displacement (mm)	Type of displacement	Requirements for actuators
10	70	2	30	50	3	Vertical and positive	no

Experimental validation of the genetic algorithm has been performed for a rigid optimized wing model based on the ATR42 airfoil; details of the results, as well as of the manufacturing and the experimental setup were given by (Koreanschi, Sugar-Gabor and Botez, 2016b). Additional details on the morphing wing model and its control system are given by (Kammegne et al., 2014).

For the theoretical supercritical airfoil, considered under the name MDO 505 wing demonstrator airfoil, the approach was more conservative, as multiple industrial structural requirements and constraints were taken into account when performing the optimization.

The MDO 505 wing demonstrator was developed based on a real aircraft wing tip structure, fully equipped with an aileron, but without a winglet. Therefore, respecting the structural requirements was as important as achieving the aerodynamic objectives. The length of the morphing upper surface was restricted by the front and rear spars' positions, and the positions of the actuators were determined based on the morphing surface length. The actuators' maximum and minimum displacements were determined in an iterative process between aerodynamic optimization and morphing surface structural optimization, in which a compromise was reached between the main aerodynamic objectives (influencing the

transition region on the upper-surface of the wing): the structural objectives for a structurally rigid morphing surface, and the need to minimize the actuator forces and size.

The number of actuators was determined based on the number of ribs situated inside the wing box and on the aerodynamic performances obtained through optimization. Several tests were conducted for combinations of four, three, two and one actuators installed on each internal rib; the solution retained was of two actuators per rib.

An additional structural requirement was added to limit the variation in displacement between the two actuators situated on the same rib. This requirement was considered an additional safety measure to those already implemented through the control system to avoid overcharging the morphing surface, and surpassing the maximum allowed force developed by the actuators. Table 6.2 presents the morphing surface limits, the number and position of the actuators on each rib and the maximum displacements.

Table 6.2 Morphing problem variable values for the ATR-42 wing airfoil

Morphing skin start point (%c)	Morphing skin end point (%c)	No. of actuators/ chord	LE actuator (%c)	TE actuator (%c)	Maximum displacement (mm)	Type of displacement	Requirements for actuators
20	65	2	32	48	3.5	Vertical, in both directions	Δactuators < 6mm

The problem of airfoil upper-surface morphing to improve the aerodynamic behavior of wings does not have a single solution. More often, as presented in Section 2.4 of this paper, there is an optimum region where several possible solutions coexist, and any of them could be considered as the final solution to the problem.

6.3.3 Genetic algorithm methodology

Based on the problem description in Section 2.2., the genetic algorithm (GA) was designed to incorporate all variables presented in Tables 6.1 and 6.2 in a general manner, in order to

easily adapt to different requirements in the projects and to find the optimal solution for the actuator displacements situated on the same rib. This GA could therefore accomplish the given objective of improving the airfoil's and implicitly the wing's aerodynamic behavior.

6.3.3.1 Genetic algorithm input

The GA allows the user to choose from a number of structural and aerodynamic variables as well as optimization parameters. The input contains all the data needed to control the optimization, from the problem definition to the effective optimization parameters and objectives.

The 'in-house' genetic algorithm internal design and the interactions between the input variables, the aerodynamic solver XFoil and the components of the optimization routine are presented in Figure 6.6.

Table 6.3 presents the input blocks and the parameters that were needed for the genetic algorithm to start an optimization. The third column in Table 6.3 presents the recommended parameter values used to obtain the best convergence speeds and optimization results, for problem of the MDO 505 wing demonstrator morphing upper-surface shape optimization.

A first generation was created based on the maximum actuator displacement and the number of individuals. An individual in a generation is defined by its genes, which correspond with the actuator displacements for our problem.

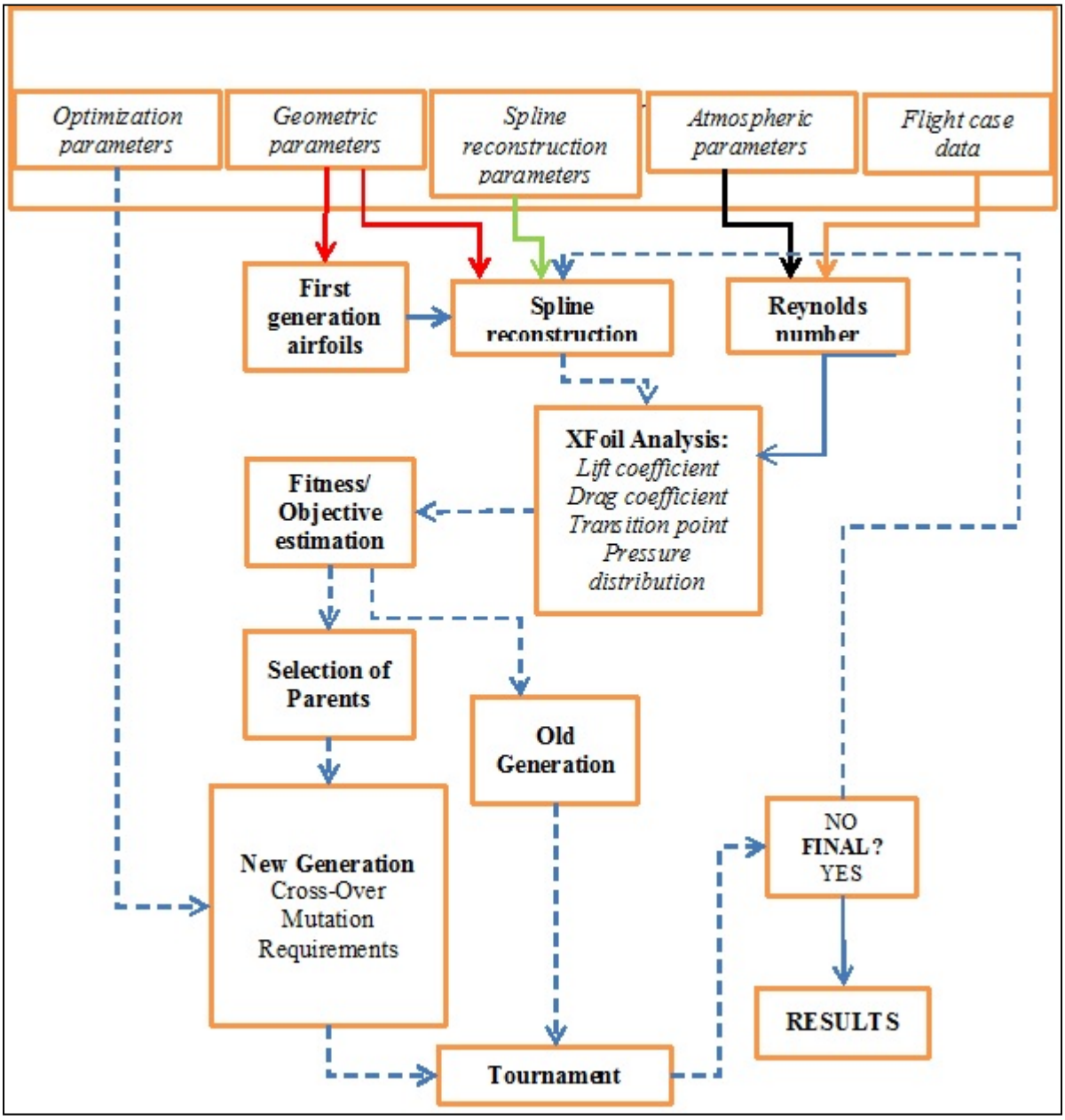

Figure 6.6 Diagram of the ‘in-house’ genetic algorithm

Table 6.3 Input blocks and parameters for the MDO 505 demonstrator airfoil

Input block	Parameter	Values	Observations
Optimization	No. of individuals	40	-
	No. of generations	20	-
	Probability of mutation	1%	% of the total population
	Amplitude of mutation	2%	% of the maximum displacement value
	Optimization objective	-	The objective is given through weights associated with aerodynamic characteristics, such as lift and drag coefficients and the transition location
Geometry	Airfoil coordinates	-	-
	Chord of the airfoil	1.332	m
	Morphing surface start point	20%	% of chord
	Morphing surface end point	65%	% of chord
	No. of actuators	2	Can accept up to 4
	LE actuator	32%	% of chord
	TE actuator	48%	% of chord
	Maximum actuator displacements	3.5	mm
	Type of displacement	both directions	Allows both positive (push) and negative (pull) actions
Spline reconstruction	Number of splines	8	-
Atmosphere data	Density	1.22	kg/m^3
	Dynamic viscosity	1.82E-05	Pa s
	Temperature	293	K
	Altitude	0	m
Flight data	Number of cases	16	-
	Speed	-	range of Mach speeds
	Angle of attack	-	range of angles
	Aileron deflection	-	range of angles

6.3.3.2 Airfoil reconstruction and aerodynamic analysis

In order to analyze the optimization level of each of these individuals, they needed to be transformed from displacements to airfoil shapes. The process of reconstructing the airfoils is based on cubic spline interpolation and requires the displacements associated with each individual, the coordinates of the original airfoil, the morphing surface limits, the number and positions of the actuators and the number of spline points.

Spline functions are characterized by their shape on subintervals, between two control points. They are also known as piece-wise polynomial real functions. In interpolation problems, spline interpolation is often referred to as polynomial interpolation, as it yields similar results. With lower-degree splines (such as bi-splines or cubic splines), the resulting curve is rebuilt as accurately as if it had been interpolated with high degree polynomials, but with the benefit of avoiding instability due to Runge's phenomenon, (Berbente, Mitran and Zancu, 1997; Piegl and Tiller, 2012).

The most-used spline interpolation is the *cubic spline*, which ensures continuity up to the second order derivatives, thus allowing the calculation of the curvature radius. For the problem of the morphing upper surface, cubic splines were found to be sufficiently accurate to reconstruct the wing airfoil shape as function of the actuator displacements, (Fincham and Friswell, 2015; Kulfan and Bussoletti, 2006).

The reconstructed airfoils were refined and analyzed using the XFoil aerodynamic solver, based on the free stream conditions and the considered flight cases. XFoil is an open source aerodynamic solver developed by (Drela and Youngren, 2001) that allows both inviscid and viscous calculation. It also includes the estimation of the boundary layer parameters, including the transition position, and function for modifying the airfoil geometry, such as curvature change and flap deflection.

In XFoil, the inviscid calculations were performed using a *linear vorticity stream function panel method.* A Karman-Tsien compressibility correction, (Drela, 1989b), was added to the panel method, which allowed for more accurate predictions in subsonic flow. For the viscous flow calculations, XFoil uses a two-equation lagged dissipation integral boundary layer formulation, (Drela, 1989a), and incorporates the e^N transition criterion, (Drela, 2003). The flow in the boundary layer and in the wake interacts with the inviscid potential flow by using the *surface transpiration model*.

The XFoil code was chosen because its precision and effectiveness for rapid design and assessment have proven to be acceptable, and because of the code's rapid convergence. The latter attribute is especially important in an optimization using the genetic algorithm, where a large number of individuals and generations are analyzed simultaneously.

The parameters that resulted from the Xfoil analysis were the lift, drag and moment coefficients, the upper-surface transition point and the skin friction coefficient, a critical parameter for understanding the flow's boundary layer behaviour.

6.3.3.3 Optimization evaluation

The results of the analysis were integrated into a single point multi-objective fitness function, expressed by equation (6.1), and paired with user-defined weights that must be provided according to the optimization objective desired in the input.

The *fitness function* calculates a fitness value that estimates the quality level of each analyzed airfoil. The goal of the optimization was to find the airfoil that had the maximum fitness value, and the algorithm was set up in a manner to avoid user-determined values for this problem. Thus, the algorithm was allowed to search the maximum fitness value across the number of generations introduced in the input block (Table 6.3).

$$F_f = w_1 \cdot \left(\frac{C_{l\_morphed} - C_{l\_original}}{C_{l\_original}} \right)^{w_2} + w_3 \cdot \frac{1}{C_d} + w_4 \cdot \left(\frac{Up_{Tr\_morphed} - Up_{Tr\_original}}{Up_{Tr\_original}} \right)^{w_5} + w_6 \cdot \left(\frac{\left(\frac{C_l}{C_d} \right)_{morphed} - \left(\frac{C_l}{C_d} \right)_{original}}{\left(\frac{C_l}{C_d} \right)_{original}} \right)^{w_7} + w_7 \cdot \frac{Up_{Tr}}{C_d} \quad (6.1)$$

When all the airfoils from a generation were analyzed and a fitness value was associated to the corresponding individuals, the individuals were sorted from the highest to the lowest fitness values and awarded grades. Since the fitness value varies from individual to individual, fitness value groups were created and a single grade was associated to each group. For example, if 5 individuals had fitness values between 60 and 65 and these values were the highest in a generation, they would be assigned to one group and all airfoils from this group would be given a grade of 10.

The awarded grades were given values between 1 and 10, with a step of 1, where 1 was the grade given to the group containing the worst individuals and 10 was given to the group containing the best individuals.

6.3.3.4 New generations and individuals

The main part of the genetic algorithm was the evolution from the current generation towards the next one. Two main processes were used to determine the evolution of a generation: cross-over and mutation.

6.3.3.4.1 Cross-over

Cross-over is a process in which two or more individuals are paired and their genes (which were the actuator displacements here) are mixed to obtain a new set of genes which defines a new individual.

For the cross-over process, the parent individuals were randomly selected from the present generation; not all of the individuals had the same chance of being chosen as parents. The

individuals with higher grades had more chances to be selected than those with lower grades, thus allowing the best genes to propagate to the next generation without endangering the convergence of the optimization by a minimization of the genetic pool. This particularity of the individual is called the *attraction factor*, which shows how an individual with a high grade is more attractive and thus more likely to be chosen to become a parent.

A probability function was developed based on the attraction factor and a random value; it gave values between 1 and 10 to individuals, based on which they were chosen to become parents.

$$P_s = 11 - x, x \in \mathbb{N}, P_s \in \mathbb{N} \tag{6.2}$$

$$x = \begin{cases} y, y \geq 1 \\ 1\ , y \leq 1 \end{cases}; x, y \in \mathbb{N} \tag{6.3}$$

$$y = \begin{cases} z^{A_f}, z^{A_f} \leq 10 \\ 10\ , z^{A_f} \geq 10 \end{cases}; y, z \in \mathbb{N} \tag{6.4}$$

$$\begin{gathered} z = \begin{cases} \lfloor \varepsilon, \varepsilon \geq 0 \\ \varepsilon \rceil\ , \varepsilon \leq 0 \end{cases}; \varepsilon \in \mathbb{Z} \\ \varepsilon = \ \delta * 10^{\frac{1}{A_f}}; random\ \delta \in [0,1] \end{gathered} \tag{6.5}$$

where P_S is the *probability of selection* and A_f represents the *attraction factor*, which was set at 2 in the present case.

The cross-over process used in the 'in-house' genetic algorithm has two step functions, based on the convergence rate observed during tests. It was observed that the algorithm converged towards the optimal region from the first 10 generations (Figure 6.7) when using a single cross-over function.

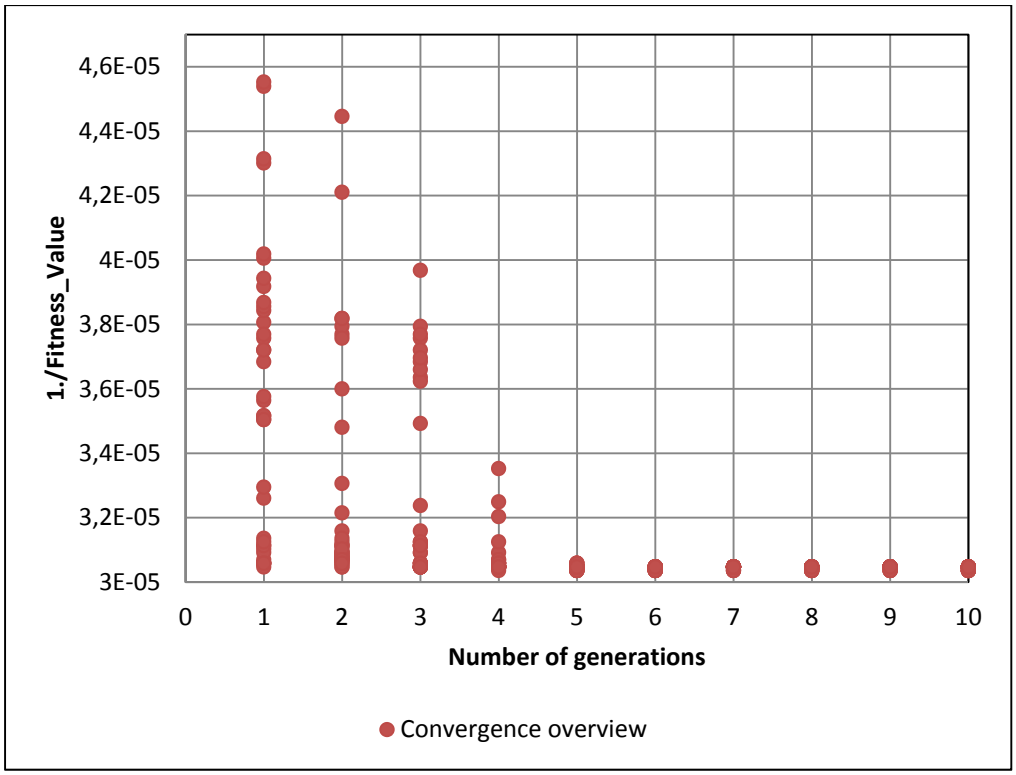

Figure 6.7 Convergence overview for optimization at speed 51 m/s, angle of attack -4.1° and aileron deflection 1° down

However, since there was the possibility that after 10 generations the algorithm would only be situated in the vicinity of the optimal region, instead of finding a solution inside this region, a two-step function was implemented.

The first step is a function that mixes the parents' genes in equal proportions; it was used for the first 10 generations when the algorithm closed to the solution region. At the tenth generation, the algorithm was switched to use the second function, which was developed based as a variation on a binary cross-over function, (Deb and Agrawal, 1994). The second function was applied throughout the remainder of the generations until the last generation was reached.

$$child = \begin{cases} child_{=}, generation \le 10 \\ child_{\neq}, generation > 10 \end{cases}$$
$$'='\text{– equal share}$$
$$'\neq'\text{– not equal share} \tag{6.6}$$

$$child_{equalshare}(gene_i) = gene_{i\_parent_j};$$
$$i \in [1, \text{number of genes}],$$
$$j \in [2, \text{number of parents}] \tag{6.7}$$

$$child_{\neq} = \begin{cases} \frac{1}{2} \cdot (1+\delta) \cdot gene_{i,parent_j}, \delta \ge 0.5 \\ \frac{1}{2} \cdot (1+\delta) \cdot gene_{i,parent_{j+1}}, \delta < 0.5 \end{cases};$$
$$random\ \delta \in [0,1];$$
$$i \in [1, \text{number of genes}],$$
$$j \in [2, \text{number of parents}] \tag{6.8}$$

6.3.3.5 Mutation

At each generation, after the new individuals were created by cross-over, they were subject to the mutation process. The effect of the mutation depended on the *probability of mutation* and on the *amplitude of each mutation*, both parameters being provided in the input by the user.

The probability of mutation dictates the percentage of individuals in a generation that will have their genes affected by the mutation process. For the present problem, the probability of mutation was set at 1% of the number of individuals in a generation. The individuals that would be affected were selected at random from the new generation.

The amplitude of mutation determines with how much the genes (displacements) are modified. For the given problem of airfoil upper-surface morphing, where there was a

maximum displacement requirement, the amplitude of mutation was set as a percentage of that displacement value, and it was selected to be 2% of the maximum possible displacement.

Both the probability and the amplitude of mutation are sensitive parameters that should be handled with care, because setting a value too low or too high would affect the convergence of the GA or could cause divergence. The upper-surface morphing airfoil problem had a small number of optimization parameters – two actuator displacements – and it was found to be stable; Figures 6.8 to 6.10 present the effects of various combinations of probability and amplitude of mutation on the convergence for this problem.

Figure 6.8 displays three combinations of the probability of mutation (P_m) with constant amplitude of mutation (A). It can be observed that when the P_m was 0, the convergence was very fast and almost all the individuals reached the optimum region in 5 generations; for the next 9 generations the individuals varied between 2 possible solutions, and starting with the 15^{th} generation they stabilized around a single value. Although this behavior would normally be considered excellent, there was still a high probability that it had found a local optimum in the vicinity of the global one, as there was no perturbation in the genetic pool that would ensure that this was indeed the global optimum. When P_m was at 10%, the algorithm also converged towards the optimal region very quickly, but with the 7^{th} generation it started to oscillate between different solutions and did not stabilize even after all the generations had passed. This indicated that to achieve convergence the algorithm needed a higher number of generations and individuals. The last combination, when P_m was at 1%, the one recommended for this problem, converged as quickly as the other two combinations, and obtained a stable solution starting with the 14^{th} generation, which had the same value as the $P_m = 0$ case. At generations 16, 19 and 20 it searched outside the optimum zone but returned to the same optimum value, confirming that it was indeed in the global optimum area.

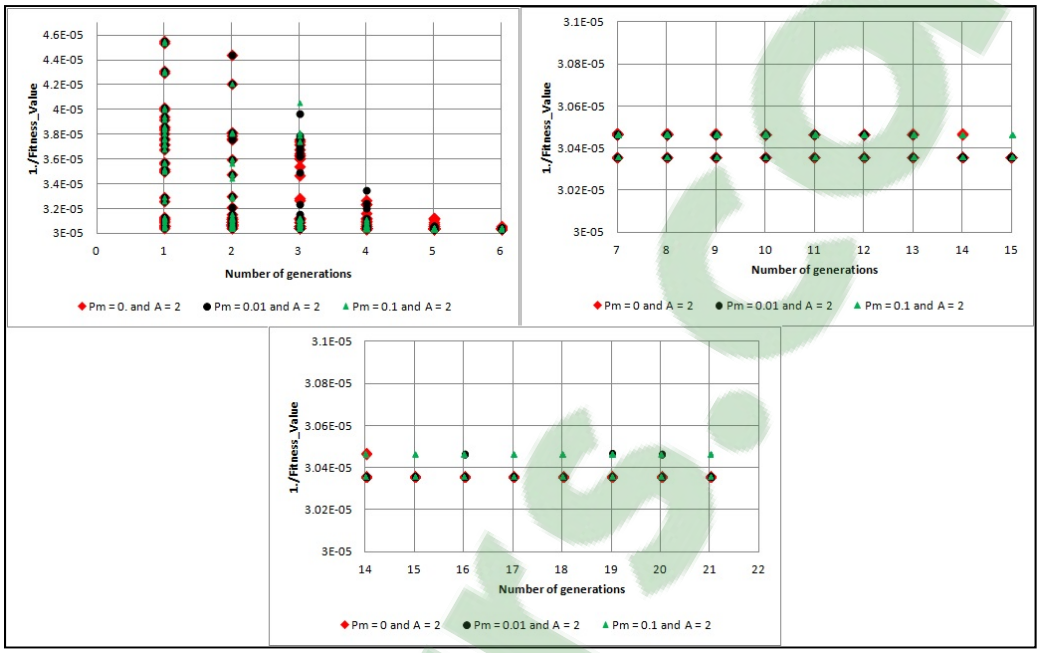

Figure 6.8 Effect of a variable probability of mutation (P_m) at constant amplitude (A) – optimizations for speed 51 m/s, angle of attack -4.1° and aileron deflection down by 1°

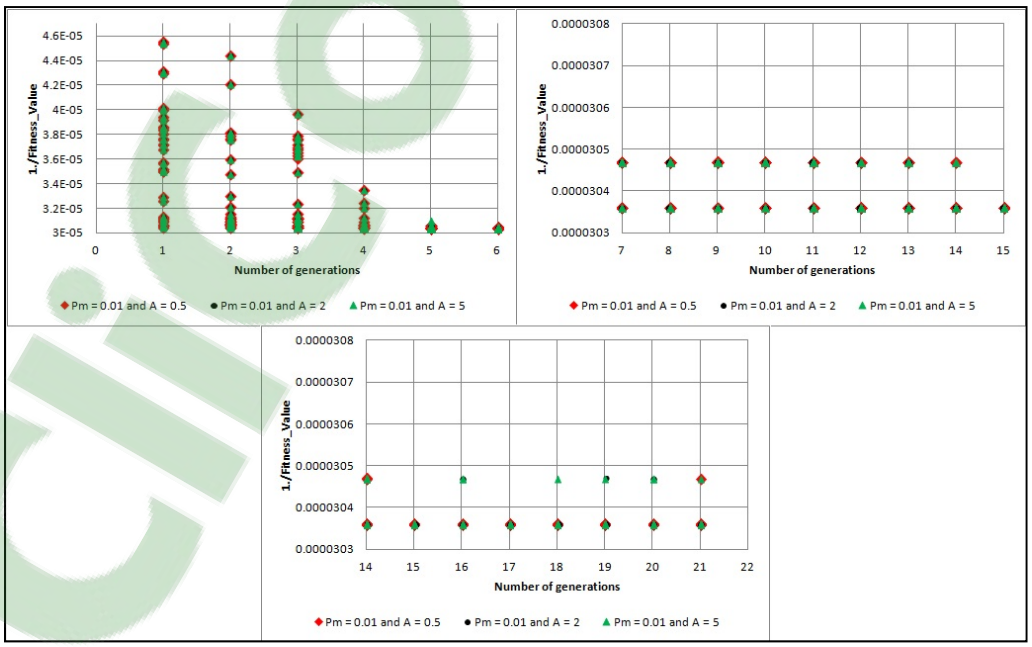

Figure 6.9 Effect of variable amplitude (A) at constant probability of mutation (Pm) – optimizations for speed 51 m/s, angle of attack -4.1° and aileron deflection down 1°

Figure 6.9 shows three combinations of amplitude of mutation (A) with constant probability of mutation (P_m). It can be observed that, for this problem, varying the amplitude up to 5% of the maximum displacement value did not affect the convergence in a critical manner. However, when A = 5% of the maximum displacement value, oscillations appeared during the last four generations, which could increase the probability of outputting a local optimum. The effect of high amplitude was observed mainly from the number of times the algorithm had to repeat the process of generating new individuals, as not all of them respected the requirements. This aspect delayed the optimization process, slowing it down and giving it a high rate of divergence because of the lack of individuals that complied with the desired requirements.

Figure 6.10 presents two extreme combinations of P_m and A that were compared with the recommended combination given in Table 6.3. It can be observed that both the extreme combinations of high P_m - low A (P_m = 0.1, A = 0.5) and high P_m - high A (P_m = 0.1, A = 5) did not converge throughout 21 generations, which implied that for a good convergence they needed more generations and possibly more individuals per generation.

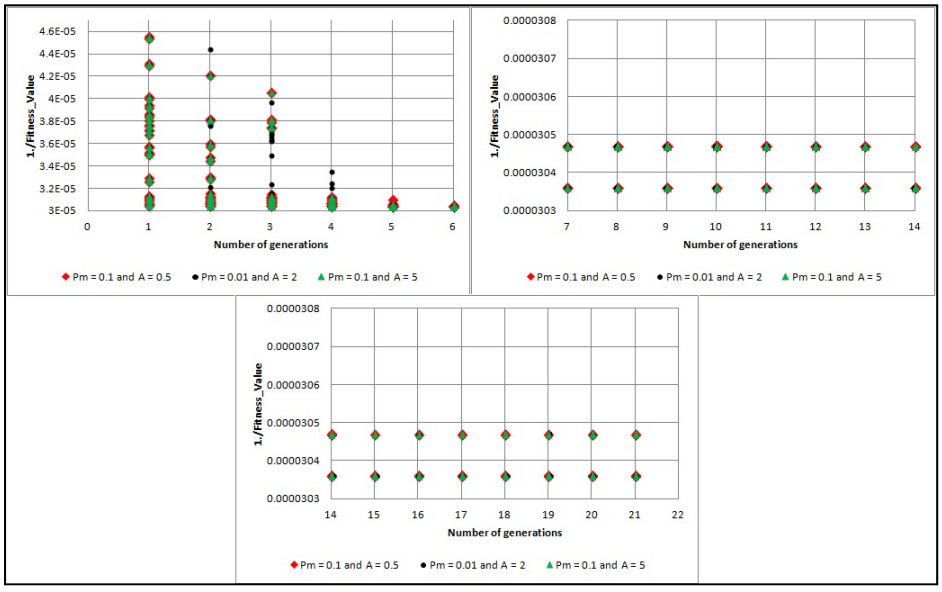

Figure 6.10 Combinations of probability of mutation (Pm) and amplitude (A) – optimizations for speed 51 m/s, angle of attack -4.1° and aileron deflection 1° downwards

The airfoils that resulted from the cross-over and mutation processes were not guaranteed to respect the requirements; for example, they might have a displacement value higher than the maximum value, or they may not respect the maximum relative displacement value between actuators. Therefore, requirement verification was applied to each new individual, and if they did not comply with the user-defined constraints, the process of selecting parents and applying the cross-over and mutation was repeated until an individual complying with the requirements was found. If after 10000 iterations no individual was found the optimization was stopped.

If the variations in the probability and amplitude were high enough, the probability that the new airfoils would not comply with the requirements was high and led to a premature end of the optimization.

6.3.3.6 Tournament

Starting with the second generation of the optimization, a tournament was introduced before the selection of parents for the subsequent generation. The tournament ensured that some airfoils from the previous generation that had good performances (a grade of 8 or higher), were given a new chance at reproducing by replacing some of the worst individuals from the current generation that had very poor performances (a grade of 4 or lower). This form of selection provided a higher chance of converging towards the optimum in fewer generations.

Figure 6.11 presents the effect of the tournament on the optimization convergence for a test case at a speed of 51m/s, angle of attack of -4.1° and aileron deflection angle of 1° down. It can be observed that in the absence of the tournament operation, the case converged slowly towards the optimum area (7^{th} generation), and then it continued to oscillate between 2 possible solutions until the final generation.

When the total number of generations was reached, the program produced a file containing the aerodynamic performances of the best airfoil from the previous generation and the

aerodynamic performances of the original airfoil on which the optimization was performed. The other result files output by the optimization contained the airfoil coordinates, the pressure coefficient and the skin friction coefficient distributions for the best airfoil shape.

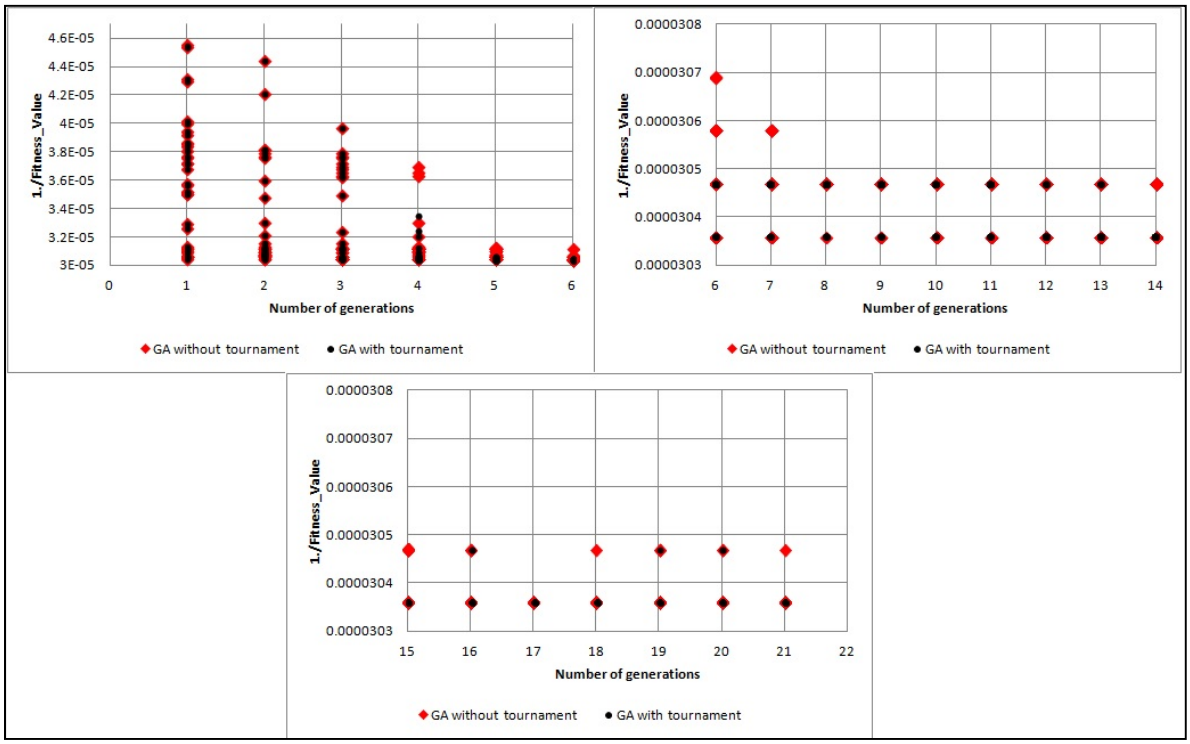

Figure 6.11 Effect of the tournament on the convergence

Figures 6.12 and 6.13 present the optimization convergence for all the individuals analyzed within each generation, and the convergence of the best individual in each generation, using the parameters provided in Table 3 for a speed of 51 m/s, angle of attack of -4.1° and aileron deflection of 1° down.

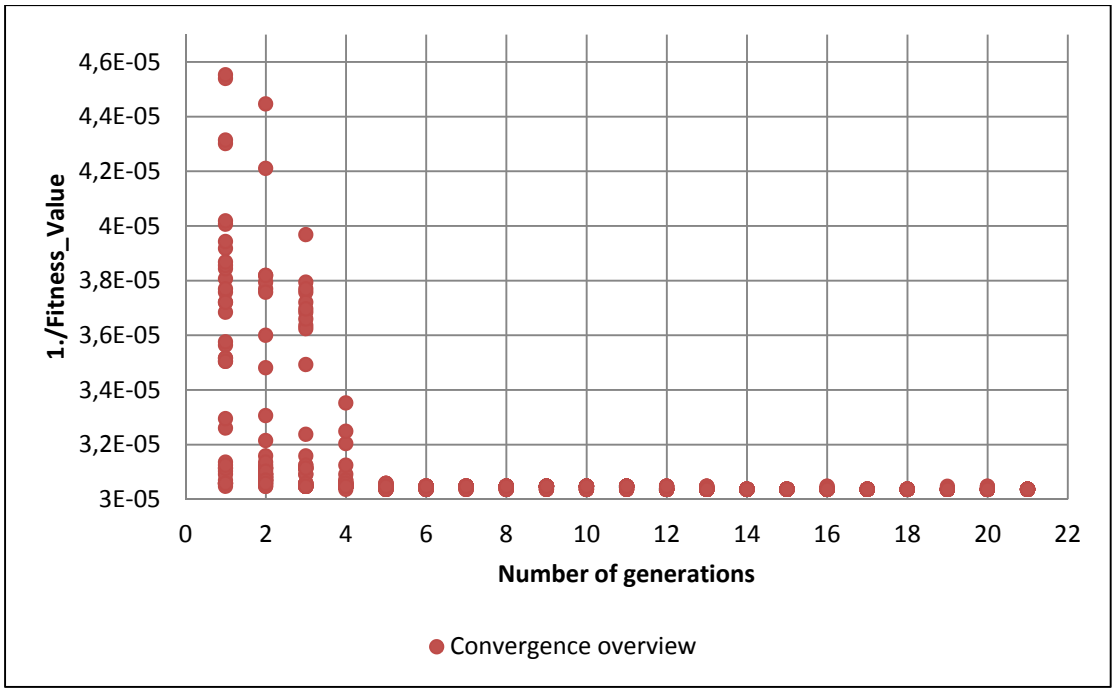

Figure 6.12 Evolution of the convergence for the optimization at speed 51 m/s and angle of attack -4.1°

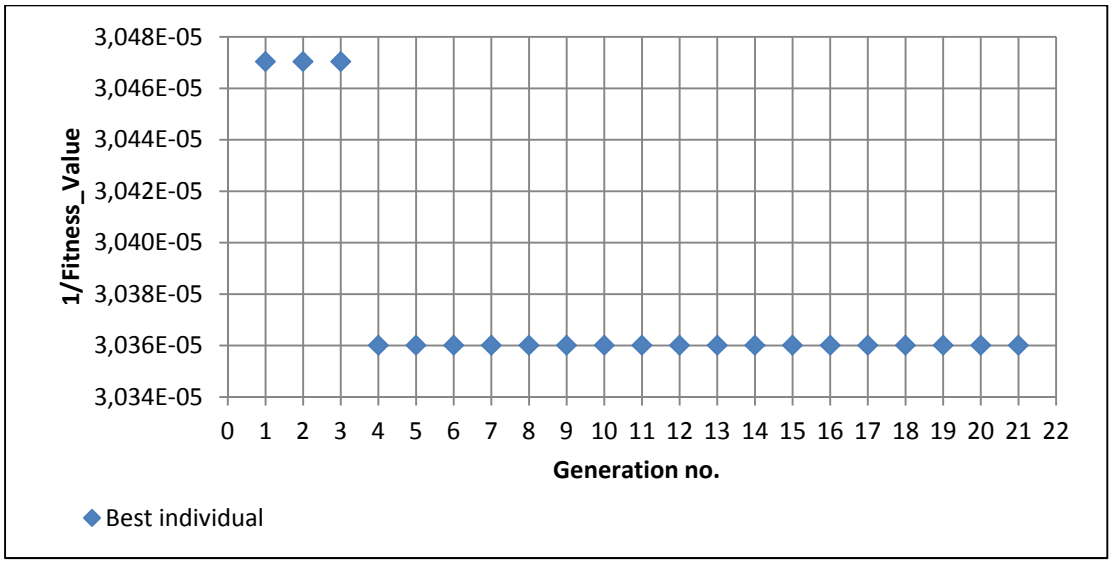

Figure 6.13 Evolution of the best individual convergence for the optimization at speed 51 m/s and angle of attack -4.1°

6.3.4 Genetic algorithm in comparison with two other optimization methods

To ensure that the genetic algorithm found the global optimum for each flight case, twenty cases were analyzed for two fitness objectives: *minimization of the drag coefficient* and *transition position optimization* towards the wing's trailing edge. The results obtained from these 20 cases test were compared to the results obtained with two other optimization methods: the Bee Colony algorithm and the Gradient Descent method.

The *Bee Colony (BC) algorithm* mimics the strategy of honeybees to find the best solution to a problem. The colony's scouts constantly search for new food sources (a solution of the optimization problem) while the other bees serve as guides. Each time a bee reaches a source, it evaluates the profitability (optimization level) and returns to the hive to communicate the value and location of the source to all onlooker bees. Rich sources have a higher probability of being revisited, and the onlooker bees will search around these rich sources (good solutions). Some of the scouts will also go searching around the rich sources, while others will look for new sources.

Multiple types of Bee Colony algorithms, (Karaboga and Basturk, 2007a; 2007b; Sugar Gabor et al., 2015a), were developed by authors, but for this study an 'in-house' developed version BC algorithm, that considered 30 bees, randomly placed in the displacement constraints (-3.5 mm, 3.5 mm) range, was used. One bee represents an airfoil with its corresponding (x_1, x_2) displacements. The airfoil was analyzed with the Xfoil solver to find the flow transition point on the upper surface or its corresponding drag coefficient. The value of the aerodynamic objective (transition point or drag coefficient) represents the profitability associated with that bee. After communicating the profitability value to the hive, each bee continues to search around the source where it was sent for a given number of cycles. At the end of the searching process, only the source with the best profitability is kept, and all other bees are again randomly placed. Usually, a good result was found after 7 searching cycles.

The *Gradient Descent method* is a first-order optimization algorithm. To find a local minimum of a function using gradient descent, steps proportional to the negative value of the gradient (or of the approximate gradient) of that function at the current point are taken. When steps proportional to the positive of the gradient are taken, a local maximum of that function is approached; the procedure is known as Gradient Ascent, (Snyman, 2005; Yuan, 2008).

The search started from the un-morphed airfoil, with (0 mm, 0 mm) displacements. At this point, the gradient was calculated using *finite differences approximations*. The finite differences were calculated so that they gave the direction to find the maximum of the objective function. For the present problem there were two distinct objective functions – minimization of the drag coefficient and delay of the transition point towards the trailing edge – basically a minimization and a maximization problem. Therefore, the algorithm needed to switch from solving one problem to solving the other problem, as a function of the user input.

In addition to direction tracking, a step was needed to find new displacements. After trying different versions, a step of 1E-06 was chosen in addition to the gradient's value. The displacements were then modified according to the following equation:

$$\begin{aligned} Displ_{new} &= Displ_{old} \pm step * gradient \\ Displ &= displacement \end{aligned} \tag{6.9}$$

The method converged very quickly, in only a few iterations, but the disadvantage was that it covered a small search area. The algorithm stopped when it found a local minimum, and so the quality of the results was very random and depended upon individual cases. This aspect could be improved by coupling it with another algorithm such as the Bee Colony. This method was also very sensitive to aerodynamic solver convergence as the results were improved gradually. Therefore, if the solver did not converge during the iterative procedure, the calculation of the new gradient value was not possible, with consequences on the optimization process convergence.

Table 6.4 Flight cases used for the comparison test

Case	Speed (m/s)	AOA (°)	Aileron deflection (°)*
1	0.15	-4	0
2	0.15	-3.5	0
3	0.15	-3	0
4	0.15	-2.5	0
5	0.15	-2	0
6	0.15	-1.5	0
7	0.15	-1	0
8	0.15	-0.5	0
9	0.15	0	0
10	0.15	0.5	0
11	0.15	1	0
12	0.15	1.5	0
13	0.15	2	0
14	0.15	2.5	0
15	0.15	3	0
16	0.2	-1	-2
17	0.2	-0.5	-2
18	0.2	0	-2
19	0.2	0.5	-2
20	0.2	1	-2

Some results of the three optimization methods were plotted on maps obtained with the Monte Carlo method, that created an envelope of all the displacement combinations for the given fitness objective. The cases for which the results were plotted were Cases 5, 8 and 16 from Table 6.4. Table 6.4 presents the twenty cases for which the comparison was made. All the aerodynamic analyses were performed using the XFoil solver. The aileron deflection angle convention is (+) positive angles for downward deflections and (-) negative angles for upward deflection.

To minimize the amount of time needed to run the optimization process for all twenty cases with all three methods, several computation machines were used. To ensure that no errors were introduced from the type of machine used, various analyses were conducted on five different machine configurations. It was observed that different operating systems and different machine hardware had a negligible influence on the analyses' results. Figure 6.14 presents a comparison between the flow transition results for all five machines, obtained using the GA optimizer. Table 6.5 presents details about the five machines on which the tests were done. All the analyses were done for the same atmospheric conditions: density, temperature and air dynamic viscosity at sea level and altitude of 0 m.

Table 6.5 Description of operating system and type of machines used for tests

Machine	**Operating system**	**Type of machine**	**Processor type**
Machine I	Windows 7	PC desktop	Xeon E3
Machine II	OS X	Mac Pro Apple	Advanced Intel Core i5 4th generation
Machine III	Windows 7	PC desktop	Intel Core i5 3rd generation
Machine	**Operating system**	**Type of machine**	**Processor type**
Machine IV	Windows 7	PC desktop	Intel Core i5 2nd generation
Machine V	Windows 7	HP Pavilion g6	AMD A6-3400M

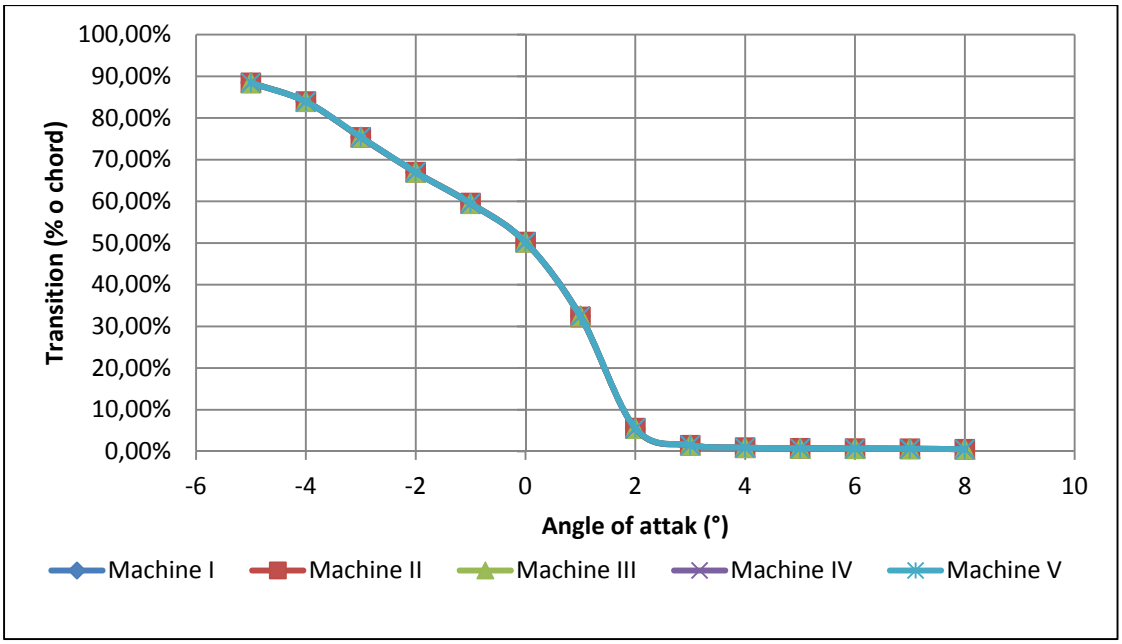

Figure 6.14 XFoil transition results comparison between five different machine configurations

For the comparison with the two other optimization methods, the optimization was done for the two fitness objectives: drag coefficient minimization and transition optimization towards the trailing edge. The fitness functions associated with these objectives were derived from Equation (6.1) using appropriate weight factors. For the drag coefficient optimization the comparison was done between the genetic algorithm and the bee colony algorithm, and for the transition optimization the comparison was done with all three optimization methods. The comparison results are presented in Figures 6.15 to 6.20. The drag coefficient in the following figures is presented in counts, where one drag count equals to a drag coefficient value of 10^{-4}.

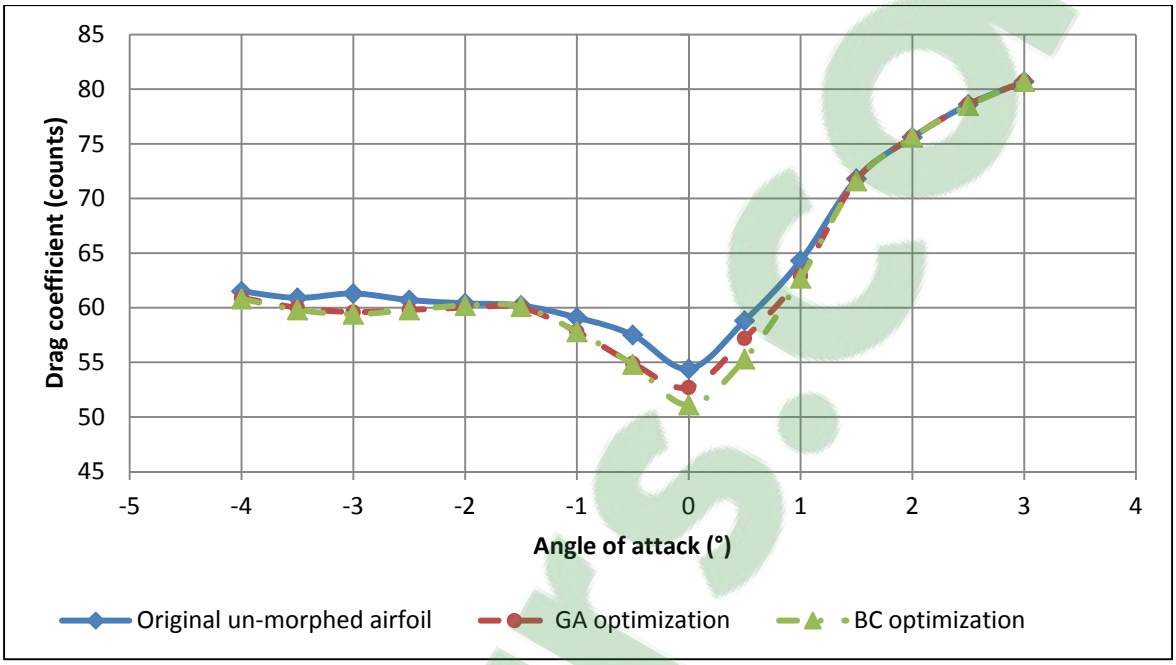

Figure 6.15 Comparison for the drag coefficient optimization – cases 1 to 15 from Table 6.4

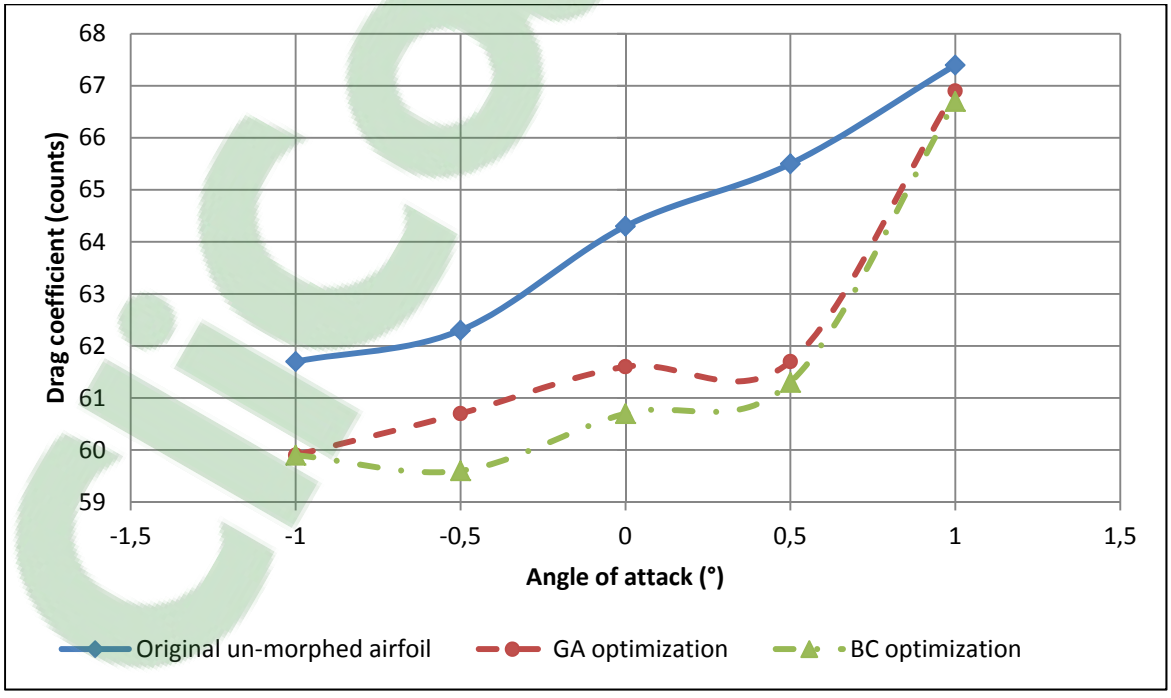

Figure 6.16 Comparison for the drag coefficient optimization – cases 16 to 20 from Table 6.4

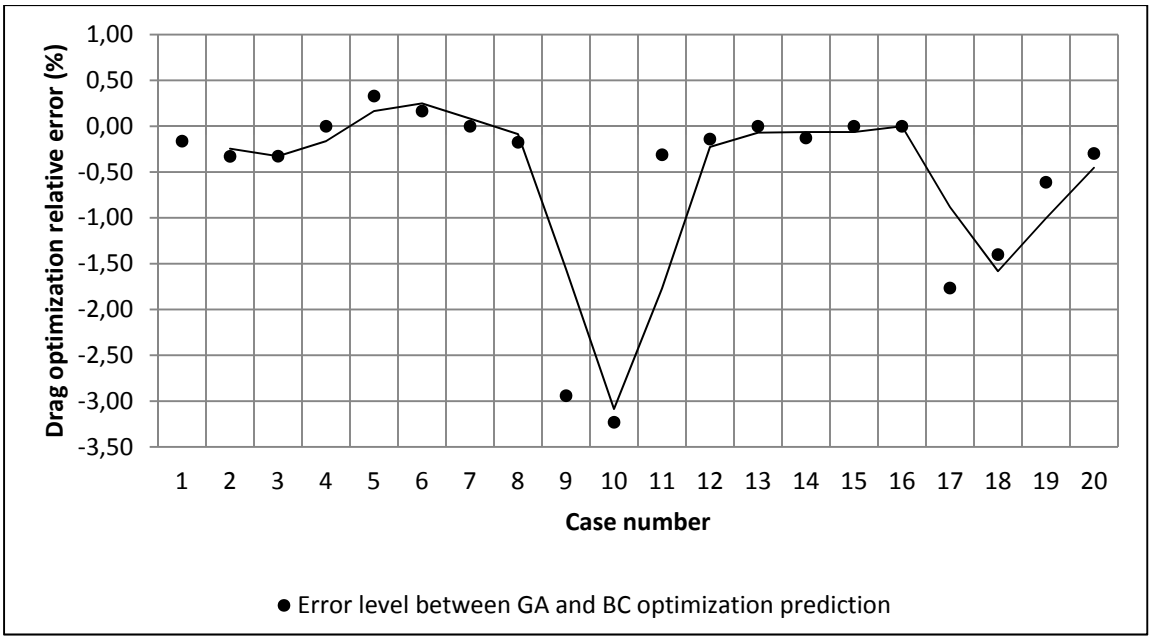

Figure 6.17 Error between the GA and BC algorithms for the drag coefficient optimization – cases 1 to 20 from Table 6.4

From Figures 6.15 to 6.17 it can be observed that, for three cases, the Bee Colony (BC) algorithm had found a drag coefficient smaller than the one found with the Genetic Algorithm (GA), and in those cases, the actual difference was less than 1.5 drag counts. Overall, for the objective of minimizing the drag coefficient, the algorithms were considered to give similar results. The few cases where the Genetic algorithm did not score better than the Bee Colony could be considered as minor local optimums inside the global optimum area.

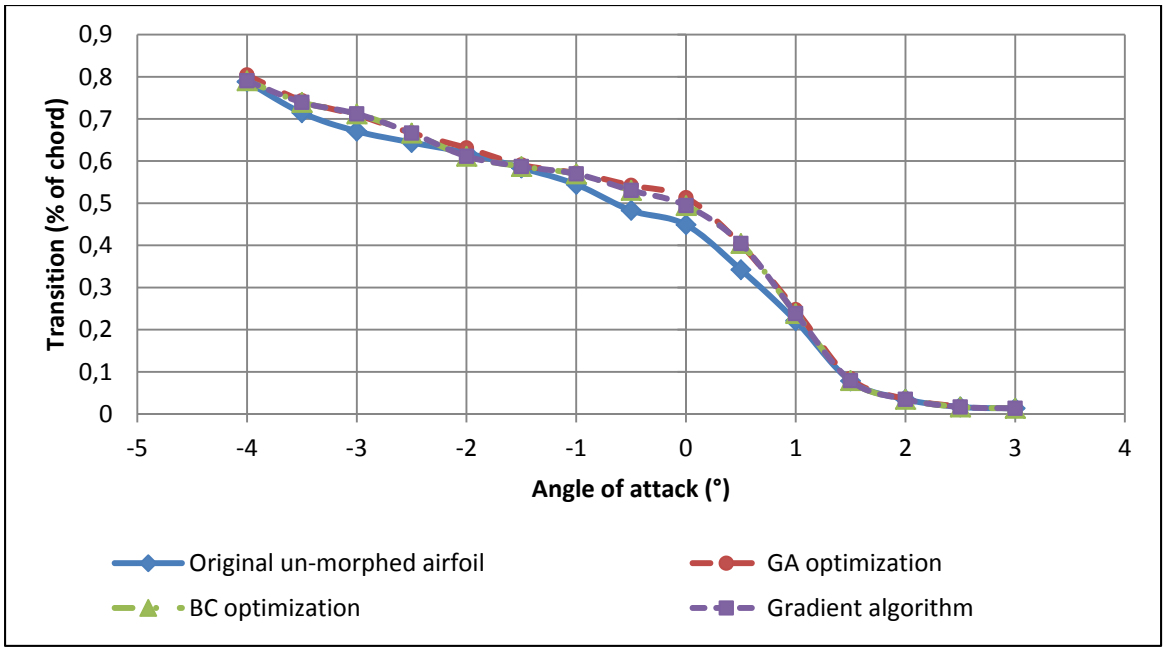

Figure 6.18 Comparison for the flow transition optimization – cases 1 to 15 from Table 6.4

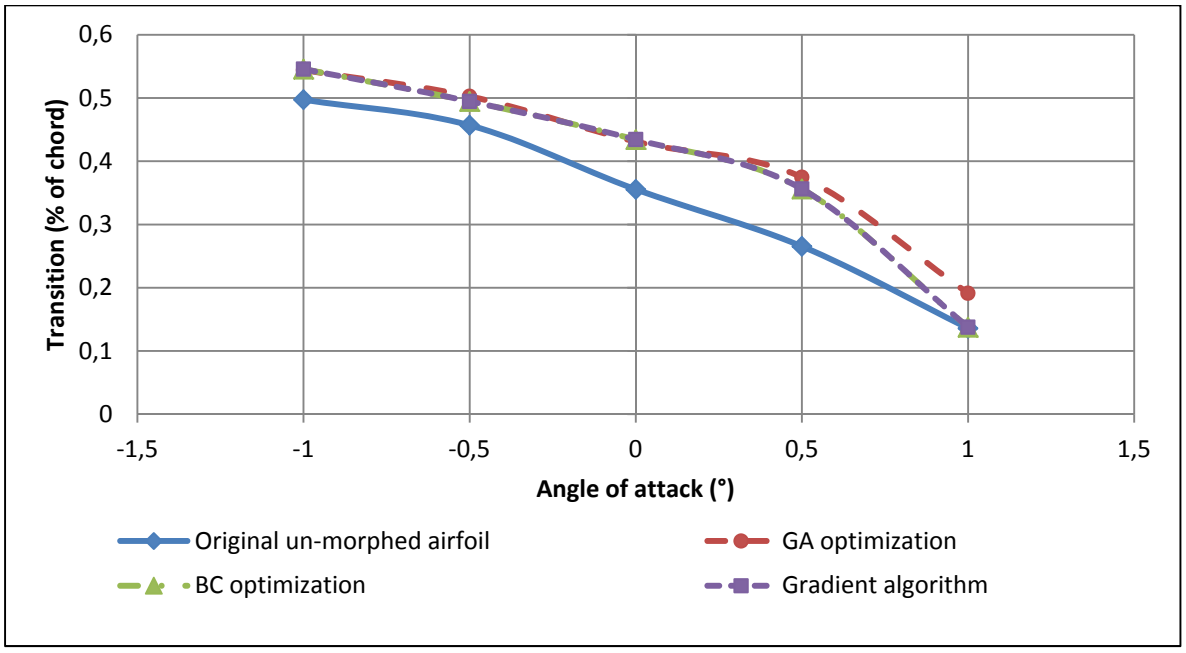

Figure 6.19 Comparison for the flow transition optimization – cases 16 to 20 from Table 6.4

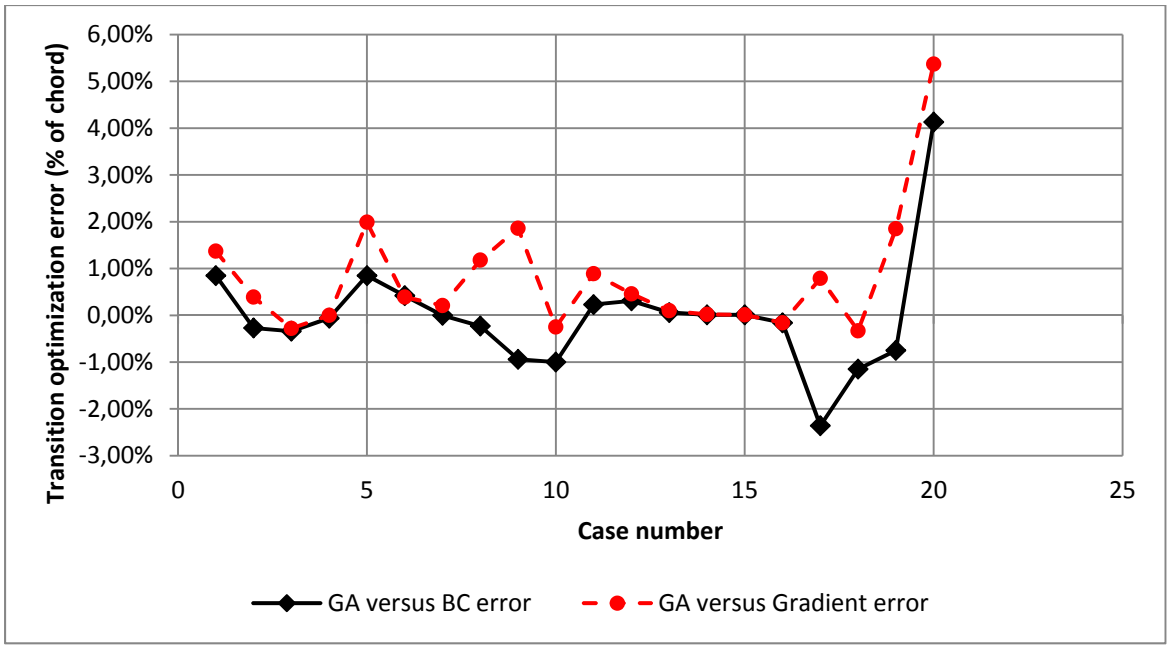

Figure 6.20 Error between the GA, BC and Gradient algorithms for the flow transition optimization – cases 1 to 20 from Table 4

The error presented in Figure 6.20 was calculated as the difference between the GA and the BC transition point results or the difference between the GA and the GD method transition point results, with the results presented as a percentage of the chord.

Figures 6.18 to 6.20 present the results for the transition optimization towards the trailing edge objective for all three methods. It can be observed that the three algorithms gave close results; in some cases, the Genetic algorithm obtained results 4% of the chord better than those of either the Bee Colony Algorithm or the Gradient Descent Method, with only one case where the Bee Colony outperformed the Genetic algorithm by 2% of the chord. These results confirmed the superiority of the Genetic algorithm in 95% of the cases, for the problem of transition delay.

Figures 6.21 to 6.23 present the Monte Carlo maps with the three algorithms' results for the drag coefficient reduction objective (case 4) and for the transition delay objective, for cases 8 and 19 (as presented in Table 6.4).

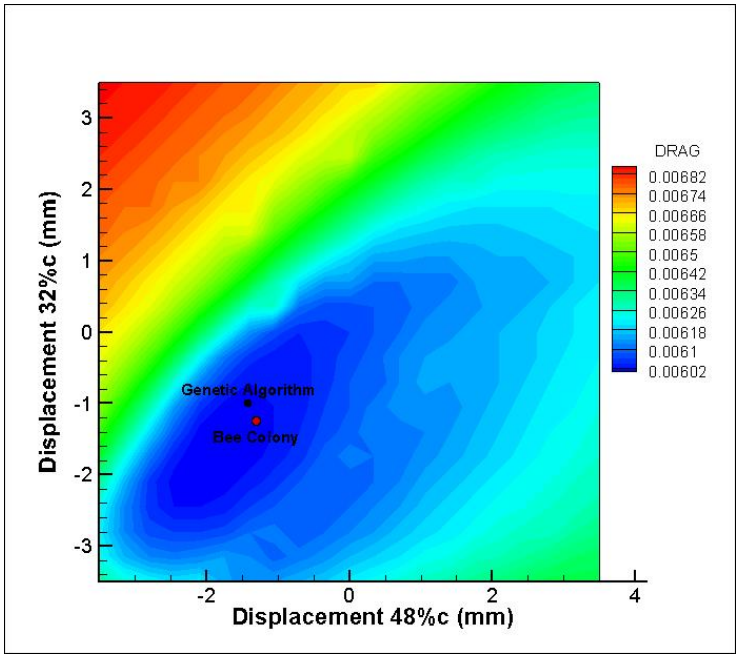

Figure 6.21 Case 4 – Genetic algorithm and Bee Colony results for drag coefficient optimization on Monte Carlo map

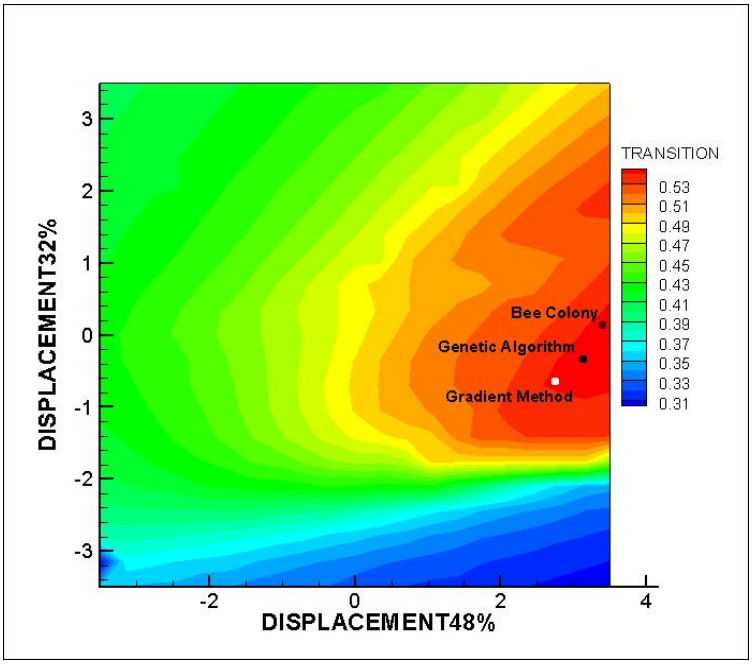

Figure 6.22 Case 8 – Genetic algorithm, Bee Colony and Gradient method results for transition delay towards TR optimization on Monte Carlo map

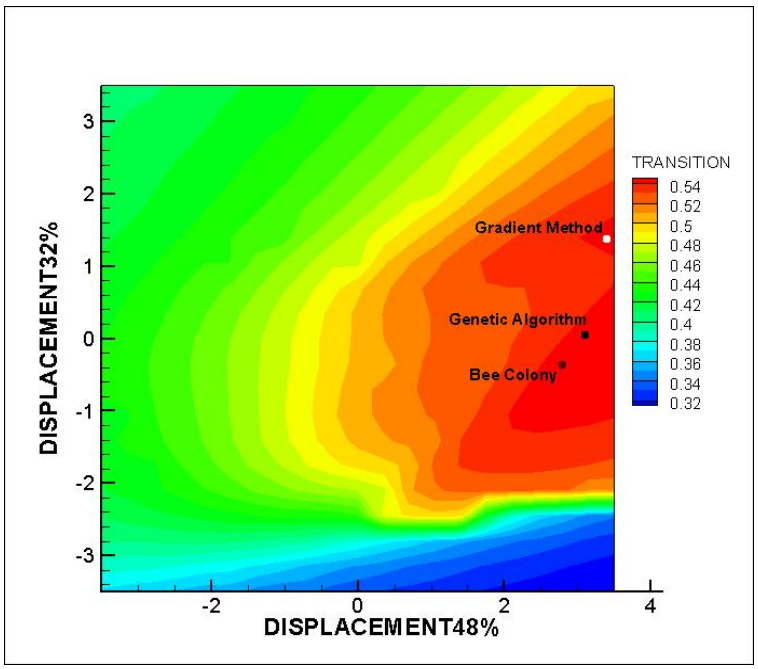

Figure 6.23 Case 19 – Genetic algorithm, Bee Colony and Gradient method results for transition delay towards TR optimization on Monte Carlo map

It was observed that for the problem of upper-surface airfoil morphing, where there are two parameters to optimize, the three optimization methods found the global optimum area in almost all the cases and situated their results inside that region, with the Gradient Descent method having the lowest quality results.

The Monte Carlo maps showed that there was no particular unique solution to the optimization of an airfoil upper-surface, as there was a region in which various combinations of actuator displacements had obtained relatively the same transition point location or drag coefficient value. For any given test case out of the 20 cases, the three algorithms could give three different solutions (where a solution refers to a combination of displacements) located inside the global optimum region. Nonetheless, the genetic algorithm has proven its reliability and that it obtained similar and even better results than the Bee Colony algorithm for most of the test cases, therefore it was further used for the optimization of the cases

experimentally tested in the NRC wind tunnel for the morphing wing tip technology demonstrator.

Table 6.6 presents the 16 wind tunnel test cases optimized by the Genetic Algorithm. Two objectives were considered by influencing the transition from laminar to turbulent flow: delay of the transition towards the trailing edge of the wing (to achieve a reduction in the drag coefficient) and advancement of the transition towards the leading edge of the wing tip demonstrator (to provide a more stable, turbulent flow when the aileron was deflected).

The improvement was calculated as the difference between the transition point obtained for the optimized airfoils and the transition obtained for the original airfoil of the wing tip demonstrator.

Table 6.6 Optimization cases and results for the wing tip demonstrator

Case no.	Mach	AoA (°)	Aileron deflection (°)	Type of optimization	Original airfoil Transition (%c)	Optimized airfoil Transition (%c)	Improvement (%c)
1	0.15	0.68	0	delay transition	53.62	54.47	0.85
2	0.15	1.50	0	delay transition	48.35	53.85	5.5
3	0.15	2.10	0	delay transition	46.09	52.41	6.32
4	0.15	-2.39	2	delay transition	63.71	66.19	2.48
5	0.15	1.93	-2	delay transition	43.34	52.97	9.63
6	0.2	1.88	4	delay transition	41.91	53.82	11.91

Case no.	Mach	AoA (°)	Aileron deflection (°)	Type of optimization	Original airfoil Transition (%c)	Optimized airfoil Transition (%c)	Improvement (%c)
7	0.2	3.03	4	delay transition	33.44	50.62	17.18
8	0.2	3.45	-4	delay transition	30.35	41.3	10.95
9	0.15	-0.33	5	advance transition	74.90	43.05	-31.85
10	0.15	-0.95	-2	advance transition	60.01	50.92	-9.09
11	0.25	-2.99	1	advance transition	60.09	44.92	-15.17
12	0.25	-2.26	3	advance transition	59.46	45.05	-14.41
13	0.15	-2.30	2	advance transition	65.58	44.01	-21.57
14	0.15	-1.64	3	advance transition	67.43	43.48	-23.95
15	0.15	-3.22	-2	advance transition	64.83	44.27	-20.56
16	0.25	-1.52	5	advance transition	64.52	41.77	-22.75

Figures 6.24 and 6.25 present the visual comparison between the original airfoil transition and the optimized airfoil transition for the two objective functions, using wind tunnel flow conditions and the parameters provided in Table 6.6.

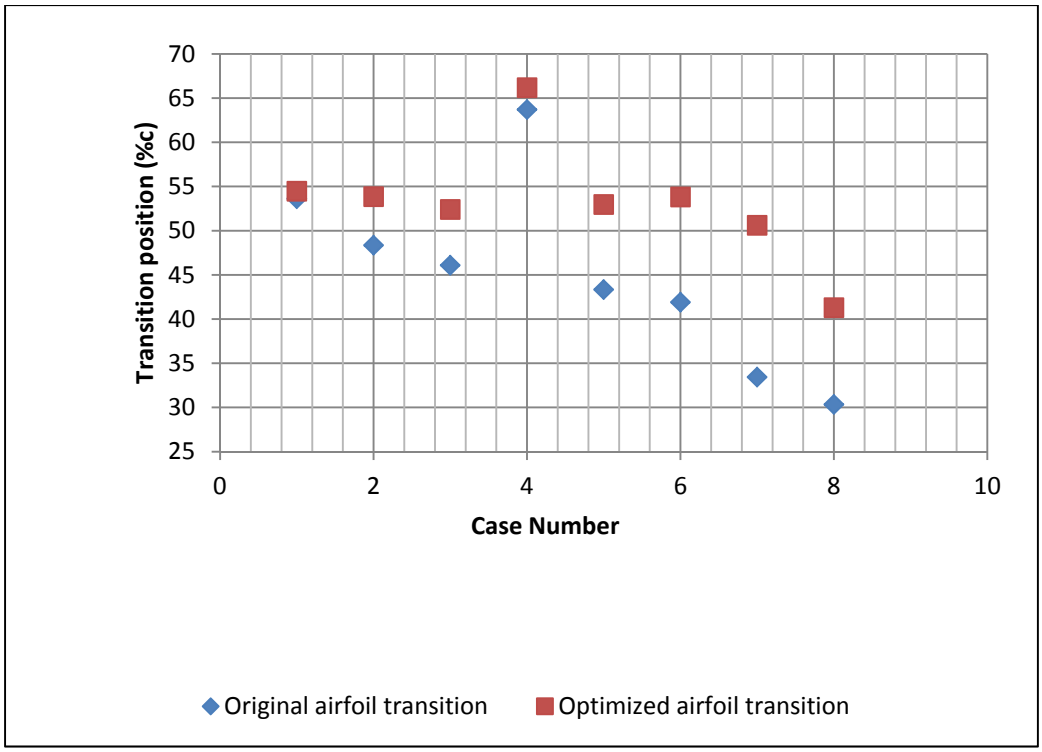

Figure 6.24 Original versus optimized airfoil transition for the objective of delaying the transition towards trailing edge

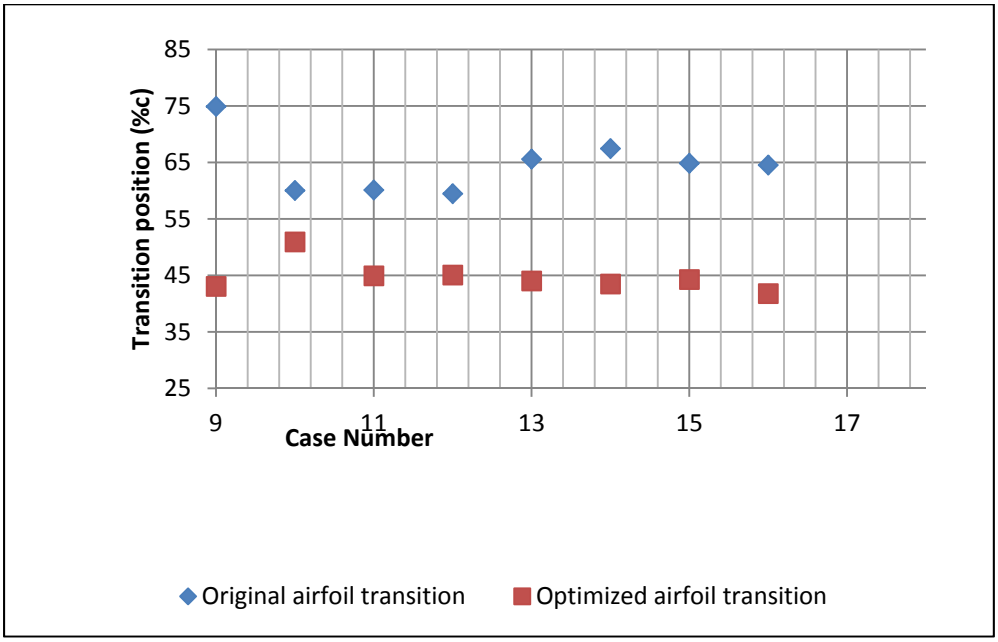

Figure 6.25 Original versus optimized airfoil transition for the objective of advancing the transition towards leading edge

6.4 Conclusions

The present paper presents an ‘in-house’ genetic algorithm that was applied to the problem of optimizing the shape of the upper surface of an airfoil by using actuator displacements. The method was applied to two different wing airfoils, the ATR 42 wing airfoil and the MDO 505 morphing wing demonstrator airfoil, using a multidisciplinary approach in which structural, aerodynamic, control and experimental requirements were combined to configure all the aspects of the optimization.

The genetic algorithm functions were described using the MDO 505 wing’s airfoil configuration. By using the recommended configuration, the algorithm converged towards the optimum region in less than 10 generations, and in 20 generations stabilized itself at the optimum point. The Genetic Algorithm (GA) was compared to two other optimization methods, the Bee Colony algorithm and the Gradient method, for two optimization objectives: minimization of the drag coefficient and delay of the transition point from laminar towards turbulent flow. These results showed that the GA provided similar or better results than the other two methods for most of the cases for which it was tested. By plotting the results on Monte Carlo maps, it was shown that the global optimum area was always reached.

The genetic algorithm was then used to optimize 16 cases for two objectives: delay of the transition towards the trailing edge of the airfoil and advancement of the transition towards the leading edge. The results indicate improvements of up to 17% of the chord for the former (transition delay), and of up to 31% of the chord for the latter (transition advancement).

The displacements resulted from the optimization were used for the upper surface morphing controller during wind tunnel testing on the MDO 505 wing tip demonstrator, and comparisons were conducted between the experimental transition regions of the morphed and un-morphed wing section, using infrared photography. The validation of the numerical optimizations for all the 16 cases is documented in the second part of this paper.

Acknowledgements

We would like to thank Bombardier Aerospace, Thales Canada, the Consortium in Research and Aerospace in Canada (CRIAQ) and the Natural Sciences and Engineering Research Council of Canada (NSERC) for their financial support. Special thanks are due to our collaborators and leaders in this project: Mr. Patrick Germain and Mr. Fassi Kafyeke from Bombardier Aerospace, Mr. Eric Laurendeau from Ecole Polytechnique, Mr. Philippe Molaret from Thales Canada, and Mr. Erik Sherwood and his team from DFS-NRC for the wing model design and fabrication.

CHAPTER 7

OPTIMIZATION AND DESIGN OF A MORPHING AIRCRAFT WING-TIP DEMONSTRATOR AT LOW SPEED FOR DRAG REDUCTION PART II – VALIDATION WITH INFRA RED TRANSITION MEASUREMENT IN A WIND TUNNEL TEST

Andreea Koreanschi, Oliviu Şugar Gabor, Joran Acotto, Guillaume Brianchon, Gregoire Portier and Ruxandra Mihaela Botez
LARCASE Laboratory of Applied Reasearch in Active Controls,
Avionics and Aeroservoelasticity
École de Technologie Supérieure, 1100 rue Notre Dame Ouest,
Montréal, H3C1K3, Québec, Canada

Mahmoud Mamou and Youssef Mebarki
Aerodynamic Laboratory
NRC Aerospace,
National Research Council Canada,
Ottawa, K1A0R6, Ontario, Canada

This article was accepted for publication in *The Chinese Journal of Aeronautics*

Résumé

L’article présente une nouvelle formulation non-linéaire de la méthode classique Vortex Lattice, qui est utilisée pour calculer les propriétés aérodynamiques de surfaces portantes. Le modèle mathématique est construit à l'aide des analyses bidimensionnelles visqueuses des sections de l’aile en long de son envergure, après la théorie des bandes, et ensuite par le couplage des forces visqueuses de bande avec les forces générées par les anneaux tourbillonnaires répartis sur la surface de la cambrure de l'aile, et calculées avec une loi entièrement en trois dimensions. Les résultats numériques obtenus avec la méthode proposée

sont très bien validés avec les données expérimentales et montrent un bon accord en termes des coefficients de la portance et du moment de tangage, mais aussi pour la prédiction de la traînée de l'aile. Les coûts de calcul faibles transforment cette méthode en un bon outil pour les procédures de conception des ailes ou les procédures d'optimisation. La méthode est appliquée pour modifier l'aile d'un système autonome de vol afin d'augmenter son efficacité aérodynamique, et pour calculer les réductions de traînée obtenues par une technique de déformation de la surface supérieure pour une aile d'avion de transport.

Abstract

In the present paper an 'in-house' genetic algorithm was numerically and experimentally validated under the CRIAQ MDO 505 project frame. The genetic algorithm was applied to an optimization problem for improving the aerodynamic performances of an aircraft wing-tip through upper surface morphing. The optimization was performed for 16 flight cases expressed in terms of various combinations of speeds, angles of attack and aileron deflections. The displacements resulted from the optimization were used during the wind tunnel tests of the wing-tip demonstrator for the actuators control to change the upper surface shape of the wing. The results of the optimization of the flow behavior for the airfoil morphing upper-surface problem were validated with wind tunnel experimental transition results obtained with Infra-red Thermography on the wing-tip demonstrator. The validation proved that the 2D numerical optimization using the 'in-house' genetic algorithm was an appropriate tool in improving various aspects of a wing's aerodynamic performances.

7.1 Introduction

Nowadays, applications of optimization algorithms can be found in almost all industrial and academic research venues, such as optimization electric circuitry, stock market predictions, image quality problems, software implementation problems, to optimization of aircraft structures, aerodynamics or flight trajectories, etc., (Bacanin, 2012; Cui et al., 2013; Majhi et al., 2009; Zhang and Ye, 2012).

In the aerospace field, many research projects and collaborations include the successful implementation of the more traditional metaheuristic optimization algorithms such as genetic algorithm, bee colony algorithm, artificial neural networks, or ant colonies optimization in

their research for new optimized flight trajectories, for new optimized wing shapes or improved control, (Mosbah, Botez and Dao, 2013; Mosbah et al., 2013; Sugar Gabor, Koreanschi and Botez, 2012; Sugar Gabor et al., 2015a).

One such collaboration took place between the teams from the LARCASE laboratory and CMC Electronics-Esterline on the GARDN project, which was funded by the Green Aviation Research Development Business Led Network (GARDN) in its second round (Patron, Botez and Labour, 2013; Patrón, Kessaci and Botez, 2014). The main objective of the collaboration was to optimize the vertical and horizontal paths of the aircraft within the Flight Management System by taking into account the Required Time of Arrival, the wind grids and meteorological conditions. The main motivation of the project was to reduce overall carbon emissions and flight costs.

Morphing also consists in changing the structure or appearance of an aircraft during flight by modifying the wing sweep, (Joo et al., 2006), span, (Neal et al., 2004), chord, (Reed Jr et al., 2005) or camber, (Monner, Hanselka and Breitbach, 1998; Poonsong, 2004), by the high lift devices, (Pecora et al., 2011; Pecora et al., 2013), or the fuselage, for small aircraft and for UAV's, (Sugar Gabor, Koreanschi and Botez, 2013a; Sugar Gabor et al., 2015b).

Applications of optimization techniques for UAVs were described by (Gamboa et al., 2009) who designed an Unmanned Aerial Vehicle (UAV) wing capable of independent span and chord changes, using a telescopic spar and a rib system. The numerical analysis demonstrated a drag reduction of up to 23% when compared to its non-morphing base geometry. (Falcão, Gomes and Suleman, 2011) designed and tested a morphing winglet for a military UAV and achieved important performance improvements by changing the winglet cant and toe angles. Other research on UAV wing morphing was done by (Sugar Gabor, Koreanschi and Botez; Sugar Gabor et al., 2014), where the upper-surface of the wing was optimized on a segment between its leading edge and 55% of the chord, and also explored morphing of the full wing's geometry. (Tianyuan and Xiongqing, 2009) developed a multi-disciplinary optimization for improving aerodynamic, stealth and structural performances of an

unmanned aerial combat vehicle. (Peifeng et al., 2012) developed a methodology for aerodynamic optimization aimed at demonstrating the performances of a blended wing body transport, while (Xie et al., 2013) studied the effects of static aeroelastic phenomena on very flexible wings.

Few projects concentrate on the effect of the morphing technologies on the aerodynamic performances of the wing; the majority concentrate mostly on aerodynamic and structural interactions for the purpose of demonstrating the increased safety against undesired aeroelastic phenomena such as flutter, (Liauzun, 2010; Pecora, Amoroso and Lecce, 2012; Pecora et al., 2014).

A recent research on the subject of morphing wings was performed in the CRIAQ 7.1 project, in which collaboration took place between aerospace industrial teams at Bombardier Aerospace and Thales Canada, academic partners from the École de Téchnologie Supérieure (ETS) and École Polytéchnique of Montreal, and researchers at the Canadian National Research Council (NRC). The purpose of this project was to demonstrate the capabilities of morphing wings in a wind tunnel for developing the flow transition from laminar to turbulent (Botez, Molaret and Laurendeau, 2007; Popov et al., 2009). Morphing was achieved by replacing the upper surface of the wing, spanned between 7% and 70% of the wing chord, with a flexible carbon-Kevlar composite skin. The skin morphing was achieved using two Shape Memory Alloy (SMA) actuation lines to obtain an optimized shape for each flight condition tested in the wind tunnel (Grigorie et al., 2012a). The optimization was done using a genetic algorithm method coupled with the aerodynamic solver XFoil. The wind tunnel tests had proven that the concept of upper surface morphing was viable, controllable, and provided tangible results confirming the delay of the transition from laminar to turbulent flow, thereby inducing a substantial reduction in the drag coefficient (Sainmont et al., 2009). Proportional – Integrator – Derivative (PID), (Grigorie, Botez and Popov, 2012), and neuro-fuzzy controllers, (Grigorie et al., 2011a), were tested to prove the ability of the flexible upper surface and the morphing mechanisms towards the transition delay. The controllers

demonstrated an excellent performance in both open and closed loops (Popov et al., 2010a; 2010b).

The research presented in this present paper was done within the framework of the international CRIAQ MDO505 Morphing Wing project, which was a continuation of the previous research project CRIAQ 7.1, and aimed at a higher technical readiness level by considering a real wing internal structure and a certifiable electric control system and controllers. The participants in this project were Ecole de Technologie Superieure (ETS), Ecole Polytehnique and University of Naples 'Federico II' as academia research partners, the Canadian National Research Council (CNRC) and the Italian Aerospace Research Center (CIRA) as research center partners and Bombardier Aeronautique, Thales Canada and Alenia Aermacchi as industrial partners.

The objectives of the project were to design, manufacture and control a wing demonstrator based on an aircraft wing-tip equipped with both a conventional and adaptive aileron. The novelty of the CRIAQ MDO 505 project consisted in its multidisciplinary approach, where structure, aerodynamics, control and experimental design were combined to design and manufacture an active morphing wing demonstrator and test it under subsonic wind tunnel conditions.

Part I of this paper established the design and optimization of a wing-tip demonstrator airfoil using an 'in-house' genetic algorithm coupled with the XFoil aerodynamic 2D solver that used the e^N method for the numerical determination of the transition point (Drela, 2003; Drela and Youngren, 2001). The algorithm was described in detail, and its results were compared with the results obtained by other optimization methods, namely the bee colony method and the gradient method. Also, another experimental validation of the genetic algorithm was performed for the ATR-42 wing airfoil in (Koreanschi, Sugar-Gabor and Botez, 2016b). Validation of the optimization technique and numerical results were achieved through experimental data obtained through wind tunnel tests of a wing model demonstrator. The optimization concentrated on the improvement of the upper-surface behavior of the flow

by manipulating the position of transition from fully laminar to fully turbulent flow. The optimization was carried at the airfoil level and in practice, was applied to a full scale wing tip with aircraft-look-alike internal structure. The validation was done though comparison of the numerical and experimental results for a specific region on the wing, where kulite sensors were installed for pressure measurements.

7.2 Wing tip demonstrator with conventional aileron

The full-scale morphing wing model was an optimized structure with a 1.5 m span and 1.5 m root chord, a taper ratio of 0.72 and leading and trailing edges sweep angle of 8°. The wing box and its internal structure (spars, ribs, and lower skin) were manufactured from aluminum alloy material, while the adaptive upper surface was positioned between 20% and 65% of the wing chord. The adaptive upper surface skin was specifically designed and optimized to meet industrial partner's requirements. The adaptive skin was manufactured using carbon fiber composite materials (Michaud, 2014).

The deformation of the skin shape, driven by actuators placed inside the wing box structure, was a function of the flight condition (defined in terms of Mach number, Reynolds number and angle of attack). These actuators were specifically designed and manufactured to meet in-flight and wind tunnel test requirements. Four electrical actuators were installed on two actuation lines; two actuators were installed on each line, were placed at 37% and 75% of the wing span, and were fixed to the ribs and to the composite skin. Each actuator has the ability to operate independently from the others. On each actuation line, the actuators were positioned at 32% and 48% of the local wing chord.

The aileron's hinge was located at 72% of the chord. Two ailerons type were designed and manufactured. One aileron was structurally rigid, while the other one represented a new morphing aileron concept. Both ailerons were designed to be attached to the same hinge axis of the wing box, and both were able to undergo a controlled deflection between -7° and +7°.

Figure 7.1 presents a sketch of the morphing wing model concept as it was mounted and tested at the NRC subsonic wind tunnel.

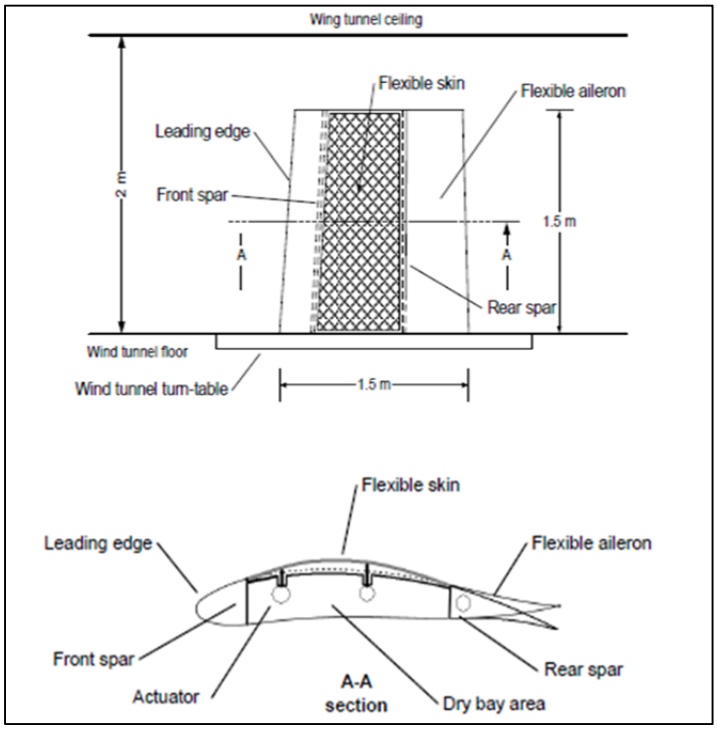

Figure 7.1 CRIAQ MDO 505 morphing wing concept

7.3 Wind tunnel description and Infrared data aquisition

The wind tunnel tests were performed at the 2 m x 3 m atmospheric closed circuit subsonic wind tunnel of the National Research Council Canada. This atmospheric wind tunnel can operate at a maximum Mach number of 0.33.

The upper surface flexible skin was equipped with 32 high precision Kulite piezoelectric-type transducers, (Kulite, 2015), for pressure measurement on the flexible skin that were further processed to determine the laminar-to-turbulent transition location. These sensors were installed in two staggered lines (with 16 Kulite sensors on each line), situated respectively at 0.600 m and 0.625 m from the wing root section. In addition to the Kulite piezoelectric sensors, at the same two spanwise stations, 60 static pressure taps were installed

(30 taps on each line) on the wing leading edge, lower surface and aileron, thus providing complete experimental pressure distribution around the wing cross section at 40% of the wing span. The pressure sensors were installed in a staggered fashion to minimize the interference between sensors.

The experimental measurements also included the use of a wake rake pressure acquisition system for the purpose of measuring the wing profile drag at different span-wise positions, and also the use of a wind tunnel balance for measuring the aerodynamic forces and moments. Figure 7.2 presents the MDO 505 morphing wing model installed in the tunnel test section, viewed from both the leading edge (7.2(a)) and the trailing edge (7.2(b)).

Infra-red (IR) thermography camera visualizations were performed for capturing the transition region over the entire wing model surface. The wing leading edge, its upper surface flexible skin and the aileron interface were coated with high emissivity black paint to improve the quality of the IR photographs. The span-wise stations, where the two pressure sensors lines were installed, were not painted, in order to not influence the pressure reading quality. A Jenoptik Variocam camera, (Mebarki, Mamou and Genest, 2009), with a resolution of 640 by 480 pixels, was used to measure the surface temperatures. This camera was equipped with 60^{o} lens in order to capture the flow transition on the entire upper surface of the wing.

The IR thermography visualization allowed the identification of the transition region between laminar and turbulent regimes, based on the analysis of the model surface temperature. Examples of Infrared Photography results are given in Section 7.5. The turbulent flow regime increases the convective heat transfer between the model and the flow with respect to the laminar boundary layer. As a result, a flow temperature change, introduced by the wind tunnel heat exchanger system, will cause different temperature changes over the model, depending on the behavior of the boundary layer.

a) b)

Figure 7.2 MDO 505 wing model setup in the wind tunnel test section;
(a) front view, (b) rear view

7.4 Optimization algorithm

The genetic algorithm was applied to the problem of airfoil upper-surface morphing. The problem objective was the search of the optimum shapes for an airfoil through local thickness modifications with the aim to improve the upper surface flow and thus the aerodynamic performances of the wing's airfoil.

The local wing thickness modification was obtained through four actuations points, as described in the previous section. The shape of the flexible upper-surface was obtained by an optimized combination of the four vertical displacements, representing the local 'pushing and pulling' actions of four electric actuators installed inside the wing box. The vertical displacements resulted from the genetic optimization of the wing's airfoil.

For the theoretical thin airfoil provided by Bombardier, considered under the name CRIAQ MDO 505 wing demonstrator airfoil, the optimization and design approach was more conservative in nature, as many structural requirements and constraints were taken into account when performing the optimization.

Table 7.1 presents the morphing surface limits, number and position of actuators on each rib as well as the maximum displacements.

Table 7.1 Morphing problem variable values for the MDO 505 wing demonstrator airfoil

Morphing surface start point (%c)	Morphing surface end point (%c)	No. Of actuators/ chord	LE actuator (%c)	TE actuator (%c)	Maximum displacement (mm)	Type of displacement	Requirements for the actuators
20	65	2	32	48	3.5	vertical in both directions	Δactuators < 6mm

The problem of airfoil upper-surface morphing for improvement of the aerodynamic behavior of wings is not a problem with a single solution. More often than not, as it was presented in Part I of this paper, there is an optimum region where several possible solutions coexist and any of them can be considered as the final solution to the problem.

A full description of the methodology used for the optimization algorithm and its numerical results was provided in Part I of this paper. Figure 7.3 presents the workflow diagram of the algorithm that was used for the optimization.

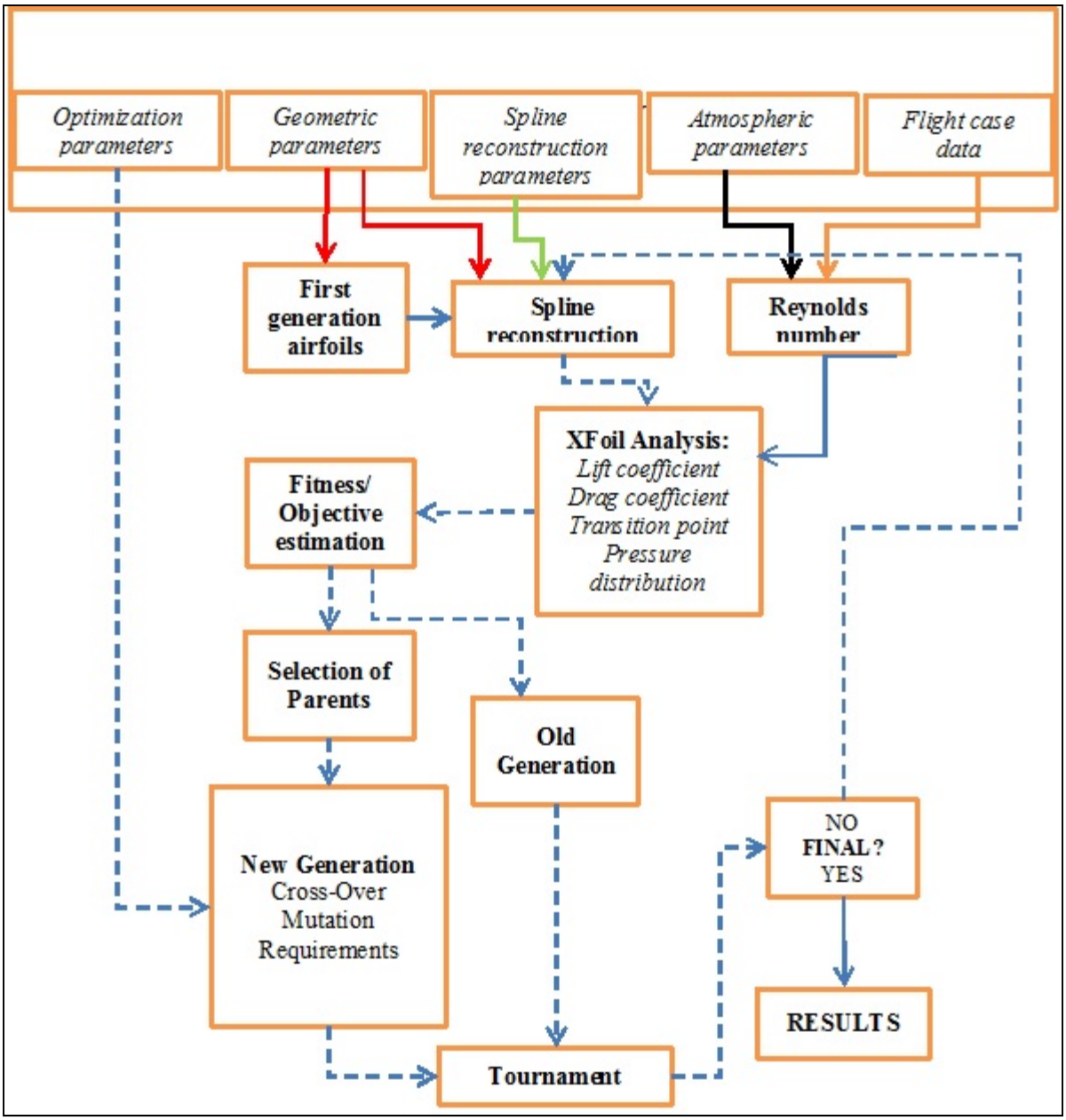

Figure 7.3 Diagram of the 'in-house' genetic algorithm

Table 7.2 presents the parameters used for the optimization of the 16 cases tested during the wind tunnel tests of the wing demonstrator.

Table 7.2 Input blocks and parameters for the CRIAQ MDO 505 demonstrator airfoil

Input block	Parameter	Values	Observations
Optimization	No. of individuals	40	-
	No. of generations	20	-
	Probability of mutation	1%	% of the total population
	Amplitude of mutation	2%	% of the maximum displacement value
	Optimization objective	-	The objective is given through weights associated with aerodynamic characteristics, such as lift and drag coefficients and the transition location
Geometry	Airfoil coordinates	-	-
	Chord of the airfoil	1.332	m
	Morphing surface start point	20%	% of chord
	Morphing surface end point	65%	% of chord
	No. of actuators	2	Can accept up to 4
	LE actuator	32%	% of chord
	TE actuator	48%	% of chord
	Maximum actuator displacements	3.5	mm
	Type of displacement	both directions	Allows both positive (push) and negative (pull) actions
Spline reconstruction	Number of splines	8	-
Atmosphere data	Density	1.22	kg/m³
	Dynamic viscosity	1.82E-05	Pa s
	Temperature	293	K
	Altitude	0	m
Flight data	Number of cases	16	-
	Speed	-	range of Mach speeds
	Angle of attack	-	range of angles
	Aileron deflection	-	range of angles

7.5 Optimization simulation results versus experimental results

In this section, the optimization of the CRIAQ MDO 505 wing airfoil is presented. The optimization was performed using the parameters provided in Section 7.4, Table 7.2. The optimization results, provided as actuator displacements in mm, were used by the control team to perform the upper-surface morphing of the wing-tip demonstrator during the wind tunnel tests.

The two sets of results, numerical and experimental, were firstly compared to assess the agreement between numerical and experimental values, and secondly to assess the optimization success during experimental tests and compare it to the numerical optimization expectation.

The optimization was run for two main objectives: transition delay towards the trailing edge (equation 7.1), which means possible drag coefficient reduction, and transition advancement towards the leading edge (equation 7.2), which could stabilize the boundary layer at high speeds or high angles of attack and aileron deflections.

$$F_f = 100 \cdot \left(\frac{Up_{Tr\_morphed} - Up_{Tr\_original}}{Up_{Tr\_original}} \right) \tag{7.1}$$

$$F_f = 100 \cdot \left(\frac{Up_{Tr\_morphed} - Up_{Tr\_original}}{Up_{Tr\_original}} \right)^2 \tag{7.2}$$

Table 7.3 presents the 16 cases studied and the numerical results obtained with the genetic algorithm optimization for both objective functions.

Table 7.3 Optimization cases and results for the CRIAQ MDO 505 wing demonstrator

Case no.	Mach	AoA (°)	Aileron deflection (°)	Type of optimization	Original airfoil Transition (%c)	Optimized airfoil Transition (%c)	Improvement (%c)
1	0.15	0.68	0	delay transition	53.62	54.47	0.85
2	0.15	1.50	0	delay transition	48.35	53.85	5.5
3	0.15	2.10	0	delay transition	46.09	52.41	6.32
4	0.15	-2.39	2	delay transition	63.71	66.19	2.48
5	0.15	1.93	-2	delay transition	43.34	52.97	9.63
6	0.2	1.88	4	delay transition	41.91	53.82	11.91
7	0.2	3.03	4	delay transition	33.44	50.62	17.18
8	0.2	3.45	-4	delay transition	30.35	41.3	10.95
9	0.15	-0.33	5	advance transition	74.90	43.05	-31.85
10	0.15	-0.95	-2	advance transition	60.01	50.92	-9.09
11	0.25	-2.99	1	advance transition	60.09	44.92	-15.17
12	0.25	-2.26	3	advance transition	59.46	45.05	-14.41

Case no.	Mach	AoA (°)	Aileron deflection (°)	Type of optimization	Original airfoil Transition (%c)	Optimized airfoil Transition (%c)	Improvement (%c)
13	0.15	-2.30	2	advance transition	65.58	44.01	-21.57
14	0.15	-1.64	3	advance transition	67.43	43.48	-23.95
15	0.15	-3.22	-2	advance transition	64.83	44.27	-20.56
16	0.25	-1.52	5	advance transition	64.52	41.77	-22.75

The experimental tests were done at the National Research Council (NRC) subsonic wind tunnel located in Ottawa/Ontario. The wind tunnel and the CRIAQ MDO 505 wing demonstrator used during the experiments were described in the above Section 7.2 of the present paper.

The experimental transition location results were obtained with Infrared (IR) Thermography; the results for the section of interest on the wing were extracted using Matlab software; the IR system was described in Section 7.2.1. The IR data post-processing steps consisted of: correction of the lens distortions, of the perspective view and projection onto the physical geometry. The detection of the transition region was fully automated by looking at the local temperature gradients on the wing surface. The final outputs of the data analysis were: the transition region (delimited by white dotted lines on the images), the mean transition front spanning the whole wing span, and the mean transition at the kulite pressure sensors station to compare with the CFD simulations. Figures 7.4 and 7.5 present examples of IR results for three of the cases from Table 7.3.

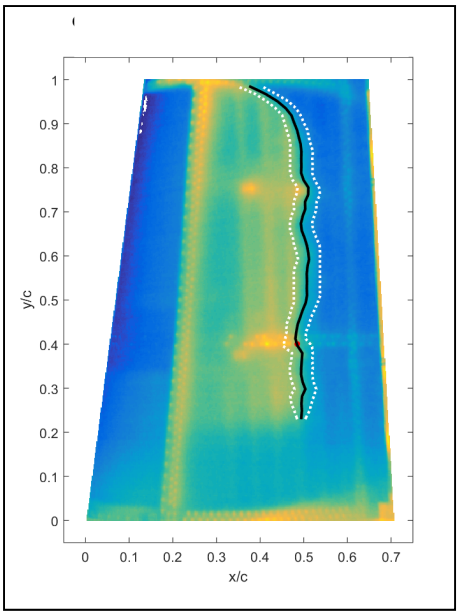

Figure 7.4 Example of Infrared results
for case 3 from Table 3 –
un-morphed wing demonstrator
shown without the aileron

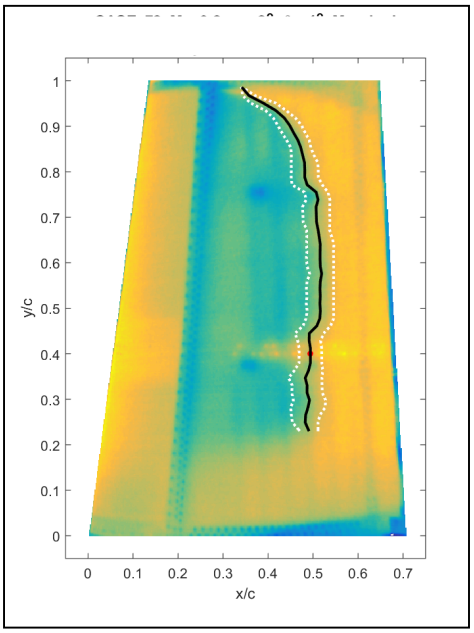

Figure 7.5 Example of Infrared results
for case 7 from Table 3 –
morphed wing demonstrator
shown without the aileron

The white dashed lines in Figures 7.4 and 7.5 correspond to the section of the wing demonstrator where the Kulite pressure sensors were installed, and also, represents the section chord for which the optimization was performed. The optimization was done for the section where the first line of actuators was installed, then it was linearly extrapolated for the second line of actuators, which is close to the tip of the wing demonstrator.

The experimental transition was presented as a 'region' and the numerical transition point obtained with XFoil's e^N method was matched to this region. If the numerical transition point was inside the experimental transition region, then it was considered that the numerical and experimental results were in good agreement. If the numerical transition was outside the experimental transition region, then an error was calculated between the numerical value and the closest boundary value. If the calculated error was less than 6%, the error was considered as acceptable, (Robitaille, Mosahebi and Laurendeau, 2015).

Figure 7.6 presents an example where the numerical transition matched the experimental transition region and an example where the numerical transition did not match.

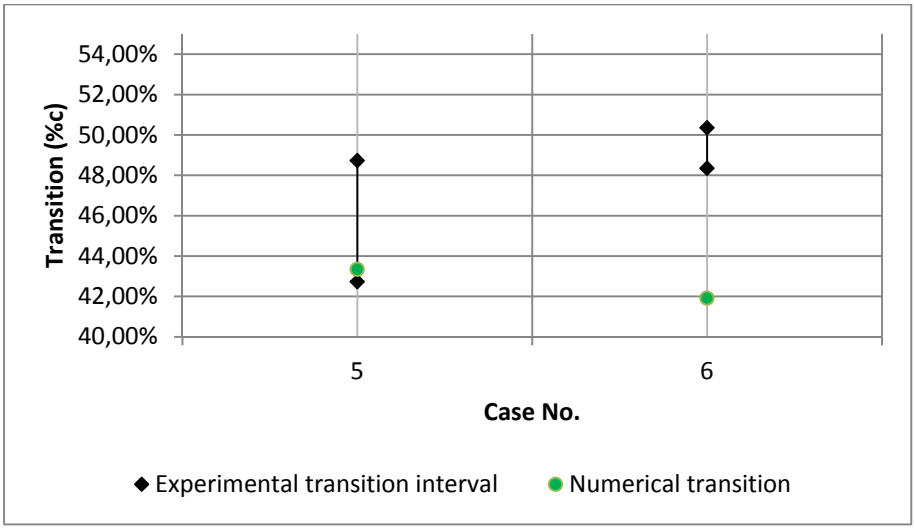

Figure 7.6 Comparison between Case 5 when the numerical transition has matched the experimental region and Case 6 when the numerical transition was found outside the experimental region

As shown in Figure 7.6, the numerical transition point was found to be situated inside the experimental transition region boundaries for Case 5, and in this case, a good agreement between numerical and experimental data existed, while in Case 6, the numerical transition was situated with 6% of the chord outside the lowest boundary of the experimental transition region, and it was viewed as having an acceptable error between numerical and experimental transition

7.5.1 Comparison between numerical and experimental transition data

Figures 7.7 to 7.10 show the comparison that was made between the numerically determined transition point and the experimental transition region from Infrared readings for the un-morphed, and for the morphed wing demonstrator. This comparison was done to show the agreement between the numerical and the experimental transition data.

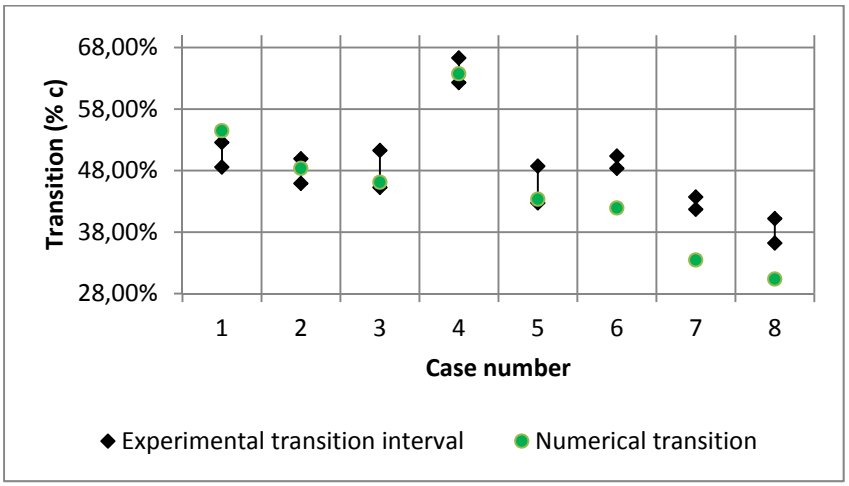

Figure 7.7 Comparison between numerical transition point and the experimental transition region for the first 8 cases – un-morphed wing demonstrator

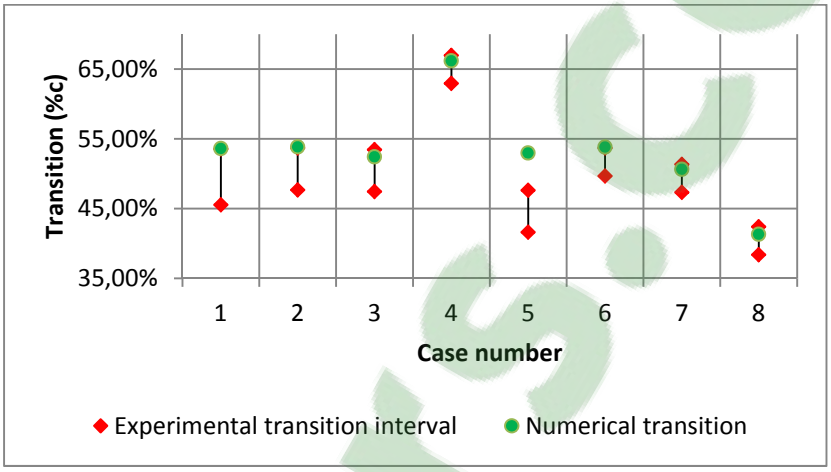

Figure 7.8 Comparison between numerical transition point and the experimental transition region for the first 8 cases - wing demonstrator optimized for transition delay towards TE

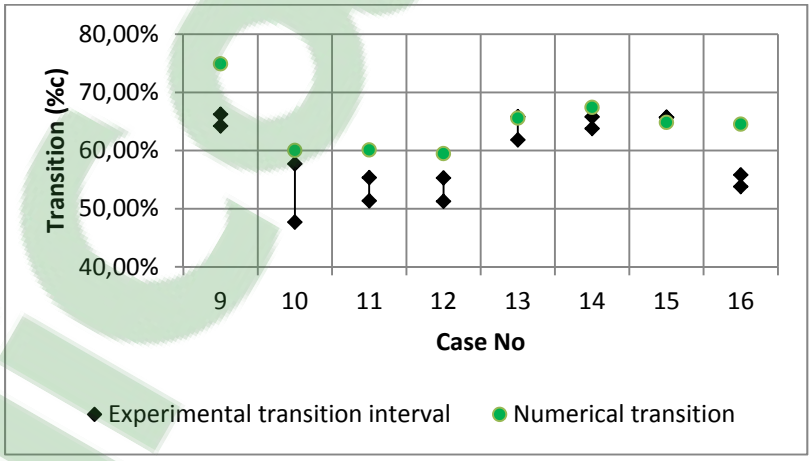

Figure 7.9 Comparison between numerical transition point and the experimental transition region for the second set of 8 cases from 9 to 16 – un-morphed wing demonstrator

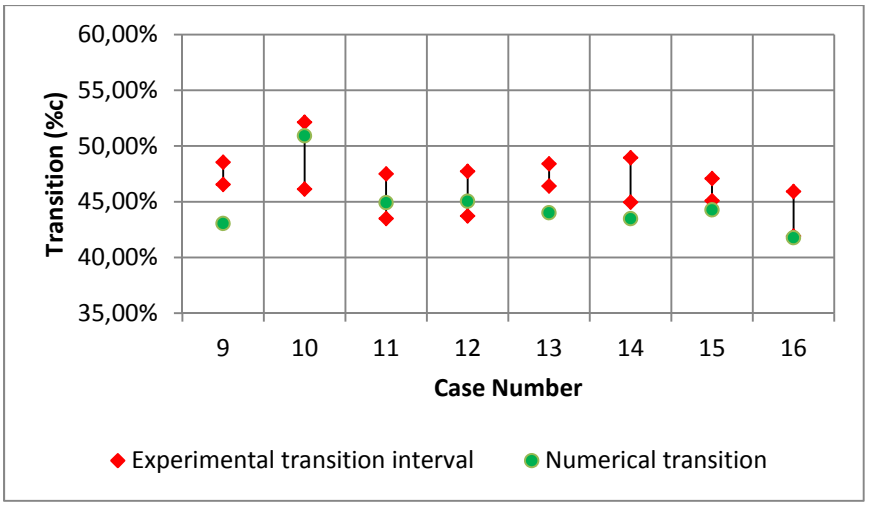

Figure 7.10 Comparison between numerical transition point and the experimental transition region for the first 8 cases - wing demonstrator optimized for transition delay towards LE

It was possible to successfully compare the numerical results obtained for the wing's airfoil to the experimental transition results extracted for a specific section corresponding to kulite sensors localization from the global experimental results of the entire wing demonstrator.

In Figures 7.7 to 7.10, the presented results show that with the exception of 3 un-morphed wing cases (cases 6, 7 and 9), the numerical transition was situated inside the experimental transition boundaries.

Tables 7.4 and 7.5 present the errors found for the 16 cases described in Table 7.3. Table7.4 presents the errors for the un-morphed wing demonstrator transition results and Table 7.5 for the morphed wing demonstrator transition results:

Table 7.4 Transition intervals and values for the numerical and experimental cases and the error between the results

Case no.	Xfoil UM *(%c)	Experimental UM*(%c)			Error (%c)
		Upper Boundary(%c)	Lower Boundary (%c)	Average(%c)	
1	53.62	52.57	48.57	50.57	1.09
2	48.35	49.91	45.91	47.91	0
3	46.09	51.26	45.26	48.26	0
4	63.71	66.30	62.30	64.30	0
5	43.34	48.73	42.73	45.73	0
6	41.91	50.35	48.35	49.35	-6.44
7	33.44	43.69	41.69	42.69	-8.25
8	30.35	40.20	36.20	38.20	-5.85
9	74.90	66.22	64.22	65.22	8.68
10	60.01	57.70	47.70	52.70	2.31
11	60.09	55.35	51.35	53.35	4.74
12	59.46	55.28	51.28	53.28	4.18
13	65.58	65.83	61.83	63.83	0
14	67.43	65.79	63.79	64.79	1.64
15	64.83	65.73	65.73	65.73	0
16	64.52	55.80	53.80	54.80	8.72

Table 7.5 Transition intervals and values for the numerical and experimental cases and the error between the results

Case no.	Xfoil UM *(%c)	Experimental M*(%c)			Error (%c)
		Upper Boundary(%c)	Lower Boundary (%c)	Average(%c)	
1	54.47	53.54	45.54	49.54	0.93
2	53.85	53.67	47.67	50.67	0.18
3	52.41	53.44	47.44	50.44	0
4	66.19	66.95	62.95	64.95	0
5	52.97	47.63	41.63	44.63	5.34
6	53.82	53.68	49.68	51.68	0.14
7	50.62	51.34	47.34	49.34	0
8	41.3	42.39	38.39	40.39	0
9	43.05	48.55	46.55	47.55	-3.50
10	50.92	52.13	46.13	49.13	0
11	44.92	47.49	43.49	45.49	0
12	45.05	47.73	43.73	45.73	0
13	44.01	48.41	46.41	47.41	0
14	43.48	48.95	44.95	46.95	-1.47
15	44.27	47.09	45.09	46.09	-0.82
16	41.77	45.91	41.91	43.91	-0.14

The error was calculated as the difference between the numeric transition value and the closest experimental transition region boundary:

$$Error = Transition_{num} - Transition_{\exp} \quad (7.3)$$

num = numerical

exp = closest boundary of the experimental region

When the error is 0 the numerical transition was situated inside the experimental transition region.

7.5.2 Evaluation of the experimental transition optimization

This section presents the behavior of the upper-surface morphing during experimental testing on the MDO 505 wing demonstrator. In Figures 7.11 and 7.12, the experimental un-morphed and morphed wing section transition regions were overlapped for a better view of the effects of the upper-surface morphing on the length and position of the transition region in the studied section.

The experimental transition region is characterized by an upper and a lower boundary. The lower boundary of the transition region represents the point where the flow starts its transition from fully laminar flow towards turbulent, while the upper boundary of the transition region represents the location at which the flow can be considered as being fully turbulent. Therefore, the optimization of the transition region refers to modifications in the desired direction of the upper and lower boundaries, depending on the optimization objective to be accomplishedr.

As such, two parameters were calculated: $\boldsymbol{\tau}$, which represented the difference between the morphed and un-morphed transition region (TR) upper boundary values and described with how much the onset of the fully turbulent flow was modified,

$$\begin{aligned} \tau &= MorphedTr_{UB} - UnmorphedTR_{UB} \\ UB &= upper - boundary \end{aligned} \tag{7.4}$$

and $\boldsymbol{\lambda}$, which represented the difference between the morphed and un-morphed transition region (TR) lower boundary values and described with how much the boundary of the fully laminar flow was modified.

$$\lambda = MorphedTr_{LB} - UnmorphedTR_{LB}$$
$$LB = lower - boundary \tag{7.5}$$

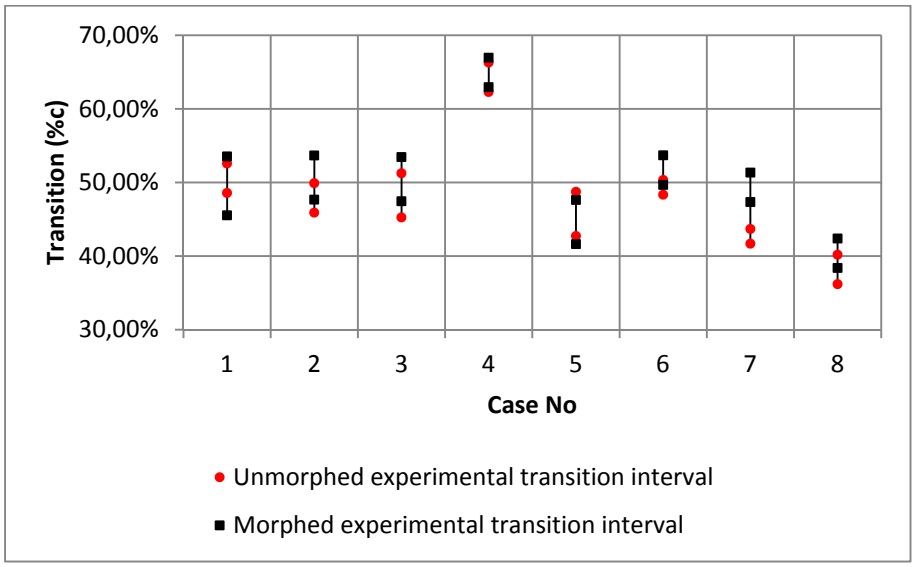

Figure 7.11 Comparison between the experimental un-morphed and morphed transition regions with the objective of transition delay towards the TE

Figure 7.11 shows the comparison between the un-morphed and morphed wing transition regions for the objective of flow transition delay from fully laminar to fully turbulent.

It could be observed from the above figure that the onset of the fully turbulent flow was delayed for 7 cases out of 8, with the maximum delay being achieved for case 7 with 7.65%c. The end of the laminar flow was also delayed in 6 cases, with the maximum delay being again for case 7 with 5.65%c. For case 1, the transition region of the morphed wing was extended in comparison with the original wing, while for case 4 the difference between the two regions was almost negligible. Case 5 was the one case where the transition optimization was not successful, but the difference between the two transition regions was also very small.

Table 7.6 presents the values for the two parameters described in the first part of the section, τ and λ, for the cases where the optimization was aimed at delaying the transition from laminar towards turbulence of the upper-surface flow.

Table 7.6 Parameters λ and τ describing the effects of the morphing wing on the flow behavior for the transition delay objective.

Case No	Mach	AoA (°)	Aileron deflection (°)	τ (%c)	λ (%c)
1	0.15	0.68	0	0.97	-3.03
2	0.15	1.50	0	3.76	1.76
3	0.15	2.10	0	2.19	2.19
4	0.15	-2.39	2	0.66	0.66
5	0.15	1.93	-2	-1.10	-1.10
6	0.2	1.88	4	3.33	1.33
7	0.2	3.03	4	7.65	5.65
8	0.2	3.45	-4	2.19	2.19

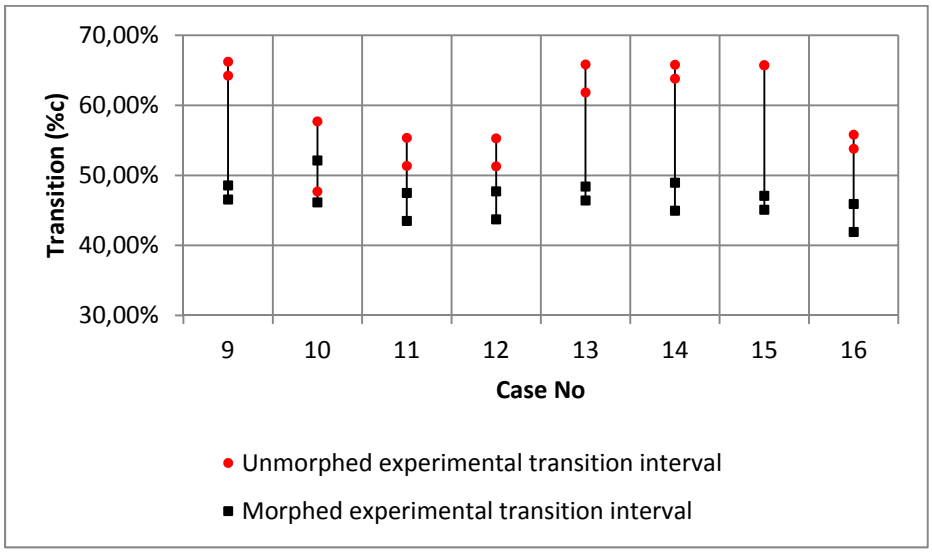

Figure 7.12 Comparison between the experimental un-morphed and morphed transition regions with the objective of transition advancement towards the LE

Figure 7.12 shows the comparison between the un-morphed and morphed wing transition regions for the objective of advancing transition towards the leading edge.

From Figure 7.12, it appeared that the onset of the fully turbulent flow was advanced towards the leading edge for all cases, with the maximum advancement being achieved for case 15 with 18.64 %c. The end of the laminar flow was also advanced towards the leading edge in all cases, with the maximum advancement being again for case 15 of 20.64 %c. For cases 10 and 13 the length of the transition region was reduced through the morphing of the upper surface, while for cases 14 to 16 the length of the transition region was a little bit extended; all the other cases had an unchanged length of the transition region.

Table 7.7 presents the values for the two parameters described in the first part of the section, $\boldsymbol{\tau}$ and $\boldsymbol{\lambda}$, for the cases where the optimization was aimed at advancing the transition on the wing upper-surface.

Table 7.7 Parameters λ and τ describing the effects of the morphing wing on the flow behavior, for transition advance towards the leading edge objective

Case No	Mach	AoA (°)	Aileron deflection (°)	τ (%c)	λ (%c)
9	0.15	-0.33	5	17.67	17.67
10	0.15	-0.95	-2	5.57	1.57
11	0.25	-2.99	1	7.86	7.86
12	0.25	-2.26	3	7.55	7.55
13	0.15	-2.30	2	17.42	15.42
14	0.15	-1.64	3	16.84	18.84
15	0.15	-3.22	-2	18.64	20.64
16	0.25	-1.52	5	9.89	11.89

Figures 7.13 and 7.14 display a comparison between the numerical transition optimization prediction and the resulted experimental optimization. Figure 7.13 shows the comparison between the numerical optimization prediction based on XFoil results and the $\boldsymbol{\tau}$ and $\boldsymbol{\lambda}$ results

with the objective to delay transition, while Figure 7.14 presents the comparison between the numerical prediction and the **τ** and **λ** results with the objective of advancing transition. The two figures assess the differences between the numerical optimization predictions and the experimental results.

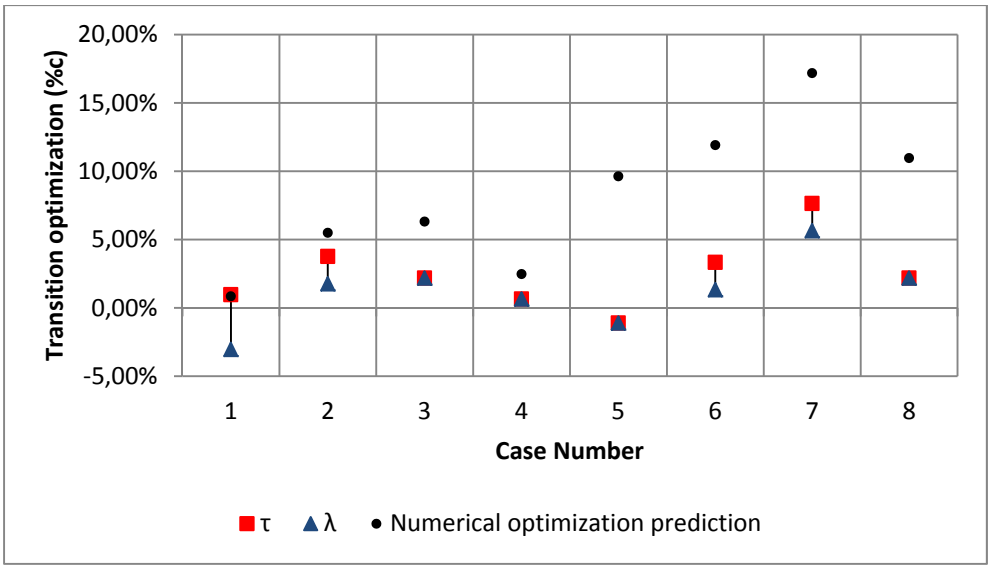

Figure 7.13 Comparison of the numerical optimization transition and the experimental resulted optimization for the transition delay objective

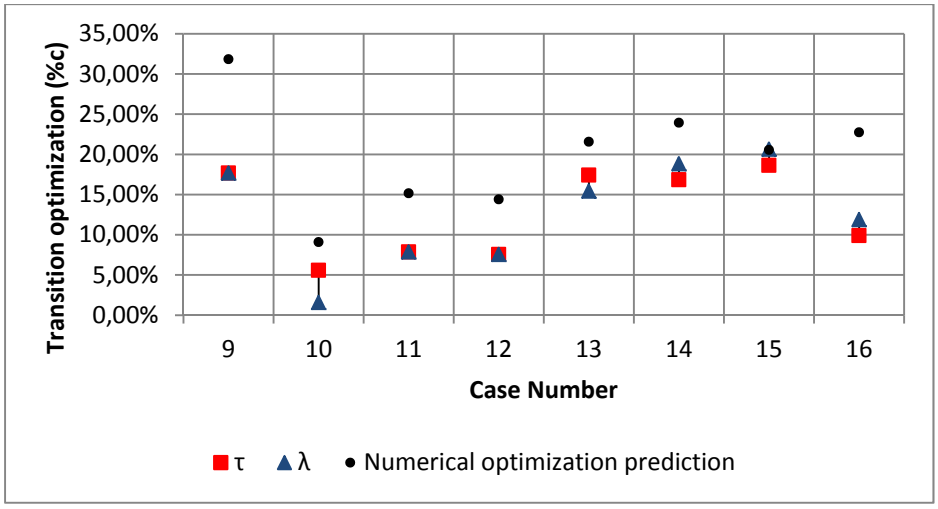

Figure 7.14 Comparison of the numerical optimization transition and the experimental resulted optimization for the transition advancement objective

From both figures, it could be observed that for most of cases the numerical optimization had overestimated the transition delay or advancement, with some cases where the difference is almost double. For Cases 1 to 4, 10 and 15 the numerical prediction was close to the transition obtained experimentally during the wind tunnel tests.

The overestimation of the transition optimization cannot be imputed to a single aspect or point in a single direction where an error could be found; as the designed and manufactured MDO 505 wing demonstrator was the result of a multidisciplinary project, where many aerospace disciplines interacted, any variation of any of the multiple variables pertaining to structure, aerodynamics, control, integration or experiment could have affected the outcome of the results. Nonetheless, despite the existing differences between the numerical predictions and the experimental results, the optimization of the MDO 505 wing through morphing of the upper surface by using actuator displacements resulted from a numerical optimization with an 'in-house' Genetic Algorithm coupled with a bi-dimensional aerodynamic solver using the e^n method was considered as successful.

7.6 Conclusions

In this paper, an 'in-house' genetic algorithm was applied to the problem of optimizing the shape of the upper surface of an airfoil by using actuator displacements. In the first part of the paper it was shown that the genetic algorithm used for the optimization of the wing tip demonstrator airfoil gave very good results in comparison with two other optimization methods and it always reached the global optimum region. It was shown that the algorithm was robust and that it converged towards the optimum area in less than 10 iterations or generations, while other 10 generations were used to ensure the stability of the solution and that this solution was found in the global optimum area.

Finally, the genetic algorithm was used to optimize the airfoil shape for 16 cases, with the aim to satisfy two objectives: delay of the transition towards the trailing edge of the airfoil, and advancement of the flow transition towards the leading edge. The displacements resulted

from the optimization were used for the upper surface morphing controller during wind tunnel testing on the MDO 505 wing demonstrator and comparisons were conducted between the experimental transition regions of the morphed and un-morphed wing – section by using Infrared Theromography. For the success of this optimization, two new parameters were introduced, τ and λ, to describe the behavior of the flow when it passed from fully laminar to fully turbulent. Both objectives were successfully attained for most of the cases, , using the displacements provided by the numerical optimization. Maximum delays of the transition region were up to 7.6% of the chord and for the forward displacement of the transition region were of up to 20% of the chord..

The experimental optimization results were then compared with the numerical simulation results, it was found that the numerical optimization was overestimated due to a multitude of factors starting with the numerical solver, and ending with the multidisciplinary aspect of the project that introduced a high number of variables that could affect the numerical optimization. Nonetheless, the numerical optimization was an important tool for preliminary estimation and evaluation of the morphing possibilities and the Genetic Algorithm presented in this paper and could be successfully used for performing optimization of the wing's upper-surface morphing problem,. Also it would be interesting to compare its results to those that could be obtained with more recent optimization methods such as those based on mathematical behavior.

Acknowledgments

We would like to thank to Bombardier Aerospace, Thales Canada, The Consortium in Research and Aerospace in Canada (CRIAQ), and to the Natural Sciences and Engineering Research Council of Canada (NSERC) for their financial support. Special thanks are dues to our collaborators and leaders in this project: Mr. Patrick Germain and Mr. Fassi Kafyeke from Bombardier Aerospace, Mr. Eric Laurendeau from Ecole Polytechnique, Mr. Philippe Molaret from Thales Canada, and Mr. Erik Sherwood and his team from DFS-NRC for the wing model design and fabrication.

DISCUSSION OF RESULTS

The research included in chapters 3 to 7 represents the general framework for analysing the performances of a morphing wing. Chapters 3 to 7 present the development of the tools needed for the optimization and analysis processes. Thsese concern optimization algorithms, geometrical studies and parameterizations, aerodynamic, aeroealastic calculations, and the improvements obtained, numerically and experimentally, from their application on two different projects. While the results were presented separately in the aforementioned chapters, in the present chapter, they will be summarised and analysed from a global perspective for each of the research projects: ATR-42 'Morphing Wing' and CRIAQ MDO 505 'Morphing Architectures and Related Technologies for Wing Efficiency Improvement'.

Chapter 3 presented the numerical and experimental results obtained for the rigid ATR-42 wing models, while chapters 4 to 7 presented the numerical and experimental results obtained for the CRIAQ MDO 505 wing – tip demonstrator.

Discussion of Results for the ATR-42 'Morphing Wing' Project

The first paper, which is shown in Chapter 3, was concentrated on the development of the multidisciplinary framework (design, optimization, manufacturing and testing) for the ATR-42 wing. This framework was developed to be applied, later in the project, on an ATR-42 active morphing wing.

The framework was validated on two rigid wing models: one wing model based on the baseline ATR-42 wing airfoil, and another wing model based on a morphed shape of the ATR-42 wing airfoil. The morphed shape was obtained by applying the optimization procedure on the original airfoil for Mach number 0.1 and angle of attack 0°.

- **Description of the Wing Models**

Upper surface morphing of the ATR-42 wing airfoil was the concept on which the multidisciplinary framework was applied. The design phase was focused on establishing the parameters necessary for conducting the optimization, such as skin length, skin flexibility, number of actuators, displacements directions, and maximum allowed displacements. The wing's airfoil upper surface was considered flexible between 10% and 70% of the chord, with the constraint that the total length of the morphed skin would remain within +/- 0.3% of the original length. The morphing shape was achieved through vertical displacements at 30% and 50% of the chord. The upper surface section, between 10% and 70% of the chord, was reconstructed with cubic spline interpolation. Natural boundary conditions were introduced to allow a smooth connection between the flexible and rigid parts of the airfoil shape. A high degree of liberty was given to the user of the numerical optimization tool, in the sense that the number of spline control points can be adjusted.

From the spanwise perspective, the wing was equipped with the flexible upper surface between 15% and 80% of the wing model span, allowing enough space at each end for the junction with the rigid part of the upper surface.

- **Aerodynamic Optimization of the Wing Models**

The optimization phase was carried for three Mach numbers between 0.08 and 0.1, several angles of attack between -2° and 2° and three Reynolds numbers ($4.5 \cdot 10^5 \rightarrow 5.7 \cdot 10^5$) as calculated using the mean aerodynamic chord. These cases were chosen as function of the Price-Païdoussis wind tunnel characteristics.

The genetic algorithm was developed using single step cross-over, mutation and tournament functions. The algorithm used equal sharing of the genes that described the individual airfoils forming a generation. The genes were represented by the control points displacements, which also served as reconstruction points for the cubic spline interpolation. The algorithm allowed

the selection of the morphing skin length, the maximum actuator displacements in percentage of the airfoil chord, and the chordwise positions of the control points, in order to allow flexibility of the optimization procedure.

The fitness function that evaluated the individual airfoils optimization level was embedded in the software. This function was developed as a weighted sum of the aerodynamic parameters calculated by Xfoil, to which the algorithm was coupled. The optimization objective was the minimization of the drag coefficient through manipulation of the flow transition from laminar to turbulent. The more extended the laminar region on the upper surface of the wing, the more the drag coefficient would be reduced.

- **Interpretation of Numerical and Experimental Results**

From the manufacturing perspective, the ATR-42 rigid wing models were used for validating the design and optimization procedures for the fiber glass-epoxy composite material. The composite material was used for manufacturing the entire wing models, not only the upper surface. Based on the aerodynamic analysis results, for each rigid model a different chordwise step was chosen between two consecutive pressure taps. This installation allowed the estimation of which of the two ATR-42 wing models was best suited to determine the transition region using the second derivative of the pressure distribution method.

The results have shown that the numerical optimization was successful, as the the aerodynamic calculations performed with a critical number equal to 5.5 (corresponding to the turbulence level of 0.3% specific to the Price-Païdoussis wind tunnel) gave numerical results within +/- 5% of the experimental transition location. For all the cases tested in the wind tunnel, it was shown that the rigid morphed shape wing model outperformed the original shape wing model, not only for the specific flight case at which the optimization was performed, but also for off-design conditions.

Numerically, the laminar region was extended towards the trailing edge with up to 20.5% of the chord, while experimentally it was extended with up to 23% of the chord. Based on the experimental transition estimated using the second derivative of the pressure distribution, the variable step used for installing the pressure taps on the original shape wing model has given more precise results than the constant step used for installing the pressure taps on the morphed shape wing model. In addition to the increased laminarity of the flow, a reduction of up to 10% of the model's drag coefficient was obtained. More detailed numerical results on the optimization of the ATR-42 airfoil are provided in Appendix I.

From a manufacturing point of view, the wind tunnel testing has shown that the design and optimization of the fiber glass-epoxy composite based on preliminary aerodynamic optimization results was a success, and thus it was developed further in order to be applied for the upper surface of the active morphing wing model.

Discussion of Results for the CRIAQ MDO 505 'Morphing Architectures and Related Technologies for Wing Efficiency Improvement'

The research presented in Chapters 4 to 7 focused on the development of the tools needed for the aerodynamic optimization, aerodynamic and aeroelastic analyses, and experimental validation of an upper surface morphing wing tip equipped with conventional and morphing aileron.

- **Design, Optimization and Manufacturing of the CRIAQ MDO 505 Wing Demonstrator**

The morphing concept applied for the CRIAQ MDO 505 project was described in detail in Chapters 2 and 4 to 7. A wing-tip structure of 1.5 m at root chord by 1.5 m span was equipped with a flexible upper surface. The morphing surface was limited to the area between the fore and aft spars, corresponding to 20% and 65% of the chord, and it was fixed on all four sides in similar way as for a conventional aircraft. The skin was designed and optimized using Hypermesh and Optistruct softwares and carbon fiber composite properties.

For the design and optimization process, preliminary aerodynamic optimizations were conducted to determine possible skin shapes. For this stage, a maximum displacement of 10 mm was investigated, and this value was transferred to the structural team to determine the forces needed for the electrical actuators used to deform the skin.

Based on the structural design and optimization, the aerodynamic optimization was adjusted in terms of maximum displacements and constraints imposed to the allowed elongation of the skin. Several steps of aerodynamical – structural optimization were done until a stable wing structure and upper surface skin were obtained. An aerodynamic optimization – control process design coupling was conducted after the finalization of the wing and aileron structures.

The final structural characteristics of the upper surface morphing wing were: morphing skin extended between 20% and 65% of the chord on the full span; elongation of the composite skin when it would morph was less than 0.3% of the non-morphed length; two actuation lines situated on the two center ribs; each actuation line contained two electrical actuators situated at 32% and 48% of the chord; the maximum allowed displacement was 3.5 mm (in both pushing and retracting directions).

The lower surface of the wing, the leading edge and the conventional aileron were manufactured using aluminium. The design and optimization of the wing equipped with the aileron was done while also trying to minimize the total weight of the complete wing system (internal control system included).

- **Morphing Aileron Description**

The morphing aileron was designed, optimized and manufactured by the Italian team. It was transported in Canada for testing together with the wing structure at the IAR-NRC wind tunnel in Ottawa. The morphing aileron was designed as a finger-like structure, using a rigid leading edge segment from which electrical actuators displaced a second middle segment, which in turn caused the deployment of the third and final segment. Two electrical actuators were used for the deployment of the second segment. The morphed shapes that the aileron was capable of obtaining were based on the aerodynamic optimization of the wing's airfoil using the camber morphing method integrated in the genetic algorithm software.

- **Wind Tunnel Testing of the CRIAQ MDO 505 Wing Demonstrator**

The manufactured wing-tip and ailerons were equipped with pressure sensors on both their upper and lower surfaces to collect pressure data for the various flight cases. 32 Kulite pressure sensors and 60 pressure taps were installed in two parallel staggered lines on the wing mode. Initially, two different configurations were proposed for the pressure sensorsinstalation: the parallel staggered and the V shaped pressure sensors lines. It was decided that the pressure sensors should be installed close to the first actuation line, as validation of the numerical results would be easier to perform experimentally. Since the area between the two center ribs was designed so that its shape under morphed and un-morphed conditions would allow a quais-two-dimensional flow, it was considered that the staggered lines configuration was the best suited.

Three sets of wind tunnel tests were performed between April and December 2015, at the subsonic wind tunnel facility at IAR-NRC in Ottawa. The first set of tests was focused on the control system calibration, infrared thermography tests, data post-processing procedures for the interpretation of experimental results, preliminary verification of the numerical results and the calibration of the aerodynamic optimization procedure. 38 flight cases for the wing-tip equipped with conventional aileron and for two objective functions were used in this set

of tests. The second series of wind tunnel tests included 97 flight cases, including the previous 38 flight cases, which were repeated for comparison purposes. For the first two series of tests, only the wing model equipped with the conventional aileron was considered, while two optimization objectives were investigated. The third set of tests was focused on evaluating the performances of the morphing wing –tip equipped with the morphing aileron. 49 flight cases were chosen for this set of tests, including 41 of the second series cases, with the objective of comparing the aerodynamic performances of the morphing aileron versus those of the conventional aileron. The chosen flight cases were aerodynamically optimized and analyzed for a number of four objective functions.

- **Aerodynamic Optimization using Genetic Algorithm**

The genetic algorithm used in the ATR-42 Morphing Wing project was further developed and used for the aerodynamic optimization of the CRIAQ MDO 505 project airfoil. The new algorithm included a two-step cross-over function, with the second step introduced to replace the first step after the first 10 generations. The first step is an equal mix of the parent airfoils genes, realized in order to obtain an individual of the new generation, while the second step of the cross-over represents a binary combination function. The new version of the algorithm also includes two methods of morphing the aileron. The first method is similar to the morphing of the airfoil upper surface, with control points simulating actuator displacements. The second method for morphing the aileron was developed as an extension of the conventional method of deflection, using control points on the camber line of the aileron to smooth the slope of its deflection.

Other modifications brought to the new optimization algorithm included:

- A greater flexibility in the choice and external input of the fitness function;
- The introduction of several options for the parameters affecting the morphing wing optimization procedure such as: number of generations, number of individual airfoils, probability of mutation, amplitude of mutation, number of control points, airfoil chord, control points maximum displacement, direction of the displacement, aerodynamic

calculation with angle of attack or lift coefficient, critical amplification factor, atmospheric parameters.

- Several options were introduced for performing the shape optimization of the airfoil: 1) optimization of upper surface only; 2) optimization of upper surface coupled with conventional aileron deflection; 3) optimization of upper surface coupled with morphing aileron (choice of either of the two methods presented); 4) optimization of morphing aileron only (fixed optimization or free optimization).

A *fixed optimization* of the morphing aileron shape refers to finding a single optimal shape at each deflection angle, that would respect specific constraints regarding constant thickness, deviation for the given deflection angle, slope of the aileron's camber line, regardless of the aerodynamic objective function. A *free optimization* of the morphing aileron shape refers to finding an optimal shape without constraints related to the deflection angle or to the slope of the aileron's camber line. This type of optimization focuses on both the aerodynamic loads and aileron shape optimization, obtaining different optimized aileron shapes based on the desired aerodynamic objective, but all shapes having the same deflection angle.

The first objective of the aerodynamic optimization of the wing equipped with conventional aileron was to extend the laminar region of the boundary layer towards the trailing edge, thus stabilizing the boundary layer, avoiding separation and minimizing the drag coefficient. A presentation of the numerical predictions for the CRIAQ MDO 505 wing airfoil without aileron deflection is given in the research paper presented in Chapter 4.

A secondary objective was introduced later to validate the optimization algorithm, focusing on extending the turbulent region of the boundary layer, with minimal loss in drag or lift. Such a behavior was considered as a possible solution for the detachment of the boundary layer at high angles of attack and high aileron deflections. Due to the design of the airfoil, to the wind tunnel limitations regarding speeds, angles of attack and aileron deflection, the conditions in which boundary layer detachment occurs were not fulfilled. Thus, this objective was studied from the numerical versus experimental optimization success perspective.

For the wing equipped with morphing aileron, the global objective was the evaluation of the performances of the morphing aileron compared with the conventional aileron, with regards to the pressure distribution over the upper surface, and especially the negative pressure peak usually encountered at the region where the camber changes slope. The numerical and experimental studies performed for the morphing aileron were done by considering flight cases that were also studied during the second series of tests, in order to be able to perform comparisons. The optimization was focused on several combinations:

- New optimization of the upper surface of the wing coupled with fixed optimization of the aileron shape,in order to observe the performances of the wing in terms of both lift and boundary layer behaviour (extension of the laminar region towards the trailing edge);
- Identical wing upper surface morphing as for the equivalent cases from the second set of tests, coupled with a fixed optimization of the aileron shape. The aim was to observe the performances in terms of lift and to understand how maintaining the upper surface deformation from the previous set of tests, while changing the aileron shape, affects the behaviour of the boundary layer;
- New optimization of the upper surface of the wing coupled with free optimization of the aileron shape at constant lift coefficient, in order to observe the how the aileron's deflection angle compares with the conventional deflection from the previous tests;
- No optimization of the upper surface coupled with a fixed optimization of the aileron shape, in order to observe the performance of the morphing aileron while subjected to a deflection angle sweep.

- **Aeroelastic study of the CRIAQ MDO 505 Wing Demonstrator**

Once all the flight cases were established for all aerodynamic objectives and the wing tip structure design, optimization and analysis was done, an aeroelastic analysis was performed. For the aeroelastic analysis, generalized Finite Element Models (FEMs) of the wing and aileron were developed using Hypermesh software. FEMs modeled the wing and aileron structures using uni-, two- and three- dimensional elements, with focus on representations

with two-dimensional elements of type SHELL. Dimensions and materials provided by Bombardier and IAR-NRC teams were used to describe the properties of these models.

A coupled FEM of the wing with aileron was exported to the Flight, Loads and Dynamics Solution (FLDS) toolbox from the MSC/Patran/Nastran software. The flutter analysis was then performed using MSC/Nastran solver and the results were exported and post-processed using HyperView. A detailed description of the FEMs, flutter analysis set-up and interpretation of results, both numerical and experimental, was given in the research paper presented in Chapter 5. From the results of the flutter analysis it was concluded that the designed structure equipped with a morphing (and thus more flexible) upper surface was as rigid as its version with aluminium skin, and neither was flexible enough to allow the appearance of flutter phenomena at the speeds that were considered for wind tunnel testing.

During the experimental testing, accelerometers were installed on the wind tunnel balance, inside the wing box and on the aileron as a safety precaution against the minor possibility of damaging vibrations occurence. The data recorded by the accelerometers have shown that no problems were encountered and that numerical predictions were sufficiently accurate.

- **Interpretation of Experimental and Numerical Results**

During wind tunnel tests, infrared, kulite and pressure taps data was recorded. The kulite pressure data was post processed to determine the transition region as seen by the kulites at the region where they were installed, and to calculate the pressure distribution over the morphing upper surface skin. The transition region obtained from the post-processing of the kulite recorded data was compared to the transition region recorded by the infrared thermography technique. Because the results from the two techniques were very close, only the infrared transition data was used for the purpose of comparing and validating the numerical optimization and analysis results.

The experimental results from the second set of tests have shown that the optimization objective of extending the turbulence region was successful in the majority of the cases, which was expected (as the perturbation of the boundary layer is easier to achieve), while the objective related to the extension of the laminar region was successful for half of the studied cases.

A comparison between the numerical optimization predictions obtained using the genetic algorithm coupled with XFoil and the experimental optimization that was measured during testing showed that for all cases, regardless of the optimization objective, the numerical optimization results were overestimated. Comparisons were performed between the performances of the genetic algorithm and two other optimization methods (Artificial Bee Colony and Gradient Descent). The results, presented in Chapter 6, have shown that all of the three algorithms performed in the same manner, with the Gradient Descent method obtaining the lowest improvements. The plots of the airfoil performance results against all possible actuators displacements combinations have shown that all three algorithms converge towards the same optimal area, which is also the global optimal area for the airfoil used in CRIAQ MDO 505 project. These results have shown that the genetic algorithm performed excellently and that the results would not have been improved by the use of another optimization algorithm.

The numerical results presented a tendency of overestimating the transition point motion caused by the upper surface morphing, as shown in the results presented in the research paper from Chapter 7, for some cases this overestimation being higher than 10%. However, for the objective of delaying the transition from laminar to turbulent, the experimental results showed transition point improvements of up to 6-7% of the chord. These results, though not as high as those obtained for the previous projects (ATR-42 Morphing Wing and CRIAQ 7.1) are very encouraging, as they were obtained for a real wing structure. This implied many structural constraints imposed during the aerodynamic optimization, and the use of a supercritical airfoil, which has already been highly optimized, having very good

performances for both low speeds and cruise conditions, as it can be observed from the results presented in Appendix II.

For the aerodynamic numerical analysis performed before the wind tunnel tests, the turbulence rate parameter which contributes to the calculation of the transition point in the XFoil e^n method was set at 7.6 corresponding to a wind tunnel turbulence rate of 0.14%. Also, the experimental results have shown that, naturally, the transition region is not stable in flight or wind tunnel conditions, as the flow over the wing has an unstable behaviour. The amplification factor N is a key parameter in the e^n method for determining the transition point for two-dimensional aerodynamic analysis. Normally, the amplification factor is selected as function of the expected turbulence rate. In absence of precise knowledge regarding the turbulence rate, it is assumed that the amplification factor is 9, which corresponds to real flight through air. The lower the amplification factor value, the more the transition point will move towards the airfoil leading edge.

The initial difference (obtained after the first set of wind tunnel tests) between experimental infrared transition and numerical transition on the non-morphed scanned airfoil ranged between -20% and + 20% of the chord. Therefore, a calibration procedure was developed to account for this natural instability of the flow for each flight case and improve the aerodynamic optimization analyses conditions. The calibration procedure was based on a cyclic correction of the aerodynamic parameters (temperature, density, Reynolds number and turbulence rate) as function of the experimental transition results in order to take into account the differences due to 3D flow effects. Therefore the turbulence rate has changed from one set of wind tunnel tests to another. Thus, the turbulence rate parameter, N_{crit}, or critical amplification factor has varied between the initial value of *7.6* and *6*, as function of the speed and aileron deflections, which were observed to affect the results, and the error between the numerical transition and the experimental infrared results was lowered to +/- 6%, with some exceptional cases falling outside this range. This difference between what was supposed to be the amplification factor specific for the IAR-NRC wind tunnel and the final amplification

factor value used it is believed to be caused by the three-dimensional flow effects that XFoil cannot take into account.

The new amplification factor was used for the aerodynamic optimization and analysis for the cases studied during the third set of tests, where the wing was equipped with a morphing aileron. Preliminary analysis of the experimental results for the 49 cases have shown that the morphing aileron deflection was not obtained as desired, with differences between the desired deflection angle and the actual deflection angle being up to 6 degrees, where the maximum allowed deflection was in the range of 6 degrees down and 6 degrees up. These limits were imposed by both the Italian and NRC teams on account of high aerodynamic loads, which could possibly damage the structure of the aileron or the integrity of the wind tunnel measurement equipments.

From an experimental optimization perspective, more than half of the studied cases obtained an extension of the laminar region, with improvements of up to 8% of the chord. Appendix III presents the preliminary results obtained from the analysis of the infrared experimental data.

GENERAL CONCLUSIONS

The work presented in this thesis was focused on researching the aerodynamic improvements of airfoils through morphing of their upper surface. To this end, optimization tools were developed and used with aerodynamic solvers such as XFoil, XFLR 5 and ANSYS/Fluent to obtain new airfoil shapes. These new shapes were optimized versions of the baseline airfoils for different flight cases and were obtained using Genetic Algorthim optimization. The Genetic Algorithm optimization tool was tested against other optimization methods, such as Artificial Bee Colony and Gradient Descent, for their performances comparison. The results have shown that the chosen method, namely Genetic Algorithm, performed as well or better than the other two methods, and it was capable of finding the global optimum for each flight case studied, regardless of the initial optimization parameter values.

In order to verify how much of the numerical performance increase could be achieved in wind tunnel experimental conditions, the optimization tools, above described, were used in the following two morphing wing projects: ATR-42 'Morphing Wing' project and the CRIAQ MDO 505 'Morphing Architectures and Related Technologies for Wing Efficiency Improvement' project. The main objective for both projects was to improve the boundary layer behaviour through extension of the laminar region. This manipulation of the boundary layer behaviour is associated with reduction of the drag force, which in turn is associated with fuel consumption reduction and to the reduction of the green-gas print in atmosphere.

In the ATR-42 'Morphing Wing' project two rigid and one active morphing wind tunnel models were designed, manufactured and tested. The two rigid models were designed and manufactured based on the shape of the original ATR-42 wing airfoil and the optimized shape of the ATR-42 wing airfoil for Mach number of 0.1 and angle of attack of 0°. They were wind tunnel tested with the purpose of validating 1) the composite material design and optimization, 2) the aerodynamic performances of the optimized shape for more flight cases than the one for which it was obtained and 3) the use of the second derivative of the experimental pressure distribution for determining the transition region. The analysis of the

experimental results has shown that all three of the researched aspects were validated and good agreement was found between numerical and experimental pressure and transition data.

In the CRIAQ MDO 505 ‘Morphing Architectures and Related Technologies for Wing Efficiency Improvement’ a wind tunnel wing-tip demonstrator equipped with conventional and morphing aileron was designed, manufactured, bench and wind tunnel tested. This project was realized as an international collaboration between Canadian and Italian industry and academia, represented by Bombardier Aerospace, Thales Canada, Ecole de Technologie Superieure, Ecole Politechnique and the National Research Council on the Canadian side and Alenia Aermacchi, Italian Aerospace Research Center and University of Naples for the Italian side. The CRIAQ MDO 505 project was developed with the aim to evaluate whether morphing of the upper surface of the wing combined with a real wing internal structure and an aileron would provide performance benefits that would overcome any deterrents that a morphing system might have, such as increase in weight or complexity of the internal control system.

Improved genetic algorithm optimization tools, with two new shape optimization methods for the morphing aileron, were used. The aerodynamic optimization was performed in a multidisciplinary process, in connection with the structural optimization of the upper surface carbon composite skin, and with the controller design. Several aerodynamic-structural cycles were needed before a final composite skin design for the wing’s upper surface was agreed upon. Aeroelastic studies were performed for the wing structure equipped with conventional aileron and composite skin, and were compared with the aeroelastic analysis results obtained for the wing structure equipped with conventional aileron and aluminium skin. The results have shown that the composite skin, although more flexible than the aluminium one, had no impact on the frequencies resulted from the analysis of the modal behaviour of the wing. No aeroelastic phenomena, particularly flutter, was found to be a risk for the wing-tip demonstrator at the speeds used during wind tunnel testing.

After manufacturing, the wing-tip demonstrator was bench tested for 1g loads, under both morphing and non-morphing conditions. The bench tests results have shown that a morphing composite surface capable of sustaining flight loads under morphing conditions was obtained through the aerodynamic optimization – structural skin optimization process.

Three wind tunnel tests were performed at the IAR-NRC subsonic wind tunnel in Ottawa for over 150 flight cases. The wing-tip was equipped with 32 high precision kulite pressure sensors, 60 pressure taps and three accelerometers. In addition, infrared thermography photography was used to detect the laminar to turbulent flow transition behaviour and a balance was used for loads measurements.

The first set of tests was done for calibration purposes and for observing the real wing surface deformation through scanning under static conditions. The data obtained from the first set of tests was used for adjusting actuator calibrations, infrared thermography measurement parameters and for calibrating the aerodynamic optimization analyses.

The second and the third sets of tests were dedicated to studying the effects of upper surface morphing using test case matrices. The wind tunnel test case matrices represent tables of the flight cases for which the aerodynamic optimization was done

The second set of tests was focused on the morphing effects for the wing-tip demonstrator equipped with a conventional aileron, and the test case matrice contained over 90 flight cases. The results have confirmed that the numerical aerodynamic optimization was correctly done, but also have shown that the numerical analyses have overestimated the values of the optimization objectives. The results obtained for the optimization of the laminar region have shown that the multi-disciplinary optimization of the wing was a complex process and that some of the assumptions, such as related to the aerodynamic solver, optimization parameters, optimization objective, structural complexity, actuation system, etc., made in the beginning of the project were not sufficient to guarantee its full success. The results and observations

made during the second set of tests were also used for recalibration of the aerodynamic optimization and analyses in view of the third set of tests.

The third set of tests was focused on the testing of the wing-tip demonstrator equipped with a morphing aileron, in collaboration with the Italian team. The numerical optimization of both wing upper surface and morphing aileron were part of the research presented in this thesis. The experimental results of the third set of tests have shown that the optimization of the upper surface in conjunction with the morphing of the aileron has produced optimistic results for the objective of extending the laminar region on the upper surface of the wing, despite the fact that the morphing aileron control did not manage to obtain the desired deflection angles. The main problem of the morphing aileron was that at the wind tunnel speeds at which it was tested, maximum of 75 m/s or Mach number of 0.2, the aileron structure elastically deflected under the influence of the aerodynamic loads. Because of the fact that no sensors were installed to measure the rib blocks' relative rotations, the actuators actions was not tunned to counteract elastic deflections in a precise way.

Based on the observations made during the project, especially during the experimental testing, the results (both positive, such as success of the optimization procedure validated with successful experimental optimization, and negative, such as cases where the numerical optimization was not validated by the experimental data due to various complication in the morphing wing system) cannot offer a firm conclusion on the success or failure of upper surface aerodynamic optimization (delay or advancement of the transition region), regardless of its objective. Based on the experimental results and observations provided by the three wind tunnel sets of tests, it cannot be concluded whether morphing of the upper surface of the wing was an advantage at the studied flow cases.

The optimization results obtained during the ATR-42 and the CRIAQ MDO 505 projects were encouraging at both numerical and experimental levels. It was found that the metaheuristic algorithms were useful for determining the airfoil optimal shapes for different flight conditions, especially when coupled with high speed aerodynamic solvers, such as

XFoil. Also, during the research conducted on these projects, it was observed that high accuracy and high speed during optimization could not be achieved with the methods existing today, thus a compromise needed to be made for each particular case.

Other observations made during the research were related to: the influence of the numerical airfoil shape on the optimization, especially when coupled with the morphing concept used, influence of the morphing concept itself and its relationship with the influence other disciplines involved in the project, such as structural optimization. The research conducted in this thesis has shown, however, that *morphing* represents a possible viable solution for aerodynamic and aeroelastic optimization of the performances of an aircraft wing, and that further research was needed to develop the concept of morphing wings. All the results and observations made during this research represent a stepping stone for the future of morphing aircrafts.

RECOMMENDATIONS

Several recommendations can be made regarding the research presented in this thesis based on observations made during the two morphing wing projects in which this research was part:

1. Aerodynamic solver recommendations

Based on the observations made during wind tunnel tests, there is a high probability that the XFOIL code was not the best choice for the CRIAQ MDO 505 project.

The advantages of using XFOIL are numerous, as it was observed during the ATR-42 'Morphing Wing' project: fast, easy to use, reliable results for 2D analysis at low speeds and Reynolds numbers, easily coupled with 'in-house' developed software, needs few input data. But for the CRIAQ MDO 505 project its disadvantages are more important and bear a greater impact on the results: not robust enough when confronted with a high amount of analyses in a cycle of optimization, showed some sensitivity to small variations in Reynolds number, speed or angles of attack, insuffient for predicting 3D flow behaviour, the 2D transition results obtained with XFOIL cannot be easily extrapolated to match the experimental infrared transition results.

Therefore, the recommendation would be to either find an effiecient method of using the 2D aerodynamic results to extrapolate the data to obtain better estimates, or to use a high precision CFD solver, such as FLUENT, CFX or OpenFoam.

If due to various reasons, the XFOIL solver is deemed as more useful for analysing a section of a 3D wing, then some experimental testing and analysis are recomended in order to evaluate how far from the experimental results the numerical estimations will be.

For example, an experimental test could be done for a scaled version of the real wing (only the shape without internal structure) at small speeds, record data related to pressure, loads

and transition region and compare with XFOIL results at different span sections. This analysis should give an idea on the order of difference between the numerical prediction and actual real results and verify if the variation between numeric and experimental is influenced by the speed or other controllable factors, such as recording sample for example.

2. Aerodynamic analyses recomendations

After analysing the balance and Infrared experimental results and the information provided by the first and second set of tests, the conclusion was that there was an additional analysis that could have helped in better understanding the obtained results, and even in improving them. Therefore I would recommend the CFD analysis of wing mounted in wind tunnel. It is an analysis that takes time, thus it should be started as early as possible in the project, but it could yield information related to the behaviour of the wing and of the flow in the wind tunnel conditions. The results can be compared to CFD analyses of the wing in free flow to observe the differences between the two manners of analysing the wing model.

3. Optimization methodology recomendations

During both projects, three optimization methods were explored: the Genetic Algorithm, Artificial Bee Colony and Gradient Descent. As shown in Chapters 2 and 6, many other optimization methods are available, and some of them hold promise for high performances in the morphing wing objectives.Therefore, more optimization methods should be explored, and function of the desired objectives, the morphing concept and the type of wing analysed, one or more optimization methods should be chosen.

The main objective of the airfoil optimization for the ATR 42 and CRIAQ MDO 505 projects was the delay of the transition region towards the trailing edge. No exact amount for the optimization objective was given, but instead a general approach was preferred. This approach, in which the optimization objective had no particular specification, for example push the transition region with 10% of the chord towards the trailing edge, has lead to

frustrations with the obtained results as it seemed that the percentage of optimization was considered insufficient for this particular application. My recomandation would be that the research should concentrate in exhausting all the possibilities for obtaining a particular value a small number or flight cases, especially in the begining, and not be too broad in its approach trying to find the best optimization values for all cases.

At the beginning of the CRIAQ MDO 505 project, too much focus was given to maintaining the connection between the optimization constraints, the manufacturing and structural reality of the wing. For example, too much attention was given to the actual number of actuators in relation to the optimization results. My recomandation would be to let the optimization be free of most of the constraints (exception those that were of fixed structural nature, such as the positions of the spars or the elasticity of the skin) and let the optimizer find the best combination of shape and morphing nodes on its own. When the best shapes would be achieved for a small number of cases, then an actuation mechanism would be researched to try and recreate through active control the desired shapes.

4. Wind tunnel testing recomendation

Another recomandation is related to the number of flight cases studied during an optimization procedure. During the CRIAQ MDO 505 project no less than 1265 flight cases were studied. Due to high number of cases and results, the wind tunnel test matrices were determined only a few months before the first set of wind tunnel tests. Threfore, a preliminary wind tunnel test matrix, an information which is useful also for establishing procedures during wind tunnel testing; should be determined very early in the project to limit the amount of unnecessary analysis and optimization. A first limited range of speeds, angles of attack and aileron deflections should be chosen, and if the optimization results are not satisfactory for this initial set of cases, then it can be expanded, otherwise the amount of data obtained is extremely high, imposing difficulties in the choice of the best wind tunnel fligh cases. A high quantity of flight cases also limits the amount of time of research spent per case which limits the chances of success in finding the optimal shape for each case.

APPENDIX I

ATR-42 WING AIRFOIL NUMERICAL AERODYNAMIC OPTIMIZATION

The code used for the aerodynamic optimisation of the ATR-42 airfoil was based on a genetic algorithm. Genetic algorithms are numerical optimisation algorithms inspired by natural selection and natural genetics of living organisms. The algorithm was initialised with a population of guessed individuals, and used three operators: selection, crossover and mutation, to direct the population towards convergence to the global optimum, over a series of generations.

In the optimisation problem of the ATR-42 wing airfoil, each individual in the population was defined by two real values: the actuators displacements δ_1 and δ_2. These displacements can have any values between 0 (which correspond to the original, un-morphed airfoil), and $\delta_{\max}$ (which depends on the characteristics and limitations of the actuators, and their interaction with the flexible skin). By considering the relatively small chord of the airfoil (a chord of 25 cm was considered the maximum chord to be used for an airfoil model in the Price-Païdoussis subsonic wind tunnel), and the thickness of the airfoil, as well as the maximum displacements of different actuators available on the market (actuators that are small enough to fit inside the wind tunnel airfoil model), the value chosen for $\delta_{\max}$ was 10 mm.

In order to evaluate all the individuals in the population, an objective function or a fitness function, was defined. Because the goal of the optimisation was to move the transition point on the upper surface towards the trailing edge of the airfoil, thus to delay the flow transition and to reduce the drag coefficient, the following fitness function was defined in the code:

$$F = \frac{1}{Cd} + 100 x_{TR}^{TOP} \qquad \text{(A I-1)}$$

The factor of 100 that multiplies the value of the transition point x_{TR}^{TOP} was introduced, so that both terms in the fitness function have the same order of magnitude.

A demonstration of the functionality of the aerodynamic optimisation code is given below by comparing the results for the original ATR 42 airfoil and a morphed airfoil obtained using the code, for a selected test case.

Table A I – 1 Wing model optimization parameters

Parameter	Value
Airfoil chord	0.244 m
Mach number	0.2
Reynolds number	1142747
Starting point of the flexible skin	0.1
Ending point of the flexible skin	0.7
Position of the first actuator	0.3
Position of the second actuator	0.5
Angle of attack	2 degrees

The optimal solution obtained by the genetic algorithm code had the following actuator displacements: $\delta_1 = 2.972$ mm, $\delta_2 = 4.049$ mm. The morphed airfoil had considerably better aerodynamic characteristics than the original airfoil, as presented in Table 2.

Table A I – 2 Wing model numerical optimization results

Parameter	Original airfoil	Morphed airfoil	Relative error (%)
CL	0.4177	0.4825	+15.51
CD	0.00755	0.00608	-19.48
Upper surface transition point	27.31	52.71	+93
Inner surface transition point	90.91	90.39	-0.58

For the same angle of attack, the morphed airfoil had an increased lift coefficient; the drag coefficient had reduced by 19.48%, but the most significant gain was found in the transition point location, which moved towards the trailing edge of the airfoil by 25.4 % of the chord.

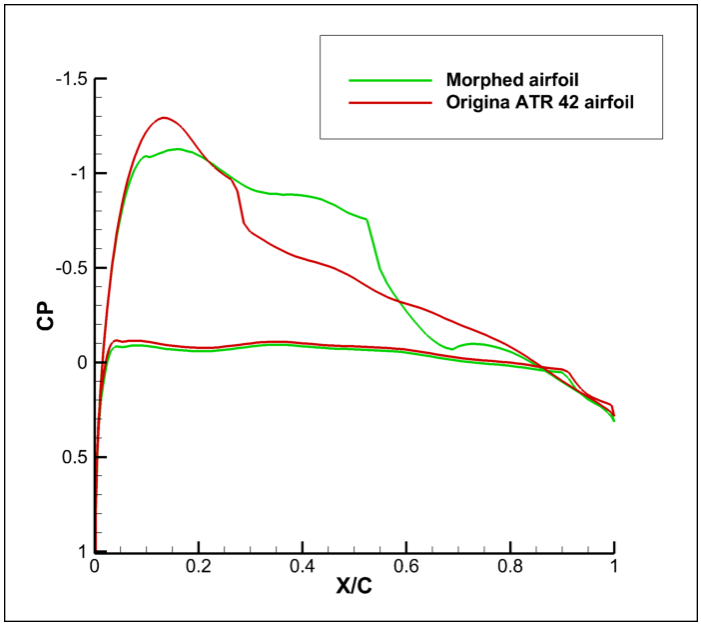

Figure A I-1 Comparison between the pressure coefficients of the original airfoil and morphed airfoil

Another result of the aerodynamic optimization is presented below. Figures A I-2, A I-3 and A I-4 present the results obtained for the original airfoil and for the optimized morphed airfoil, placed at the angle of attack of -2°. These results were expressed in terms of variation of the lift coefficient with the Mach number (Figure A I-2), variation of the drag coefficient with the Mach number (Figure A I-3) and variation of the Mach number with the transition point location (Figure A I-4).

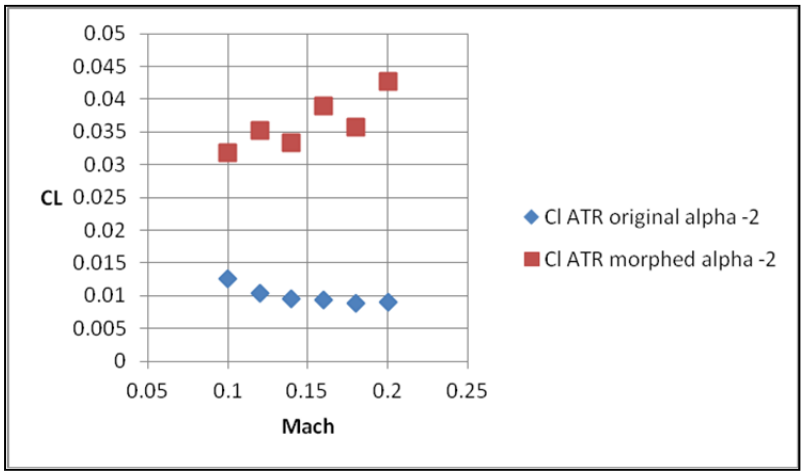

Figure A I-2 Lift coefficient versus Mach number
for -2° angle of attack

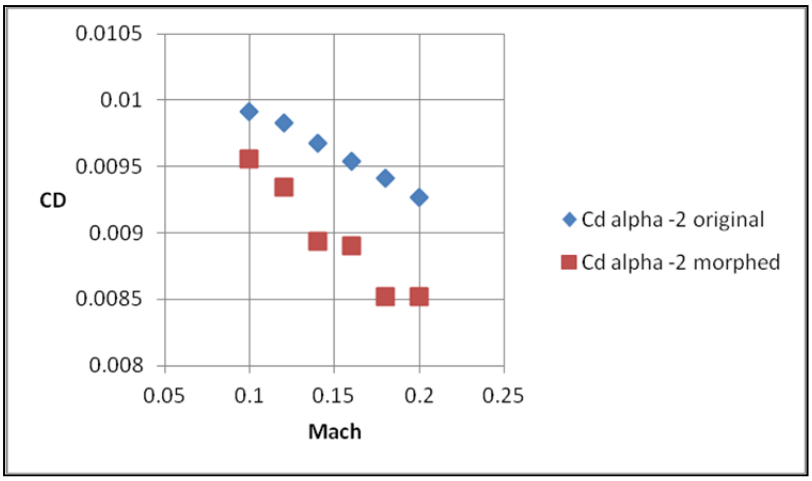

Figure A I-3 Drag coefficient versus Mach number
for -2° angle of attack

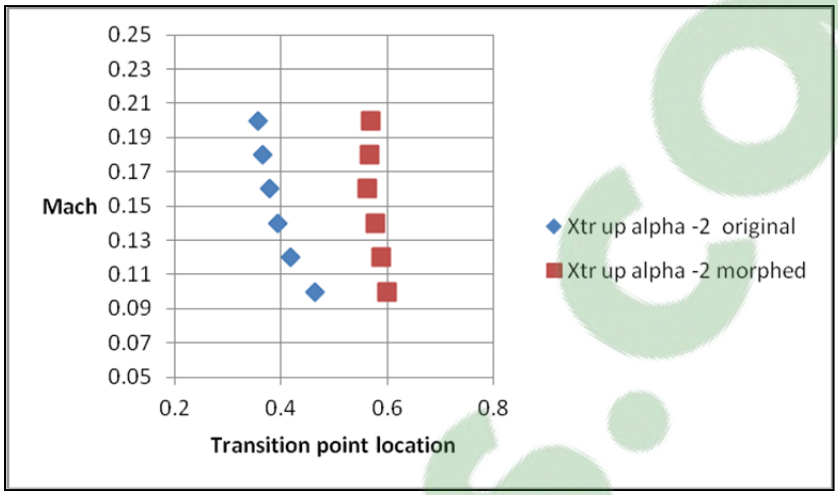

Figure A I-4 Mach number versus Transition position (%c) for -2° angle of attack

APPENDIX II

EXPERIMENTAL OPTIMIZATION ANALYSIS BASED IN THE INFRARED THERMOGRAPHY DATA COLLECTED FROM THE THIRD SET OF TESTS

The 3rd set of tests were done at the subsonic wind tunnel at NRC facilities in Ottawa. The objective was the experimental testing of an upper surface morphing wing equipped with a morphing aileron.

During the third set of wind tunnel tests, 49 cases were tested in the wind tunnel and the infrared experimental transition corresponding to them was recorded. No comparison was done between numerical simulation and experimental results for transition delay and loads, as further numerical and experimental data was needed for a good analysis.

For 32 of the cases, the objective of delaying the passage from laminar to turbulent regions was accomplished. The 32 cases are presented in Table A II-1:

Table A II – 1 The 32 wind tunnel cases for which the objective of transition delay towards the trailing edge was accomplished

Case No	Mach number	Wing geometrical Angle of Attack (°)	Adaptable Aileron Deflection (°)
1	0.15	-3	-2
8	0.15	0.5	-2
9	0.15	1	-2
10	0.15	1.5	-2
11	0.15	-0.5	0
12	0.15	-0.25	0
13	0.15	0	0
14	0.15	0.25	0
15	0.15	0.5	0
16	0.15	0.75	0
17	0.15	1	0
18	0.15	1.25	0
19	0.15	1.5	0

Case No	Mach number	Wing geometrical Angle of Attack (°)	Adaptable Aileron Deflection (°)
20	0.15	2	0
22	0.15	3	0
23	0.2	0	4
24	0.2	0.5	4
25	0.2	1	4
26	0.2	1.5	4
27	0.2	2	4
29	0.20	-1.4	3
30	0.20	-0.9	3
31	0.20	-0.5	3
32	0.20	0.6	2.5
36	0.20	0.00	4
37	0.20	0.50	4
38	0.20	1.00	4
39	0.20	1.50	4
40	0.20	2.00	4
41	0.15	0	6
44	0.15	0	3
45	0.15	0	2

Table A II-2 presents the values of parameters λ, τ, which were defined in Chapter 7 and the chapter dedicated to the Discussion of the Results, and difference between the average values of the un-morphed and morphed transition region for all 32 cases.

There are 6 cases for which the extension of the laminar region is less than 1% of the chord. For 2 of these 6 cases the contraction of the turbulent region is also less than 1% of the chord. Under these circumstances, in these 2 cases, it was considered that no actual modification took place, in essence the transition performances were the same between the un-morphed and morphed wing. However, for these 2 flight cases, this aspect does not imply that other aerodynamic parameters of the wing (lift, drag and moment) have remained unchanged. For the other four cases, the turbulent region has a contracted length in the range of 2 to 4% of the chord. One case has a small negative contraction of the turbulent region (τ) but is counterbalanced by almost 2% of the chord of laminar region extension.

The other 15 cases have an extension of the laminar region (λ) between 1.3 and 7% of the chord, with the average being 3% of the chord. The contraction of the turbulent region (τ) is situated between 0.3 and 6.5% of the chord, with the average being also 3% of the chord.

Table A II – 2 Wing model numerical optimization results

Case No	Extension of the Laminar region λ (%c)	Transition Region average (%c)	Contraction of the turbulent region τ (%c)
1	1.38	2.88	4.38
8	2.84	3.84	4.84
9	2.28	2.28	2.28
10	4.84	3.84	2.84
11	0.92	1.92	2.92
12	1.47	1.97	2.47
13	1.98	2.68	3.38
14	0.30	1.30	2.30
15	3.09	2.09	1.09
16	5.15	4.15	3.15
17	0.51	0.51	0.51
18	2.06	2.06	2.06
19	2.90	2.90	2.90
20	3.00	3.00	3.00
22	0.65	0.65	0.65
23	2.54	2.54	2.54
24	3.74	3.74	3.74
25	6.43	6.43	6.43
26	1.52	4.02	6.52
27	1.29	1.29	1.29
29	1.80	0.80	-0.20
30	3.87	2.87	1.87
31	1.71	1.71	1.71
32	2.54	3.54	4.54
36	1.66	2.66	3.66
37	0.64	2.64	4.64
38	3.79	3.29	2.79
39	6.80	5.80	4.80
40	5.04	4.54	4.04
41	3.40	3.90	4.40

Case No	Extension of the Laminar region λ (%c)	Transition Region average (%c)	Contraction of the turbulent region τ (%c)
44	1.30	0.80	0.30
45	0.91	1.41	1.91

Figures A II-2 to A II-5 present, in contrast, the transition region for the un-morphed and morphed wing for all 32 cases discussed above. In these figures it can be clearly observed the modification of the transition region between un-morphed and morphed states.

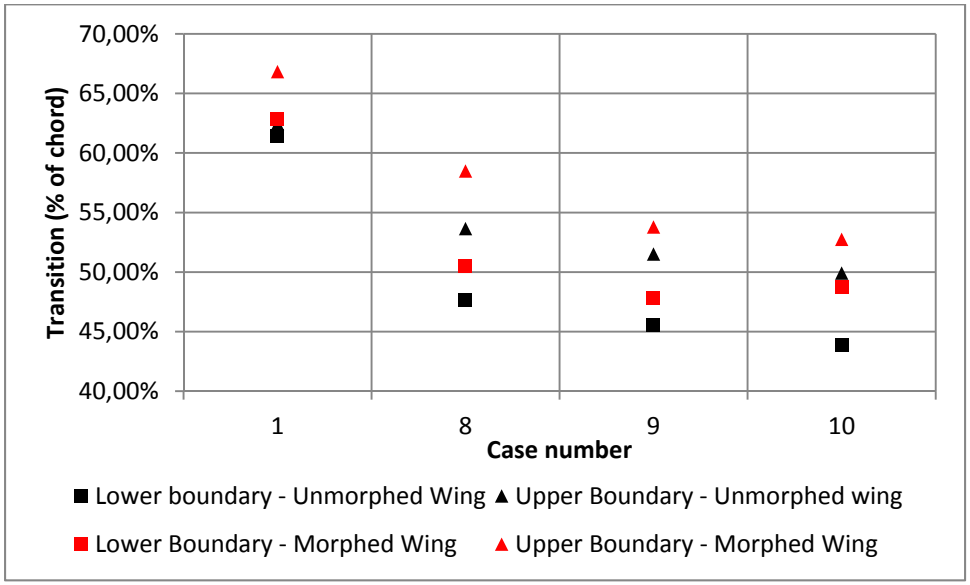

Figure A II-2 Morphed versus Un-morphed state – transition region comparison – cases of the wing with aileron deflected 2° up

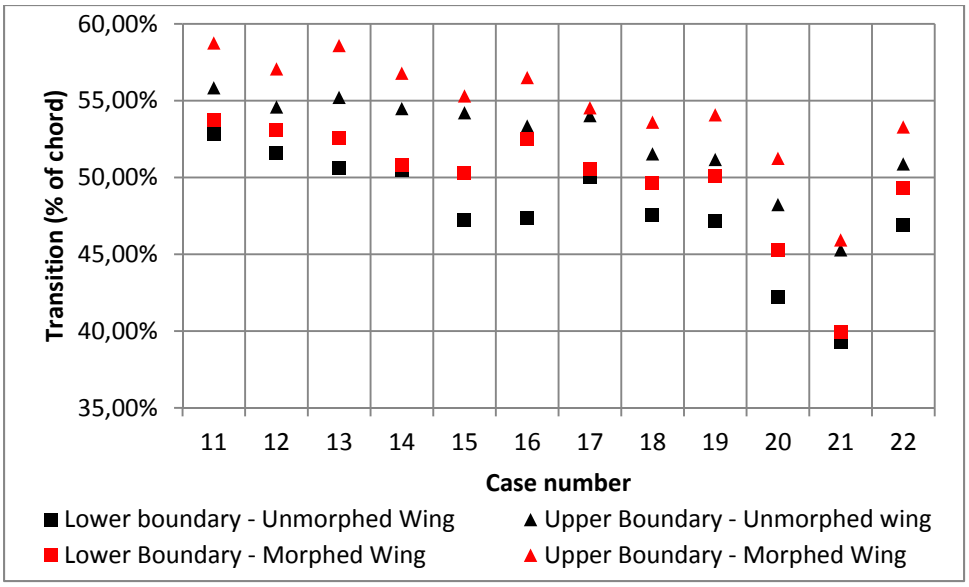

Figure A II-3 Morphed versus Un-morphed state –
transition region comparison – cases of the wing with aileron deflected 0°

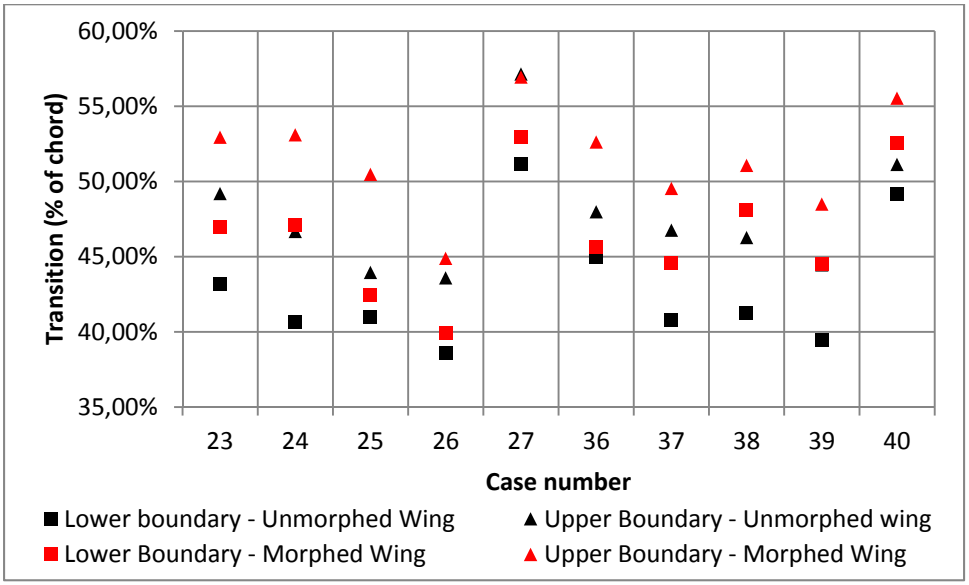

Figure A II-4 Morphed versus Un-morphed state –
transition region comparison – cases of the wing with
aileron deflected 4° down

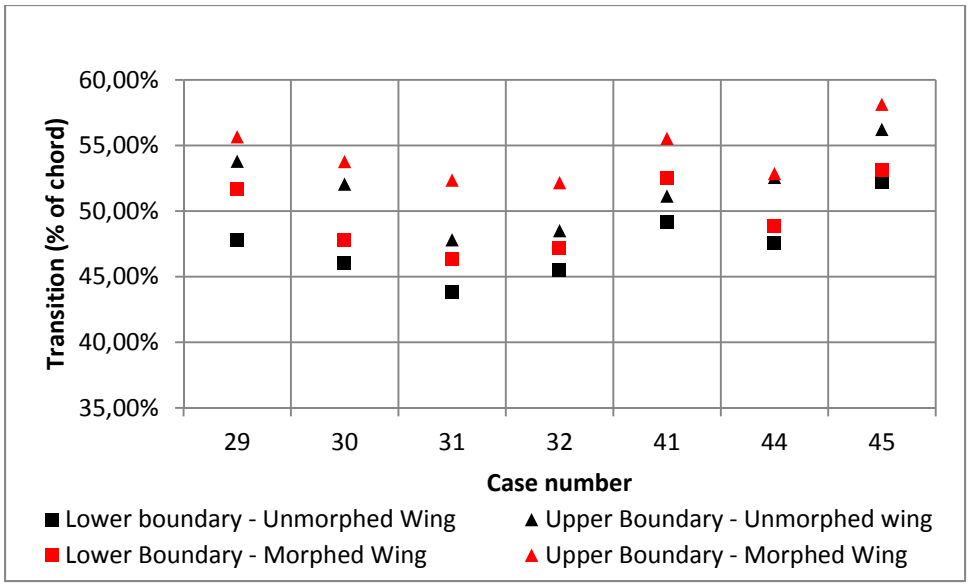

Figure A II-5 Morphed versus Un-morphed state – transition region comparison – cases of the wing with various aileron deflections down

Based on the results presentd above, it can be said that most of the cases were successful, as almost half of them gave a positive modification of the laminar and turbulent flow boundary of more than 3% of the chord, with the maximum being 7% of the chord.

APPENDIX III

MORPHING AILERON DEFLECTIONS OBTAINED DURING THE THIRD SET OF WIND TUNNEL TESTS

During the third set of tests, the morphing wing – tip demonstrator was equipped with a morphing aileron system. The morphing aileron had a finger-like architecture with three articulated sections. The first section was the leading edge, and it was immovable. The second section was connected to the first, and it was deployed using two electric actuators. While the third section of the aileron, or the trailing edge, was connected to the previous section through a cinematic mechanism. The second and the third sections were deployed together with different deflection angles for each section.

During the wind tunnel tests, it was observed that the aileron deflection angles obtained with the Italian team control system, did not match the desired aileron deflection angles. The desired deflection angles were deduced from the aerodynamic optimization and were also used during the second set of tests when the rigid aileron was tested. Table A III – 1 presents the correspondence between the desired aileron deflection angles and the obtained angles, or true angles, for each speed used in the third set of tests.

Because of these differences in the aileron deflection angles, the numerical validation of the optimization resultswith the wind tunnel experimental results was very difficult to be done. The analysis of the results, from pressure coefficient variation with with the chord, is on its way.

Table A III – 1 Conversion table between desired morphing aileron deflection angles and real morphing aileron deflection angles obtained during wind tunnel tests

Speed m/s	**Conversion table**	
	Desired aileron deflection (°)	**True angle (°)**
50	-2	-4.01
	-1	-2.45
	0	-1.13
	1	-0.06
	2	0.77
	3	1.35
	4	1.68
	5	1.76
	6	1.6
70	-2	-5.66
	-1	-4.03
	0	-2.67
	1	-1.59
	2	-0.78
	3	-0.24
	4	0.03
	5	0.3
	6	0.56

LIST OF REFERENCES

Abbott, Ira Herbert, and Albert Edward Von Doenhoff. 1959. *Theory of wing sections, including a summary of airfoil data*. Courier Corporation.

Aerolab. 2015. « Aerolab software information ». < http://www.aerolab.com/products/data-acquisition-systems/ >. Consulté le January 2015.

Analog. 2015. « Analog Devices ». < http://www.analog.com/en/products/mems/mems-accelerometers/adxl326.html#product-overview >. Consulté le October 2015.

Anderson, Kevin, and Alice Bows. 2008. « Reframing the climate change challenge in light of post-2000 emission trends ». *Philosophical Transactions of the Royal Society of London A: Mathematical, Physical and Engineering Sciences,* vol. 366, n° 1882, p. 3863-3882.

ATAG. 2015. « Influence of Aerospace on the CO2 ». < http://www.atag.org/facts-and-figures.html >. Consulté le February 2016.

Austin, Fred, Michael J Rossi, William Van Nostrand, Gareth Knowles and Antony Jameson. 1994. « Static shape control for adaptive wings ». *AIAA journal,* vol. 32, n° 9, p. 1895-1901.

Bacanin, Nebojsa. 2012. « Implementation and performance of an object-oriented software system for cuckoo search algorithm ». *International Journal of Mathematics and Computers in Simulation,* vol. 6, n° 1, p. 185-193.

Baciu, Ovidiu. 2012. *Projet d'application : Modélisation et tests d'une aile morphable dans la soufflerie de LARCASE* Coll. « Maitrise avec projet »: Ecole de Technologie Superieure. Consulté le December 2015.

Barbarino, Silvestro, Onur Bilgen, Rafic M Ajaj, Michael I Friswell and Daniel J Inman. 2011. « A review of morphing aircraft ». *Journal of Intelligent Material Systems and Structures,* vol. 22, n° 9, p. 823-877.

Bastedo, William G, and TJ Mueller. 1986. « Spanwise variation of laminar separation bubbles on wings at low Reynolds number ». *Journal of aircraft,* vol. 23, n° 9, p. 687-694.

Baxevanou, CA, PK Chaviaropoulos, SG Voutsinas and NS Vlachos. 2008. « Evaluation study of a Navier–Stokes CFD aeroelastic model of wind turbine airfoils in classical flutter ». *Journal of wind engineering and industrial aerodynamics,* vol. 96, n° 8, p. 1425-1443.

Berbente, Corneliu, Sorin Mitran and Silviu Zancu. 1997. *Metode numerice*. Editura Tehnica.

Bharti, Smita, Mary Frecker, George Lesieutre and Jamie Browne. 2007. « Tendon actuated cellular mechanisms for morphing aircraft wing ». In *The 14th International Symposium on: Smart Structures and Materials & Nondestructive Evaluation and Health Monitoring*. p. 652307-652307-13. International Society for Optics and Photonics.

Blevins, Robert D, and R Plunkett. 1980. « Formulas for natural frequency and mode shape ». *Journal of Applied Mechanics,* vol. 47, p. 461.

Blondeau, Julie, Justin Richeson and Darryll J Pines. 2003. « Design, development and testing of a morphing aspect ratio wing using an inflatable telescopic spar ». *AIAA paper,* vol. 1718, p. 7-10.

Bonnema, Kenneth L, and Stephen B Smith. 1988. « AFTI/F-111 mission adaptive wing flight research program ». In *AIAA Flight Test Conference, 4 th, San Diego, CA*. p. 155-161.

Botez, Ruxandra Mihaela, Philippe Molaret and Eric Laurendeau. 2007. « Laminar flow control on a research wing project presentation covering a three year period ». In *Canadian Aeronautics and Space Institute Annual General Meeting*.

Brailovski, Vladimir, Patrick Terriault, Daniel Coutu, Thomas Georges, Emeric Morellon, Charles Fischer and Sébastien Bérubé. 2008. « Morphing laminar wing with flexible extrados powered by shape memory alloy actuators ». In *ASME 2008 Conference on Smart Materials, Adaptive Structures and Intelligent Systems*. p. 615-623. American Society of Mechanical Engineers.

Buckley, Howard P, Beckett Y Zhou and David W Zingg. 2010. « Airfoil optimization using practical aerodynamic design requirements ». *Journal of Aircraft,* vol. 47, n° 5, p. 1707-1719.

Cadogan, David, Tim Smith, Frank Uhelsky and Matt MacKusick. 2004. « Morphing inflatable wing development for compact package unmanned aerial vehicles ». *AIAA Paper,* vol. 1807, p. 2004.

Veuillez sélectionner un type de document autre que « Generic » afin de faire afficher la référence bibliographique.

Campanile, LF, and D Sachau. 2000. « The belt-rib concept: a structronic approach to variable camber ». *Journal of Intelligent Material Systems and Structures,* vol. 11, n° 3, p. 215-224.

Chen, Tanggong, Youhua Wang and Jianwei Li. 2012. « Artificial tribe algorithm and its performance analysis ». *Journal of Software,* vol. 7, n° 3, p. 651-656.

Coley, David A. 1999. *An introduction to genetic algorithms for scientists and engineers*. World scientific.

Courchesne, Samuel, Andrei Vladimir Popov and Ruxandra Mihaela Botez. 2010. « New aeroelastic studies for a morphing wing ». In *Proceedings of the 48th AIAA Aerospace Sciences Meeting Including the New Horizons Forum and Aerospace Exposition, American Institute of Aeronautics and Astronautics (AIAA), Washington, DC*.

Courchesne, Samuel, Andrei Vladimir Popov and Ruxandra Mihaela Botez. 2012. « New Aeroelastic Studies for a Morphing Wing ». *INCAS BULLETIN,* vol. 4, n° 2, p. 19-28.

Coutu, D, V Brailovski, P Terriault and C Fischer. 2007. « Experimental validation of the 3D numerical model for an adaptive laminar wing with flexible extrados ». In *Proceedings of the 18th International Conference of Adaptive Structures and Technologies (ICAST'2007)*. Citeseer.

Coutu, Daniel, Vladimir Brailovski and Patrick Terriault. 2009. « Promising benefits of an active-extrados morphing laminar wing ». *Journal of Aircraft,* vol. 46, n° 2, p. 730-731.

Coutu, Daniel, Vladimir Brailovski and Patrick Terriault. 2010. « Optimized design of an active extrados structure for an experimental morphing laminar wing ». *Aerospace Science and Technology,* vol. 14, n° 7, p. 451-458.

Cui, Shi-Yu, Zhi-Hui Wang, Pei-Wei Tsai, Chin-Chen Chang and Shuai Yue. 2013. « Single bitmap block truncation coding of color images using cat swarm optimization ». In *Recent Advances in Information Hiding and Applications*. p. 119-138. Springer.

Deb, Kalyanmoy, and Ram B Agrawal. 1994. « Simulated binary crossover for continuous search space ». *Complex Systems,* vol. 9, n° 3, p. 1-15.

Deperrois, A. . 2015. « XFLR 5 v6.11 application and documentation ».

Diaconu, Cezar G, Paul M Weaver and Filippo Mattioni. 2008. « Concepts for morphing airfoil sections using bi-stable laminated composite structures ». *Thin-Walled Structures,* vol. 46, n° 6, p. 689-701.

Diodati, Gianluca, Sergio Ricci, Alessandro De Gaspari, Fabien Huvelin, Antoine Dumont and Jean-Luc Godard. 2013. « Estimated performance of an adaptive trailing-edge device aimed at reducing fuel consumption on a medium-size aircraft ». In *SPIE*

Smart Structures and Materials+ Nondestructive Evaluation and Health Monitoring. p. 86900E-86900E-16. International Society for Optics and Photonics.

Dong, Yu, Zhang Boming and Liang Jun. 2008. « A changeable aerofoil actuated by shape memory alloy springs ». *Materials Science and Engineering: A,* vol. 485, n° 1, p. 243-250.

Drela, Mark. 1989a. « Integral boundary layer formulation for blunt trailing edges ». *AIAA paper,* vol. 89, p. 2200.

Drela, Mark. 1989b. « XFOIL: An analysis and design system for low Reynolds number airfoils ». In *Low Reynolds number aerodynamics*. p. 1-12. Springer.

Drela, Mark. 2003. « Implicit Implementation of the Full en Transition Criterion ».

Veuillez sélectionner un type de document autre que « Generic » afin de faire afficher la référence bibliographique.

Engelbrecht, Andries P. 2007. *Computational intelligence: an introduction*. John Wiley & Sons.

Engineer, The. 2009. « Sustainable Flight ». < https://www.theengineer.co.uk/issues/january-2009-online/sustainable-flight/ >. Consulté le February 2016.

Eppler, Richard (163-510). 1990. *Airfoil design and data*. Springer Science & Business Media.

Falcão, Luís, Alexandra Gomes and Afzal Suleman. 2011. « Aero-structural design optimization of a morphing wingtip ». *Journal of Intelligent Material Systems and Structures,* vol. 22, n° 10, p. 1113-1124.

Falcao, Luıs, Alexandra Gomes and Afzal Suleman. 2011. « Design and Analysis of an Adaptive Wingtip ». In *52nd AIAA/ASME/ASCE/AHS/ASC Structures, Structural Dynamics and Materials Conference 19th AIAA/ASME/AHS Adaptive Structures Conference 13t*. p. 2131.

Fincham, JHS, and MI Friswell. 2015. « Aerodynamic optimisation of a camber morphing aerofoil ». *Aerospace Science and Technology,* vol. 43, p. 245-255.

Gamboa, P, J Vale, FJ P. Lau and A Suleman. 2009. « Optimization of a morphing wing based on coupled aerodynamic and structural constraints ». *AIAA journal,* vol. 47, n° 9, p. 2087-2104.

Good, Matthew G. 2004. « Development of a Variable Camber Compliant Aircraft Tail using Structural Optimization ». Virginia Polytechnic Institute and State University.

Granville, Paul S. 1953. *The calculation of the viscous drag of bodies of revolution*. DTIC Document.

Grigorie, Teodor Lucian, and Ruxandra Mihaela Botez. 2009. « Adaptive neuro-fuzzy inference system-based controllers for smart material actuator modelling ». *Proceedings of the Institution of Mechanical Engineers, Part G: Journal of Aerospace Engineering,* vol. 223, n° 6, p. 655-668.

Grigorie, Teodor Lucian, and Ruxandra Mihaela Botez. 2010. « New adaptive controller method for SMA hysteresis modelling of a morphing wing ». *Aeronautical Journal,* vol. 114, n° 1151, p. 1.

Grigorie, Teodor Lucian, Ruxandra Mihaela Botez and Andrei Vladimir Popov. 2009. « Adaptive neuro-fuzzy controllers for an open-loop morphing wing system ». *Proceedings of the Institution of Mechanical Engineers, Part G: Journal of Aerospace Engineering,* vol. 223, n° 7, p. 965-975.

Grigorie, Teodor Lucian, Ruxandra Mihaela Botez and Andrei Vladimir Popov. 2012. « Design and experimental validation of a control system for a morphing wing" ». In *AIAA Atmospheric flight mechanics conference*.

Grigorie, Teodor Lucian, Ruxandra Mihaela Botez, Andrei Vladimir Popov, Mahmoud Mamou and Youssef Mébarki. 2011a. « A new morphing mechanism for a wing using smart actuators controlled by a self-tuning fuzzy logic controller ». In. AIAA Centennial of Naval Aviation Forum.

Grigorie, Teodor Lucian, Ruxandra Mihaela Botez, Andrei Vladimir Popov, Mahmoud Mamou and Youssef Mébarki. 2012a. « A hybrid fuzzy logic proportional-integral-derivative and conventional on-off controller for morphing wing actuation using shape memory alloy-Part 1: Morphing system mechanisms and controller architecture design ». *Aeronautical Journal,* vol. 116, n° 1179, p. 433.

Grigorie, Teodor Lucian, Ruxandra Mihaela Botez, Andrei Vladimir Popov, Mahmoud Mamou and Youssef Mébarki. 2012b. « A hybrid fuzzy logic proportional-integral-derivative and conventional on-off controller for morphing wing actuation using shape memory alloy, Part 2: Controller implementation and validation ». *The Aeronautical Journal,* vol. 116, n° 1179, p. 451-465.

Grigorie, Teodor Lucian, Andrei Vladimir Popov, Ruxandra Mihaela Botez, Mahmoud Mamou and Youssef Mébarki. 2010a. « A Morphing Wing used Shape Memory Alloy Actuators New Control Technique with Bi-positional and PI Laws Optimum Combination-Part 1: Design Phase ». In *ICINCO (1)*. p. 13-19.

Grigorie, Teodor Lucian, Andrei Vladimir Popov, Ruxandra Mihaela Botez, Mahmoud Mamou and Youssef Mébarki. 2010b. « A Morphing Wing used Shape Memory Alloy Actuators New Control Technique with Bi-positional and PI Laws Optimum Combination-Part 2: Experimental Validation ». In *ICINCO (1)*. p. 13-19.

Grigorie, Teodor Lucian, Andrei Vladimir Popov, Ruxandra Mihaela Botez, Mahmoud Mamou and Youssef Mébarki. 2011b. « On–off and proportional–integral controller for a morphing wing. Part 1: Actuation mechanism and control design ». *Proceedings of the Institution of Mechanical Engineers, Part G: Journal of Aerospace Engineering*, p. 0954410011408226.

Grigorie, Teodor Lucian, Andrei Vladimir Popov, Ruxandra Mihaela Botez, Mahmoud Mamou and Youssef Mébarki. 2012c. « On–off and proportional–integral controller for a morphing wing. Part 2: Control validation–numerical simulations and experimental tests ». *Proceedings of the Institution of Mechanical Engineers, Part G: Journal of Aerospace Engineering,* vol. 226, n° 2, p. 146-162.

Herrera, Francisco, Manuel Lozano and Jose L. Verdegay. 1998. « Tackling real-coded genetic algorithms: Operators and tools for behavioural analysis ». *Artificial intelligence review,* vol. 12, n° 4, p. 265-319.

Huo, Shi-hui, Zhe Yuan, Fu-sheng Wang and Zhu-feng Yue. 2013. « Effects of static aeroelasticity on composite wing characteristics under different flight attitudes ». *Journal of Central South University,* vol. 20, p. 312-317.

HyperWorks. 2016. « User Manual and Help ». < http://www.altairhyperworks.com/hwhelp/Altair/hw12.0/help/hm/hmbat.aspx?hypermesh.htm >. Consulté le January 2016.

Icardi, Ugo, and Laura Ferrero. 2009. « Preliminary study of an adaptive wing with shape memory alloy torsion actuators ». *Materials & Design,* vol. 30, n° 10, p. 4200-4210.

Impulse, Project Solar. 2010. « HB-SIA Mission ». < http://www.solarimpulse.com/ >. Consulté le February 2016.

Irizarry, Roberto. 2005. « A generalized framework for solving dynamic optimization problems using the artificial chemical process paradigm: Applications to particulate processes and discrete dynamic systems ». *Chemical engineering science,* vol. 60, n° 21, p. 5663-5681.

Janardhan, Srinivasan, and Ramana V Grandhi. 2004. « Multidisciplinary optimization of an aircraft wing/tip store configuration in the transonic regime ». *Engineering Optimization,* vol. 36, n° 4, p. 473-490.

Jha, Ratneshwar, and Aditi Chattopadhyay. 1999. « Multidisciplinary optimization of composite wings using refined structural and aeroelastic analysis methodologies ». *Engineering Optimization,* vol. 32, n^{o} 1, p. 59-78.

Joo, James J, Brian Sanders, Terrence Johnson and Mary I Frecker. 2006. « Optimal actuator location within a morphing wing scissor mechanism configuration ». In *Smart Structures and Materials*. p. 616603-616603-12. International Society for Optics and Photonics.

Kammegne, Michel Joël Tchatchueng, Lucian Teodor Grigorie, Ruxandra Mihaela Botez and Andreea Koreanschi. 2014. « Design and Validation of a Position Controller in the Price-Paidoussis Wind Tunnel ». In *IASTED Modeling, Simulation and Control Conference, Innsbruck, Austria*. p. 17-19.

Karaboga, Dervis, and Bahriye Basturk. 2007a. « Artificial bee colony (ABC) optimization algorithm for solving constrained optimization problems ». In *Foundations of Fuzzy Logic and Soft Computing*. p. 789-798. Springer.

Karaboga, Dervis, and Bahriye Basturk. 2007b. « A powerful and efficient algorithm for numerical function optimization: artificial bee colony (ABC) algorithm ». *Journal of global optimization,* vol. 39, n^{o} 3, p. 459-471.

Katz, Joseph, and Allen Plotkin. 1991. *Low-speed aerodynamics: from wing theory to panel methods*. McGraw-Hill, Incorporated.

Khrabrov, Alexander, and Michael V Ol. 2004. « Effects of flow separation on aerodynamic loads in linearized thin airfoil theory ». *Journal of aircraft,* vol. 41, n^{o} 4, p. 944-948.

Khurana, M. 2008. « Application of an hybrid optimization approach in the design of long endurance airfoils ». In *26th Congess of the International Council of the Aeronautical Sciences*. p. 1-13. American Institute of Aeronautics and Astronautics.

Koreanschi, Andreea, Oliviu Sugar-Gabor and Ruxandra Mihaela Botez. 2016a. « Drag optimisation of a wing equipped with a morphing upper surface ». *The Aeronautical Journal,* vol. 120, n^{o} 1225, p. 473-493.

Koreanschi, Andreea, Oliviu Sugar-Gabor and Ruxandra Mihaela Botez. 2016b. « Numerical and Experimental Validation of a Morphed Wing Geometry Using Price-Païdoussis Wind Tunnel Testing ». *The Aeronautical Journal*.

Koreanschi, Andreea, Oliviu Sugar Gabor, Tristan Ayrault, Ruxandra Mihaela Botez, Mahmoud Mamou and Youssef Mebarki. 2016. « Numerical Optimization and Experimental Testing of a Morphing Wing with Aileron System ». In *24th AIAA/AHS Adaptive Structures Conference*. p. 1083.

Kota, Sridhar, Joel A Hetrick and Russell F Osborn Jr. 2006. « Adaptive structures: Moving into the maienstream ». *Aerospace America,* vol. 44, n° 9, p. 16-18.

Kota, Sridhar, Joel A Hetrick, Russell Osborn, Donald Paul, Edmund Pendleton, Peter Flick and Carl Tilmann. 2003. « Design and application of compliant mechanisms for morphing aircraft structures ». In *Smart Structures and Materials*. p. 24-33. International Society for Optics and Photonics.

Kulfan, Brenda M, and John E Bussoletti. 2006. « Fundamental parametric geometry representations for aircraft component shapes ». In *11th AIAA/ISSMO multidisciplinary analysis and optimization conference*. Vol. 6948. sn.

Kulite. 2015. « Kulite Semiconductor Products ». < Http://Kulite.Com/ >. Consulté le November 2015.

Veuillez sélectionner un type de document autre que « Generic » afin de faire afficher la référence bibliographique.

Langtry, RB, FR Menter, SR Likki, YB Suzen, PG Huang and S Völker. 2006. « A correlation-based transition model using local variables—Part II: Test cases and industrial applications ». *Journal of Turbomachinery,* vol. 128, n° 3, p. 423-434.

Liauzun, Cédric. 2010. « Aeroelastic Response to Gust Using CFD Techniques ». In *ASME 2010 3rd Joint US-European Fluids Engineering Summer Meeting collocated with 8th International Conference on Nanochannels, Microchannels, and Minichannels*. p. 269-276. American Society of Mechanical Engineers.

Love, MH, PS Zink, RL Stroud, DR Bye, Steven Rizk and David White. 2007. « Demonstration of morphing technology through ground and wind tunnel tests ». In *Proceedings of 48th AIAA/ASME/ASCE/AHS/ASC structures, structural dynamics and materials conference*. p. 23-26.

Lyu, Z., and J.R.R.A. Martins. 2014. « Aerodynamic Shape Optimization of an Adaptive Morphing Trailing Edge Wing ». In *In Proceedings of the 15th AIAA/ISSMO Multidisciplinary Analysis and Optimization Conference*. (Atlanta, Georgia, USA).

Majhi, Ritanjali, Ganapati Panda, Babita Majhi and Gadadhar Sahoo. 2009. « Efficient prediction of stock market indices using adaptive bacterial foraging optimization (ABFO) and BFO based techniques ». *Expert Systems with Applications,* vol. 36, n° 6, p. 10097-10104.

Majji, Manoranjan, and John L Junkins. 2006. *Robust control of redundantly actuated dynamical systems*. Texas A & M University.

Mamou, Mahmoud, Weixing Yuan, Mahmood Khalid, Ralf Wokoeck and Rolf Radespiel. 2006. « Transition Prediction in Low Reynolds Airfoil Flows Using Finite Element/Difference Solvers Coupled with the en Method: A Comparative Study ». *AIAA Paper,* vol. 3176.

Manan, Abdul, GA Vio, MY Harmin and JE Cooper. 2010. « Optimization of aeroelastic composite structures using evolutionary algorithms ». *Engineering Optimization,* vol. 42, n^{o} 2, p. 171-184.

Veuillez sélectionner un type de document autre que « Generic » afin de faire afficher la référence bibliographique.

Marwala, Tshilidzi. 2010. *Finite element model updating using computational intelligence techniques: applications to structural dynamics*. Springer Science & Business Media.

Maskew, Brian. 1987. « Program VSAERO theory document ». *NASA CR-4023*.

McGowan, Anna-Maria R, Anthony E Washburn, Lucas G Horta, Robert G Bryant, David E Cox, Emilie J Siochi, Sharon L Padula and Nancy M Holloway. 2002. « Recent results from NASA's morphing project ». In *SPIE's 9th Annual International Symposium on Smart Structures and Materials*. p. 97-111. International Society for Optics and Photonics.

Veuillez sélectionner un type de document autre que « Generic » afin de faire afficher la référence bibliographique.

Mebarki, Youssef, Mahmoud Mamou and M. Genest. 2009. « Infrared Measurements of the Transition Detection on the CRIAQ Project Morphing Wing Model ». *NRC LTR AL-2009-0075*.

Menter, Florian R, RB Langtry, SR Likki, YB Suzen, PG Huang and S Völker. 2006. « A correlation-based transition model using local variables—part I: model formulation ». *Journal of turbomachinery,* vol. 128, n^{o} 3, p. 413-422.

Michaud, Francois. 2014. « Design and Optimization of a Composite Skin for an Adaptive Wing ». *Master Of Science Thesis, Ecole De Technologie Superieure, Montreal, Canada*.

Michaud, François, Simon Joncas and RM Botez. 2013. « Design, Manufacturing and Testing of a Small-Scale Composite Morphing Wing ». In *19th International Conference on Composite Materials, Montréal, Québec, Canada, July*.

Michel, R. 1951. « Etude de la Transition sur les Profiles d'Aile; Etablissement d'un Critére de Determination de Point de Transition et Calcul de la Trainee de Profile Incompressible ». *ONERA Rept,* vol. 1.

Mitchell, Melanie. 1998. *An introduction to genetic algorithms*. MIT press.

Monner, Hans P, Holger Hanselka and Elmar J Breitbach. 1998. « Development and design of flexible fowler flaps for an adaptive wing ». In *5th Annual International Symposium on Smart Structures and Materials*. p. 60-70. International Society for Optics and Photonics.

Mosbah, Abdallah Ben, Ruxandra Botez and Thien My Dao. 2013. « New methodology for calculating flight parameters with neural network–EGD method ». In *AIAA Modeling and Simulation Technologies (MST) Conference, Boston, MA, USA, Aug*. p. 19-22.

Mosbah, Abdallah Ben, Manuel Flores Salinas, Ruxandra Mihaela Botez and Thien-my Dao. 2013. « New Methodology for Wind Tunnel Calibration Using Neural Networks-EGD Approach ». *SAE International Journal of Aerospace,* vol. 6, n^{o} 2, p. 761-766.

Mueller, Thomas J. 2013. *Low Reynolds Number Aerodynamics: Proceedings of the Conference Notre Dame, Indiana, USA, 5–7 June 1989*, 54. Springer Science & Business Media.

Murua, Joseba, Rafael Palacios and Joaquim Peiró. 2010. « Camber effects in the dynamic aeroelasticity of compliant airfoils ». *Journal of Fluids and Structures,* vol. 26, n^{o} 4, p. 527-543.

Navy, United States. 2003. *F-14 Tomcat Fighter Fact File*. United States Navy. Consulté le January 2015.

Neal, David A, Matthew G Good, Christopher O Johnston, Harry H Robertshaw, William H Mason and Daniel J Inman. 2004. « Design and wind-tunnel analysis of a fully adaptive aircraft configuration ». *Proceedings of AIAA/ASME/ASCE/AHS/ASC SDM, Palm Springs, California*.

News, CBS. 2008. « Airline flies jumbo jet powered by biofuel ». < http://www.cbc.ca/news/technology/airline-flies-jumbo-jet-powered-by-biofuel-1.754085 >. Consulté le February 2016.

Nir, Adi, and Haim Abramovich. 2010. « Design, analysis and testing of a smart fin ». *composite structures,* vol. 92, n^{o} 4, p. 863-872.

Okamoto, Nicole DeJong, Jinny Rhee and Nikos J Mourtos. 2005. « Educating students to understand the impact of engineering solutions in a global/societal context ». In *8th UICEE Annual Conference on Engineering Education*. Citeseer.

Pagès, L, O Trifu and I Paraschivoiu. 2007. « Optimized laminar flow control on an airfoil using the adaptable wall technique ». In *Proceedings of the Canadian Aeronautics and Space Institute Annual General Meeting*.

Patran/Nastran, MSC. 2016. « Aeroelasticity User Manual ». < http://www.mscsoftware.com >. Consulté le January 2016.

Patron, Felix Salvador Roberto, Ruxandra Mihaela Botez and D Labour. 2013. « New altitude optimisation algorithm for the flight management system CMA-9000 improvement on the A310 and L-1011 aircraft ». *Royal Aeronautical Society,* vol. 117, p. 787-805.

Patrón, Félix Salvador Roberto, Aniss Kessaci and Ruxandra Mihaela Botez. 2014. « Horizontal flight trajectories optimisation for commercial aircraft through a Flight Management System ». *The Aeronautical Journal,* vol. 118, n° 1209.

Pecora, Rosario, Francesco Amoroso and Gianluca Amendola. 2014. « Validation of a smart structural concept for wing-flap camber morphing ». *Smart Structures and Systems,* vol. 14, n° 4, p. 659-678.

Pecora, Rosario, Francesco Amoroso and Leonardo Lecce. 2012. « Effectiveness of wing twist morphing in roll control ». *Journal of aircraft,* vol. 49, n° 6, p. 1666-1674.

Pecora, Rosario, Silvestro Barbarino, Leonardo Lecce and Salvatore Russo. 2011. « Design and functional test of a morphing high-lift device for a regional aircraft ». *Journal of Intelligent Material Systems and Structures,* vol. 22, n° 10, p. 1005-1023.

Pecora, Rosario, Marco Magnifico, Francesco Amoroso and Ernesto Monaco. 2013. « Trade-off flutter analysis of a morphing wing trailing edge ». In *6th ECCOMAS Conference on Smart Structures and Materials, SMART2013*.

Pecora, Rosario, Marco Magnifico, Francesco Amoroso and Ernesto Monaco. 2014. « Multi-parametric flutter analysis of a morphing wing trailing edge ». *Aeronautical Journal,* vol. 118, n° 1207, p. 1063-1078.

Peeters, Paul, J Middel and A Hoolhorst. 2005. « Fuel efficiency of commercial aircraft ». *An overview of historical*.

Peifeng, LI, Binqian Zhang, CHEN Yingchun, YUAN Changsheng and LIN Yu. 2012. « Aerodynamic design methodology for blended wing body transport ». *Chinese Journal of Aeronautics,* vol. 25, n° 4, p. 508-516.

Piegl, Les, and Wayne Tiller. 2012. *The NURBS book*. Springer Science & Business Media.

Poonsong, Prasobchok. 2004. « Design and analysis of a multi-section variable camber wing ».

Popov, Andrei Vladimir, Ruxandra Mihaela Botez and Michel Labib. 2008. « Transition point detection from the surface pressure distribution for controller design ». *Journal of Aircraft,* vol. 45, n° 1, p. 23-28.

Popov, Andrei Vladimir, Ruxandra Mihaela Botez, Mahmoud Mamou, Youssef Mébarki, B Jahrhaus, M Khalid and Teodor Lucian Grigorie. 2009. « Drag reduction by improving laminar flows past morphing configurations ». In *AVT-168 NATO Symposium on the Morphing Vehicles*.

Popov, Andrei Vladimir, Teodor Lucian Grigorie, Ruxandra Mihaela Botez, Mahmoud Mamou and Youssef Mebarki. 2010a. « Closed-loop control validation of a morphing wing using wind tunnel tests ». *Journal of Aircraft,* vol. 47, n° 4, p. 1309-1317.

Popov, Andrei Vladimir, Teodor Lucian Grigorie, Ruxandra Mihaela Botez, Mahmoud Mamou and Youssef Mebarki. 2010b. « Real time morphing wing optimization validation using wind-tunnel tests ». *Journal of Aircraft,* vol. 47, n° 4, p. 1346-1355.

Rae, William H, and Alan Pope. 1984. *Low-speed wind tunnel testing*. John Wiley.

Reed Jr, John L, Christopher D Hemmelgarn, Bryan M Pelley and Ernie Havens. 2005. « Adaptive wing structures ». In *Smart structures and materials*. p. 132-142. International Society for Optics and Photonics.

Reynolds, Osborne. 1883. « An experimental investigation of the circumstances which determine whether the motion of water shall be direct or sinuous, and of the law of resistance in parallel channels ». *Proceedings of the royal society of London,* vol. 35, n° 224-226, p. 84-99.

Robitaille, Martin, Ali Mosahebi and Éric Laurendeau. 2015. « Design of adaptive transonic laminar airfoils using the transition model ». *Aerospace Science and Technology,* vol. 46, p. 60-71.

Rocha, J, P Moniz and A Suleman. 2007. « Aeroelastic control of a wing with active skins using piezoelectric patches ». *Mechanics of Advanced Materials and Structures,* vol. 14, n° 1, p. 23-32.

Veuillez sélectionner un type de document autre que « Generic » afin de faire afficher la référence bibliographique.

Rodden, William P, and E Dean Bellinger. 1982. « Aerodynamic lag functions, divergence, and the British flutter method ». *Journal of Aircraft,* vol. 19, n° 7, p. 596-598.

Sainmont, C, I Paraschivoiu, D Coutu, V Brailovski, E Laurendeau, MMY Mamou and M Khalid. 2009. « Boundary layer behaviour on an morphing wing: simulation and wind tunnel tests" ». In *Canadian Aeronautics and Space Institute AERO09 Conference*.

Sanders, B, FE Eastep and E Forster. 2003. « Aerodynamic and aeroelastic characteristics of wings with conformal control surfaces for morphing aircraft ». *Journal of Aircraft,* vol. 40, n° 1, p. 94-99.

Schlichting, Herrmann, and Klaus Gersten. 2003. *Boundary-layer theory*. Springer Science & Business Media.

Secanell, Marc, Afzal Suleman and Pedro Gamboa. 2005. « Design of a morphing airfoil for a light unmanned aerial vehicle using high-fidelity aerodynamic shape optimization ». *Journal of American Institute of Aeronautics and Astronautics (AIAA 2005-1891)*, p. 1-20.

Shaw, R. 1960. « The influence of hole dimensions on static pressure measurements ». *Journal of Fluid Mechanics,* vol. 7, n° 04, p. 550-564.

Shili, Liu, Ge Wenjie and Li Shujun. 2008. « Optimal design of compliant trailing edge for shape changing ». *Chinese Journal of Aeronautics,* vol. 21, n° 2, p. 187-192.

Shyy, Wei, Hikaru Aono, Satish Kumar Chimakurthi, P Trizila, C-K Kang, Carlos ES Cesnik and Hao Liu. 2010. « Recent progress in flapping wing aerodynamics and aeroelasticity ». *Progress in Aerospace Sciences,* vol. 46, n° 7, p. 284-327.

Silisteanu, Paul-Dan, and Ruxandra M Botez. 2010. « Transition-flow-occurrence estimation: A new method ». *Journal of Aircraft,* vol. 47, n° 2, p. 703-708.

Silisteanu, Paul Dan, and Ruxandra Mihaela Botez. 2012. « Two-dimensional airfoil design for low speed airfoils ». In *AIAA Atmospheric Flight Mechanics conference*.

Sivells, James C, and Robert H Neely. 1947. *Method for calculating wing characteristics by lifting-line theory using nonlinear section lift data*. DTIC Document.

Skillen, Michael D, and William A Crossley. 2008. « Morphing Wing Weight Predictors and Their Application in a Template-Based Morphing Aircraft Sizing Environment II. Part 2; Morphing Aircraft Sizing via Multi-level Optimization ».

Smith, Stephen B, and David W Nelson. 1990. « Determination of the aerodynamic characteristics of the mission adaptive wing ». *Journal of Aircraft,* vol. 27, n° 11, p. 950-958.

Snyman, Jan. 2005. *Practical mathematical optimization: an introduction to basic optimization theory and classical and new gradient-based algorithms*, 97. Springer Science & Business Media.

Sofla, AYN, SA Meguid, KT Tan and WK Yeo. 2010. « Shape morphing of aircraft wing: status and challenges ». *Materials & Design,* vol. 31, n° 3, p. 1284-1292.

Storms, Bruce L, Timothy T Takahashi and James C Ross. 1995. *Aerodynamic influence of a finite-span flap on a simple wing*. SAE Technical Paper.

Sugar Gabor, Oliviu, Andrea Koreanschi and M. Ruxandra Botez. « Numerical optimization of the S4 Éhecatl UAS airfoil using a morphing wing approach ». In *American Institute of Aeronautics and Astronautics AIAA 32nd Applied Aerodynamics Conference*.

Sugar Gabor, Oliviu, Andreea Koreanschi and Ruxandra Mihaela Botez. 2012. « Low-speed aerodynamic characteristics improvement of ATR 42 airfoil using a morphing wing approach ». In *IECON 2012-38th Annual Conference on IEEE Industrial Electronics Society*. p. 5451-5456. IEEE.

Sugar Gabor, Oliviu, Andreea Koreanschi and Ruxandra Mihaela Botez. 2013a. « Optimization of an Unmanned Aerial Systems' Wing Using a Flexible Skin Morphing Wing ». *SAE International Journal of Aerospace,* vol. 6, n° 2013-01-2095, p. 115-121.

Sugar Gabor, Oliviu, Andreea Koreanschi and Ruxandra Mihaela Botez. 2013b. « Unmanned Aerial System Hydra Technologies Éhecatl wing optimization using a morphing approach ». In *AIAA Atmospheric Flight Mechanics (AFM) Conference*. p. 5164.

Sugar Gabor, Oliviu, Antoine Simon, Andreea Koreanschi and Ruxandra Botez. 2014. « Application of a Morphing Wing Technology on Hydra Technologies Unmanned Aerial System UAS-S4 ». In *ASME 2014 International Mechanical Engineering Congress and Exposition*. p. V001T01A037-V001T01A037. American Society of Mechanical Engineers.

Sugar Gabor, Oliviu, Antoine Simon, Andreea Koreanschi and Ruxandra M Botez. 2015a. « Aerodynamic performance improvement of the UAS-S4 Éhecatl morphing airfoil using novel optimization techniques ». *Proceedings of the Institution of Mechanical Engineers, Part G: Journal of Aerospace Engineering*, p. 0954410015605548.

Sugar Gabor, Oliviu, Antoine Simon, Andreea Koreanschi and Ruxandra Mihaela Botez. 2015b. « Improving the UAS-S4 Éhecal airfoil high angles-of-attack performance characteristics using a morphing wing approach ». *Proceedings of the Institution of Mechanical Engineers, Part G: Journal of Aerospace Engineering*.

Talay, Theodore A. 1975. *Introduction to the Aerodynamics of Flight*, 367. Scientific and Technical Information Office, National Aeronautics and Space Administration.

Tavoularis, S. 2005. *Measurement in Fluid Mechanics*. Cambridge University Press.

Thill, C, J Etches, I Bond, K Potter and P Weaver. 2008. « Morphing skins ». *The Aeronautical Journal,* vol. 112, n° 1129, p. 117-139.

Tianyuan, Hu, and Yu Xiongqing. 2009. « Aerodynamic/stealthy/structural multidisciplinary design optimization of unmanned combat air vehicle ». *Chinese Journal of Aeronautics,* vol. 22, n° 4, p. 380-386.

Van Ingen, JL. 2008. *The eN method for transition prediction: historical review of work at TU Delft*. AIAA.

van Zyl, Louw H, and Motodi S Maserumule. 2001. « Unrestrained aeroelastic divergence and the pk flutter equation ». *Journal of aircraft,* vol. 38, n° 3, p. 588-590.

Vasista, Srinivas, Liyong Tong and KC Wong. 2012. « Realization of morphing wings: a multidisciplinary challenge ». *Journal of Aircraft,* vol. 49, n° 1, p. 11-28.

Vercauteren, J, W Bosschaerts, M Baelmans and T Persoons. 2010. « Numerical Investigation on the Measurement Error of Static Pressure Taps in Small Scale Channels ». *Proceedings Power MEMS*, p. 1-3.

Wang, Donny P, Jonathan D Bartley-Cho, Christopher A Martin and Brian J Hallam. 2001. « Development of high-rate large-deflection hingeless trailing-edge control surface for the Smart Wing wind tunnel model ». In *SPIE's 8th Annual International Symposium on Smart Structures and Materials*. p. 407-418. International Society for Optics and Photonics.

Wazzan, AR, C Gazley and AMO Smith. 1979. « Tollmien-Schlichting waves and transition: heated and adiabatic wedge flows with application to bodies of revolution ». *Progress in Aerospace Sciences,* vol. 18, p. 351-392.

Whitley, Darrell. 1994. « A genetic algorithm tutorial ». *Statistics and computing,* vol. 4, n° 2, p. 65-85.

Xie, ChangChuan, Yi Liu and Chao Yang. 2012. « Theoretic analysis and experiment on aeroelasticity of very flexible wing ». *Science China Technological Sciences,* vol. 55, n° 9, p. 2489-2500.

Xie, Changchuan, Libo Wang, Chao Yang and Yi Liu. 2013. « Static aeroelastic analysis of very flexible wings based on non-planar vortex lattice method ». *Chinese Journal of Aeronautics,* vol. 26, n° 3, p. 514-521.

Xie, Li-Ping, and Jian-Chao Zeng. 2009. « A global optimization based on physicomimetics framework ». In *Proceedings of the first ACM/SIGEVO Summit on Genetic and Evolutionary Computation*. p. 609-616. ACM.

Xing, Bo, and Wen-Jing Gao. 2014. *Innovative computational intelligence: a rough guide to 134 clever algorithms*. Springer.

Yuan, Ya-xiang. 2008. « Step-sizes for the gradient method ». *AMS IP Studies in Advanced Mathematics,* vol. 42, n° 2, p. 785.

Zhang, Hao, and Dongyi Ye. 2012. « An artificial bee colony algorithm approach for routing in VLSI ». In *Advances in swarm intelligence*. p. 334-341. Springer.

Zingg, David W, Laslo Diosady and Laura Billing. 2006. « Adaptive airfoils for drag reduction at transonic speeds ». *AIAA paper,* vol. 3656, p. 2006.

Zona_Technology, Inc. 2014. « ZAERO, Version 8.5, theoretical manual. ». < http://www.zonatech.com/Documentation/ZAERO_THEORETICAL_MANUAL_8.5.pdf >. Consulté le October 2015.